University of Mississippi

eGrove

Electronic Theses and Dissertations | Graduate School

1-1-2011

Natural Products Chemistry of Leads Acting on MRSA, HCV, Malaria, and Depression Disorders

Mohamed Ali Mohamed Ali Ibrahim
University of Mississippi

Follow this and additional works at: https://egrove.olemiss.edu/etd

 Part of the Pharmacy and Pharmaceutical Sciences Commons

Recommended Citation

Ibrahim, Mohamed Ali Mohamed Ali, "Natural Products Chemistry of Leads Acting on MRSA, HCV, Malaria, and Depression Disorders" (2011). *Electronic Theses and Dissertations*. 1461.
https://egrove.olemiss.edu/etd/1461

This Dissertation is brought to you for free and open access by the Graduate School at eGrove. It has been accepted for inclusion in Electronic Theses and Dissertations by an authorized administrator of eGrove. For more information, please contact egrove@olemiss.edu.

Natural Products Chemistry of Leads Acting on MRSA, HCV, Malaria, and Depression Disorders

A Dissertation

Presented for the

Doctor of Philosophy

Degree

The University of Mississippi

Mohamed A. Ibrahim

August 2011

Copyright © 2011 by Mohamed A. Ibrahim
All rights reserved

ABSTRACT

Nature has proven to be an endless source of abundant diversity of chemical entities with varying biological activities. The World Health Organization (WHO) estimates that 80% of the world's population depends on traditional medicine for treating their everyday health problems. According to Gordon Cragg, former director of the natural products branch of the NCI, ″Nature has produced wonderfully complex molecules that no synthetic chemist could ever dream up.″ Moreover, he emphasized that over 60% of cancer therapeutics have been derived from nature whether directly through isolation or indirectly through semi-synthesis. Various examples have been reported such as extracts from *Catharanthus roseus* (Rosy Periwinkle) used for treatment of Hodgkin's disease and leukemia, digitalis from *Digitalis purpurea* (foxglove) for treatment of heart disease, galantamine from *Galanthus caucasicus* (snowdrops) for treatment of Alzheimer's disease, and paclitaxel from the bark of the Pacific yew tree to treat cancer.

During the course of these studies, we researched the potential of natural products to provide drugs for treatment of human and plant diseases for which no adequate therapy exists. For instance, methicillin-resistant *Staphylococcus aureus* (MRSA) is a destructive pathogen with a high patient mortality rate. Over 50% of the *Staph. aureus* infections around the world are caused by MRSA. In the first chapter, we will address the bioassay-guided isolation and characterization of a series of anti-MRSA active glycosides that exhibit a high degree of selectivity for MRSA from the leaves of the common American sycamore, *Platanus occidentalis*.

The isolated metabolites; *E,E*-platanoside [kaempferol 3-*O*-*α*-L-(2",3"-di-*E*-*p*-coumaroyl)rhamnoside, IC_{50} 2.0 μg/mL], *E,Z*-platanoside [kaempferol 3-*O*-*α*-L-(2"-*E*-*p*-coumaroyl-3"-*Z*-*p*-coumaroyl)rhamnoside, IC_{50} 0.8 μg/mL], *Z,E*-platanoside [kaempferol 3-*O*-*α*-L-(2"-*Z*-*p*-coumaroyl-3"-*E*-*p*-coumaroyl)rhamnoside, IC_{50} 0.7 μg/mL], and *Z,Z*-platanoside [kaempferol 3-*O*-*α*-L-(2",3"-di-*Z*-*p*-coumaroyl)rhamnoside, IC_{50} 0.4 μg/mL] have been shown to prevent growth of MRSA on surfaces and systemically.

The in vitro anti-MRSA activity of these metabolites indicated that changing the configuration of the double bond in the *p*-comaroyl units greatly affects the MRSA activity. This, in turn, encouraged us to establish economic methods to transform the less active *E,E*-platanoside to the more active *Z,* Z-platanoside. Light-mediated isomerization in platanosides provides a precise, noninvasive, and "green" approach for controlling MRSA activity. In the second chapter, the development of a simple "green" chemistry approach is described that uses light induced photoisomerization for transforming the thermodynamically stable *E,E*-platanoside to the *Z,E*-, *E,Z*- and *Z,*Z-platanosides. This provided support for the light mediated photoisomerization over the enzymatic control theory for the biosynthesis formation of the *Z*-isomers.

American sycamore is significant to the forest products industry due to its use as pulp-wood for making paper and fiberboard, and sawlogs for manufacturing butcher's blocks, furniture, interior trim, boxes, and flooring. Historically, American sycamore has held, and continues to hold, good potential as a dedicated biofuels crop grown on short rotations in

plantations. However, the growth and productivity of sycamore plantations is hampered by bacterial leaf scorch disease (BLS) caused by *Xylella fastidiosa*. Strains of this bacterium are the major cause of various plant diseases such as phony peach disease (PPD), plum leaf scald (PLS), and Pierce's disease (PD) of grapes, citrus variegated chlorosis (CVC), and leaf scorch of almond, oleander, and pear. The isolated anti-MRSA metabolites are found in greater concentrations in healthy sycamore trees versus diseased trees suggesting an ecological link between tree health and glycoside content. The third chapter describes this ecological link and presents data that demonstrates the ability of the metabolites to inhibit *X. fastidiosa* at nanomolar concentrations (MIC $\leq$ 17-67 nM). The presence of these metabolites in sycamore has the potential to be a useful analytical tool for selecting disease-resistant strains.

Depression is the most common disease of the central nervous system affecting approximately 17% of Americans each year. According to the National Institute of Mental Health (NIMH), every year about 40 million American adults suffer from anxiety disorders that frequently co-occur with other psychiatric illnesses like depression. Recently, our group reported the isolation of several marine indole alkaloids and evaluated their biological activity in the forced swim (FST) and locomotor activity tests, revealing their potential to become new antidepressant drug leads. Among the isolated compounds, 5-bromo-*N*,*N*-dimethyltryptamine was found to display a high sedative effect in the locomotor activity test. Owing to the limited amounts of this compound obtained from isolation, a synthetic approach was adopted to prepare 5-bromo-*N*,*N*-dimethyltryptamine and its derivatives to study the structure activity relationships

(SAR) and complete the dose-response experiments. In the fourth chapter, the synthesis is described of a series of 2-(5-halo-1*H*-indol-3-yl)-*N*,*N*-dimethylethanamines, as is the evaluation of their in vivo antidepressant and sedative activities using the FST and locomotor activity tests. Of the synthetically prepared compounds, 2-(1*H*-indol-3-yl)-*N*,*N*-dimethyl-2-oxoacetamide, 2-(5-chloro-1*H*-indol-3-yl)-*N*,*N*-dimethyl-2-oxoacetamide, 2-(1*H*-indol-3-yl)-*N*,*N*-dimethylethanamine, 2-(5-chloro-1*H*-indol-3-yl)-*N*,*N*-dimethylethanamine, and 2-(5-iodo-1*H*-indol-3-yl)-*N*,*N*-dimethylethanamine have been shown to possess antidepressant-like action. Dose response studies were completed for the active compounds.

Manzamine A is an alkaloid that contains a unique multi-heterocyclic ring system coupled to a β-carboline moiety. Manzamine A showed potent in vitro antimalarial activity against *P. falciparum* D6 and W2 (0.017-0.020 μM), but its toxicity hindered its development as a drug lead. Malaria, a major tropical infectious disease caused primarily by the protozoan parasite *Plasmodium falciparum*, is responsible for the death of more than 1.12 million individuals every year. Recently, Ihara reported that the π-delocalized lipophilic cationic (DLC) structures of various β-carboline natural products, display reasonable antimalarial activity against *P. falciparum* with low cytotoxicity against mammalian cells. The fifth chapter describes the synthesis of mono- and di-methylated quaternary carbolinium cations of manzamine A and evaluations of their in vitro antimalarial and antimicrobial activities, cytotoxicity, and also their potential for glycogen synthase kinase (GSK-3β) inhibition using molecular docking studies. Among the analogs, 2-*N*-methylmanzamine A exhibited antimalarial activity (IC_{50} 0.7 – 1.0

μM), but was less potent than manzamine A. However, the compound was significantly less cytotoxic to mammalian kidney fibroblasts with a selectivity index in the same range as manzamine A.

One of the most serious threats to humans is hepatitis C virus (HCV) infections affecting approximately 4 million individuals in the United States, and 200-300 million individuals worldwide, causing over 8,000 deaths each year. HCV can progress to severe liver disorders such as fibrosis, cirrhosis, and hepatocellular carcinoma. A rare Latin American plant extract provided through collaboration with the National Cancer Institute (NCI) repository (No. 77951) showed potent anti-HCV activity.

Diplostephium rhododendroides (family Asteraceae) is only found between Ecuador and Colombia and has not been subjected to phytochemical screening. The last chapter describes the isolation and identification from this rare plant of anti-HCV oleanane-triterpenes complex glycosides with *m/z* of 1700-1800. The isolated rhododendrosaponins **I-III** have shown exceptional activity (EC_{50} 0.2 μg/mL) against HCV and warrant further evaluations.

DEDICATION

This work is dedicated to my Family and my Uncle

“Saeed Mohamed Ali”

ACKNOWLEDGMENTS

I would like to gratefully acknowledge my advisor, Professor Mark T. Hamann for his guidance and continuous support towards earning my doctoral degree.

I would like to thank my committee members: Drs. Daneel Ferreira, Jordan Zjawiony, Abir T. El-Alfy, James D. McChesney, and Theodor D. Leininger for their valuable suggestions.

I would especially like to thank Dr. Raymond F. Schinazi and his research group at Emory's Center for AIDS Research, Emory University, GA for performing Hepatitis C assays, Dr. Theodor D. Leininger and his team for their help in providing bacterial leaf scorch asymptomatic and symptomatic American sycamore leaves, Dr. Abir T. El-Alfy and her group for performing the forced swim and locomotor activity tests and Dr. Khalid M. Ashfag for in vivo testing my *E*,*E*-platanoside in MRSA murine thigh infection model. Thanks are also due to Drs. Melissa Jacob, Shabana I. Khan, and Ms. Marsha Wright for antimicrobial, antimalarial and cytotoxicity testing. I would like also to acknowledge Dr. Robert Doerksen and his group members for molecular modeling, and Dr. Jiangnan Peng, Mr. John Bowling and Ms. Amanda L. Waters for acquiring 600 MHz NMR data. I would like to thank Dr. Mitchell Avery and Mr. Yunshan Wu for acquiring the X-ray data, Dr. Mohamed M. Radwan for his help in acquiring the UV spectra and the optical rotations, Dr. John S. Williamson for his help with purification of the rhododendrosaponins, and Drs. Ikhlas A. Khan, Mei Wang, and Desmond Slade for acquiring the GC data.

I am thankful to the faculty and staff in the Department of Pharmacognosy for all I have learned from them. I would like to thank Ms. Casey Stauber for her continuous help in dealing with any difficulties concerning graduate students.

I would also like to thank the Egyptian Ministry for Higher Education and Scientific Research for awarding a 4 years Ph.D. scholarship.

Many thanks are given to my colleagues in the Department of Pharmacognosy for their support and encouragement. Thanks are also due to Ms. Claire Mischker at the Writing Center-University of Mississippi for proofing my dissertation.

Finally, my deep thanks and appreciation are given to Dr. Iman Gohar and my family: my parents, my wife, my children, my sister, my brother in-law, my brother, and my sister in-law for their unbelievable support, encouragement and care.

TABLE OF CONTENTS

CHAPTER PAGE

I. METHICILLIN-RESISTANT *STAPHYLOCOCCUS AUREUS* ACTIVE METABOLITES FROM *PLATANUS OCCIDENTALIS* (AMERICAN SYCAMORE)……1

II. PHOTOISOMERIZATION AS A MECHANISM TO ENHANCE BIOLOGICAL ACTIVITY AND CONTROL RESISTANCE IN *STAPHYLOCOCCUS AUREUS* AND METHICILLIN-RESISTANT *STAPHYLOCOCCUS AUREUS* ……...48

III. LINKING THE DISCOVERY OF LEADS FOR DRUG RESISTANT HUMAN PATHOGENS TO THE GENERATION OF DISEASE RESISTANT STRAINS OF *PLATANUS OCCIDENTALIS* (AMERICAN SYCAMORE)…… …...77

IV. 2-(5-HALO-1*H*-INDOL-3-YL)-*N*,*N*-DIMETHYLETHANAMINES AS ANTIDEPRESSANT DRUG LEADS……93

V**.** 2-*N*-MODIFICATIONS AND SAR STUDIES OF MANZAMINE A ……132

VI. HCV LEADS FROM THE SOUTH AMERICA ENDANGERED PLANT *DIPLOSTEPHIUM RHODODENDROIDES* 160

BIBILIOGRAPHY…….....223

APPENDIX: HETERONEMIN ……236

VITA……...240

LIST OF FIGURES

FIGURE PAGE

Figure 1. The structures of American sycamore glycosides **1**-**4**…….....4

Figure 2. The LC/MS analysis of the crude extract shows the presence of the four metabolites **1**-**4**…….....12

Figure 3. Stability of *Z,Z*-platanoside in various solvents…….12

Figure 4. Effect of *E,E*-platanoside **1** on MRSA thigh infection in a murine model....13

Figure 5. HPLC chromatogram of Fr. **7**; H_2O-CH_3CN (5: 95) on 250 x 21.2 mm NH_2 column….....17

Figure 6. HPLC chromatogram of signal **2** on 250 x 10 mm PFP-2 column……18

Figure 7. LC/MS chromatogram of *E,E*-platnaoside……18

Figure 8. ^{1}H NMR spectrum of *E,E*-platanoside in methanol-d_4 (600 MHz)……...19

Figure 9. ^{13}C NMR spectrum of *E,E*-platanoside in methanol-d_4 (600 MHz)……..20

Figure 10. 135º DEPT spectrum of *E,E*-platanoside in methanol-d_4 (600 MHz)…....21

Figure 11. HSQC spectrum of *E,E*-platanoside in methanol-d_4 (400 MHz)…….…22

Figure 12. COSY spectrum of *E,E*-platanoside in methanol-d_4 (400 MHz)……..…..23

Figure 13. HMBC spectrum of *E,E*-platanoside in methanol-d_4 (400 MHz)……...24

Figure 14. Selected COSY and HMBC correlations of *E,E*-platanoside …..……...25

Figure 15. UV spectrum of *E,Z*-platanoside in MeOH……...……..25

Figure 16. ^{1}H NMR spectrum of *E,Z*-platanoside in methanol-d_4 (400 MHz)…..…...26

Figure 17. ^{13}C NMR spectrum of *E*,*Z*-platanoside in methanol-d_4 (400 MHz)……27

Figure 18. 135º DEPT spectrum of *E*,*Z*-platanoside in methanol-d_4 (400 MHz)……..28

Figure 19. HMQC spectrum of *E*,*Z*-platanoside in methanol-d_4 (400 MHz)…….....29

Figure 20. COSY spectrum of *E*,*Z*-platanoside in methanol-d_4 (400 MHz)…….....30

Figure 21**.** HMBC spectrum of *E*,*Z*-platanoside in methanol-d_4 (400 MHz)…….....31

Figure 22. NOESY spectrum of *E*,*Z*-platanoside in methanol-d_4 (400 MHz)…….....32

Figure 23. UV spectrum of *Z*,*E*-platanoside in MeOH…….....32

Figure 24. ^{1}H NMR spectrum of *Z*,*E*-platanoside in methanol-d_4 (400 MHz)…….....33

Figure 25. ^{13}C NMR spectrum of *Z*,*E*-platanoside in methanol-d_4 (400 MHz)…….....34

Figure 26. 135º DEPT spectrum of *Z*,*E*-platanoside in methanol-d_4 (400 MHz)…….....35

Figure 27. HMQC spectrum of *Z*,*E*-platanoside in methanol-d_4 (400 MHz)…….....36

Figure 28. COSY spectrum of *Z*,*E*-platanoside in methanol-d_4 (400 MHz)…….....37

Figure 29. HMBC spectrum of *Z*,*E*-platanoside in methanol-d_4 (400 MHz)…….....38

Figure 30. NOESY spectrum of *Z*,*E*-platanoside in methanol-d_4 (400 MHz)…….....39

Figure 31. UV spectrum of *Z*,*Z*-platanoside in MeOH……..……...….39

Figure 32. ^{1}H NMR spectrum of *Z*,*Z*-platanoside in methanol-d_4 (400 MHz)…….....40

Figure 33. ^{13}C NMR spectrum of *Z*,*Z*-platanoside in methanol-d_4 (400 MHz)..…..….41

Figure 34. 135º DEPT spectrum of *Z*,*Z*-platanoside in methanol-d_4 (400 MHz)..……...42

Figure 35. HMQC spectrum of *Z*,*Z*-platanoside in methanol-d_4 (400 MHz)..…….....43

Figure 36. COSY spectrum of *Z*,*Z*-platanoside in methanol-d_4 (400 MHz)…….....44

Figure 37. HMBC spectrum of *Z,Z*-platanoside in methanol-d_4 (400 MHz)…….....45

Figure 38. NOESY spectrum of *Z,Z*-platanoside in methanol-d_4 (400 MHz)…….....46

Figure 39. LC/MS comparison between American sycamore and bay leaves…….....51

Figure 40. Structures of *Laurus nobilis* metabolites, quercitrin, and *E*-*p*-coumaric acid…….…...…52

Figure 41. LC/MS chromatogram of 2,4-*E,E*-platanoside ……...…….…..53

Figure 42. Final purification of 2,4-*E,E*-platanoside on 250 x 21.2 mm NH_2 column……...54

Figure 43. ^{1}H NMR spectrum of 2,4-*E,E*-platanoside in methanol-d_4 (400 MHz).....55

Figure 44. ^{13}C NMR spectrum of 2,4-*E,E*-platanoside in methanol-d_4 (400 MHz).....56

Figure 45. 135º DEPT spectrum of 2,4-*E,E*-platanoside in methanol-d_4 (400 MHz)...57

Figure 46. HSQC spectrum of 2,4-*E,E*-platanoside in methanol-d_4 (400 MHz).....58

Figure 47. HMBC spectrum of 2,4-*E,E*-platanoside in methanol-d_4 (400 MHz).....59

Figure 48. ^{1}H NMR spectrum of 2,4-*Z,E*-platanoside in methanol-d_4 (400 MHz).....60

Figure 49. ^{13}C NMR spectrum of 2,4-*Z,E*-platanoside in methanol-d_4 (400 MHz).....61

Figure 50. Possible conjugation in *Z,Z*-platanoside …….…...62

Figure 51. Purification of tetra-*O*-methyl-*E,E*-platanoside (**9**) on 250 x 10 mm Si HPLC column……...……64

Figure 52. LC/MS chromatogram of tetra-*O*-methyl-*E,E*-platanoside (**9**)……....64

Figure 53. ^{1}H NMR spectrum of tetra-*O*-methyl-*E,E*-platanoside (**9**) in methanol-d_4 (400 MHz).....65

Figure 54. Selected HMBC correlations of tetra-*O*-methyl-*E,E*-platanoside (**9**) in methanol-d_4 (500 MHz)…….....65

Figure 55. Application of 0.5% mixture platanosides (**1**-**4**) on TLC plates contaminated with MRSA ……67

Figure 56. The formation of the three active metabolites (**2**-**4**) through UV irradiation of *E,E*-platanoside ……69

Figure 57. Effect of chlorophyll on the isomerization of *E*-*p*-coumaric acid…….....69

Figure 58. The suggested biosynthetic formation of the *Z*-metabolites (**2**-**4**)…….....70

Figure 59. Effect of solvent (H-bonding) on the isomerization of *E*-*p*-coumaric acid.....71
Figure 60. Effect of BHT on the isomerization of *E*-*p*-coumaric acid……..72

Figure 61. A sycamore leaf expressing symptoms of bacterial leaf scorch ……..…80

Figure 62. A colony of *Xylella fastidiosa*…….....81

Figure 63. *Homalodisca vitripennis*, the glassy-winged sharpshooter.....81

Figure 64. Anti-MRSA metabolites from *Platanus occidentalis* (American sycamore)……...82

Figure 65. LC/MS calibration curve of *E,E*-platanoside ……83

Figure 66. Percent glycosides in 14 asymptomatic and symptomatic trees…..…..84

Figure 67. Pictures of two American sycamore trees coded 17-6 (BLS-symptomatic) and 9-17 (BLS-symptomatic) ……...86

Figure 68. In vitro assay of 0.2, 0.1, and 0.025% range of semi purified mixture of glycosides (purity ≥ 70% by LC/MS) against *X. fastidiosa*……..…….....88

Figure 69. In vitro assay of 0.1, 0.025, and 0.005% range of semi purified mixture of glycosides (purity ≥ 70% by LC/MS) against *X. fastidiosa* in double compartment Petri plates (72 h)……..…….....89

Figure 70. In vitro assay of 0.005-0.00125% of *E,E*-platanoside, *Z,Z*-platanoside, mixture of glycosides (27% purity by weight), and –ve control in four compartment

Petri plates…….89

Figure 71. In vitro assay of 0.005-0.00125% of *E*,*Z*-platanoside, *Z*,*E*-platanoside, mixture of glycosides (27% purity by weight), and –ve control in four compartment Petri plates…….90

Figure 72. In vitro assay of 0.005-0.0025% of *E*,*E*-platanoside, *Z*,*Z*-platanoside, *Z*,*E*-platanoside, and *E*,*Z*-platanoside in four compartment Petri plates…….....90

Figure 73. ^{1}H NMR spectrum of 2-(5-fluoro-1*H*-indol-3-yl)-*N*,*N*-dimethyl-2-oxoacetamide (**3b**) in methanol-d_4 (400 MHz)…… 97

Figure 74. ^{13}C NMR spectrum of 2-(5-fluoro-1*H*-indol-3-yl)-*N*,*N*-dimethyl-2-oxoacetamide (**3b**) in methanol-d_4 (400 MHz)……...…..97

Figure 75. 135º DEPT spectrum of 2-(5-fluoro-1*H*-indol-3-yl)-*N*,*N*-dimethyl-2-oxoacetamide (**3b**) in methanol-d_4 (400 MHz)……..…….……98

Figure 76. ^{1}H NMR spectrum of 2-(5-chloro-1*H*-indol-3-yl)-*N*,*N*-dimethyl-2-oxoacetamide (**3c**) in methanol-d_4 (400 MHz)……..…….**.....**98

Figure 77. ^{13}C NMR spectrum of 2-(5-chloro-1*H*-indol-3-yl)-*N*,*N*-dimethyl-2-oxoacetamide (**3c**) in methanol-d_4 (400 MHz)……..99

Figure 78. 135º DEPT spectrum of 2-(5-chloro-1*H*-indol-3-yl)-*N*,*N*-dimethyl-2-oxoacetamide (**3c**) in methanol-d_4 (400 MHz)……...….99

Figure 79. GC/MS chromatogram of 2-(5-bromo-1*H*-indol-3-yl)-*N*,*N*-dimethyl-2-oxoacetamide (**3d**)…….…….....100

Figure 80. ^{1}H NMR spectrum of 2-(5-bromo-1*H*-indol-3-yl)-*N*,*N*-dimethyl-2-oxoacetamide (**3d**) in $CDCl_3$ (400 MHz)……....……100

Figure 81. The X-ray crystal structure of compound 2-(1*H*-indol-3 yl)-*N*,*N*-dimethyl-2-oxoacetamide (**3a**)……101

Figure 82. ^{1}H NMR spectrum of 2-(1*H*-indol-3-yl)-*N*,*N*-dimethylethanamine (**4a**) in methanol-d_4 (400 MHz)……...……102

Figure 83. ^{13}C NMR spectrum of 2-(1*H*-indol-3-yl)-*N*,*N*-dimethylethanamine (**4a**) in methanol-d_4 (400 MHz)……...…103

Figure 84. 135º DEPT spectrum of 2-(1*H*-indol-3-yl)-*N*,*N*-dimethylethanamine (**4a**) in methanol-d_4 (400 MHz)……...…103

Figure 85. HSQC spectrum of 2-(1*H*-indol-3-yl)-*N*,*N*-dimethylethanamine (**4a**) in methanol-d_4 (400 MHz)……...104

Figure 86. HMBC spectrum of 2-(1*H*-indol-3-yl)-*N*,*N*-dimethylethanamine (**4a**) in methanol-d_4 (400 MHz)……..….104

Figure 87. COSY spectrum of 2-(1*H*-indol-3-yl)-*N*,*N*-dimethylethanamine (**4a**) in methanol-d_4 (400 MHz)…….……..105

Figure 88. ^{1}H NMR spectrum of 2-(5-fluoro-1*H*-indol-3-yl)-*N*,*N*-dimethylethanamine (**4b**) in methanol-d_4 (400 MHz)……..….105

Figure 89. ^{13}C NMR spectrum of 2-(5-fluoro-1*H*-indol-3-yl)-*N*,*N*-dimethylethanamine (**4b**) in methanol-d_4 (400 MHz)……..……106

Figure 90. 135º DEPT spectrum of 2-(5-fluoro-1*H*-indol-3-yl)-*N*,*N*-dimethylethanamine (**4b**) in methanol-d_4 (400 MHz)……106

Figure 91. LC/MS chromatogram of 2-(5-chloro-1*H*-indol-3-yl)-*N*,*N*-dimethylethanamine (**4c**)……...……107

Figure 92. ^{1}H NMR spectrum of 2-(5-chloro-1*H*-indol-3-yl)-*N*,*N*-dimethylethanamine (**4c**) in methanol-d_4 (400 MHz)……..….107

Figure 93. ^{13}C NMR spectrum of 2-(5-chloro-1*H*-indol-3-yl)-*N*,*N*-dimethylethanamine (**4c**) in methanol-d_4 (400 MHz)……...108

Figure 94. 135º DEPT spectrum of 2-(5-chloro-1*H*-indol-3-yl)-*N*,*N*-dimethylethanamine (**4c**) in methanol-d_4 (400 MHz)……..…108

Figure 95. HSQC spectrum of 2-(5-chloro-1*H*-indol-3-yl)-*N*,*N*-dimethylethanamine (**4c**) in methanol-d_4 (400 MHz)…….……..109

Figure 96. LC/MS chromatogram of 2-(5-bromo-1*H*-indol-3-yl)-*N*,*N*-dimethylethanamine (**4d**)…….....…….109

Figure 97. ^{1}H NMR spectrum of 2-(5-bromo-1*H*-indol-3-yl)-*N*,*N*-dimethylethanamine (**4d**) in methanol-d_4 (400 MHz)……...……110

Figure 98. ^{13}C NMR spectrum of 2-(5-bromo-1*H*-indol-3-yl)-*N*,*N*-dimethylethanamine (**4d**) in methanol-d_4 (400 MHz)……..…….110

Figure 99. 135º DEPT spectrum of 2-(5-bromo-1*H*-indol-3-yl)-*N*,*N*-dimethylethanamine (**4d**) in methanol-d_4 (400 MHz)…….111

Figure 100. HSQC spectrum of 2-(5-bromo-1*H*-indol-3-yl)-*N*,*N*-dimethylethanamine (**4d**) in methanol-d_4 (400 MHz)……...111

Figure 101. HMBC spectrum of 2-(5-bromo-1*H*-indol-3-yl)-*N*,*N*-dimethylethanamine (**4d**) in methanol-d_4 (400 MHz)……..…….112

Figure 102. ^{1}H NMR spectrum of 2-(5-iodo-1*H*-indol-3-yl)-*N*,*N*-dimethylethanamine (**4e**) in methanol-d_4 (400 MHz)…….....113

Figure 103. ^{13}C NMR spectrum of 2-(5-iodo-1*H*-indol-3-yl)-*N*,*N*-dimethylethanamine (**4e**) in methanol-d_4 (400 MHz)…….……113

Figure 104. 135º DEPT spectrum of 2-(5-iodo-1*H*-indol-3-yl)-*N*,*N*-dimethylethanamine (**4e**) in methanol-d_4 (400 MHz)……...…….114

Figure 105. Effect of compounds **3a-e** (20 mg/kg, i.p.) in (A) the forced swim test and (B) locomotor activity…….…….....116

Figure 106. Effect of compounds **4a-e** (20 mg/kg, i.p.) in (A) the forced swim test and (B) locomotor activity……....117

Figure 107. Dose response curves of compound **3a** in (A) the forced swim test and (B) locomotor activity…….……....119

Figure 108. Dose response curves of compound **3d** in (A) the forced swim test and (B) locomotor activity…….....119

Figure 109. Dose response curves of compound **4a** in (A) the forced

swim test and (B) locomotor activity…….....120

Figure 110. Dose response curves of compound **4c** in (A) the forced swim test and (B) locomotor activity…….……120

Figure 111. Dose response curves of compound **4d** in (A) the forced swim test and (B) locomotor activity……..121

Figure 112. Dose response curves of compound **4e** in (A) the forced swim test and (B) locomotor activity……...…..121

Figure 113. In vitro binding affinity of **4a** and **4d** towards 5-HT_{1D}……...….123

Figure 114. In vitro binding affinity of **4a** and **4d** towards 5-HT_{1E}…….....123

Figure 115. In vitro binding affinity of **4a** and **4d** towards 5-HT_3…….....124

Figure 116. In vitro binding affinity of **4c** towards 5-HT_{2C}……124

Figure 117. In vitro binding affinity of **4d** and **4e** towards 5-HT_{1A} 125

Figure 118. In vitro binding affinity of **4d** and **4e** towards 5-HT_{1B} ……....125

Figure 119. In vitro binding affinity of **4d** and **4e** towards 5-HT_{2B} ……....126

Figure 120. In vitro binding affinity of **4d** and **4e** towards 5-HT_{5A} ……126

Figure 121. In vitro binding affinity of **4d** and **4e** towards 5-HT_6……..127

Figure 122. In vitro binding affinity of **4d** and **4e** towards 5-HT_7…….....127

Figure 123. In vitro binding affinity of **4d** and **4e** towards dopamine 2 receptor…...128

Figure 124. In vitro binding affinityof **4e** towards 5-HT_{1E}…….....128

Figure 125. β-Carboline alkaloids with potential biological activities……...134

Figure 126. Selected HMBC correlations 2-*N*-methylmanzamine A (**2**), and 2-*N*,12-*O*-dimethylmanzamine A (**3**) trifluoromethanesulfonate……137

Figure 127. Binding positions of manzamine A (**1**), 2-*N*-methylmanzamine A (**2**), and 2-*N*,12-*O*-dimethylmanzamine A (**3**) trifluoromethanesulfonate within the ATP-noncompetitive binding pocket of GSK-3β (A: **1**, B: **2**, C: **3**).....141

Figure 128. Interactions of manzamine A (A) and 2-*N*-methylmanzamine A trifluoromethanesulfonate (B) with the GSK-3β ATP-noncompetitive binding pocket residues……...……141

Figure 129. Purification of 2-*N*-methylmanzamine A trifluoromethanesulfonate **2** on 250 x 21.20 C_{18} column……...……...146

Figure 130. LC/MS chromatogram of 2-*N*-methylmanzamine A trifluoromethanesulfonate **2**……146

Figure 131. UV spectrum of 2-*N*-methylmanzamine A trifluoromethanesulfonate **2**……147

Figure 132. IR spectrum of 2-*N*-methylmanzamine A trifluoromethanesulfonate **2**……147

Figure 133. ^{1}H NMR spectrum of 2-*N*-methylmanzamine A trifluoromethanesulfonate **2** in methanol-d_4 (400 MHz)……...…148

Figure 134. ^{13}C NMR spectrum of 2-*N*-methylmanzamine A trifluoromethanesulfonate **2** in methanol-d_4 (400 MHz)……...…149

Figure 135. HSQC spectrum of 2-*N*-methylmanzamine A trifluoromethanesulfonate **2** in methanol-d_4 (400 MHz)……...…150

Figure 136. HMBC spectrum of 2-*N*-methylmanzamine A trifluoromethanesulfonate **2** in methanol-d_4 (400 MHz)……..……151

Figure 137. LC/MS chromatogram of 2-*N*,12-*O*-dimethylmanzamine A (**3**) trifluoromethanesulfonate…….…..152

Figure 138. UV spectrum of 2-*N*,12-*O*-dimethylmanzamine A (**3**) trifluoromethanesulfonate…….……..152

Figure 139. IR spectrum of 2-*N*,12-*O*-dimethylmanzamine A (**3**)

trifluoromethanesulfonate……...153

Figure 140. ^{1}H NMR spectrum of 2-*N*,12-*O*-dimethylmanzamine A (**3**) trifluoromethanesulfonate in methanol-d_4 (400 MHz)…….……...154

Figure 141. ^{13}C NMR spectrum of 2-*N*,12-*O*-dimethylmanzamine A (**3**) trifluoromethanesulfonate in methanol-d_4 (400 MHz)…….……...155

Figure 142. ^{1}H NMR spectrum of 9-*N*-methylmanzamine A (**4**) in methanol-d_4 (400 MHz)…….……..156

Figure 143. ^{13}C NMR spectrum of 9-*N*-methylmanzamine A (**4**) in methanol-d_4 (400 MHz)……..….157

Figure 144. HCV genome and polyprotein potential drug target……...163

Figure 145. Enzymatic and non enzymatic drug targets for HCV…….….164

Figure 146. Structures of selected anti-HCV active compounds……....166

Figure 147. Selected species from the genus *Diplostephium*……..167

Figure 148. HPLC chromatogram of Fr. **3**; DCM-MeOH (25:75), on 250 x 21.2 mm C_{18} column……...170

Figure 149. HPLC chromatogram of Fr. **C**; (60-80 min off C_{18}), on 250 x 21.2 mm NH_2 column, signals 1-3 indicated the presence of the rhododendrosaponins **I**-**III** in similar order……...….……171

Figure 150. Re-injection of rhododendrosaponins **I** and **II** on 250 × 4.6 mm NH_2 column…….....172

Figure 151. Co-injection of rhododendrosaponins **I** and **II** on 250 × 4.6 mm NH_2 column…….172

Figure 152**.** (+)-HRESIMS spectrum of rhododendrosaponin **I**……..173

Figure 153. ^{1}H NMR spectrum of rhododendrosaponin **I** in methanol-d_4 (600 MHz)……...174

Figure 154. ^{13}C NMR spectrum of rhododendrosaponin **I** in methanol-d_4 (600 MHz)……...175

Figure 155. 135º DEPT spectrum of rhododendrosaponin **I** in methanol-d_4 (600 MHz)……...176

Figure 156. HSQC spectrum of rhododendrosaponin **I** in methanol-d_4 (600 MHz)……...177

Figure 157. COSY spectrum of rhododendrosaponin **I** in methanol-d_4 (600 MHz)……...178

Figure 158. HMBC spectrum of rhododendrosaponin **I** in methanol-d_4 (600 MHz)……...179

Figure 159. TOCSY spectrum of rhododendrosaponin **I** in methanol-d_4 (600 MHz)……...180

Figure 160. ROESY spectrum of rhododendrosaponin **I** in methanol-d_4 (600 MHz)……...181

Figure 161**.** (+)-HRESIMS spectrum of rhododendrosaponin **II**……182

Figure 162. ^{1}H NMR spectrum of rhododendrosaponin **II** in methanol-d_4 (600 MHz)……...183

Figure 163. ^{13}C NMR spectrum of rhododendrosaponin **II** in methanol-d_4 (600 MHz)……...183

Figure 164. 135º DEPT spectrum of rhododendrosaponin **II** in methanol-d_4 (600 MHz)……...184

Figure 165. HSQC spectrum of rhododendrosaponin **II** in methanol-d_4 (600 MHz)……...185

Figure 166. COSY spectrum of rhododendrosaponin **II** in methanol-d_4 (600 MHz)……...186

Figure 167. HMBC spectrum of rhododendrosaponin **II** in methanol-d_4

(400 MHz)……...187

Figure 168. H2BC spectrum of rhododendrosaponin **II** in methanol-d_4
(400 MHz)……..188

Figure 169. TOCSY spectrum of rhododendrosaponin **II** in methanol-d_4
(600 MHz)……...189

Figure 170. NOESY spectrum of rhododendrosaponin **II** in methanol-d_4
(600 MHz)……...190

Figure 171. LC/MS chromatogram of rhododendrosaponin **III**……191

Figure 172. ^{1}H NMR spectrum of rhododendrosaponin **III** in methanol-d_4
(600 MHz)……...192

Figure 173. ^{13}C NMR spectrum of rhododendrosaponin **III** in methanol-d_4
(600 MHz)……...193

Figure 174. 135º DEPT spectrum of rhododendrosaponin **III** in methanol-d_4
(600 MHz)……..194

Figure 175. HSQC spectrum of rhododendrosaponin **III** in methanol-d_4
(600 MHz)……...195

Figure 176. HMBC spectrum of rhododendrosaponin **III** in methanol-d_4
(400 MHz)……..196

Figure 177. COSY spectrum of rhododendrosaponin **III** in methanol-d_4
(400 MHz)……..197

Figure 178. H2BC spectrum of rhododendrosaponin **III** in methanol-d_4
(600 MHz)……..197

Figure 179. TOCSY spectrum of rhododendrosaponin **III** in methanol-d_4
(600 MHz)……...198

Figure 180. NOESY spectrum of rhododendrosaponin **III** in methanol-d_4
(600 MHz)……...199

Figure 181. Selected HMBC correlations of the aglycone triterpene…….200

Figure 182. GC/MS detection of 3-hydroxybutanoate in rhododendrosaponin **III**……..200

Figure 182. HMBC correlations of 3-hydroxybutanoate dimmer in rhododendrosaponin **III**……..201

Figure 183. Stacked plot the ^{1}H NMR spectra of rhododendrosaponins **I-III**.....202

Figure 184. Stacked plot the ^{13}C NMR spectra of rhododendrosaponins **I-III**……...202

Figure 185**.** NSI-MS^{n} fragmentation of rhododendrosaponin **III**……...205

Figure 186. L- and D-glucose standards by carbohydrate analysis method…..……207

Figure 187. L- and D- glucose, xylose, and fucose standards by the carbohydrate analysis method……..…….207

Figure 188. Carbohydrate analysis for rhododendrosaponin **III**…….……208

Figure 189. The gross structure of rhododendrosaponin **III**…….…..209

Figure 190. Overlaid the carbohydrate analysis chromatograms of rhododendrosaponins **I** and **III**……210

Figure 191. Carbohydrate analysis chromatogram of rhododendrosaponin **II**……..……..210

Figure 192. Overlaid HSQC spectra of rhododendrosaponins **I** and **III**…….212

Figure 193. The expanded HSQC spectrum of rhododendrosaponin **I** in methanol-d_4 (600 MHz) shows the presence of α and β isomers at position 24……..212

Figure 194. The expanded HMBC spectrum of rhododendrosaponin **I** in methanol-d_4 (600 MHz) shows the presence of α and β isomers at position 24……..213

Figure 195. The expanded ROESY spectrum of rhododendrosaponin **I** in methanol-d_4 (600 MHz) shows the presence of α and β isomers at position 24……..213

Figure 196. 135º DEPT spectrum of rhododendrosaponin **I** in methanol-d_4 (600 MHz) shows the presence of (-CHO) for the acyclic intermediate……...214

Figure 197. Overlaid HSQC spectra of rhododendrosaponins **II** and **III**……...215

Figure 198. The ^{13}C NMR spectrum of rhododendrosaponin **II** in methanol-d_4 (600 MHz) shows the presence of (-CHO) for the acyclic intermediate……....215

Figure 199. Expanded HMBC spectrum of rhododendrosaponin **II** in methanol-d_4 (600 MHz) shows the presence of arbinofuranosyl moiety…….216

Figure 200. Co-injection of rhododendrosaponins **II** and **III** on 250 × 4.6 mm NH_2 column…….216

Figure 201. 135º DEPT spectrum of active fraction after 250 x 21.2 mm C_{18} and rhododendrosaponin **I** after 250 x 21.2 mm NH_2 in methanol-d_4 (600 MHz)…….217

Figure 202. GC chromatograms of: A) (R)-methyl 3-hydroxybutanoate, B) (S)-methyl 3-hydroxybutanoate, C) Co-injection of (R) and (S)-methyl 3-hydroxybutanoate….218

Figure 203. GC chromatograms of: A) rhododendrosaponins **I**-**III** after methanolysis, B) Co-injection of the sample and (R)-methyl 3-hydroxybutanoate, C) Co-injection of the sample and (S)-methyl 3-hydroxybutanoate…….….219

Figure 204. The proposed structures of rhododendrosaponins **I**-**III**……..….220

Figure 205. The minimized 3D structure surface generated by PyMol 1.4 for the major glycoside, rhododendrosaponin **III,** red represents oxygen while green and grey represent carbon and hydrogen……..……..221

Figure 206. ^{1}H NMR spectrum of heteronemin in $CDCl_3$ (400 MHz)……....238

Figure 207. ^{13}C NMR spectrum of heteronemin in $CDCl_3$ (400 MHz)…….….238

Figure 208. 135º DEPT spectrum of heteronemin in $CDCl_3$ (400 MHz)…….... 239

Figure 209. HMBC spectrum of heteronemin in $CDCl_3$ (400 MHz)……..239

LIST OF TABLES

TABLE PAGE

Table 1. Antimicrobial activity of various parts of *Platanus occidentalis*…….....5
.
Table 2. ^{13}C NMR data of glycosides (**1**-**4**)…… 6

Table 3. ^{1}H NMR data of glycosides (**1**-**4**)…….....7

Table 4. In vitro antimicrobial activity of glycosides (**1**-**4**)…… 10

Table 5. In vitro antimicrobial activity of compounds **1**-**9**…….…...66

Table 6. Percent glycosides in 14 asymptomatic and symptomatic trees…….84

Table 7**.** Glycoside content comparison between August 2009 and May 2010 for three asymptomatic and three symptomatic trees……..…...85

Table 8. LC/MS program for determination of rhamnose glycosides……...91

Table 9. Effect of control antidepressants on immobility time in mouse forced swim test and total locomotor activity……...118

Table 10. Binding affinities of **4a**, **4c**, **4d**, and **4e** towards serotonin receptors……..122

Table 11. In vitro antimalarial activity, selectivity index, cytotoxicity to Vero cells and docking scores of manzamine A (**1**), 2-*N*-methylmanzamine A (**2**), 2-*N*,12-*O*-dimethylmanzamine A (**3**) trifluoromethanesulfonate, and 9-*N*-methylmanzamine A (**4**)…….……..139

Table 12. In vitro antimicrobial activity for manzamine A (**1**), 2-*N*-methylmanzamine A (**2**), 2-*N*,12-*O*-dimethylmanzamine A (**3**) trifluoromethanesulfonate, and 9-*N*-methylmanzamine A (**4**),(all values in µM)…..142

Table 13. Anti-HCV activity of 2-*N*-methylmanzamine A trifluoromethanesulfonate (**2**) in the Huh-7 replicon assay.....143

Table 14. Monosaccharide analysis of rhododendrosaponin **III** by GC/MS……..203

Table 15. Glycosyl linkage analysis for rhododendrosaponin **III**……...204

Table 16. The retention times of the carbohydrate standards……..208

Table 17. Anti-HCV activity of rhododendrosaponins **I-III** in Huh-7 replicon cells.222

LIST OF SCHEMES

SCHEME PAGE

Scheme 1. Large scale fractionation of 50 gm sycamore ethanolic extract using VLC……..……...16

Scheme 2. Application of Fr. **5**; EtOAc-MeOH (75:25) on 250 x 100 mm C_8 column……..16

Scheme 3. Application of Fr. **7**; H_2O-CH_3CN (5: 95) on 250 x 21.2 mm NH_2 column…….....17

Scheme 4. Fractionation of 3.5 g bay leaves ethanolic extract using VLC…….....52

Scheme 5. Fractionation of Fr. 3; Hex-EtOAc (25:75) on 250 x 21.2 mm NH_2 column…….....53

Scheme 6. Alkylation of *E,E*-platanoside…….63

Scheme 7. The synthesis of 5-haloindole-dimethylethanamines……..96

Scheme 8. Synthesis of 2-*N*-methylmanzamine A (**2**), 2-*N*,12-*O*-dimethylmanzamine A (**3**) trifluoromethanesulfonate, and 9-*N*-methyl manzamine A (**4**)……. 136

Scheme 9. Fractionation of *Diplostephium rhododendroides* extract via solvent extraction…….....169

Scheme 10. Fractionation of Fr. **3**; DCM-MeOH (25:75), on 250 × 21.2 mm C_{18} column…….170

Scheme 11. Fractionation of Fr. **C**; (60-80 min off C_{18}), on 250 × 21.2 mm NH_2 column…….....171

Scheme 12. An investigational method for carbohydrate analysis…….....206

CHAPTER I

METHICILLIN-RESISTANT *STAPHYLOCOCCUS AUREUS* ACTIVE METABOLITES FROM *PLATANUS OCCIDENTALIS* (AMERICAN SYCAMORE)

Published in *J. Nat. Prod.* **2009**, *72*, 2141–2144.

Reproduced with permission from *J. Nat. Prod.* **2009**, *72*, 2141–2144.

Copyright 2009 American Chemical Society

Methicillin-resistant *Staphylococcus aureus* (MRSA) is a serious pathogen with significant patient mortality.[1,2] Currently, over 50% of the *Staph. aureus* infections around the world are caused by MRSA.[3,4] Hospital-acquired infections of MRSA (HA-MRSA) have been shown to be resistant to multiple antibiotics. However, MRSA has recently developed into a community-associated pathogen (CA-MRSA) infecting individuals that have not been hospitalized within a year. CA-MRSA causes skin infections with abscess formation and cellulitis and is currently sensitive to some antibiotics.[5]

The glycopeptide antibiotic vancomycin has been used as a drug of choice for MRSA infections. With a reported success rate of 35-57%, its side effects, including nosocomial pneumonia, hearing loss in the young and old, skin and soft tissue infections, and low bone penetration, limit vancomycin's utility. Moreover, the increased use of vancomycin, especially in chronic conditions, has resulted in the emergence of MRSA with reduced susceptibility to glycopeptides.[6-8]

The most effective anti-MRSA drug used currently is daptomycin, a cyclic lipopeptide derived from the fermentation of *Streptomyces roseosporus*. Daptomycin is most useful for short durations and for the treatment of persistent MRSA infections unaffected by other drug treatments such as vancomycin. Its mechanism of action involves binding to the bacterial cell membrane, causing depolarization of the membrane potential leading to inhibition of protein, DNA, and RNA synthesis. However, various side effects were reported for daptomycin, including an increase in blood creatine phosphokinase, rhabdomyolysis, skin exfoliation, and skin ulcers.

The American sycamore [*Platanus occidentalis* L. (family Platanaceae)] is a large, fast-growing tree with maximum growth up to 50 m in height and 3.2 m in diameter; it is widely distributed in the eastern United States where it grows on a variety of soils and sites and is often found near lakes and streams.[9,10] Its safe use by humans is known from its use in traditional folk medicine for the treatment of a wide variety of conditions. The species has been used frequently for its antimicrobial and antiseptic properties. Native Americans used *P. occidentalis* as a cold and cough remedy, as well as a dietary supplement like tea, dermatological, gynecological, respiratory, and gastrointestinal aid.[11] The bark was used with honey locust to relieve hoarseness and sore throats as well as to treat skin eruptions, scabs and eczema, lung problems, hemorrhage, and tuberculosis. A mixture of the bark, stems, and twigs was used to treat open wounds. In addition, the bark has been used to treat colds, to purify the blood, for weight gain, and as an analgesic.[12] The American sycamore was also generally taken as a cathartic, emetic, and antidiarrheal drug to treat dysentery.[13] Previous chemical investigations of American sycamore have shown the presence of triterpenoids. This species produces betulinic aldehyde, betulinic acid, platanic acid, β-sitosterol, tiliroside,[14] as well as kaempferol 3-*O*-rhamnosides.[15]

Because of the increasing presence of MRSA-related infections and the emerging need for effective antibiotic therapies, bioassay-guided extraction of *P. occidentalis* was performed in order to identify new antibacterial compounds. All isolated metabolites were assayed in vitro for antifungal and antibacterial activity, and *E,E*-platanoside **1** was evaluated against MRSA in vivo.

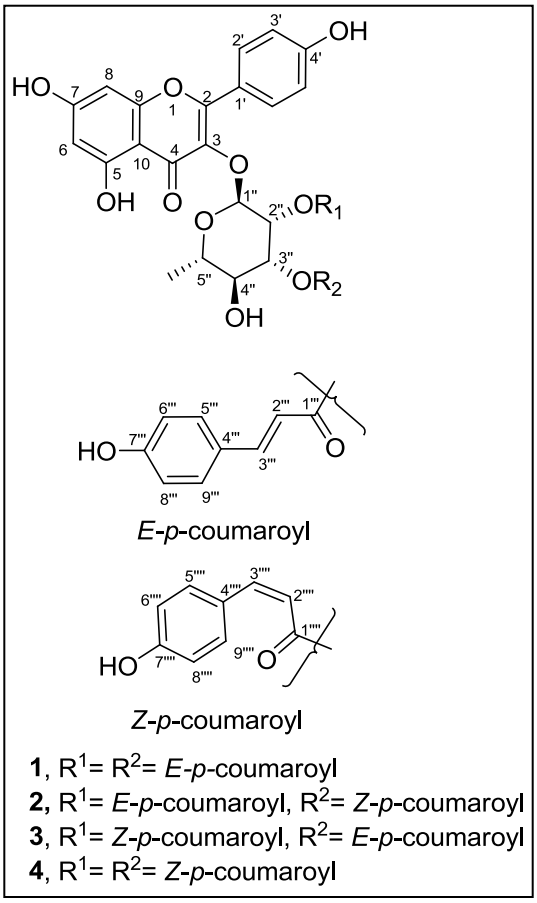

Figure 1. The structures of American sycamore glycosides **1**-**4**

Results and Discussion

The antimicrobial evaluation of extracts from various parts of *P. occidentalis* showed the leaf extract to be highly active against MRSA (Table 1).

Table 1. Antimicrobial activity of various parts of *Platanus occidentalis*

Sample Code	*C. albicans*[1]	*C. neoformans*[2]	*A. fumigatus*[3]	MRSA[4]	*E. coli*[5]	*P. aeruginosa*[6]	*M. intracellulare*[7]
SMBB	7	19	2	33	22	4	0
SL	6	4	6	55	27	24	0
SBBB	5	12	4	9	15	0	0
ST	6	25	5	30	17	15	0

[1]*Candida albicans,* [2]*Candida neoformans,* [3]*Aspergillus fumigatus,* [4]*Methicillin resistant Staphylococcus aureus,* [5]*Escherichia coli,* [6]*Pseudomonas aeruginosa,* [7]*Mycobacterium intracellulare;* Concentration= 50 µg/mL; Samples showing % Growth Inhibition; < 50 are considered inactive. SMBB: sycamore middle branches bark, SL: sycamore leaves, SBBB: sycamore big branches bark, ST: sycamore twigs

Four active metabolites, **1-4;** (Figure 2) were shown by (+)-HRESIMS to possess the same mass with *m/z* 747.1647-747.1679, for the sodium-charged $C_{39}H_{32}O_{14}Na$. The isolated compounds were shown to be L-rhamnose glycosides with different configurations of the *p*-coumaroyl functionalities. Structural assignments of the new glycosides (**2-4**) were confirmed by examination of ^{1}H and ^{13}C NMR data and comparison with literature data (Tables 2 and 3).[16]

Table 2. ^{13}C NMR data of glycosides (**1-4**)[a]

carbon	1	2	3	4
2	157.9	157.7	157.6	157.5
3	134.2	134.0	134.1	133.7
4	178.1	177.9	177.9	177.5
5	162.0	161.8	161.8	161.6
6	98.7	98.6	98.6	99.9
7	164.7	164.8	164.5	165.3
8	93.6	93.4	93.5	94.4
9	157.3	157.1	157.1	157.1
10	104.7	104.4	104.6	103.3
1’	121.2	121.0	121.2	121.1
2' 6'	130.7	130.5	130.5	130.4
3', 5'	115.6	115.4	115.4	115.4
4'	160.5	160.3	160.2	160.4
1"	99.1	98.8	98.9	98.9
2"	69.7	69.4	69.3	69.1
3"	71.9	71.4	71.7	71.5
4"	69.8	69.5	69.5	69.3
5"	71.0	70.9	70.8	70.8
6"	16.6	16.3	16.3	16.3
1‴, 1⁗	166.6, 167.3	166.4, 166.1	167.3, 165.2	166.1, 166.2
2‴, 2⁗	113.1, 113.7	112.9, 114.8	113.5, 114.1	114.0, 114.8
3‴, 3⁗	145.8, 146.5	146.2, 144.3	145.6, 145.2	144.4, 144.8
4‴, 4⁗	125.8, 125.9	125.7, 126.2	125.7, 126.0	126.0, 126.1
5‴, 9‴, 5⁗, 9⁗	130.0, 130.2	130.0, 132.4	129.8, 132.4	132.5, 132.5
6‴, 8‴, 6⁗, 8⁗	115.6, 115.7	114.5, 115.4	114.6, 115.5	114.5, 114.6
7‴, 7⁗	160.1, 160.3	160.0, 158.7	159.8, 158.7	158.8, 158.9

[a]Measured at 100 MHz for ^{13}C in methanol-d_4

Table 3. ^{1}H NMR data of glycosides (**1**-**4**)[a]

Proton	1	2	3	4
6	6.11, s	6.26, s	6.22, s	6.13, S
8	6.31, s	6.39, brs	6.41, brs	6.30, brs
2', 6'	7.77, d (8.4)	7.87, d (8.4)	7.86, d (8.8)	7.83, d (8.4)
3', 5'	6.89, d (8.8)	7.01, d (8.4)	6.98, d (8.8)	6.96, d (8.4)
1"	5.51, s	5.56, s	5.54, s	5.52, S
2"	5.73, bs	5.78, brs	5.78, brs	5.79, brs
3"	5.21, dd (9.6, 3.2)	5.27, dd (9.6, 3.2)	5.27, dd (9.2, 3.2)	5.21, dd (9.2, 3.2)
4"	3.55, t, (9.6)	3.58, t (9.6)	3.49, t (9.2)	3.48, t (9.6)
5"	3.45, m	3.52, m	3.53, m	3.52, m
6"	0.96, d (6.0)	1.04, d (6.0)	1.00, d (6.0)	0.97, d (5.6)
2‴, 2⁗	6.29, d (15.6), 6.21, d (15.6)	6.31, d (16.0), 5.72, d (12.8)	6.30, d (16.0), 5.81, d (12.8)	5.72, d (12.8), 5.74, d (12.8)
3‴, 3⁗	7.50, d (15.6), 7.52, d (15.6)	7.59, d (16.0), 6.88, d (12.8)	7.61, d (16.0), 6.94, d (12.8)	6.89, d (12.8), 6.86, d (12.8)
5‴, 9‴ 5⁗, 9⁗	7.28, d (8.8), 7.36, d (8.4)	7.47, d (8.4), 7.71, d (8.4)	7.36, d (8.8), 7.64, d (8.8)	7.71, d (8.4), 7.62, d (8.4)
6‴, 8‴, 6⁗, 8⁗	6.65, d (8.4), 6.70, d (8.4)	6.81, m, 6.81, m	6.63, d (8.8), 6.78, d (8.8)	6.81, d (8.4), 6.69, d (8.4)

[a]Measured at 400 MHz for ^{1}H in methanol-d_4. "s" singlet, "brs" broad singlet, "d " doublet, "dd" doublet of doublet,"t" triplet, "m" multiplet

The ^{1}H NMR spectra of compounds **1**-**4** clearly displayed the characteristic signals of the kaempferol nucleus as well as the anomeric α-configured sugar. The major glycoside isolated was *E*,*E*-platanoside (**1**) known as platanoside.[17] In addition, three new anti-MRSA active metabolites were isolated in smaller amounts, *E*,*Z*-platanoside (**2**), *Z*,*E*-platanoside (**3**), and *Z*,*Z*-platanoside (**4**). The isolated compounds exhibited similar UV spectra [λ_{max} (MeOH) 268, 313 nm]. The ^{1}H and ^{13}C NMR spectra of compounds **2**-**4** also resembled those of *E*,*E*-platanoside **1**.

Investigation of HMBC and COSY correlations indicated the positions of attachments of both *p*-coumaroyl units to L-rhamnose while ^{1}H NMR coupling constants and NOESY spectra revealed the configurations at C-2‴, C-3‴ and C-2⁗, C-3⁗ for the isolated metabolites **2-4**. HMBC correlations between H-2" (5.81 Hz) and C-1‴ (166.6 Hz) as well as between H-3" (5.27 Hz) and C-1‴ (167.3 Hz) and the presence of the COSY correlation between H-2" (5.81 Hz) and H-3" (5.27 Hz) confirmed the attachment of the *p*-coumaroyl units to C-2" and C-3". The large coupling constant between H-2‴ and H-3‴ (15.6 Hz) in the known compound **1** indicated the *trans* relationship of the *p*-coumaroyl units at C-2" and C-3" of L-rhamnosyl moiety. For glycoside **2,** HMBC correlations between H-2" (5.78 Hz) and C-1‴ (166.4 Hz) as well as between H-3" (5.27 Hz) and C-1⁗ (166.1 Hz) and the presence of the COSY correlation between H-2" (5.78 Hz) and H-3" (5.27 Hz), confirmed the attachment of the *p*-coumaroyl units to C-2" and C-3". The *J* value of H-2‴ and H-3‴ (16.0 Hz) of the *p*-coumaroyl functionality at C-2" of the L-rhamnose indicated an *E* configuration, while the *J* value of H-2⁗and H-3⁗ (12.8 Hz) of the *p*-coumaroyl at C-3" of the L-rhamnose indicated a *Z* configuration, which was also confirmed by the NOESY correlation between H-2⁗and H-3⁗. The opposite arrangement was shown for glycoside **3**, where HMBC correlations between H-2" (5.78 Hz) and C-1⁗ (165.2 Hz) as well as between H-3" (5.27 Hz) and C-1‴ (167.3 Hz) and the presence of the COSY correlation between H-2" (5.78 Hz) and H-3" (5.27 Hz) confirmed the attachment of the *p*-coumaroyl units at C-2" and C-3". The *J* value of H-2‴ and H-3‴ (16.0 Hz) of the *p*-coumaroyl functionality at C-3" of L-rhamnose supported the *E* configuration while the *J* value of H-2⁗and H-3⁗ (12.8 Hz) of the *p*-coumaroyl functionality at C-2" of L-rhamnose suggested a *Z* configuration which was also confirmed by the NOESY correlation between H-2⁗ and H-3⁗.

HMBC correlations in glycoside **4** between H-2" (5.79 Hz), C-1"" (166.1 Hz) as well as H-3" (5.21 Hz), C-1"" (166.2 Hz) and the presence of the COSY correlation between H-2" (5.79 Hz), H-3" (5.21 Hz) confirmed the attachment of the *p*-coumaroyl units to C-2" and C-3". The small coupling constants (12.8 Hz) between H-2""and H-3"" established the *Z* configuration[18] of the *p*-coumaroyl groups at C-2" and C-3" of L-rhamnose; this was also confirmed by the NOESY correlations between H-2"" and H-3"". The platanosides were hydrolyzed and the absolute configuration of the sugar was shown to be L-rhamnose by GC comparison of its acetylated thiazolidine derivative with that of an L-rhamnose standard. The LC/MS analysis of the crude extract showed the presence of all four metabolites (**1**-**4**), which confirmed that no significant transformation of one isomer to the others occurred during the isolation and purification process (Figure 2).

The LC/MS stability tests in various solvents revealed that water facilitated isomerization of the thermodynamically less stable isomers **3** and **4** to the most stable **1** in comparison with other solvents (methanol, ethanol, dimethylformamide, dichloromethane, ethyl acetate, Figure 3).

The in vitro anti-MRSA data of the four isolated compounds represented in Table 4, showed the bacteriostatic activity of the isolated compounds against MRSA. In addition all metabolites were relatively inactive against other test organisms including the Gram-negative bacteria *Escherichia coli* and *Pseudomonas aeruginosa*, as well as the other microorganisms *Mycobacterium intracellulare*, *Candida albicans, Cryptococcus neoformans*, and *Aspergillus fumigatus* at a maximum concentration of 100 μg/mL. In vitro Vero cell (kidney fibroblast cells) cytotoxicity was not observed up to the maximum dose of 100 μg/mL.

Table 4. In vitro antimicrobial activity of glycosides (**1**-**4**)

	MRSA		*S. aureus*	
compound	**IC_{50}[a]**	**MIC[b]**	**IC_{50}[a]**	**MIC[b]**
1	1.99 +/- 0.58	10 +/- 0	3.72 +/- 0.86	13.33 +/- 4.71
2	0.79 +/- 0.39	1.67 +/- 0.59	1.63 +/- 0.72	5.83 +/- 3.12
3	0.73 +/- 0.03	1.25 +/- 0	1.41 +/- 0.05	3.75 +/- 1.25
4	0.4 +/- 0.02	0.63 +/- 0	1.56 +/- 0.56	2.5 +/- 0
Methicillin	NA	NA	0.45 +/- 0.07	2.5 +/- 0
Piperacillin	NA	NA	NT	NT
Ciprofloxacin	0.06 +/- 0.01	0.25 +/- 0	0.1 +/- 0.01	0.38 +/- 0.13

[a]IC_{50} = the concentration that affords 50% inhibition of growth (μg/mL). [b]MIC (minimum inhibitory concentration, μg/mL) is the lowest test concentration that allows no detectable growth. [c]MBC (minimum bactericidal concentration) is the lowest test concentration that kills the organism (μg/mL). [d]NA = not active at the highest test concentration. [e]NT = not tested

The structure-activity relationship of the closely related compounds kaempferol 3-*O*-α-L-(2",4"-di-*Z*-*p*-coumaroyl)rhamnoside and kaempferol 3-*O*-α-L-(2"-*Z*-*p*-coumaroyl-4"-*E*-*p*-coumaroyl)-rhamnoside show that the presence of the flavonoid moiety connected to the *p*-coumaroyl functionality through the sugar as well as the presence of hydroxy groups at C-5, C-7, and C-4' are important for the anti-MRSA activity.[19] Additionally, we found that the configuration of the double bonds of the *p*-coumaroyl units plays a significant role in the activity of these compounds. The *Z*-configured compound **4** shows enhanced activity in comparison with the *E*-configuration represented in *E*,*E*-platanoside **1** (MIC difference is ~ 9x).

The in vivo results of *E*,*E*-platanoside **1** in Figure 4 showed that in the muscle tissue of untreated control animals (vehicle group) the MRSA cfu/g was 8.02×10^7. The number of MRSA isolated from vancomycin-treated animals was 2.2×10^7/g of tissue ($p < 0.05$), showing a reduction of 72% compared to the vehicle control. Similarly, the number of MRSA colonies

recovered after treatment with *E,E*-platanoside **1** at 3 mg/kg and 15 mg/kg was 2.6 x 10^7 and 1.8 x 10^7 respectively, which corresponded to a reduction of 67 ($p < 0.05$) and 78% ($p < 0.01$) as compared to the vehicle control. These results supported the in vitro data and indicated that the test compound was as active as vancomycin (3.0 mg/kg) against MRSA. While determining the maximal tolerated dose in the preliminary experiment, up to 20 mg/kg of *E,E*-platanoside **1** was given (i.p.), for 2 days. No adverse effect was seen in these animals indicating a lack of acute toxicity. Higher doses remain to be tested but based on the absence of detectable toxicity, the dosages could have been increased further. In summary, these plant natural products are highly promising drug leads for the control of MRSA and could be on par with the antibiotics currently used to treat drug-resistant *Staph. aureus* infections but with less potential for toxicity.

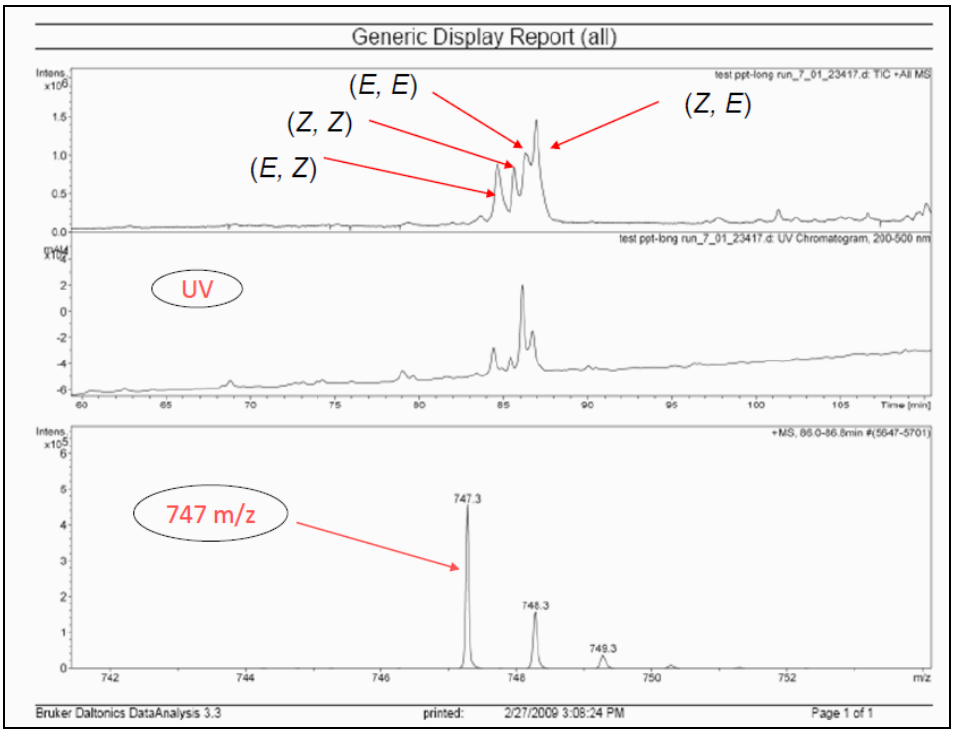

Figure 2. The LC/MS analysis of the crude extract shows the presence of the four metabolites **1**-**4**

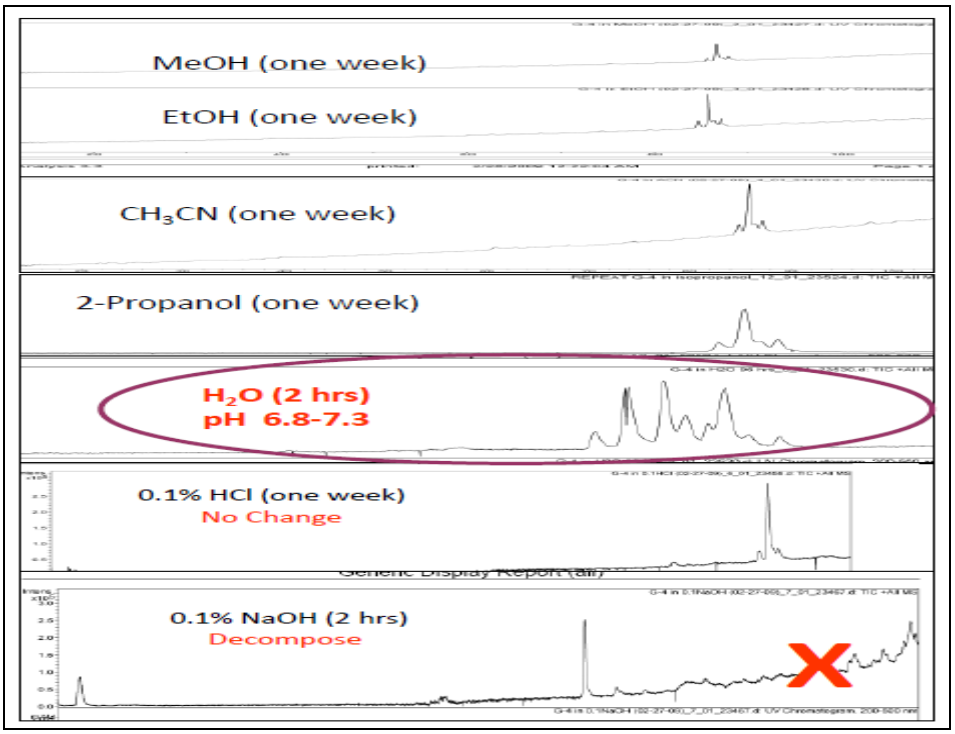

Figure 3. Stability of *Z,Z*-platanoside in various solvents

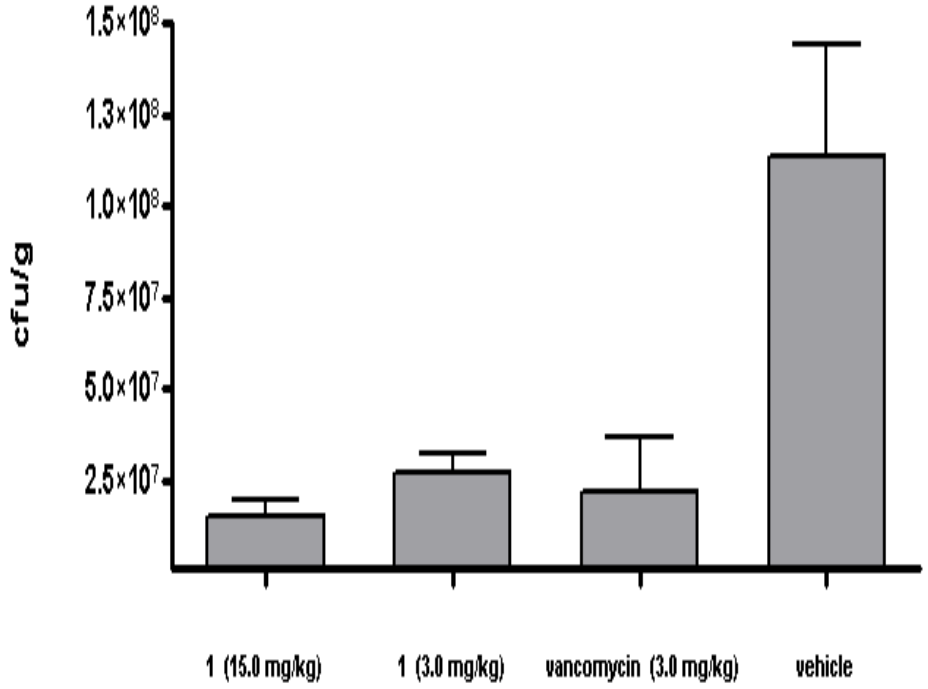

Figure 4. Effect of *E,E*-platanoside **1** on MRSA thigh infection in a murine model. Treatment with *E,E*-platanoside **1** was initiated 2 h intraperitoneally after thigh inoculation. Thigh muscle homogenate was processed for microbiological assay to determine the number of MRSA cfu/g of muscle tissue (n = 4)

Experimental Section:

General Experimental Procedures. Optical rotations were measured using a Rudolph Research Analytical Autopol IV automatic polarimeter model 589-546. UV spectra were recorded on a Varian Cary 50 Bio UV-visible spectrometer. The 1D and 2D NMR experiments were measured on a Bruker AV NMR spectrometer (Bruker Biospin, Bruker Inc.) operating at 400 MHz and the chemical shift (δ) values are expressed in ppm. The mass spectra were measured using the Bruker micrOTOF (Bruker Daltonics, Bruker Inc.) with an ESI ionization source. HPLC was carried out on a Waters Prep-LC with a 2487 dual absorbance detector.

Plant Material. The leaves and stem of *P. occidentalis* were collected in August 2007 in Oxford, Mississippi, and were identified by Dr. Charles Burandt. A voucher specimen (No. MI-SYC-04-08) is housed at the Department of Pharmacognosy, School of Pharmacy, The University of Mississippi.

Extraction and Isolation. Air-dried leaves and branches (10 Kg) of different sizes were macerated at room temperature with ethanol yielding 400 g extract residue. The ethanolic extract (50 g) was subjected to silica gel vacuum-liquid chromatography (VLC), yielding an active fraction with EtOAc-MeOH (75:25) (7 g); Scheme 1. Bioassay-guided fractionation and purification of this fraction utilized HPLC at room temperature, a Luna C_8 column (250 × 150 mm, Phenomenex, Inc.), using H_2O-CH_3CN (100→100, 90 min, λ 300 nm) in which the active fraction eluted with H_2O-CH_3CN (5:95, 85 min); Scheme 2. Following this, a Luna NH_2 column (250 × 21.20 mm, Phenomenex, Inc.) was used with *n*-hexane-CH_2Cl_2 (100→100, 30 min) and then CH_2Cl_2-MeOH (100→100, 30 min, λ 300 nm), yielding three well-resolved signals. All of the signals eluted with 100% MeOH: the first at 65 min (**1**) (20 mg), the second representing two metabolites at 77 min (**2** and **3**) (10 mg), and the third at 101 min (**4**) (3 mg); Scheme 3; Figure 5. Final purification of glycosides **2** and **3** was done using a PFP-2 (pentafluorophenyl) (250×10 mm, Phenomenex Inc.) column with CH_3CN-H_2O (0→100, 120, λ= 300 nm). Glycosides **2** and **3** eluted with CH_3CN-H_2O (50:50, λ= 300 nm) with retention times of 90 and 91 min, respectively; Figure 6. These four glycosides together represent 0.02-0.05% of leaf dry weight and the percentage of each individual glycoside is 65:25:3:7, respectively.

***E,E*-platanoside (1):** amorphous, off-white solid; $[\alpha]^{25}_{D}$ +89.6 (*c* 0.3, MeOH); UV (MeOH) λ_{max} (log ε) 268 (4.4), 313 (4.6) nm; ^{1}H NMR and ^{13}C NMR, see Tables 2 and 3; (+)-(+)-HRESIMS *m/z* calcd for $C_{39}H_{33}O_{14}Na$ $[M+Na]^{+}$ 747.1684, found 747.1664; Figures (7-14).

***E,Z*-platanoside (2):** amorphous, off-white solid; $[\alpha]^{25}_{D}$ +90.7 (*c* 0.2, MeOH); UV (MeOH) λ_{max} (log ε) 267 (4.4), 314 (4.6) nm; ^{1}H NMR and ^{13}C NMR, see Tables 2 and 3; (+)-HRESIMS *m/z* calcd for $C_{39}H_{33}O_{14}$ Na $[M+Na]^{+}$ 747.1684, found 747.1667; Figures (15-22).

***Z,E*-platanoside (3):** amorphous, off-white solid; UV (MeOH) λ_{max} (log ε) 268 (4.5), 313 (4.7) nm; ^{1}H NMR and ^{13}C NMR, see Tables 2 and 3; (+)-HRESIMS *m/z* calcd for $C_{39}H_{32}O_{14}$ Na $[M+Na]^{+}$ 747.1684, found 747.1679; Figures (23-30).

***Z,Z*-platanoside (4):** amorphous, yellowish-white solid; $[\alpha]^{25}$ +16.7 (*c* 0.1, MeOH); UV (MeOH) λ_{max} (log ε) 267 (4.1), 313 (4.2) nm; ^{1}H NMR and ^{13}C NMR, see Tables 2 and 3; (+)-HRESIMS *m/z* calcd for $C_{39}H_{32}O_{14}$ Na $[M+Na]^{+}$ 747.1684, found 747.1647; Figures (31-38).

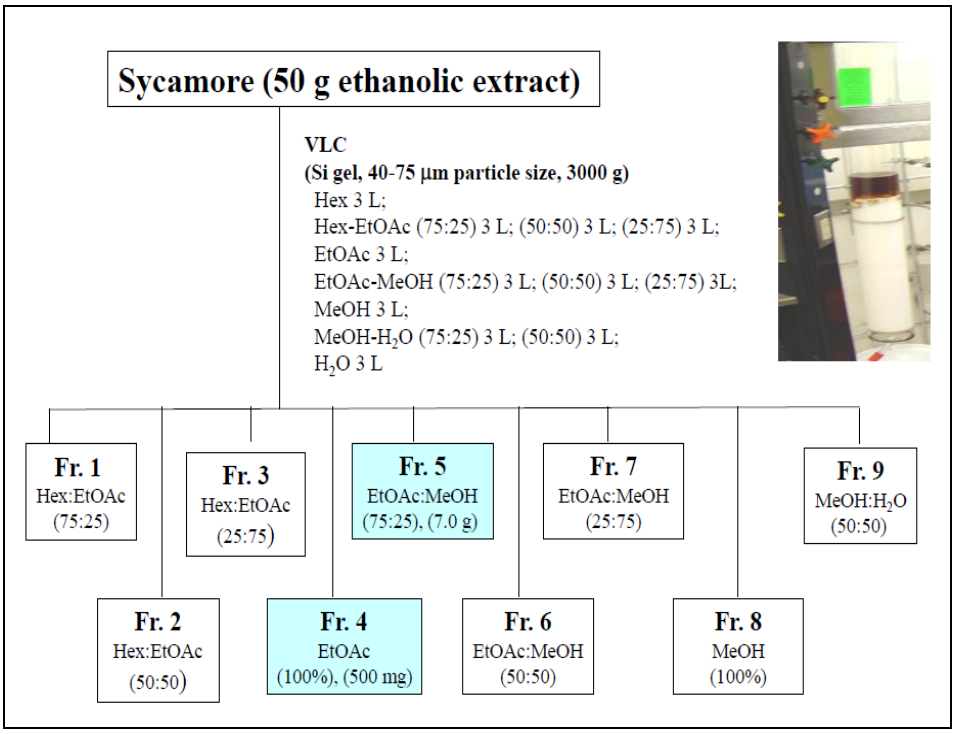

Scheme 1. Large scale fractionation of 50 gm sycamore ethanolic extract using VLC, blue color indicated the presence of the platanosides

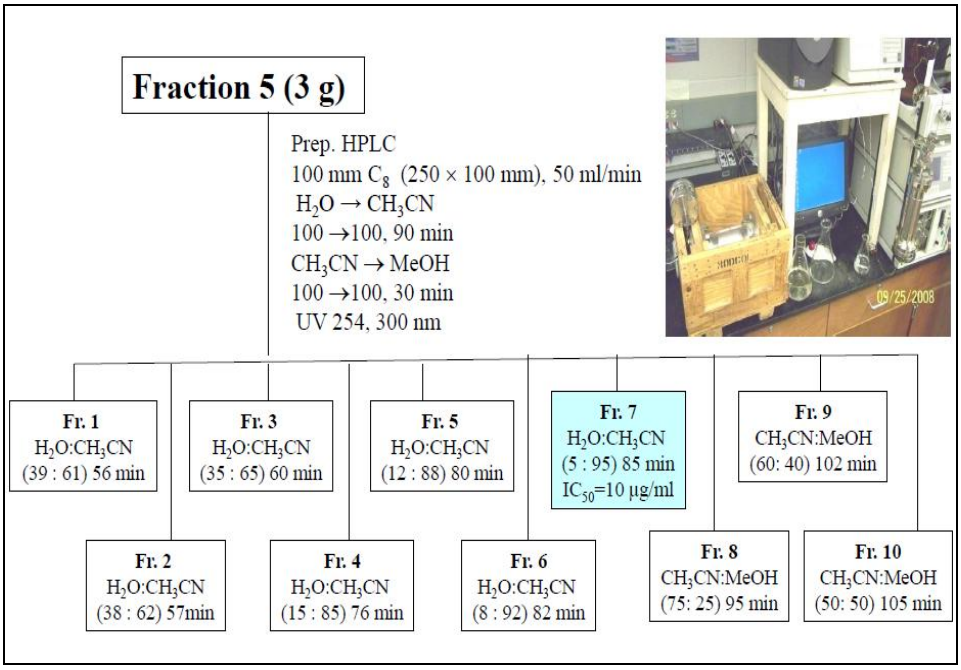

Scheme 2. Application of Fr. **5**; EtOAc-MeOH (75:25) on 250 x 100 mm C_8 column, blue color indicated the presence of the platanosides

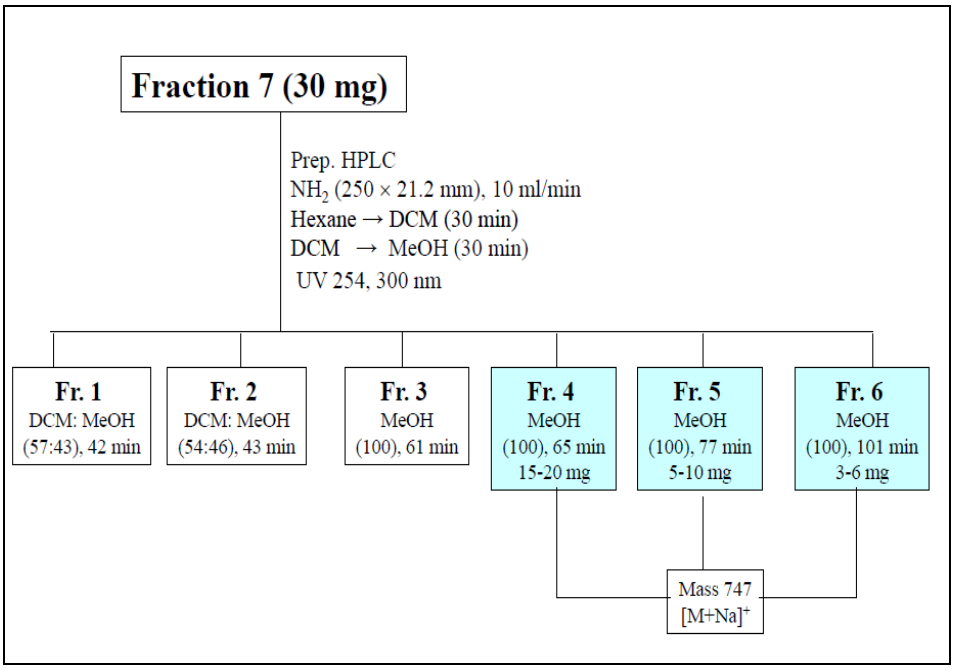

Scheme 3. Application of Fr. **7**; H_2O-CH_3CN (5:95) on 250 x 21.2 mm NH_2 column, blue color indicated the presence of the platanosides

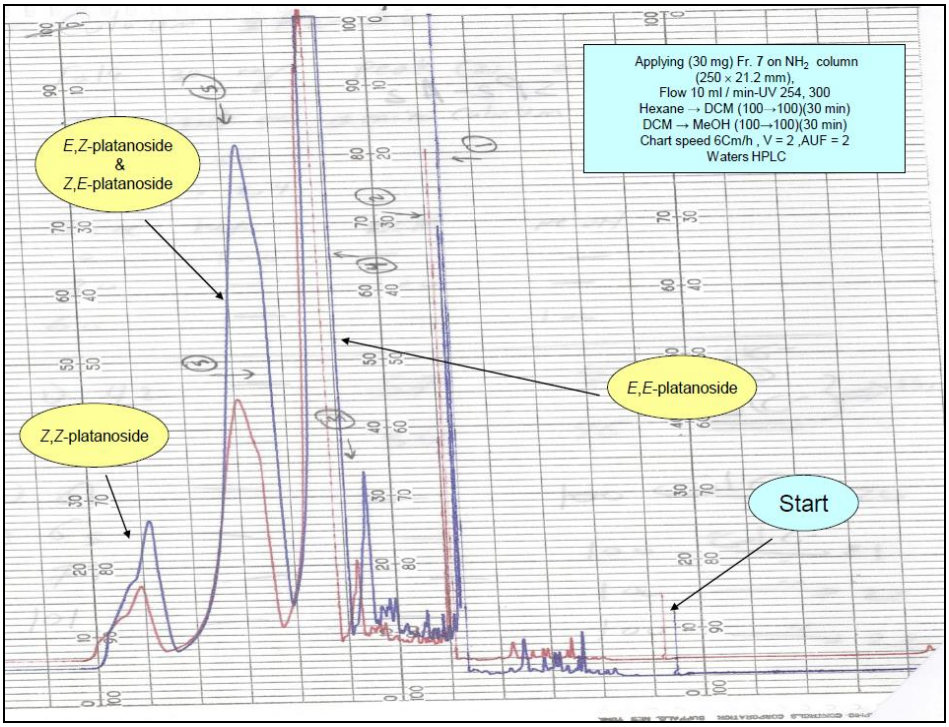

Figure 5. HPLC chromatogram of Fr. **7**; H_2O-CH_3CN (5:95) on 250 x 21.2 mm NH_2 column

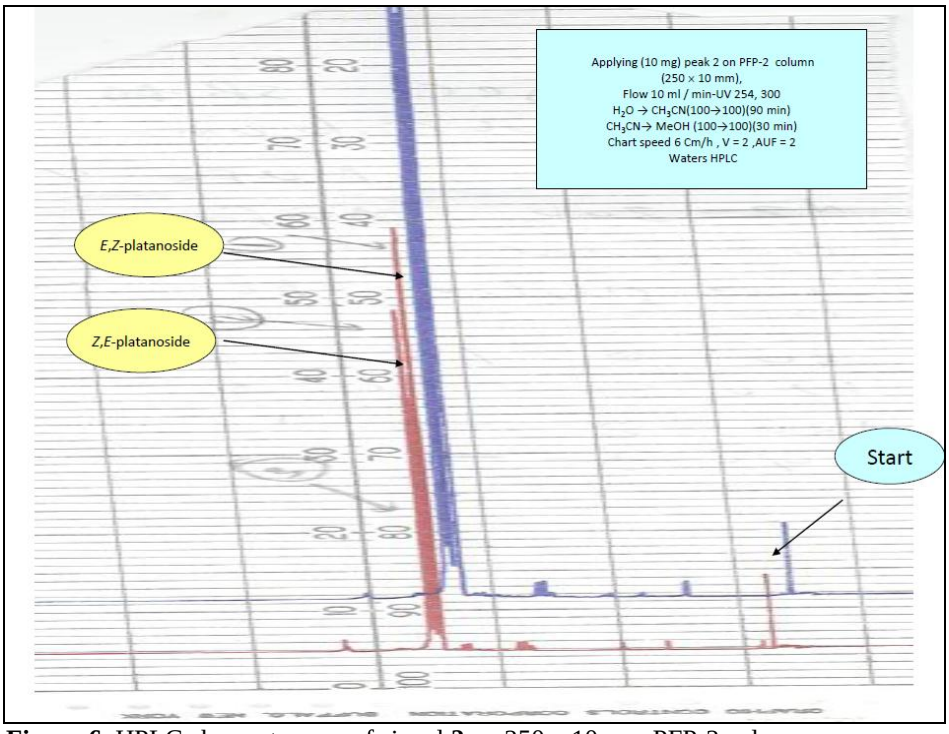

Figure 6. HPLC chromatogram of signal **2** on 250 x 10 mm PFP-2 column

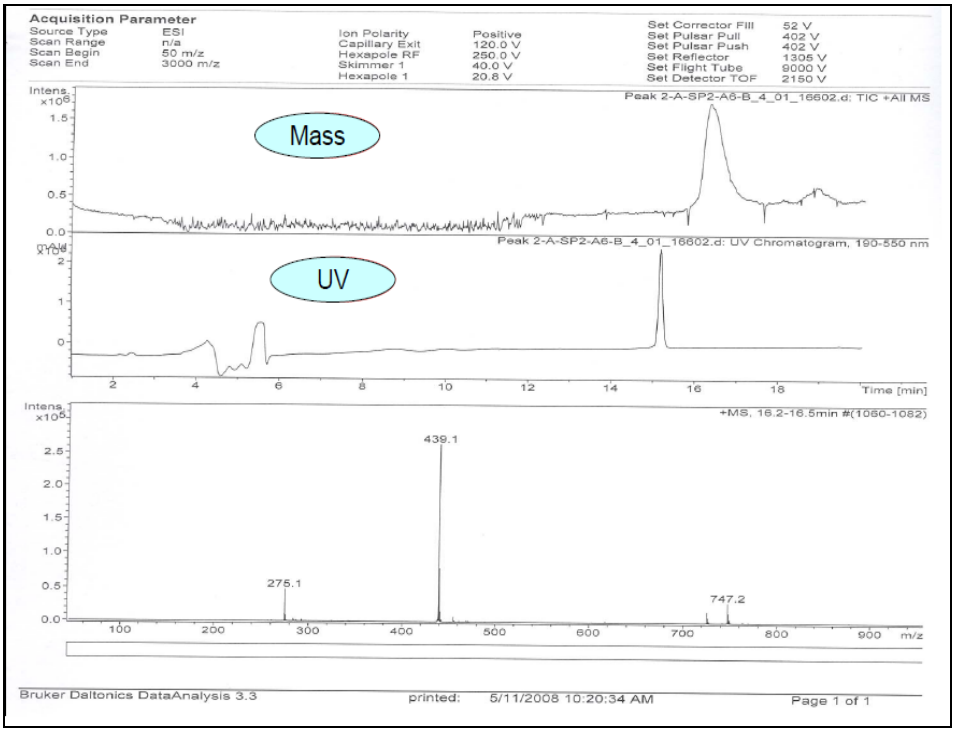

Figure 7. LC/MS chromatogram of *E*,*E*-platanoside

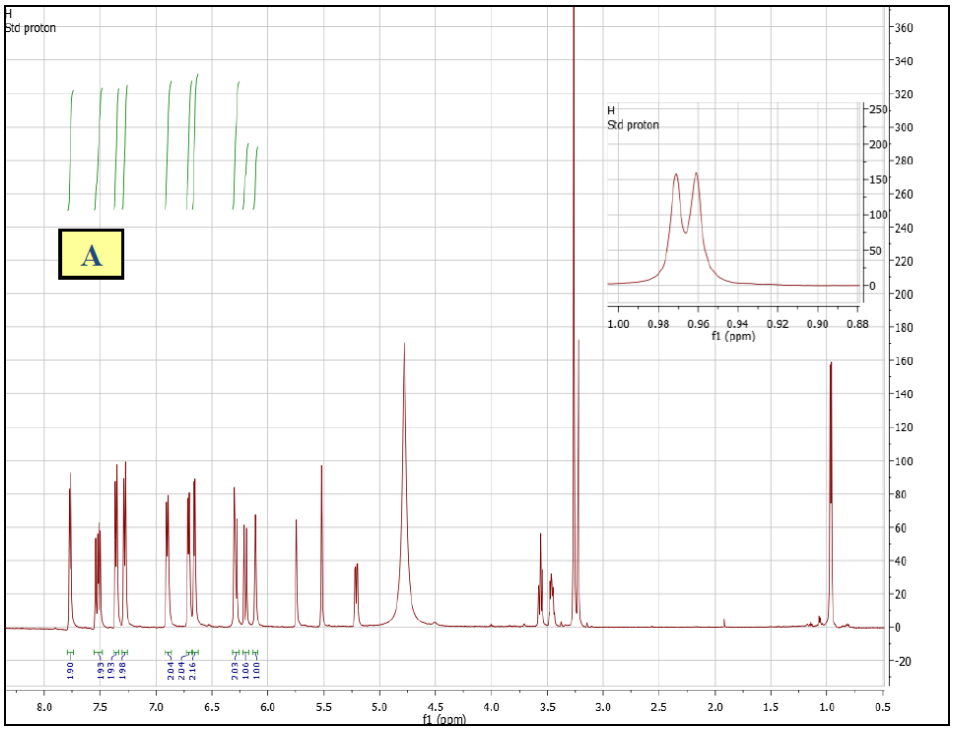

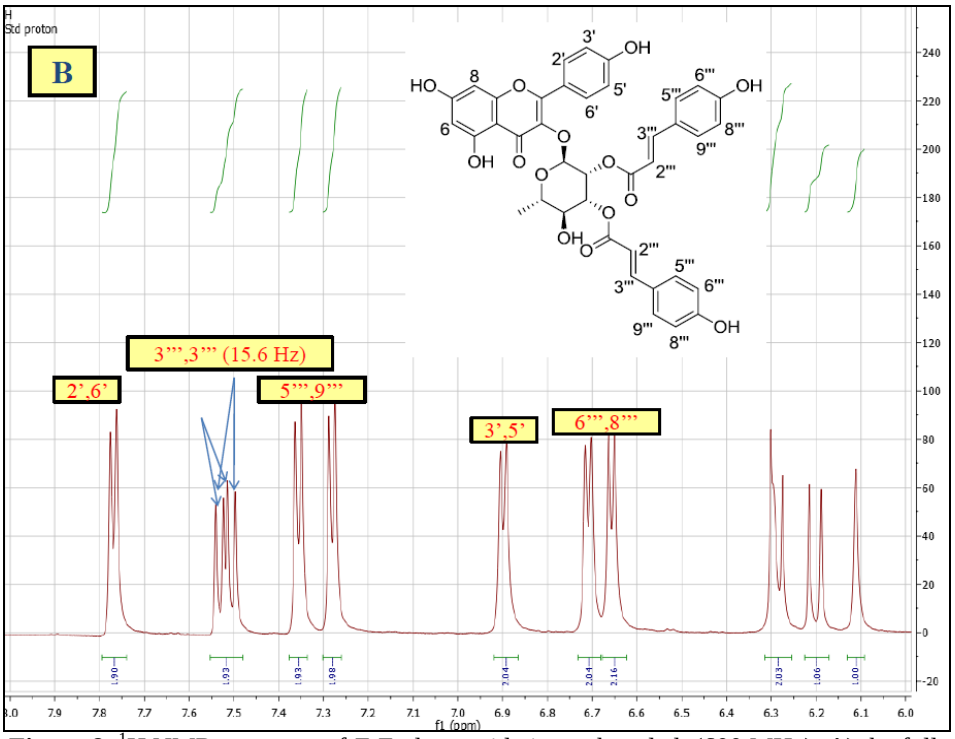

Figure 8. ^{1}H NMR spectrum of *E*,*E*-platanoside in methanol-d_4 (600 MHz); A) the full spectrum, B) the downfield region

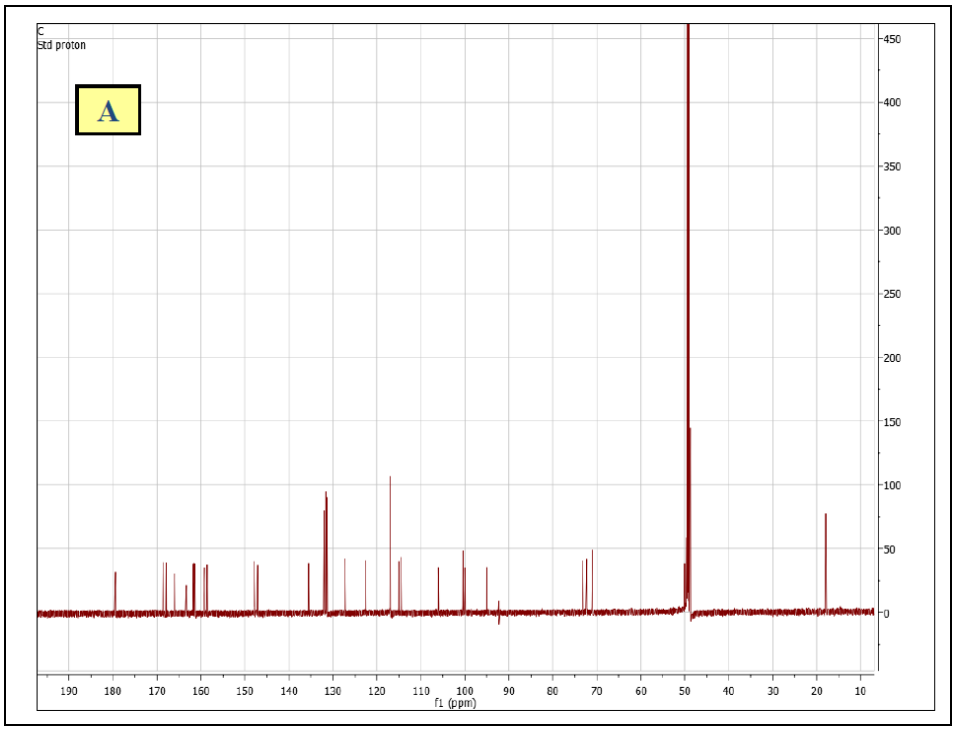

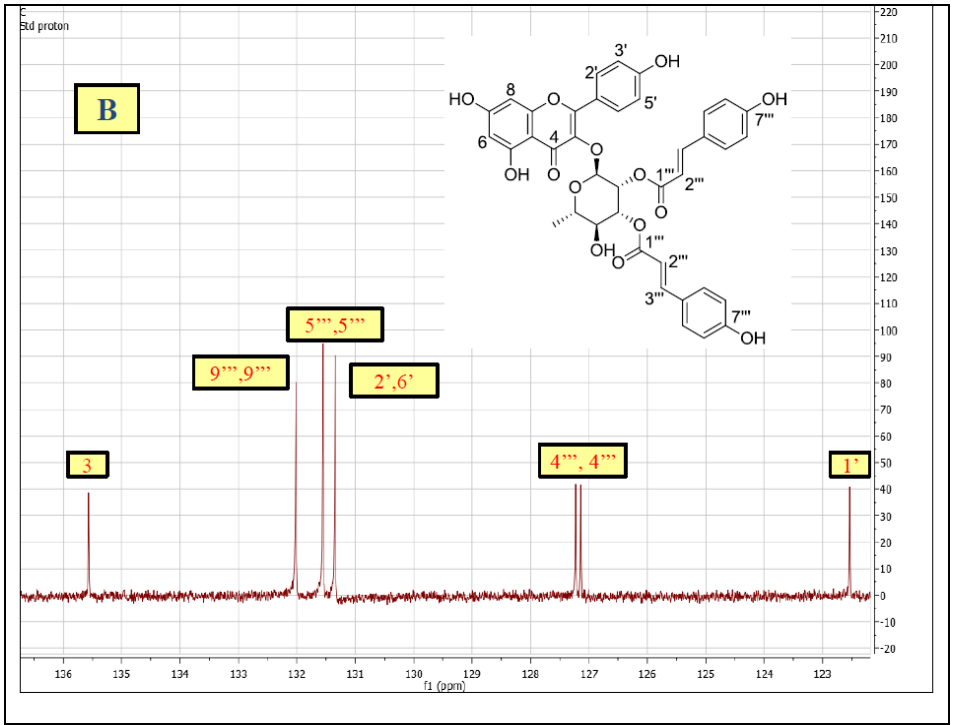

Figure 9. ^{13}C NMR spectrum of *E*,*E*-platanoside in methanol-d_4 (600MHz); A) the full spectrum, B) the downfield region

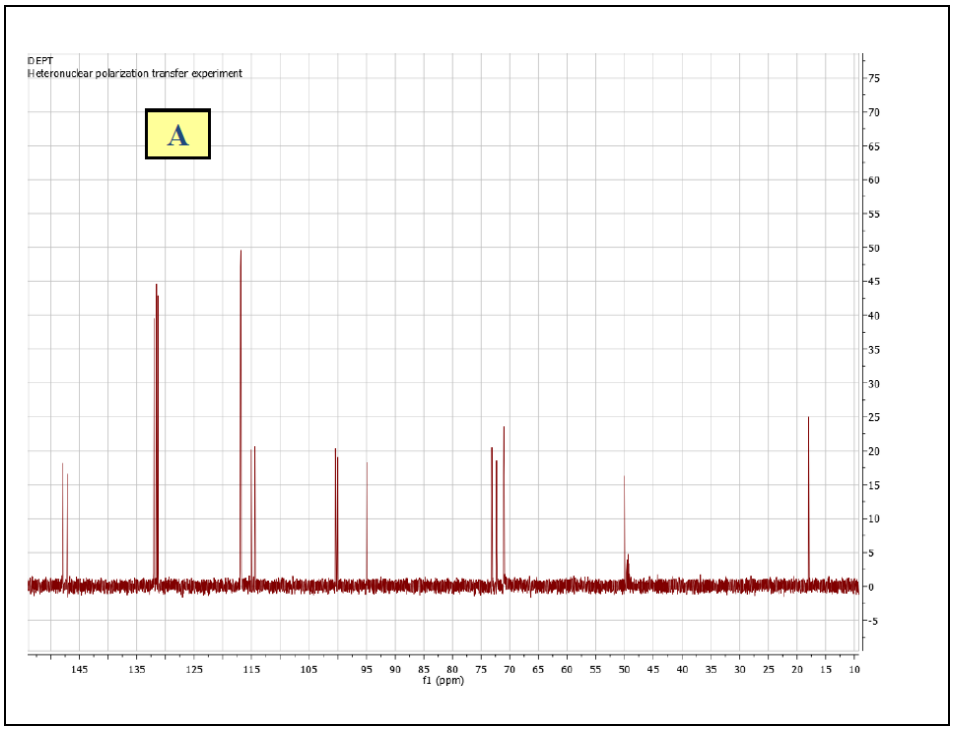

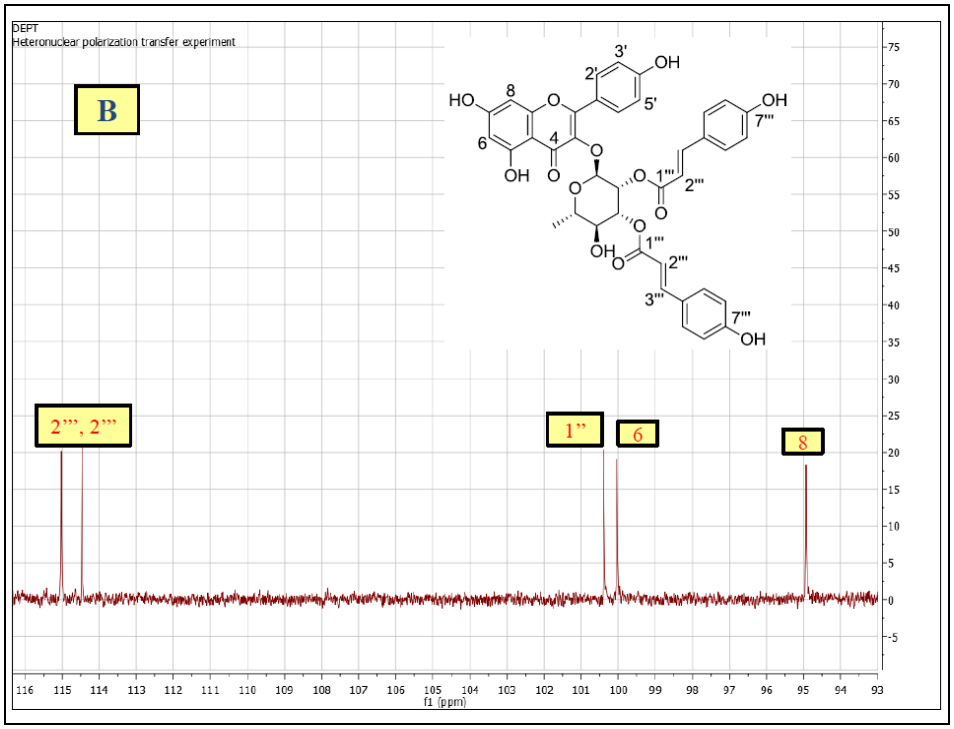

Figure 10. 135º DEPT spectrum of *E*,*E*-platanoside in methanol-d_4 (600 MHz); A) the full spectrum, B) the downfield region

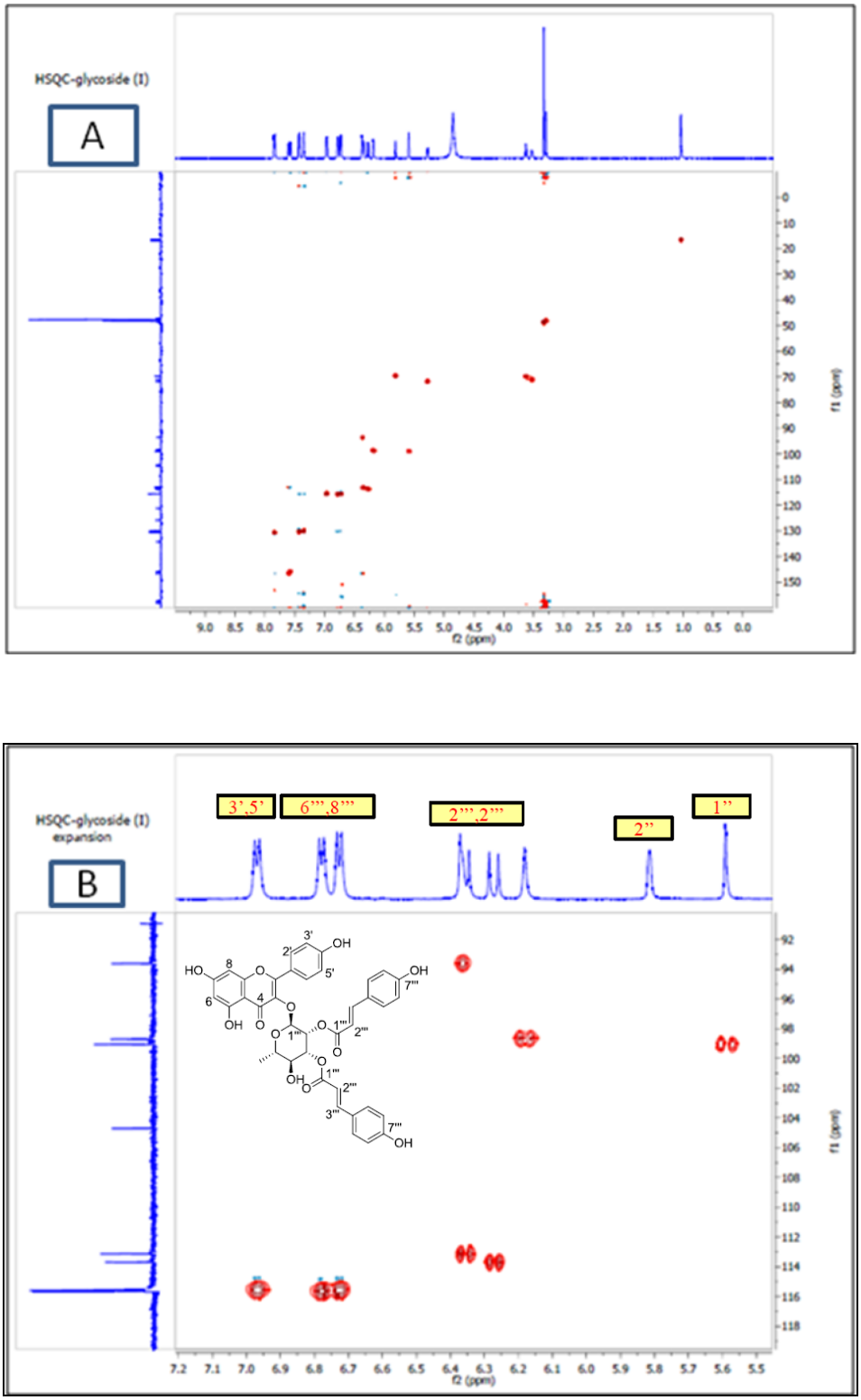

Figure 11. HSQC spectrum of *E*,*E*-platanoside in methanol-d_4 (400 MHz); A) the full spectrum, B) the downfield region

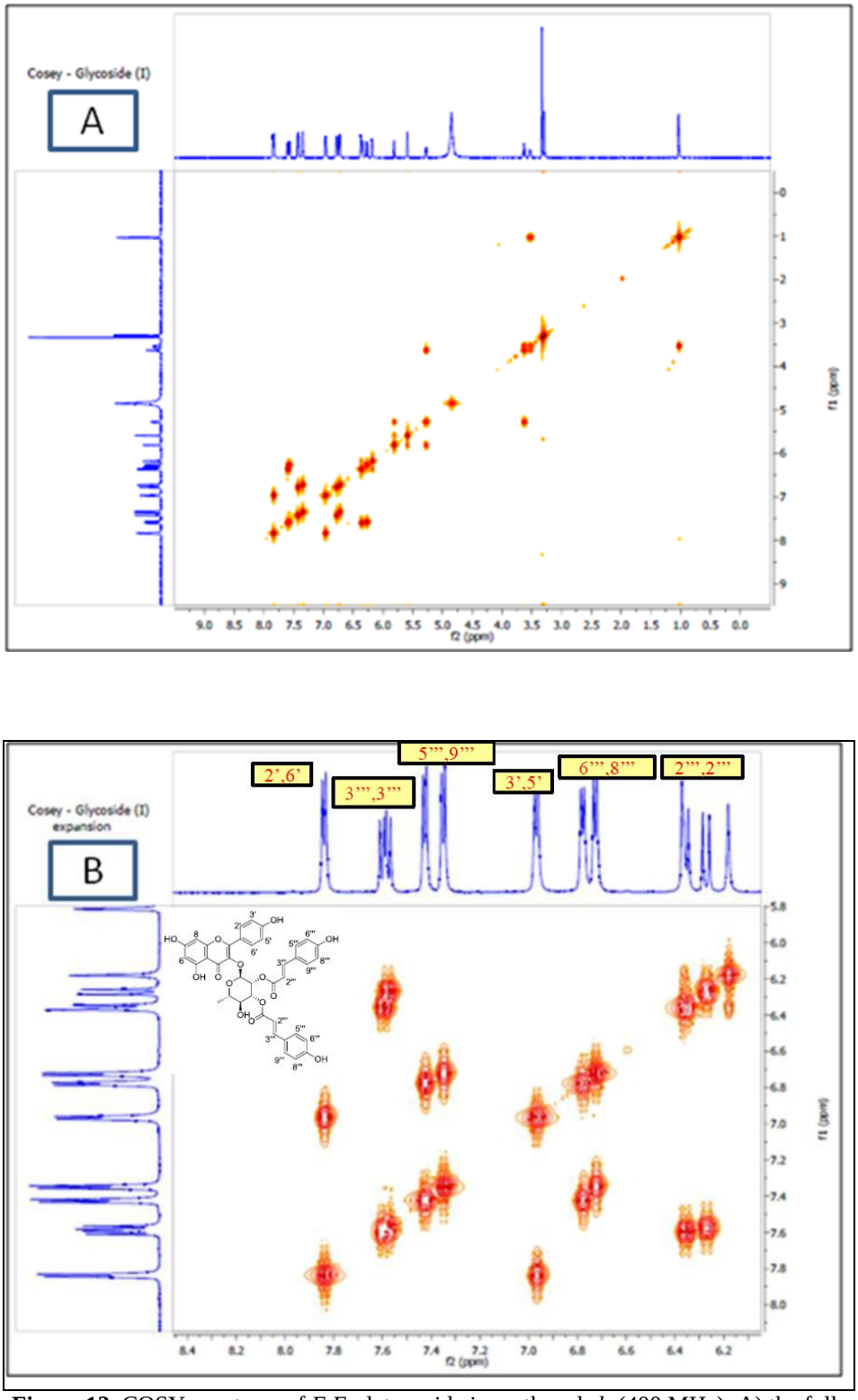

Figure 12. COSY spectrum of *E*,*E*-platanoside in methanol-d_4 (400 MHz); A) the full spectrum, B) the downfield region

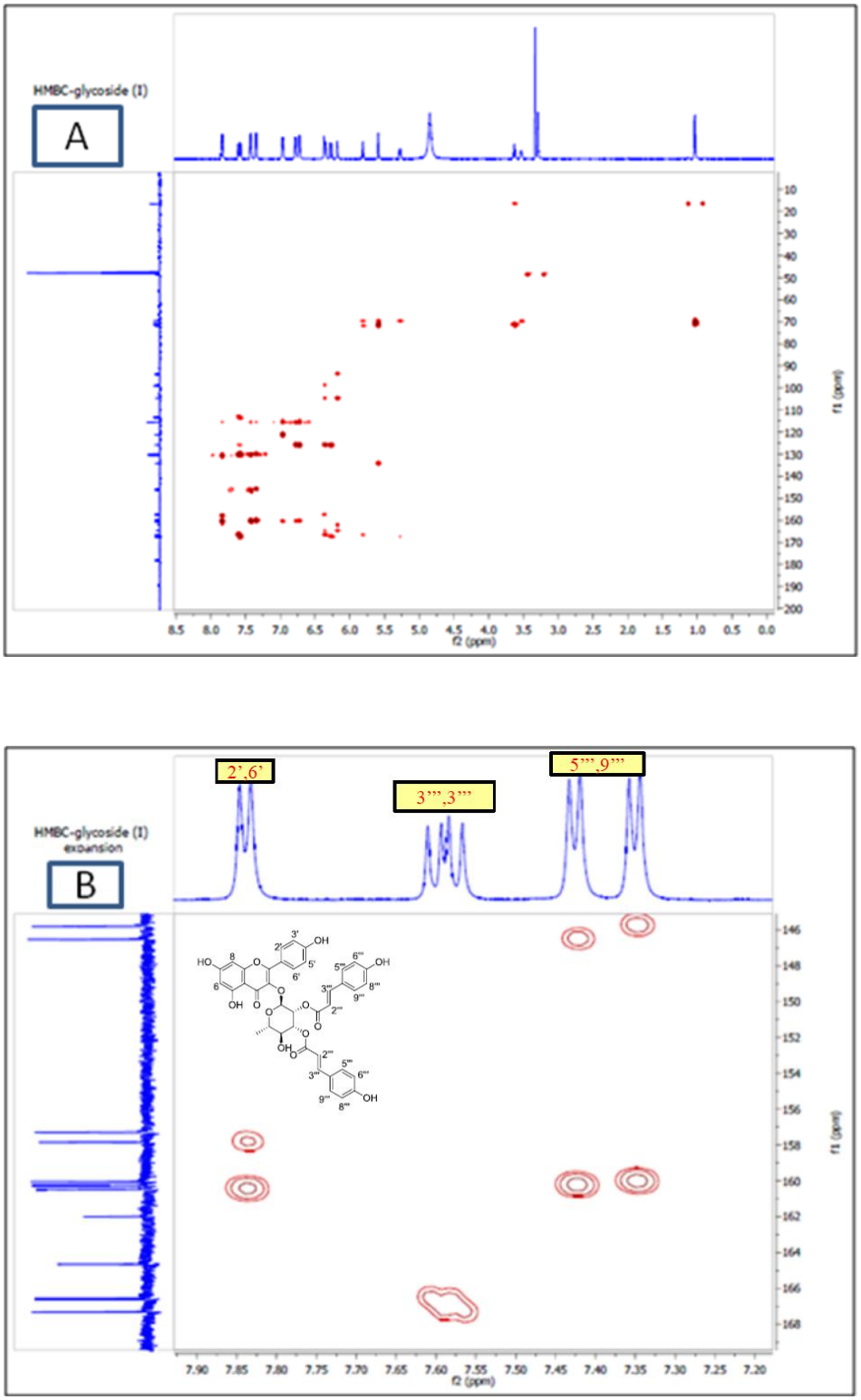

Figure 13. HMBC spectrum of *E*,*E*-platanoside in methanol-d_4 (400 MHz); A) the full spectrum, B) the downfield region

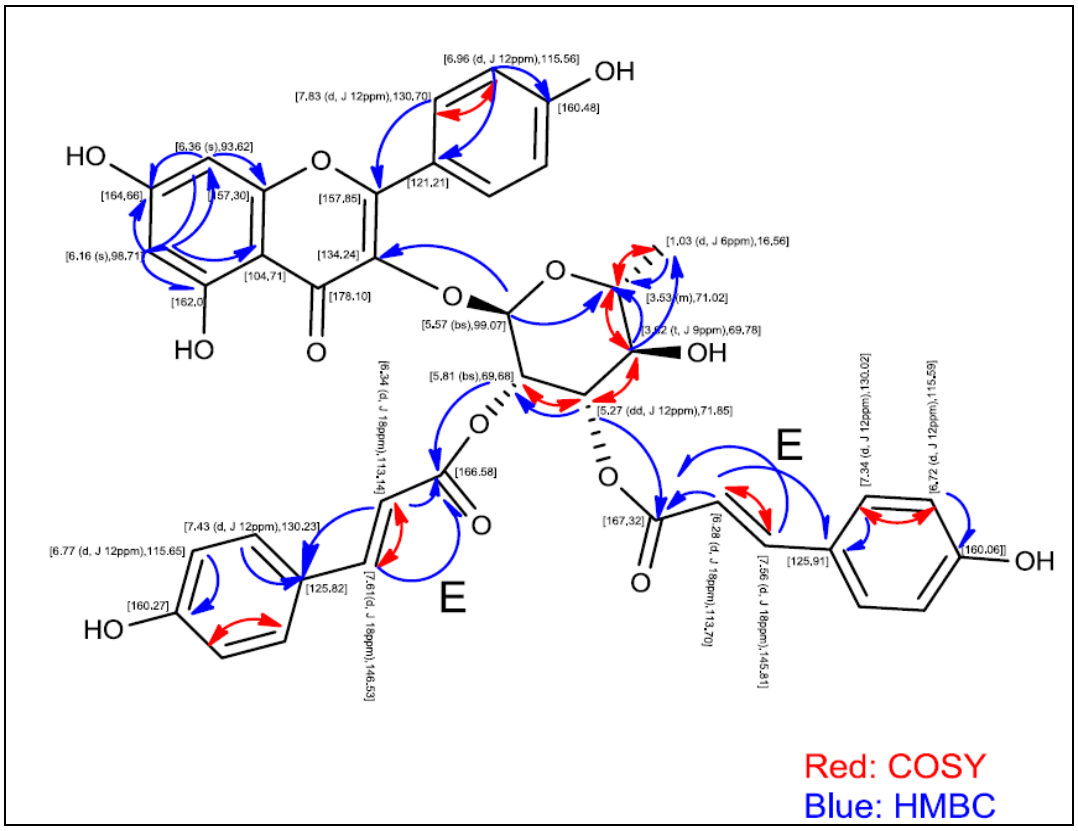

Figure 14. Selected COSY and HMBC correlations of *E*,*E*-platanoside

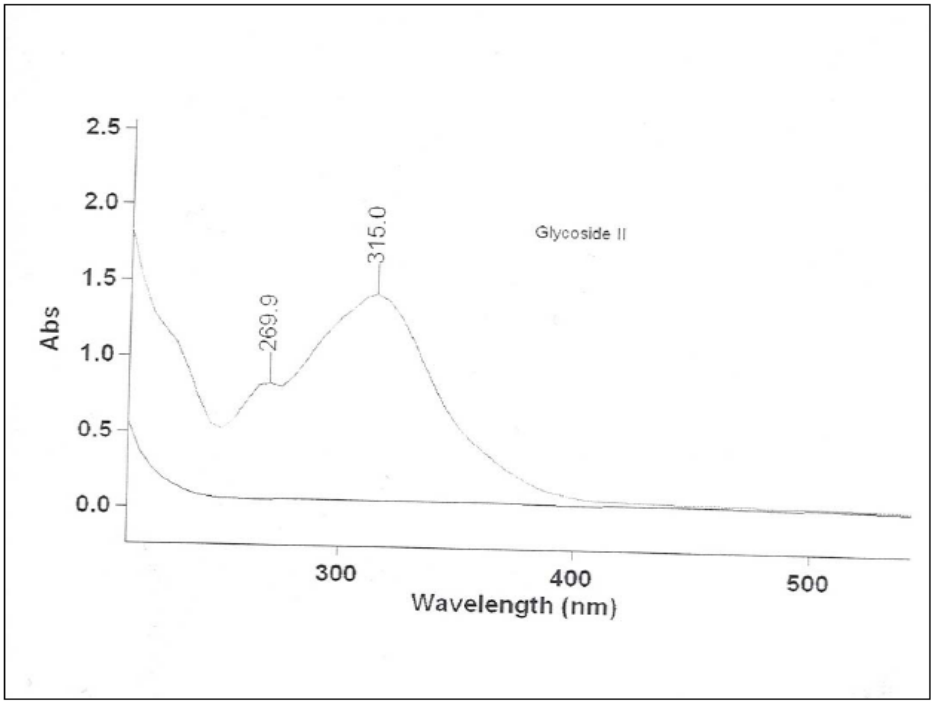

Figure 15. UV spectrum of *E*,*Z*-platanoside in MeOH

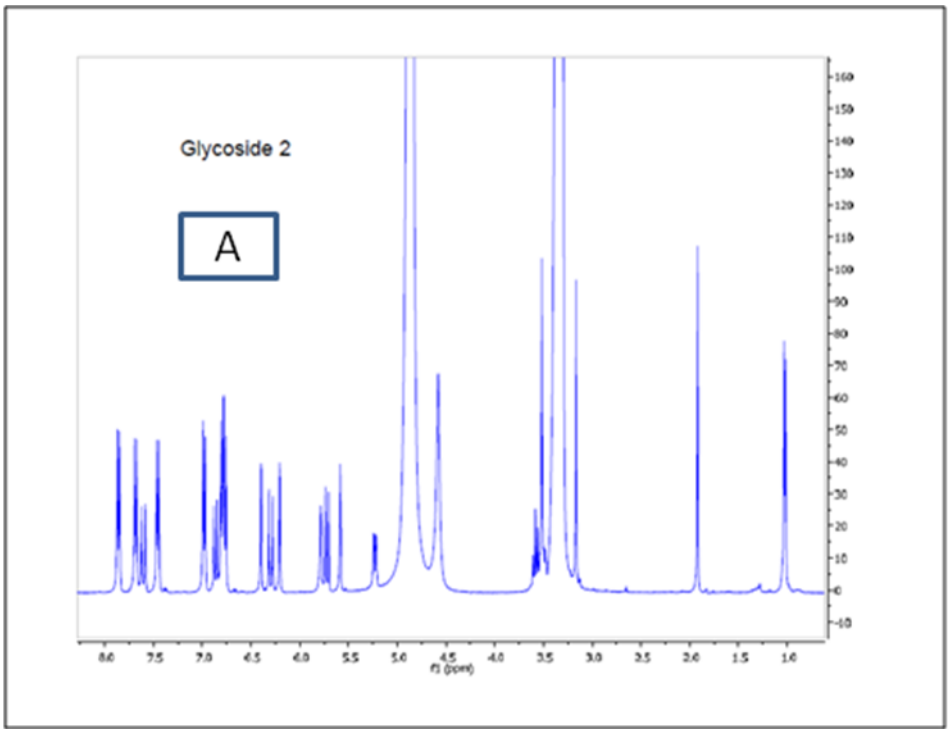

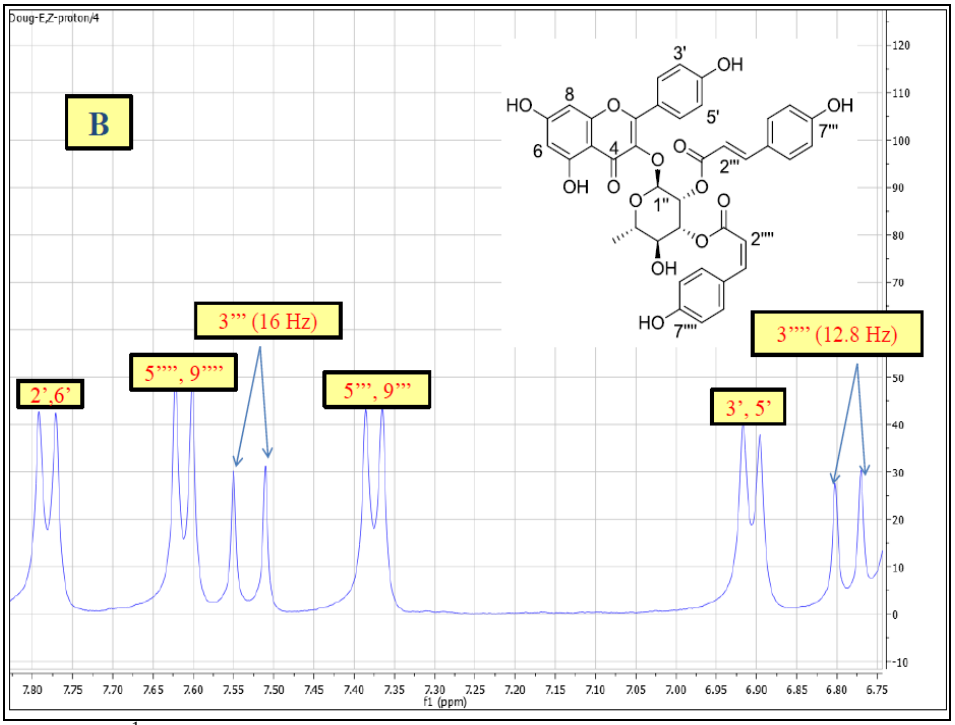

Figure 16. ^{1}H NMR spectrum of *E*,*Z*-platanoside in methanol-d_4 (400 MHz); A) the full spectrum, B) the downfield region

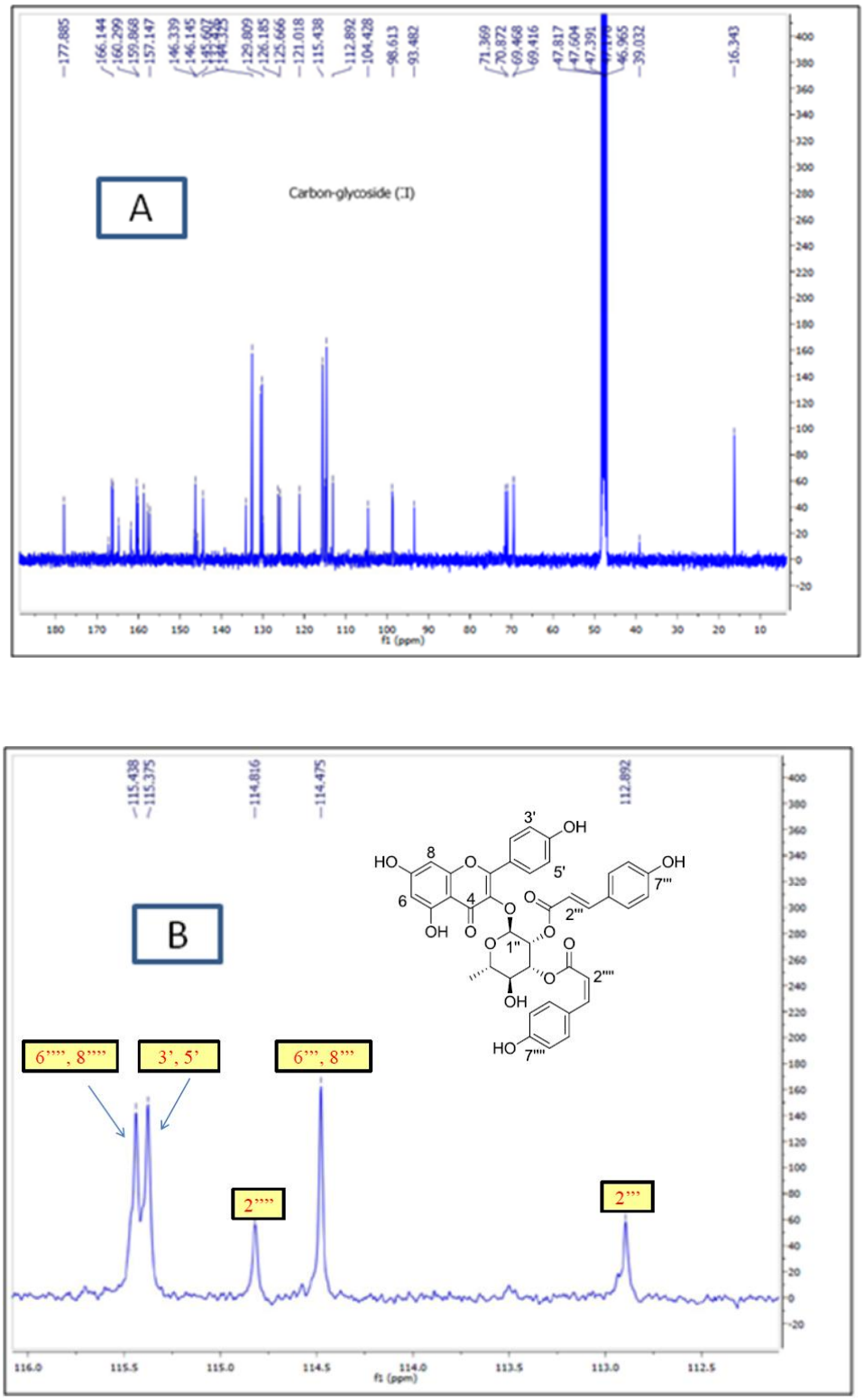

Figure 17. ^{13}C NMR spectrum of *E*,*Z*-platanoside in methanol-d_4 (400 MHz); A) the full spectrum, B) the downfield region

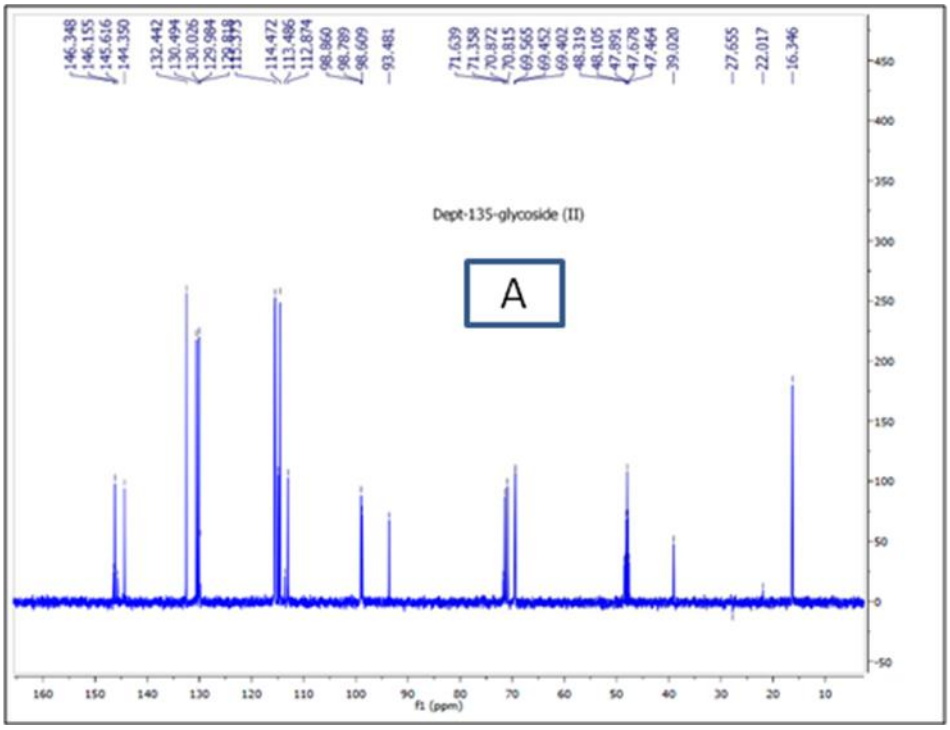

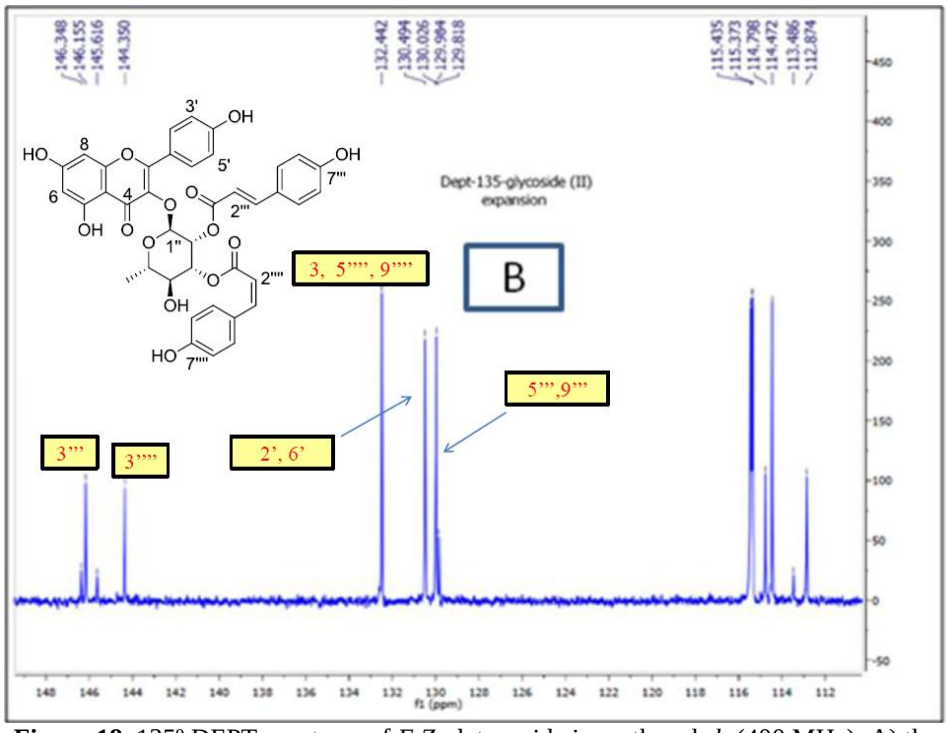

Figure 18. 135º DEPT spectrum of *E,Z*-platanoside in methanol-d_4 (400 MHz); A) the full spectrum, B) the downfield region

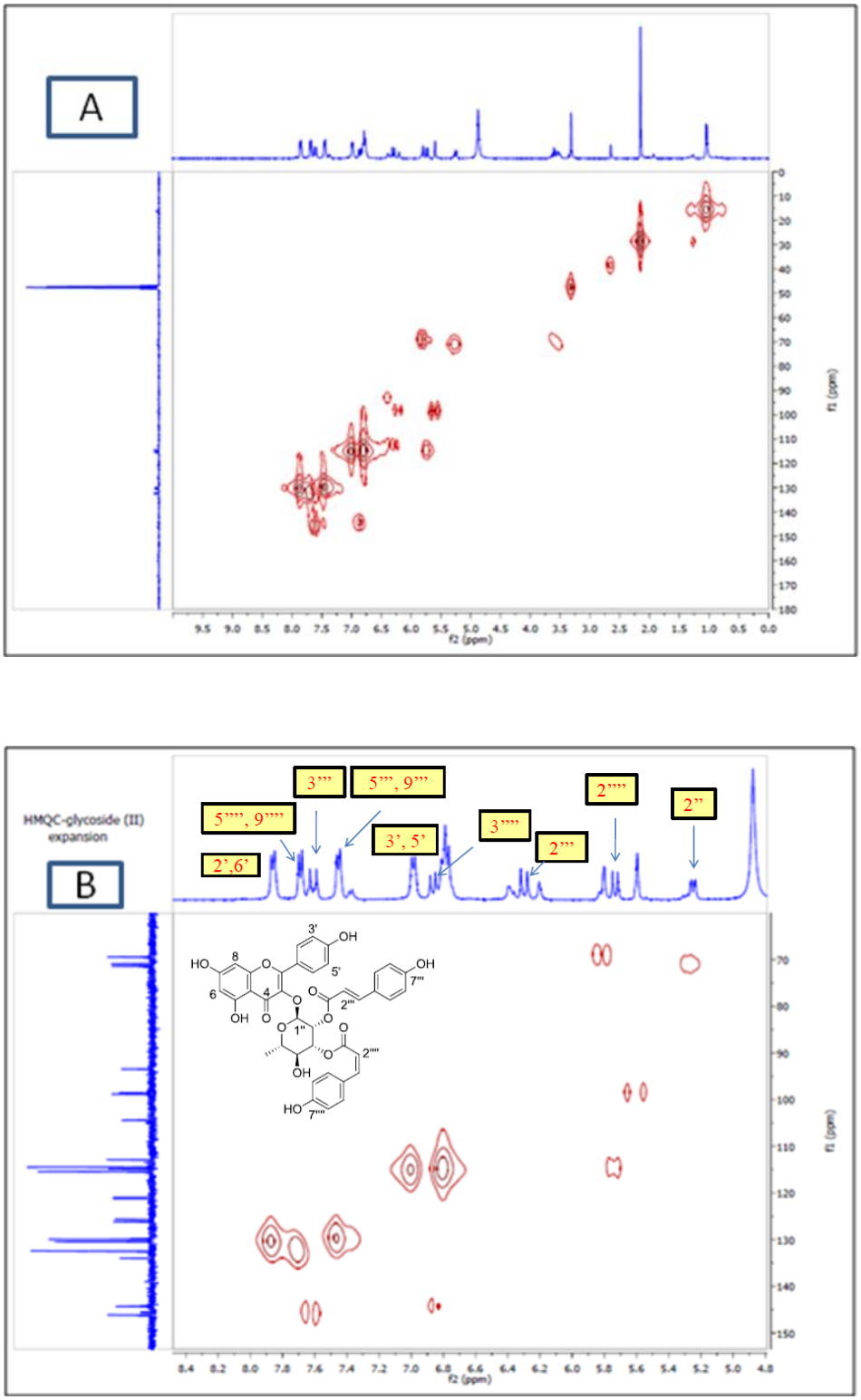

Figure 19. HMQC spectrum of *E*,*Z*-platanoside in methanol-d_4 (400 MHz); A) the full spectrum, B) the downfield region

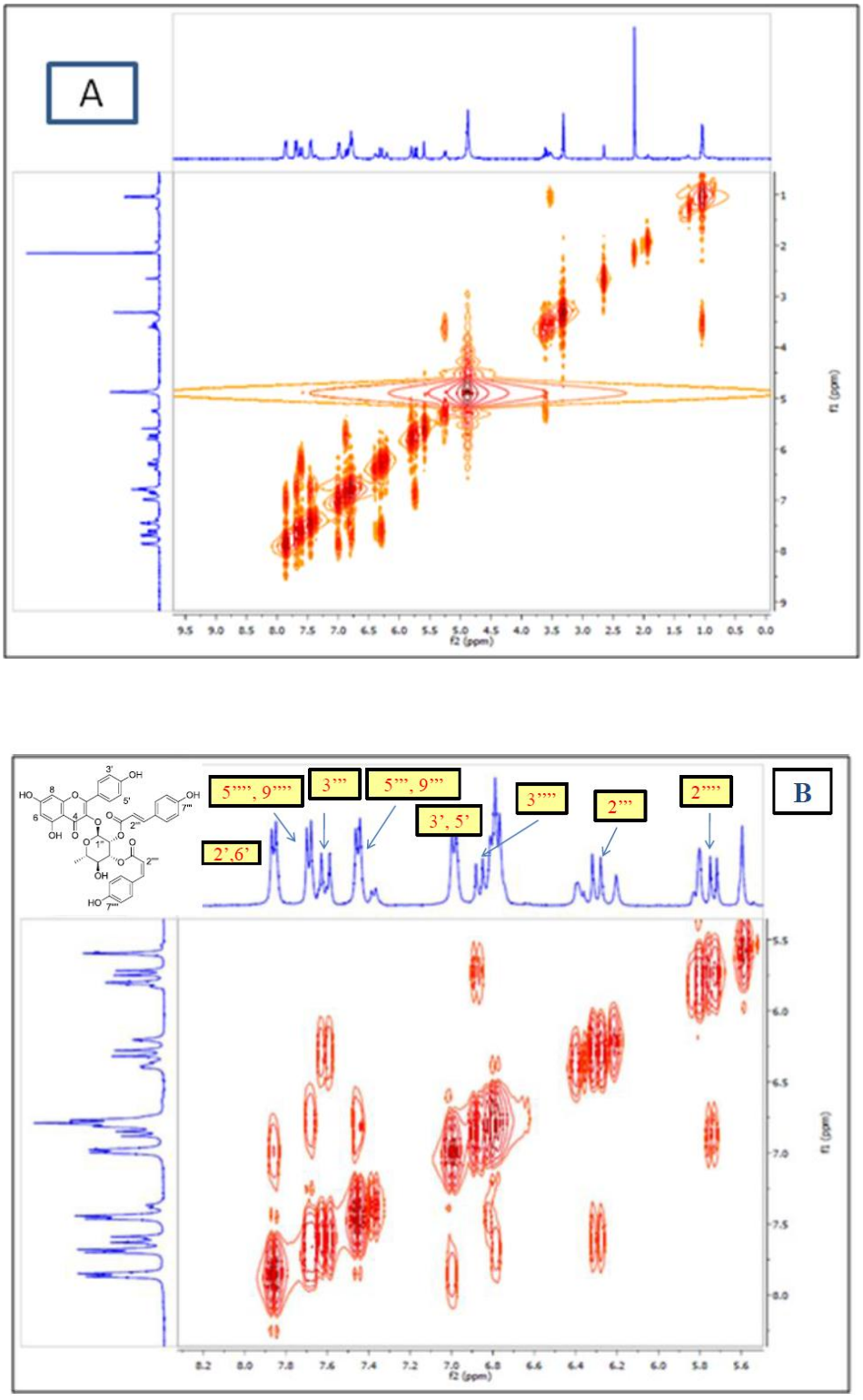

Figure 20. COSY spectrum of *E*,*Z*-platanoside in methanol-d_4 (400 MHz); A) the full spectrum, B) the downfield region

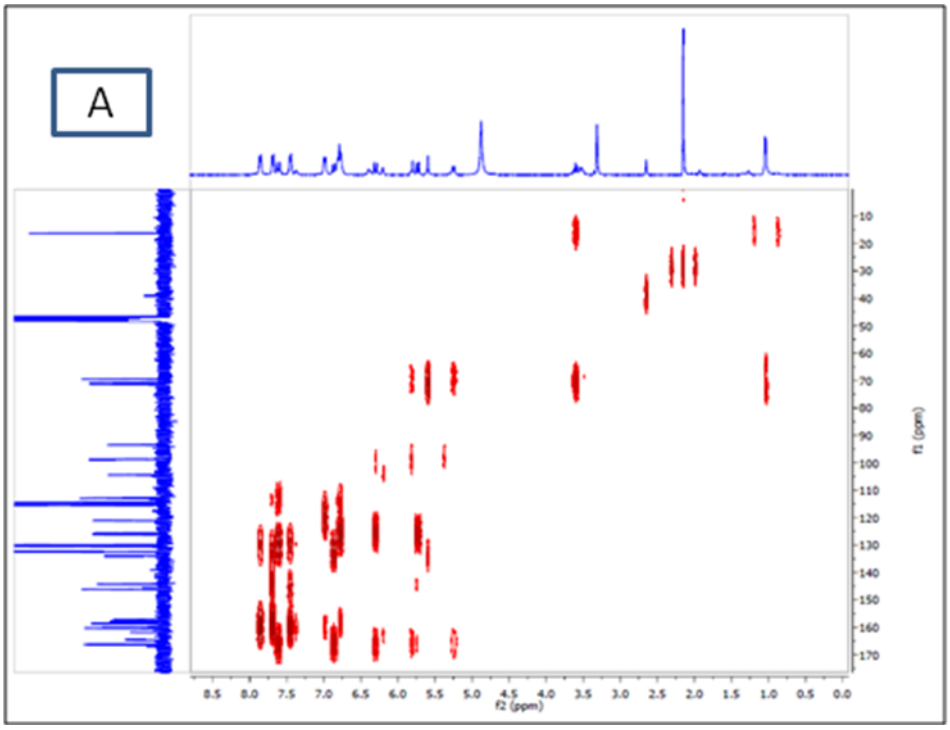

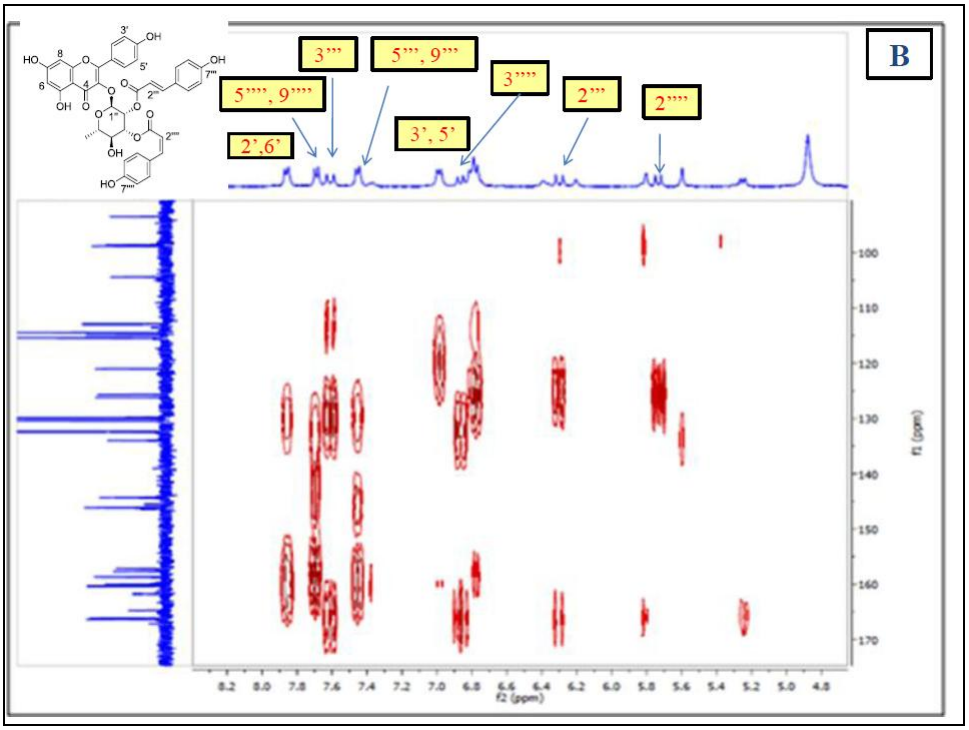

Figure 21. HMBC spectrum of *E*,*Z*-platanoside in methanol-d_4 (400 MHz); A) the full spectrum, B) the downfield region

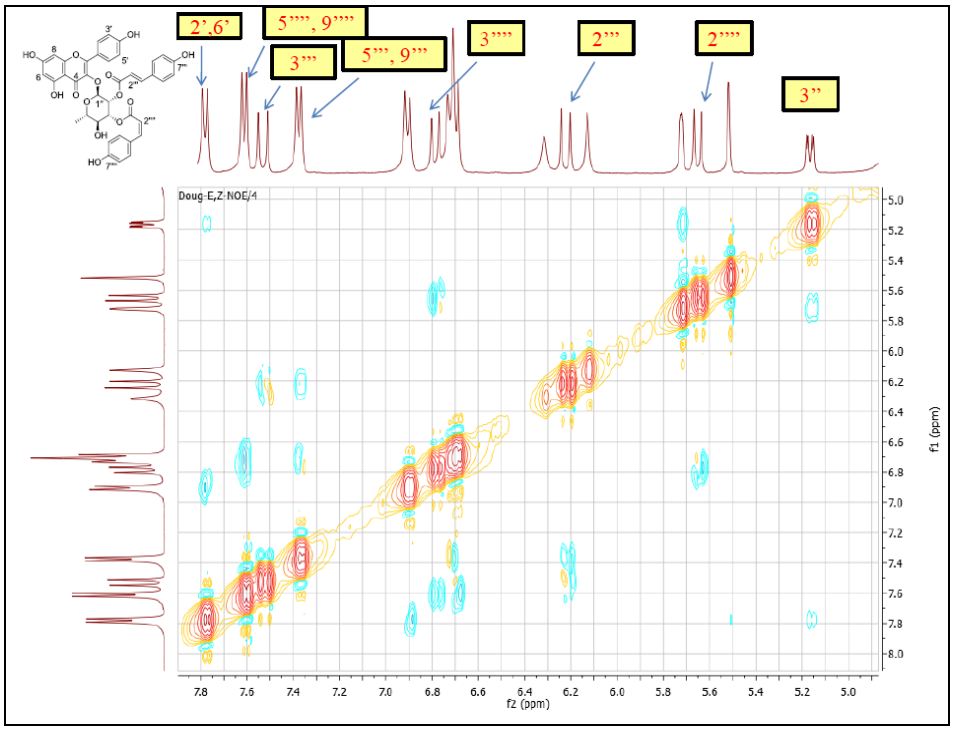

Figure 22. NOESY spectrum of *E,Z*-platanoside in methanol-d_4 (400 MHz)

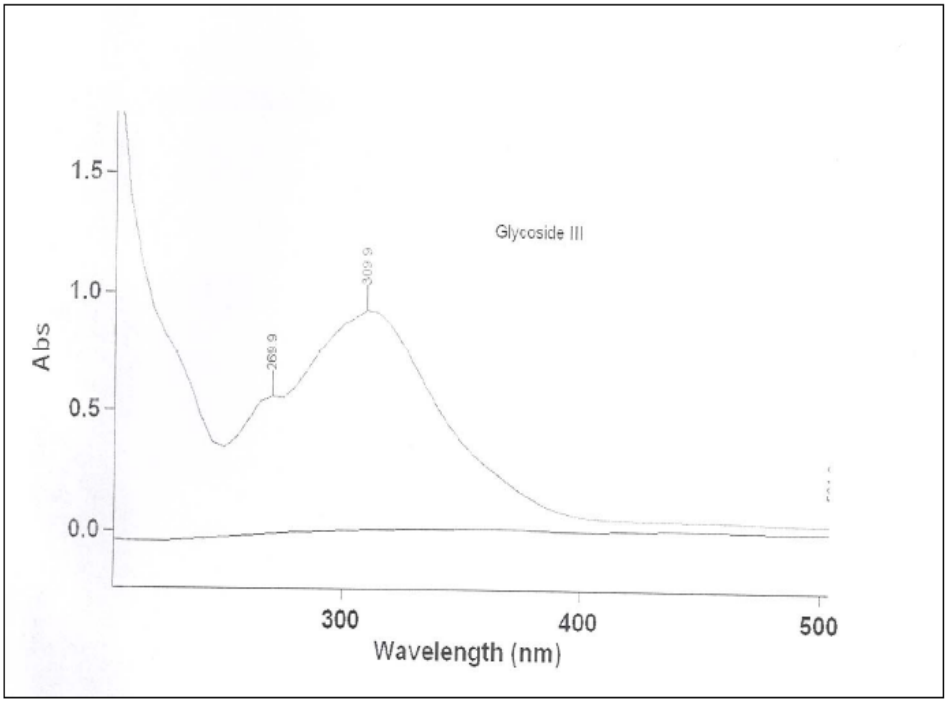

Figure 23. UV spectrum of *Z,E*-platanoside in MeOH

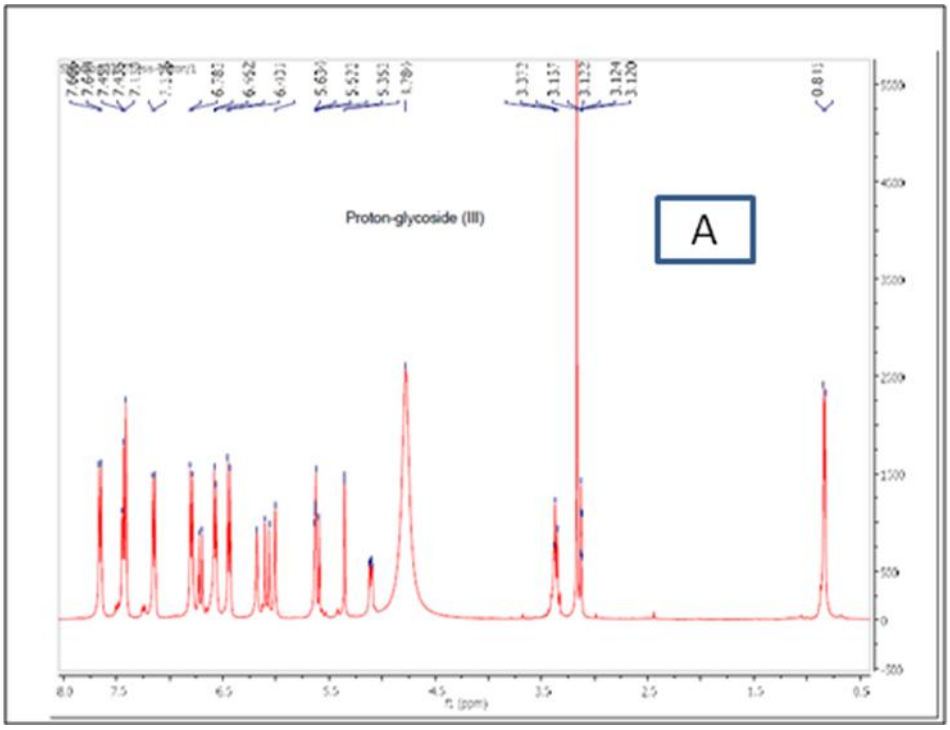

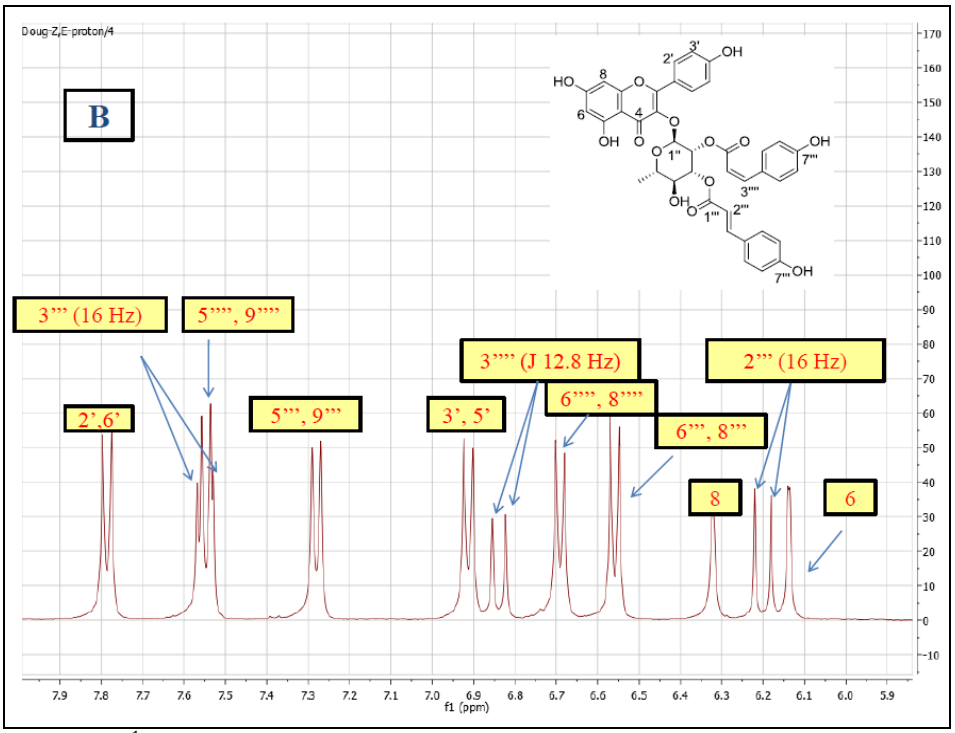

Figure 24. ^{1}H NMR spectrum of *Z,E*-platanoside in methanol-d_4(400 MHz); A) the full spectrum, B) the downfield region

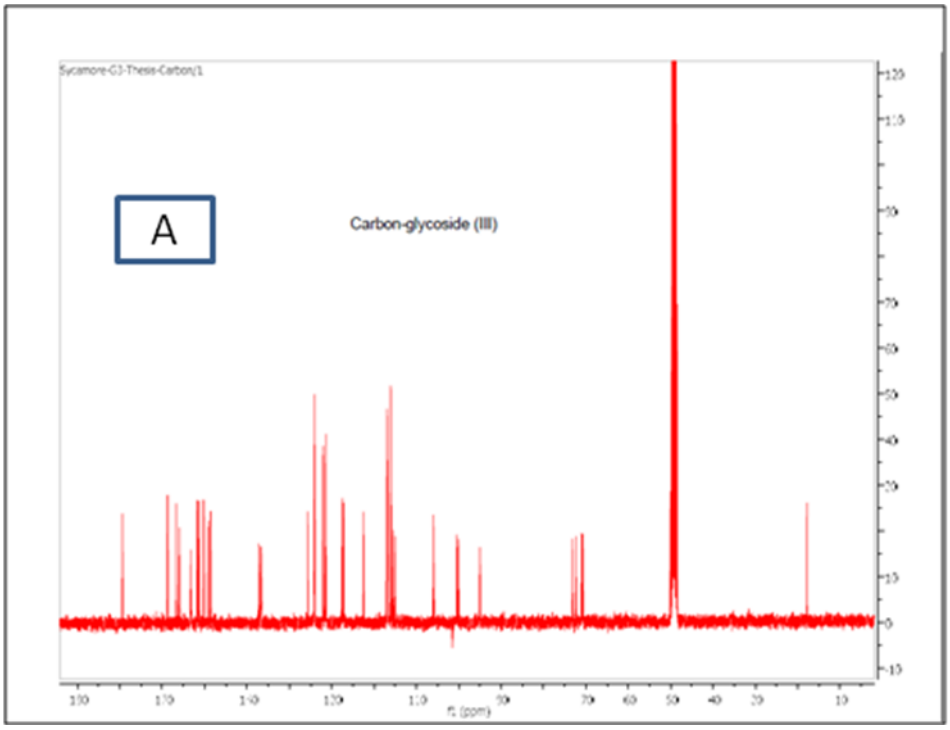

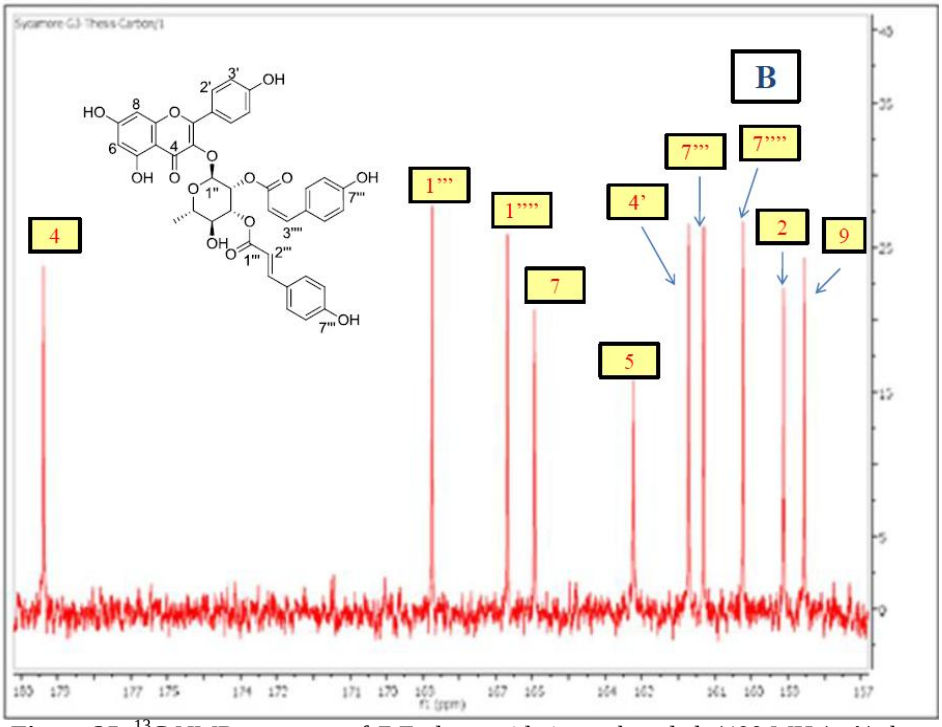

Figure 25. ^{13}C NMR spectrum of *Z,E*-platanoside in methanol-d_4 (400 MHz); A) the full spectrum, B) the downfield region

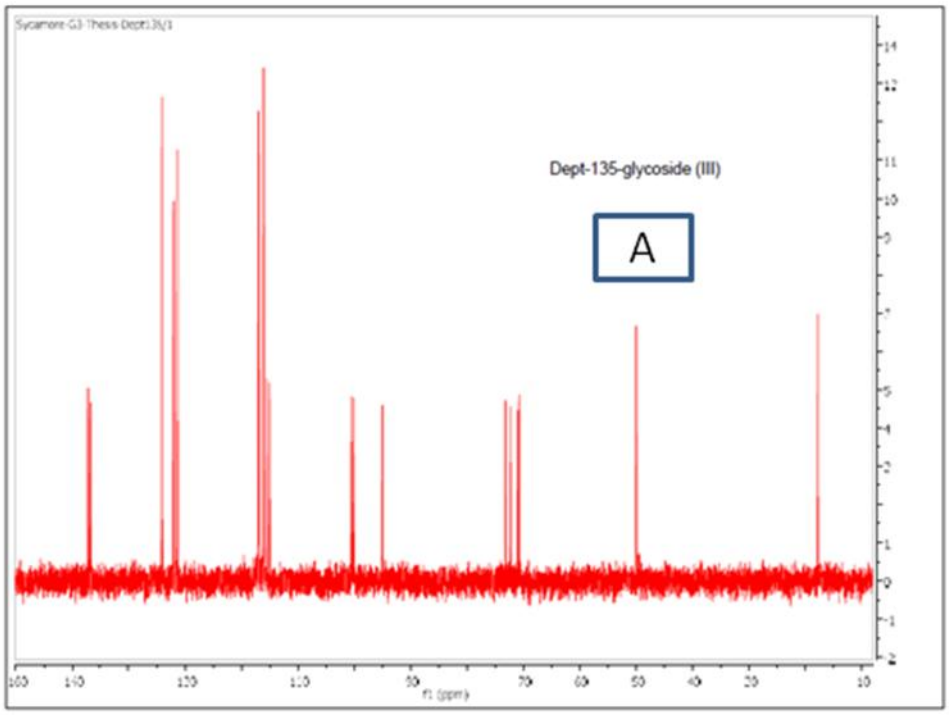

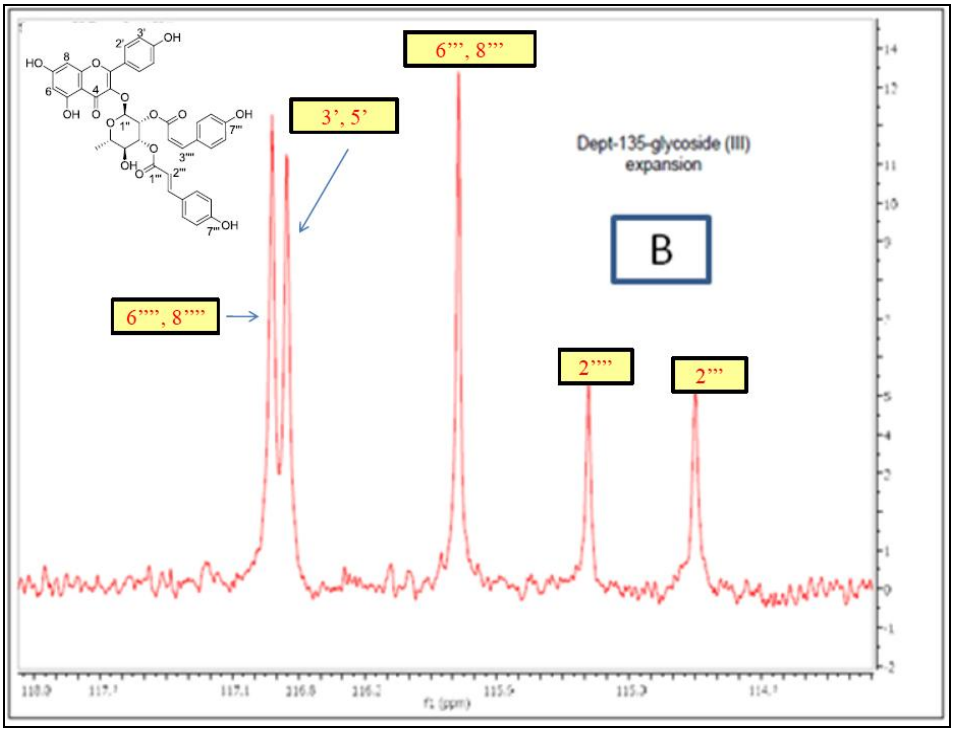

Figure 26. 135º DEPT spectrum of *Z,E*-platanoside in methanol-d_4 (400 MHz); A) the full spectrum, B) the downfield region

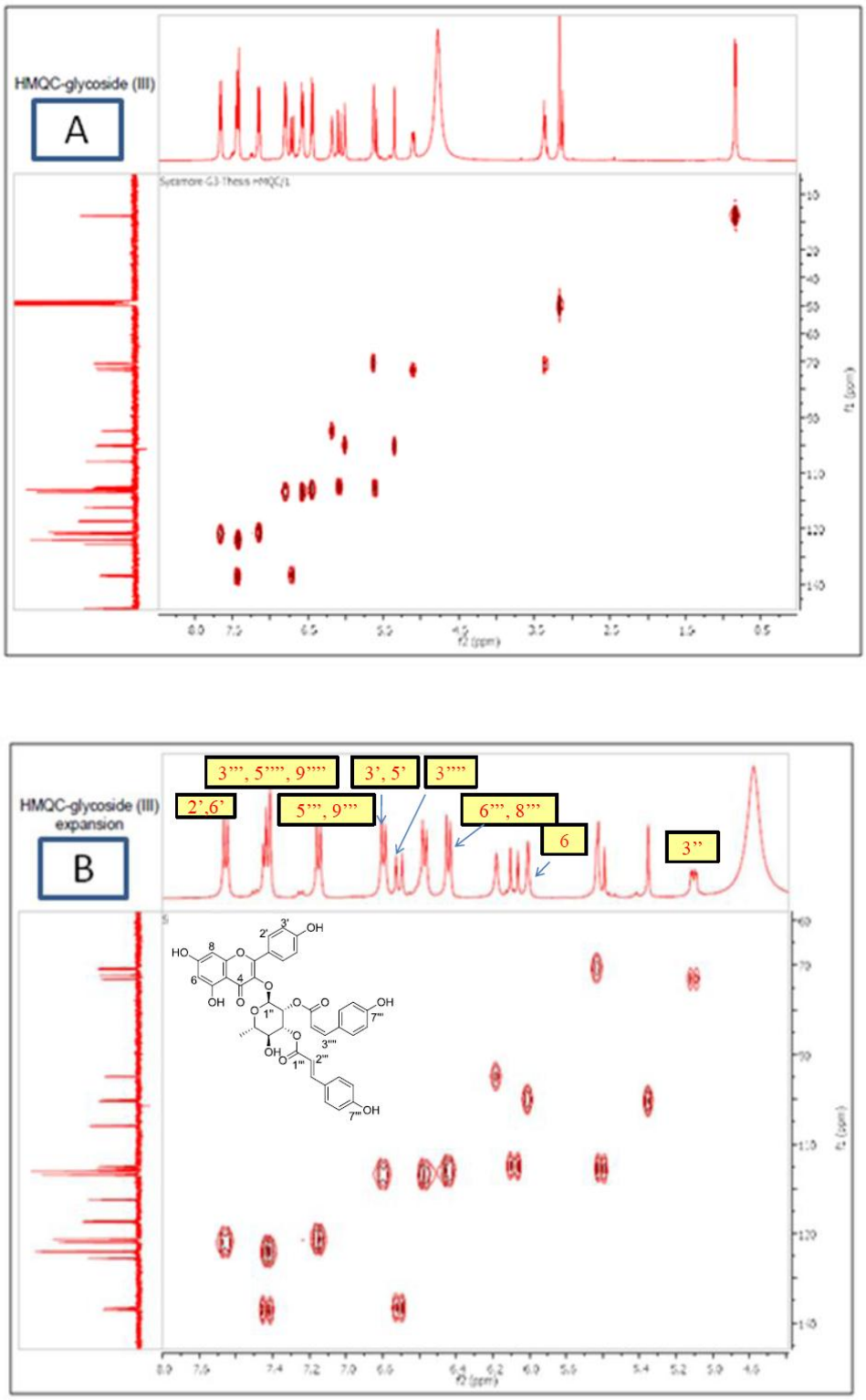

Figure 27. HMQC spectrum of *Z,E*-platanoside in methanol-d_4 (400 MHz); A) the full spectrum, B) the downfield region

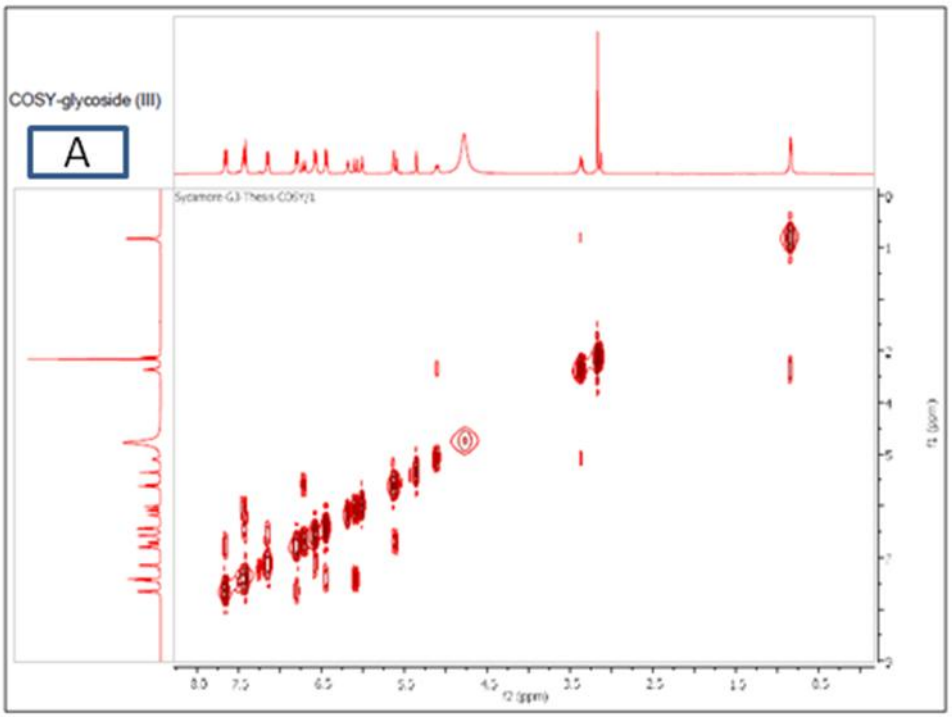

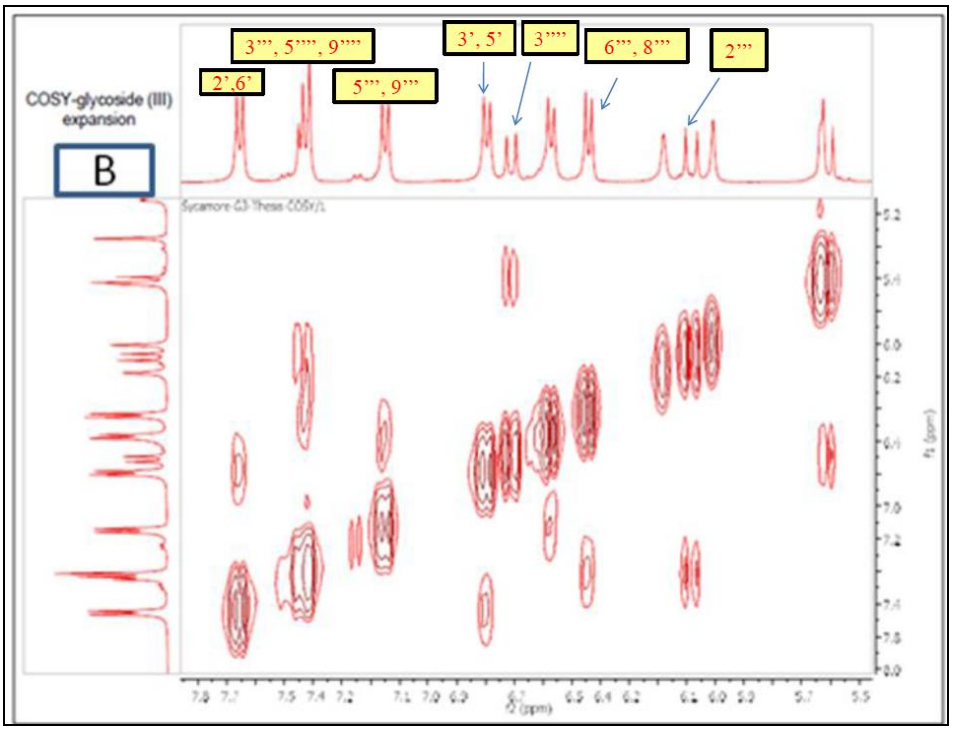

Figure 28. COSY spectrum of *Z,E*-platanoside in methanol-d_4 (400 MHz); A) the full spectrum, B) the downfield region

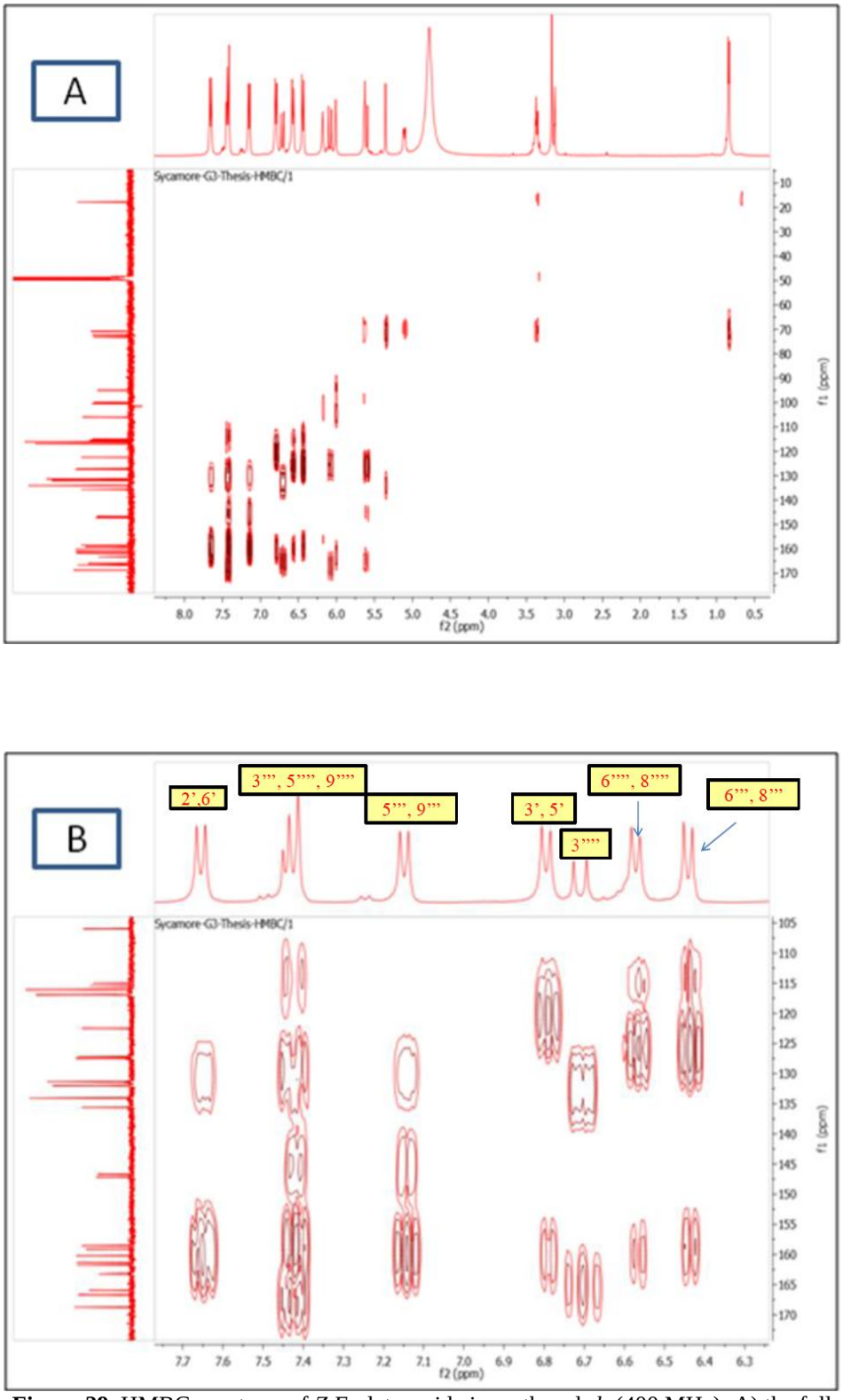

Figure 29. HMBC spectrum of *Z,E*-platanoside in methanol-d_4 (400 MHz); A) the full spectrum, B) the downfield region

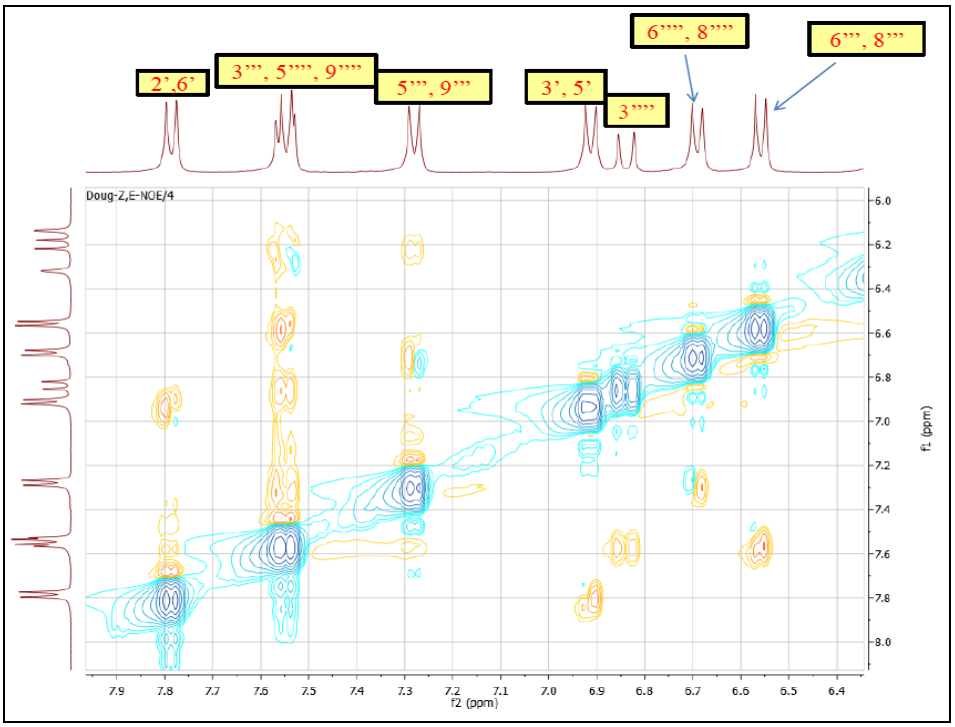

Figure 30. NOESY spectrum of *Z,E*-platanoside in methanol-d_4 (400 MHz)

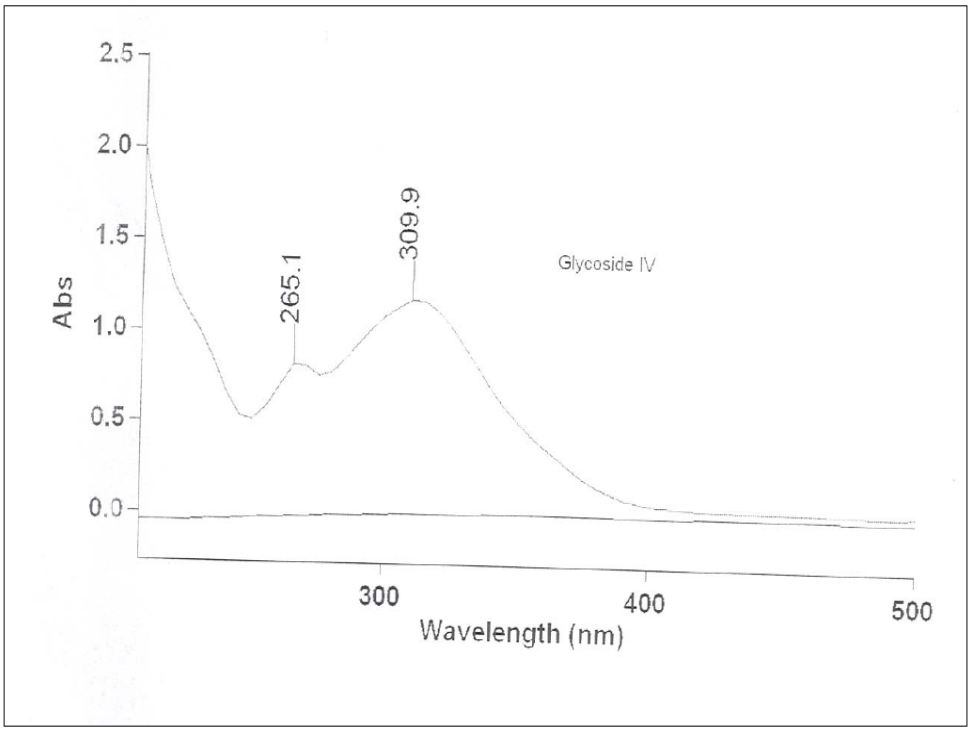

Figure 31. UV spectrum of *Z,Z*-platanoside in MeOH

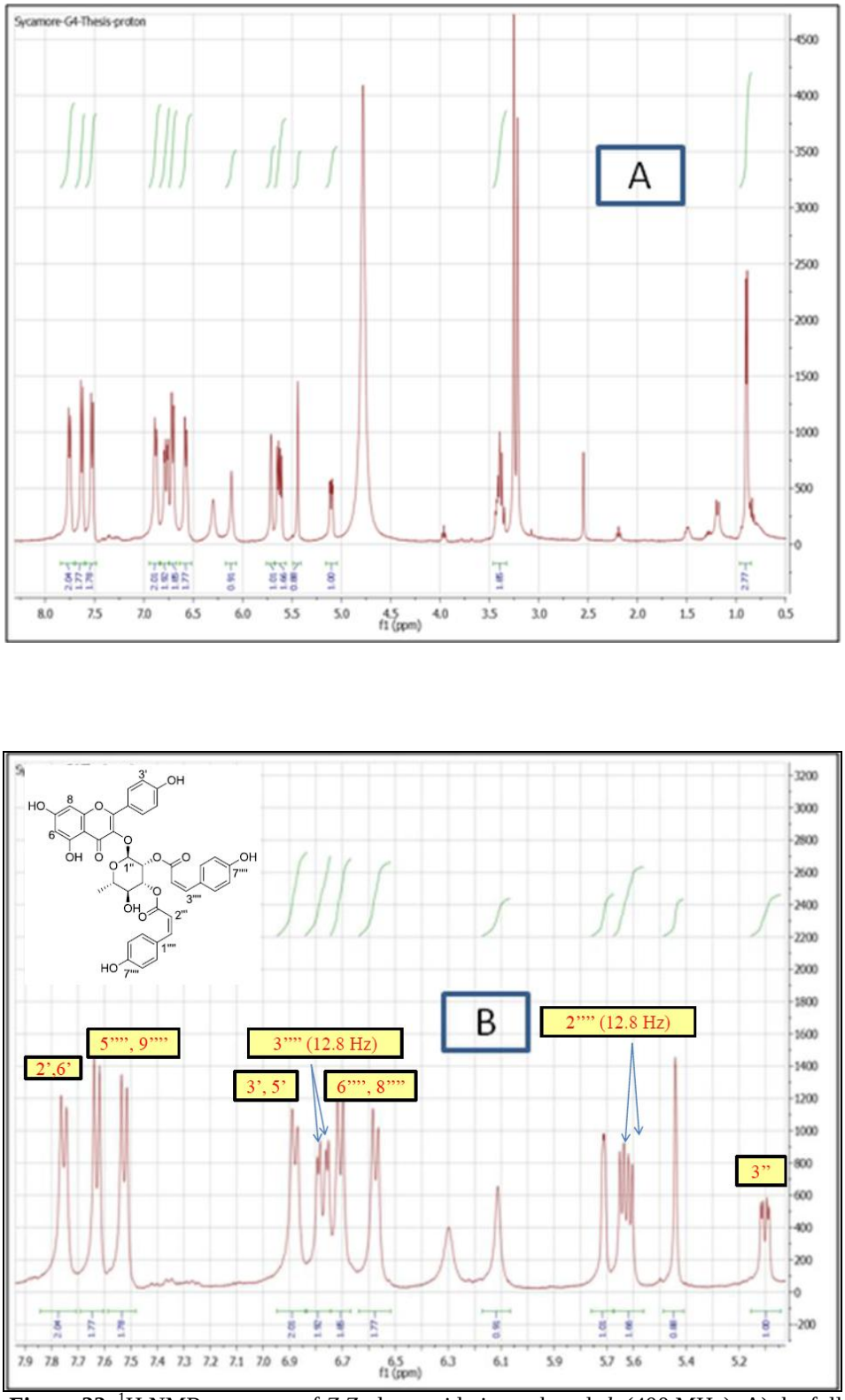

Figure 32. ^{1}H NMR spectrum of *Z,Z*-platanoside in methanol-d_4 (400 MHz); A) the full spectrum, B) the downfield region

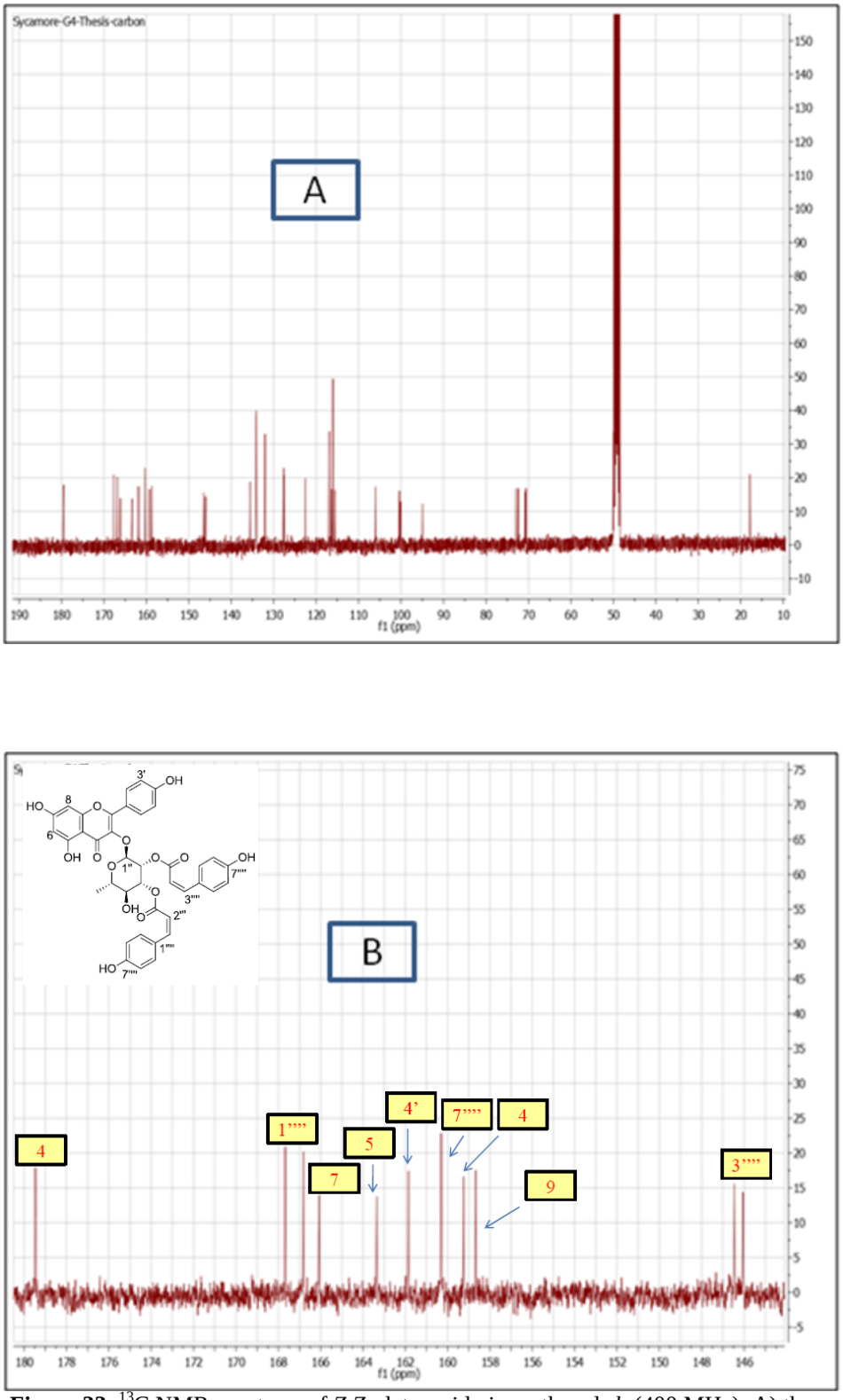

Figure 33. ^{13}C NMR spectrum of *Z,Z*-platanoside in methanol-d_4 (400 MHz); A) the full spectrum, B) the downfield region

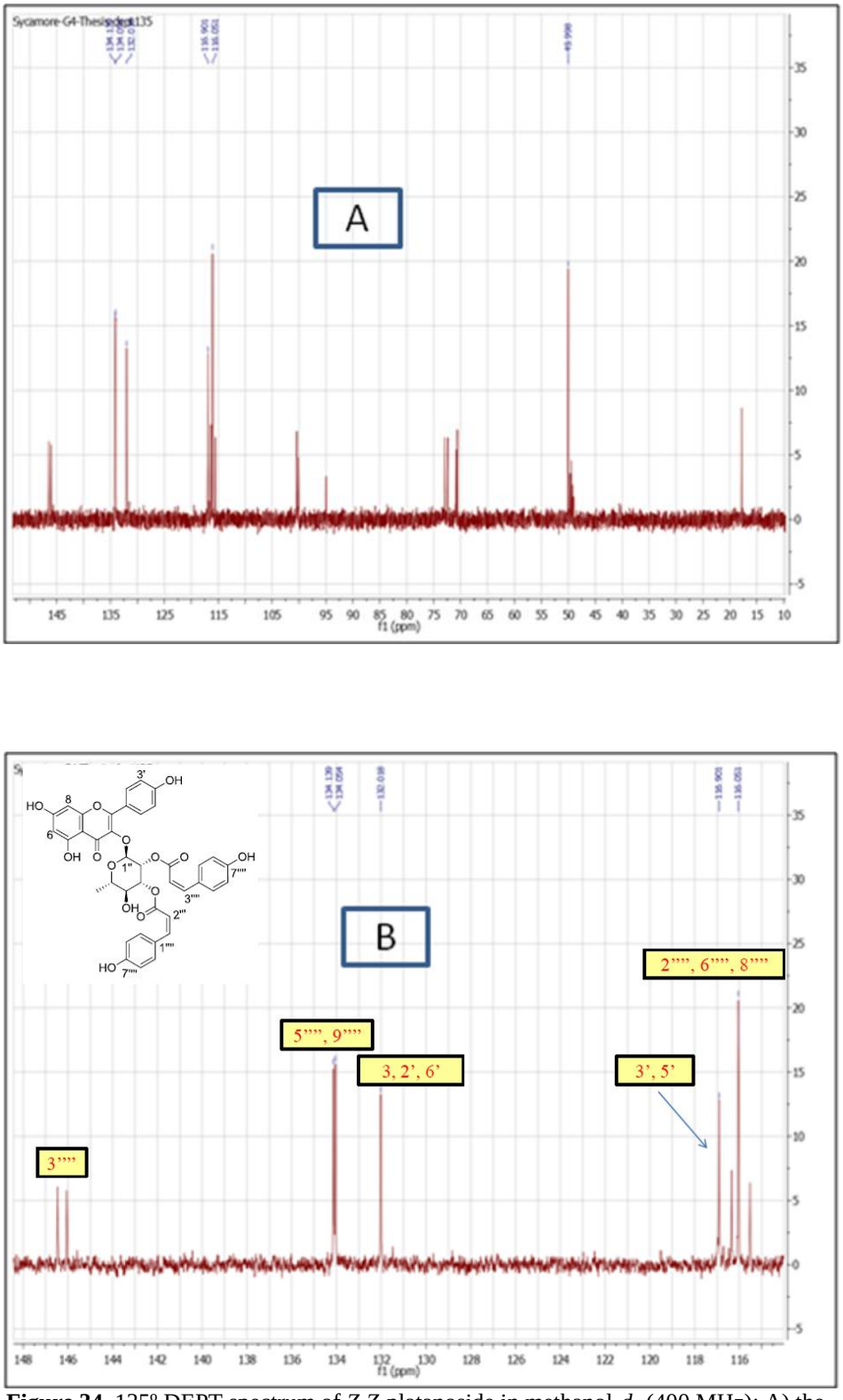

Figure 34. 135º DEPT spectrum of *Z*,*Z*-platanoside in methanol-d_4 (400 MHz); A) the full spectrum, B) the downfield region

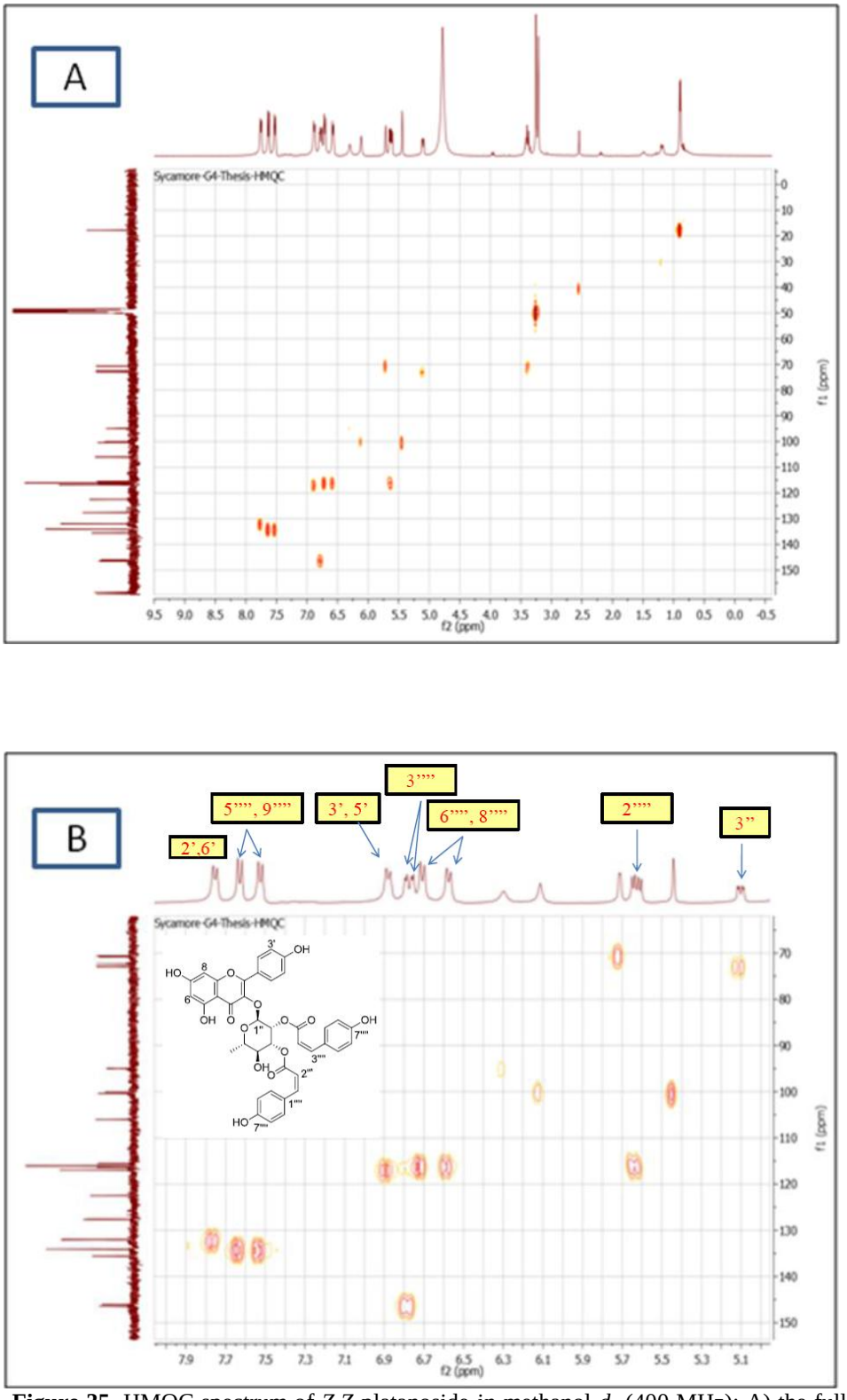

Figure 35. HMQC spectrum of *Z,Z*-platanoside in methanol-d_4 (400 MHz); A) the full spectrum, B) the downfield region

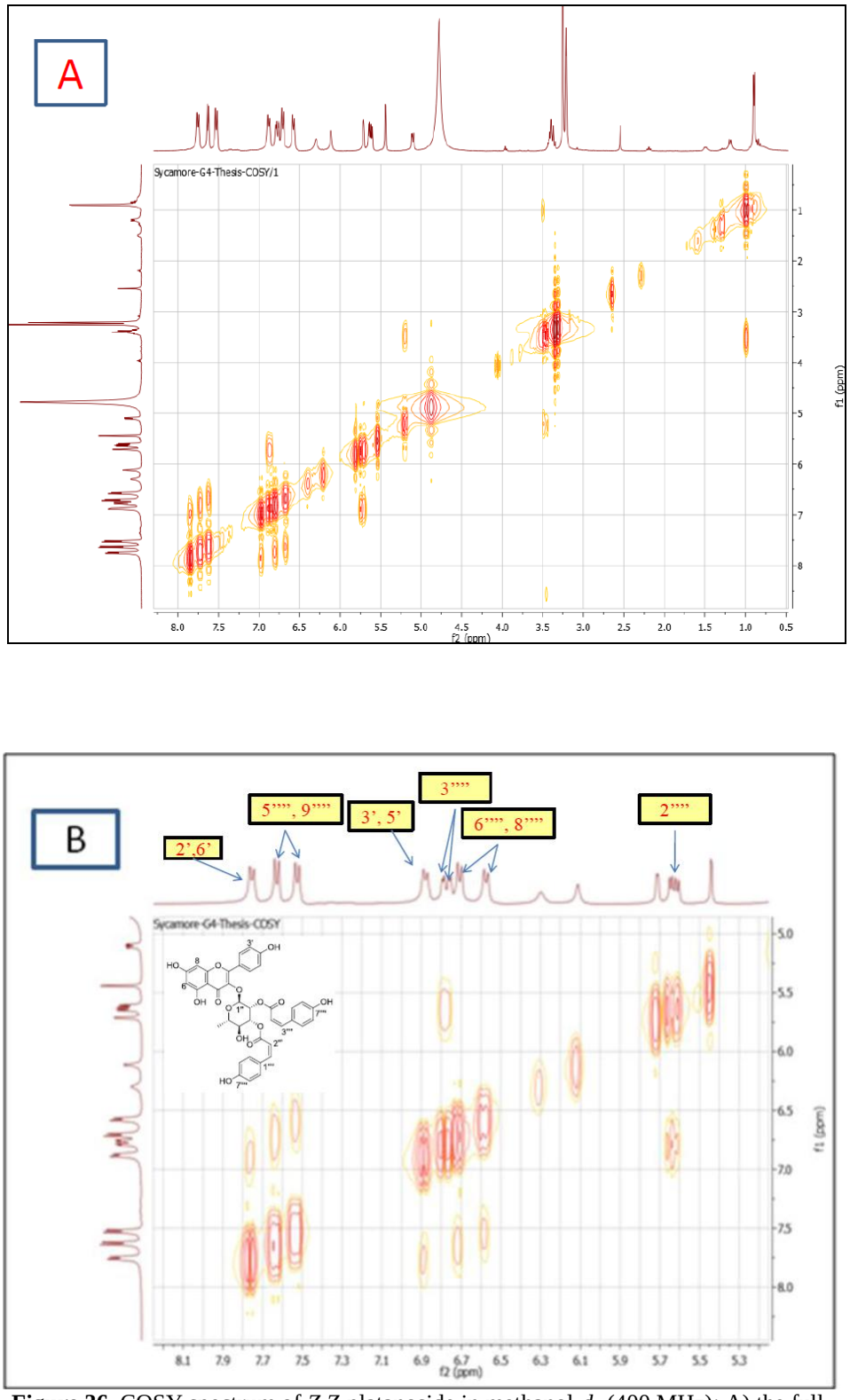

Figure 36. COSY spectrum of *Z,Z*-platanoside in methanol-d_4 (400 MHz); A) the full spectrum, B) the downfield region

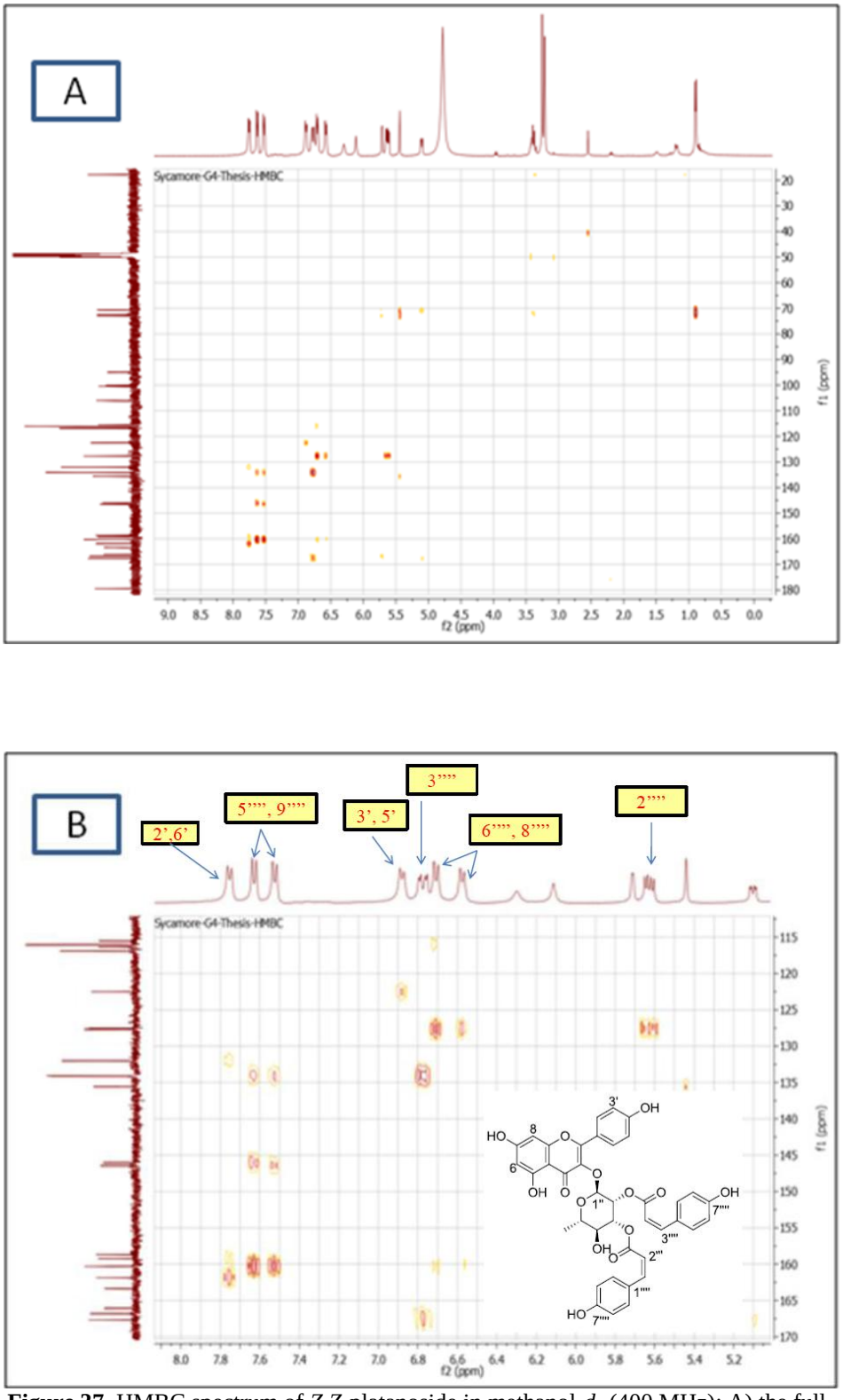

Figure 37. HMBC spectrum of *Z,Z*-platanoside in methanol-d_4 (400 MHz); A) the full spectrum, B) the downfield region

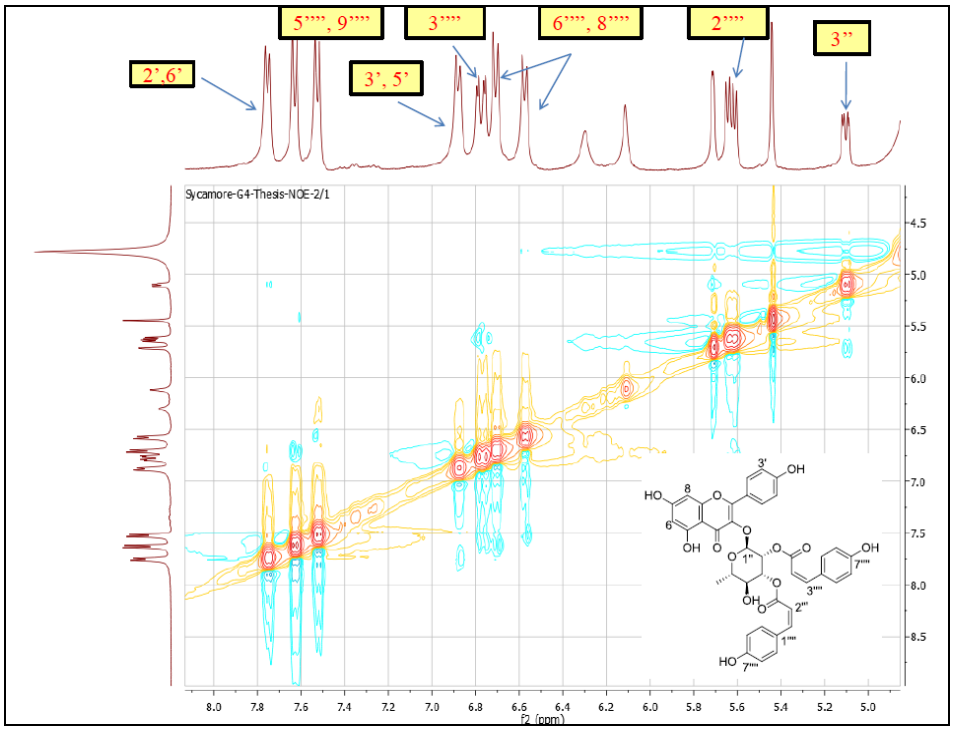

Figure 38. NOESY spectrum of *Z,Z*-platanoside in methanol-d_4 (400 MHz)

Carbohydrate Analysis. Each glycoside (0.3 mg) was hydrolyzed with 2 N HCl (1.0 mL) for 3 h at 95 ^{o}C, cooled, neutralized with NH_4OH, and extracted using EtOAc/H_2O. The aqueous layer was dried, and dissolved in a mixture of pyridine (0.3 mL) and a 0.1 M solution of L-cysteine methyl ester hydrochloride in pyridine (1.0 mL). The reaction mixture was heated for 1 hr at 60 ^{o}C, and an equal volume of Ac_2O was added with continuous heating for an extra hour. The acylated thiazolidine derivatives were subjected to GC analysis [capillary column: DB-5 ms (30 m x 0.25 mm x 0.25 μm)].[20,21] The carbohydrates were identified as L-rhamnose by comparison with the retention time of an L-rhamnose standard.

Antimicrobial Assays. The CLSI (formerly NCCLS) method[22] was used for the in vitro evaluation of test samples. Duplicate samples were transferred to 96-well microplates after diluting with 0.9% saline. The microbial cell suspensions were added to the samples to give the

required target inocula after addition to the samples. Media and solvent controls were included in each assay. The IC_{50} value was calculated by plotting percent growth versus test concentration.[23]

In Vivo MRSA Assay.[24] Mice (CD-1) were purchased from Harlan, Inc. (Houston, TX) and acclimatized up to 5 days before the test. Food and water were available *ad libitum* throughout the study. The mice were rendered neutropenic by two injections of cyclophosphamide (100 mg/kg) given intraperitoneally (i.p.), one and four days before infection. A volume of 50 μL suspension of MRSA ($1.5x10^6$ live organisms) was injected intramuscularly (im) into each of the two rear thighs. Each thigh was considered as an individual data point (a total of four data points for each treatment). These mice were randomly distributed into the control or treatment groups (n = 2/group).

Treatment with *E*,*E*-platanoside **1** (i.p.) was initiated 2 h after thigh inoculation. Control animals were concurrently administered saline (mock treatment) or vancomycin in the same volume as those receiving *E*,*E*-platanoside **1**. All animals were sacrificed after 48 h by CO_2 inhalation. Immediately following sacrifice, thigh tissue was collected from the animals, weighed, and homogenized in 5.0 mL of saline. Thigh muscle homogenate was processed for microbiological assay to determine the number of MRSA cfu/g of muscle tissue.[24,25]

CHAPTER II

PHOTOISOMERIZATION AS A MECHANISM TO ENHANCE BIOLOGICAL ACTIVITY AND CONTROL RESISTANCE IN *STAPHYLOCOCCUS AUREUS* AND METHICILLIN-RESISTANT *STAPHYLOCOCCUS AUREUS*

Bay Leaves

American Sycamore

Recently, our research group reported[26] the isolation and characterization of a group of four closely related anti-MRSA acylated kaempferol glycosides (platanosides); (Figure 1), isolated from *Platanus occidentalis* (American sycamore). We emphasized in our previous work the impact of changing the configuration from *E*- to *Z*- in the *p*-coumaric units on MRSA activity. We also showed that the isomerization from the kinetically favored *Z,Z*-platanoside (**4**) (IC_{50} 0.75 µg/mL) to the thermodynamically stable *E,E*-platanoside (**1**) (IC_{50} 6.16 µg/mL) was facilitated by an aqueous environment.

Here we report a simple, economical, and scalable "green" approach to transform the less active metabolite compound (**1**) to the most active metabolites (**2-4**) with the emphasis on the mechanism of isomerization and the biosynthesis of these metabolites. A similar approach was shown in 2008 by Fortin et al.[27] Fortin pointed out that photo-switchable affinity label (PAL) treatment in endogenous ion channels that do not rely on exogenous gene expression confers light sensitivity onto endogenous K+ channels permitting the change in configuration from *E*-azobenzene derivatives to the *Z*-isomers in isolated rat neurons, allowing rapid optical regulation of excitability without genetic modification. Moreover, Jiang reported the discovery of a bacterial photoreceptor similar to photoactive yellow protein, which is a 4-hydroxycinnamic acid-containing protein that functions as a blue-light photoreceptor in a behavioral avoidance response in the organism.[28]

RESULTS

SAR comparison between *Platanus occidentalis* and *Laurus nobilis* metabolites

Structural activity relationships were completed for this group of metabolites (**1-4**) relative to a closely related set of regioisomers isolated from *Laurus nobilis*, commonly called bay laurel or sweet bay. Leaves of bay laurel were shown by Otsuka et al., to possess anti-MRSA activity,[19] (Figures 39 and 40); kaempferol 3-*O*-*α*-L-(2",4"-di-*E*-*p*-coumaroyl)rhamnoside (**5**); (Figures 40, 41-47), and kaempferol 3-O-*α*-L-(2"-*Z*-*p*-coumaroyl-4"-*E*-*p*-coumaroyl)rhamnoside (**6**); (Figures 40, 48-49). Similar isolation schemes to those used for American sycamore were applied to bay leaves (Schemes 4 and 5).

The six isomers were shown by (+)-HRESIMS to possess similar masses with m/z 747.1647-747.1679, indicating the molecular formula to be $C_{39}H_{32}O_{14}Na$ $[M+Na]^+$. Structure assignment of the isolated glycosides was confirmed by examination of ^{1}H and ^{13}C NMR data and comparison with the reported data.[19] The anti-MRSA effects of the six metabolites confirmed the importance of changing the configuration on the *Staph. aureus* and MRSA activity as established by Ibrahim et al.[26] *Z*,*Z*-platanoside (**4**) shows an IC_{50} 0.75 µg/mL while *E*,*E*-platanoside (**1**) shows an IC_{50} 6.16 µg/mL, (Table 5). Interestingly, changing the regiochemistry on the rhamnose moiety from (2, 3) to (2, 4) was shown to be crucial for MRSA activity where kaempferol 3-*O*-*α*-L-(2",4"-di-*E*-*p*-coumaroyl)rhamnoside (**5**) shows an IC_{50} 0.53 µg/mL compared to 6.16 µg/mL for compound (**1**); (Table 5).

For a better understanding of the SAR of the isolated glycosides, the commercially available quercitrin (**7**) and *E*-*p*-coumaric acid (**8**) as two primary moieties in the glycoside structures, (Figure 40), were tested against MRSA and *Staph. aureus*, (Table 5). Both

compounds did not show any recognizable activity against MRSA and *Staph. aureus*. The kaempferol glycoside should be acylated with at least one *p*-coumaroyl unit and this is consistent with what was reported by Otsuka et al. in the MRSA activity of compounds (**5**) and (**6**), referred to as 2,4-*E*,*E*-platanoside and 2,4-*Z*,*E*-platanoside.[19] A similar trend was shown when evaluating these metabolites against *Enterococcus faecalis* (Table 5), where *E*,*E* and *Z*,*Z*-platanosides (**1**) and (**4**) show IC_{50} values of 11.15 and 2.67 µg/mL, respectively. Parallel with MRSA, changing the regiochemistry of the rhamnose moiety from (2, 3) to (2, 4) affects *E. faecalis* activity to a great extent, where 2,4-*E*,*E*-platanoside (**5**) shows an IC_{50} value of 3.09 µg/mL compared to 11.15 µg/mL for *E*,*E*-platanoside (**1**), (Table 5).

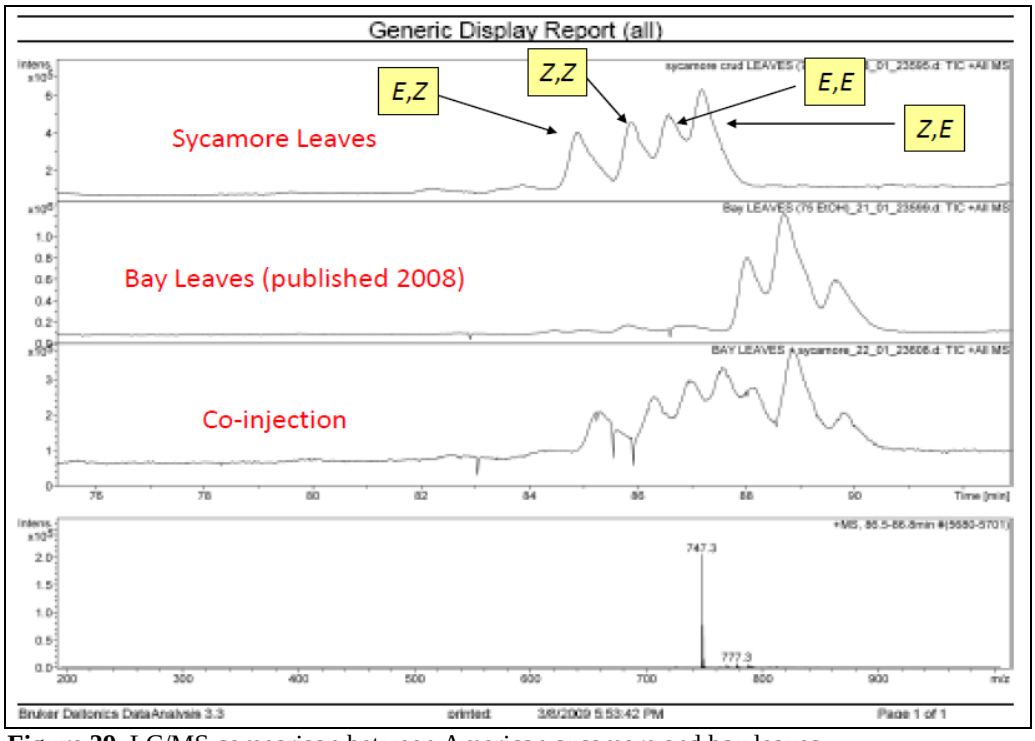

Figure 39. LC/MS comparison between American sycamore and bay leaves

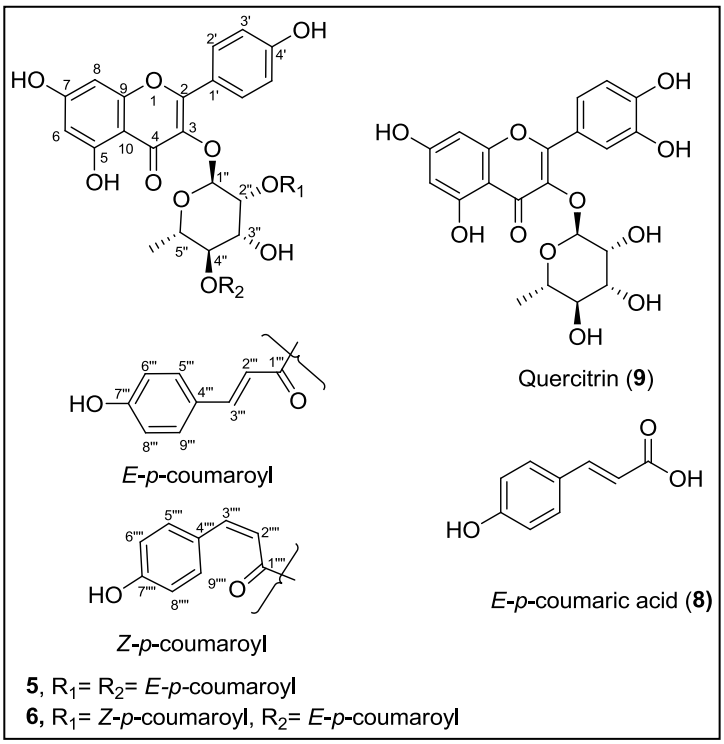

Figure 40. Structures of *Laurus nobilis* metabolites, quercitrin, and *E-p*-coumaric acid

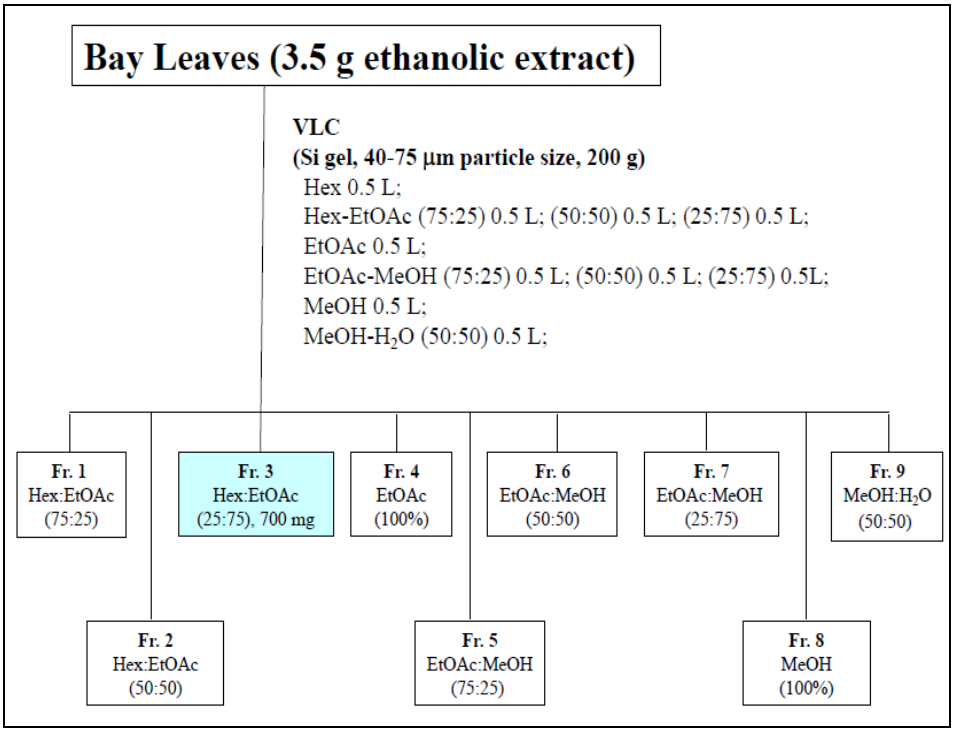

Scheme 4. Fractionation of 3.5 g bay leaves ethanolic extract using VLC, blue color indicated the presence of the bay leaf glycosides

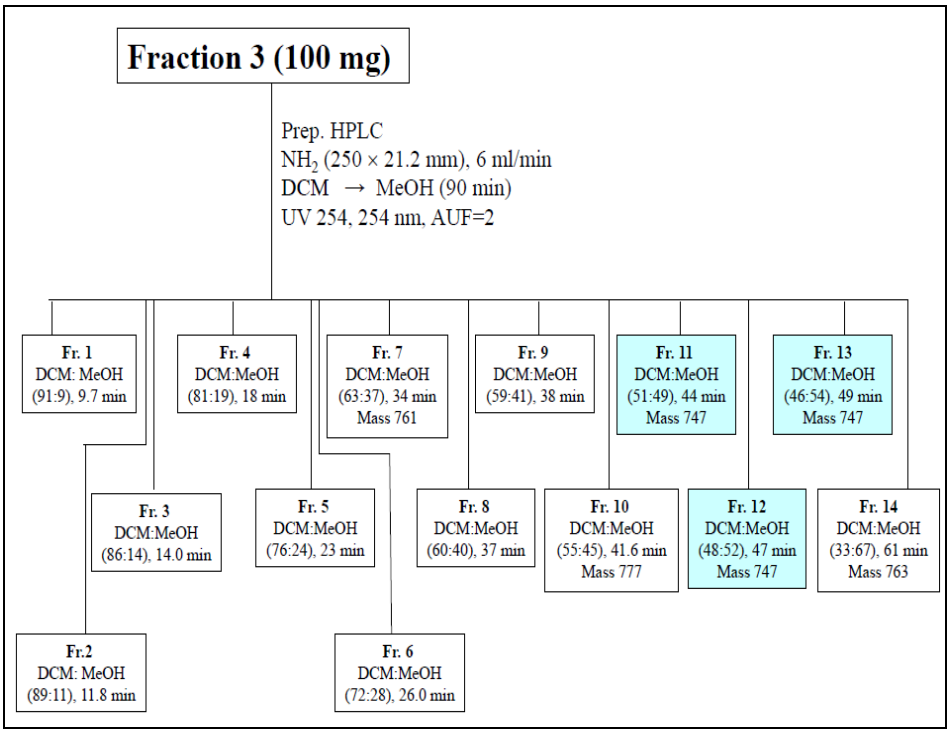

Scheme 5. Fractionation of Fr. **3**; Hex-EtOAc (25:75) on 250 x 21.2 mm NH_2 column, blue color indicated the presence of the bay leaf glycosides

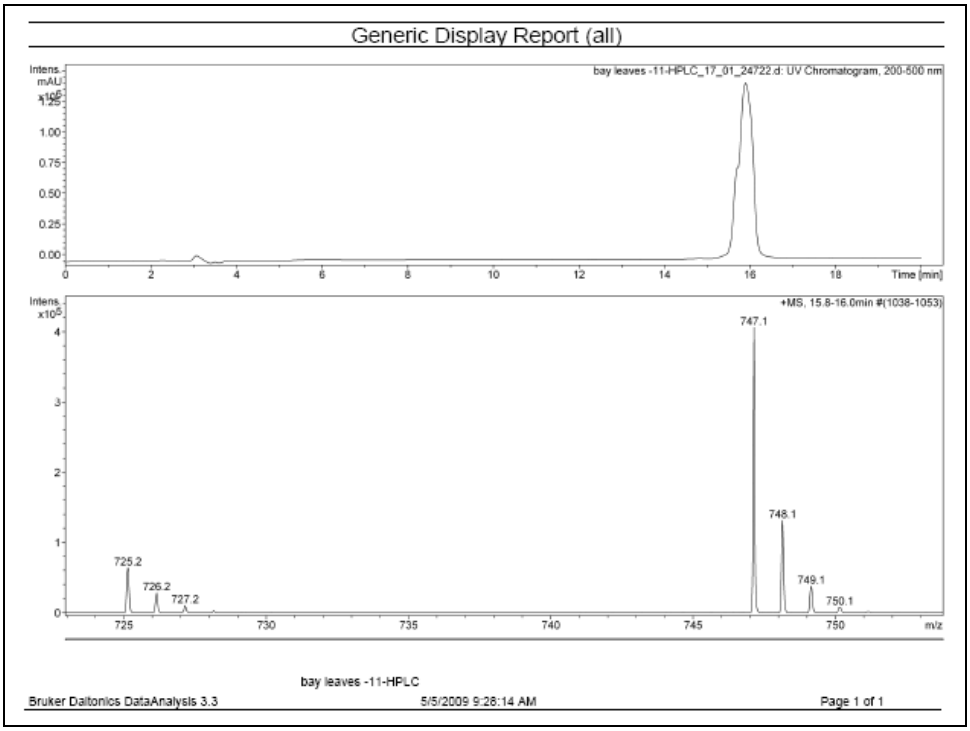

Figure 41. LC/MS chromatogram of 2,4-*E*,*E*-platanoside

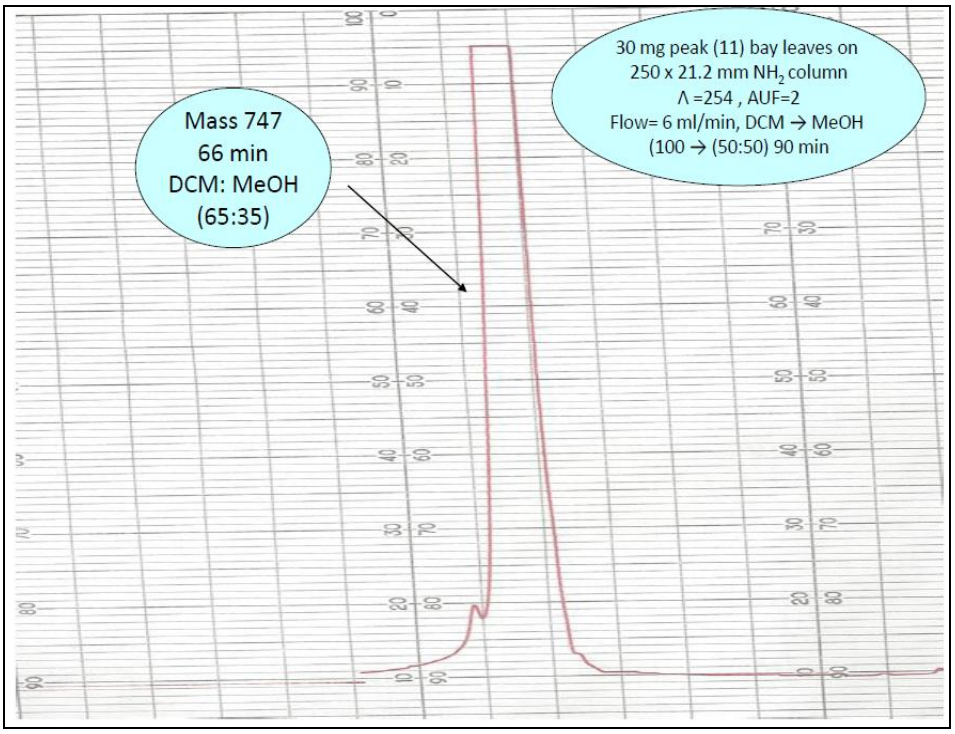

Figure 42. Final purification of 2,4-*E*,*E*-platanoside on 250 x 21.2 mm NH_2 column

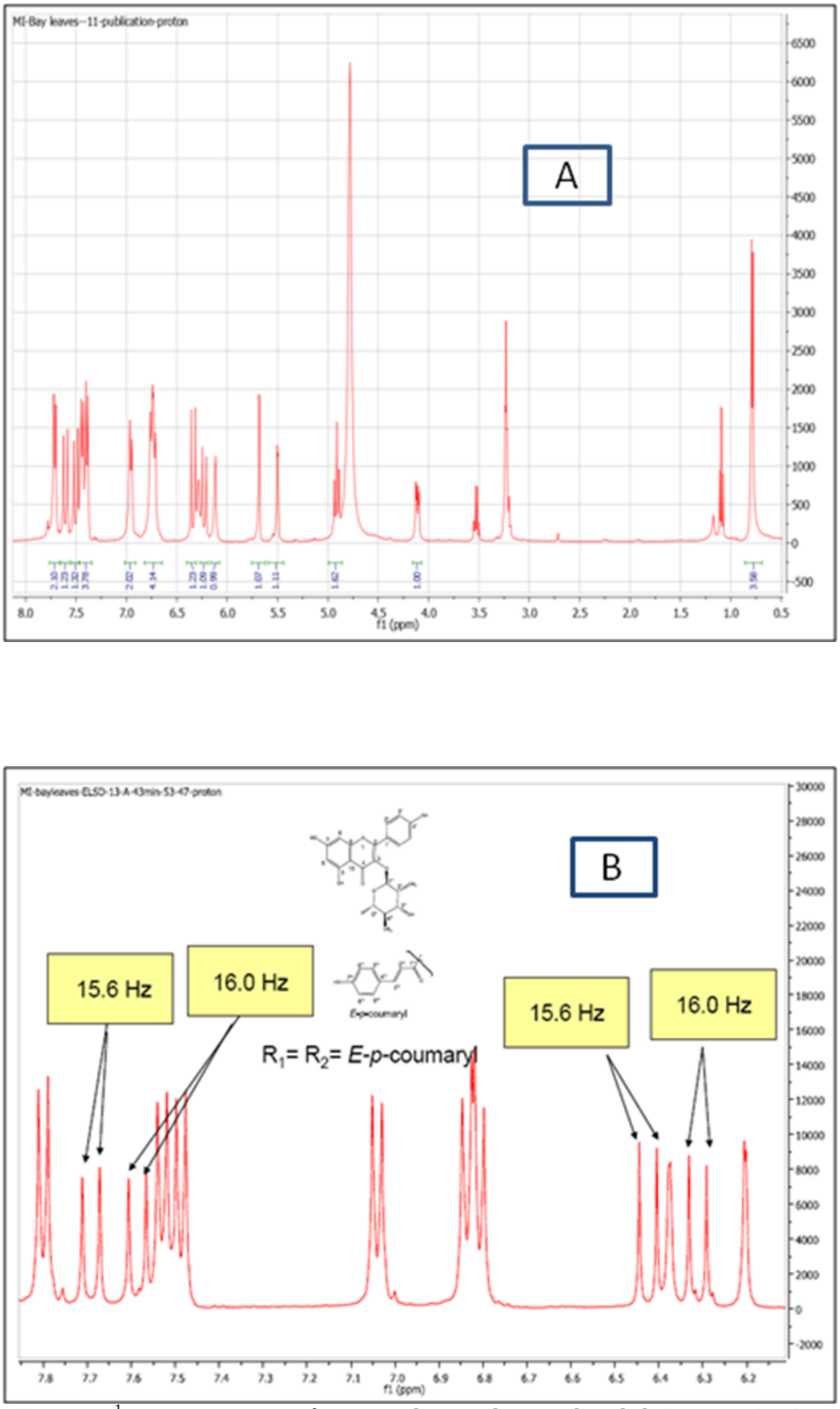

Figure 43. [1]H NMR spectrum of 2,4-*E*,*E*-platanoside in methanol-d_4 (400 MHz); A) the full spectrum, B) the downfield region

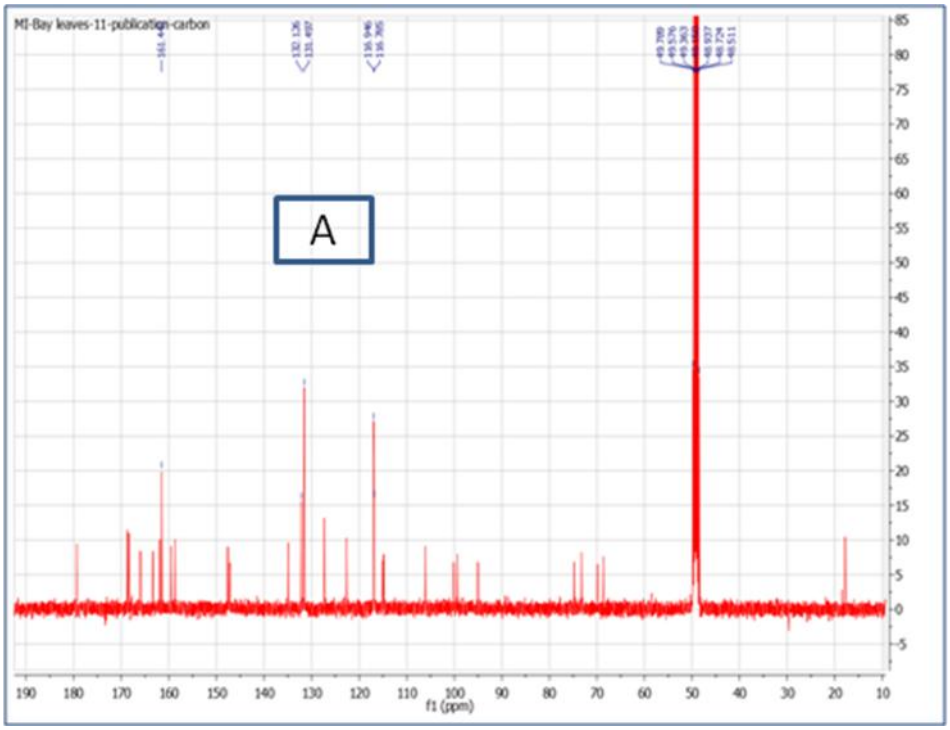

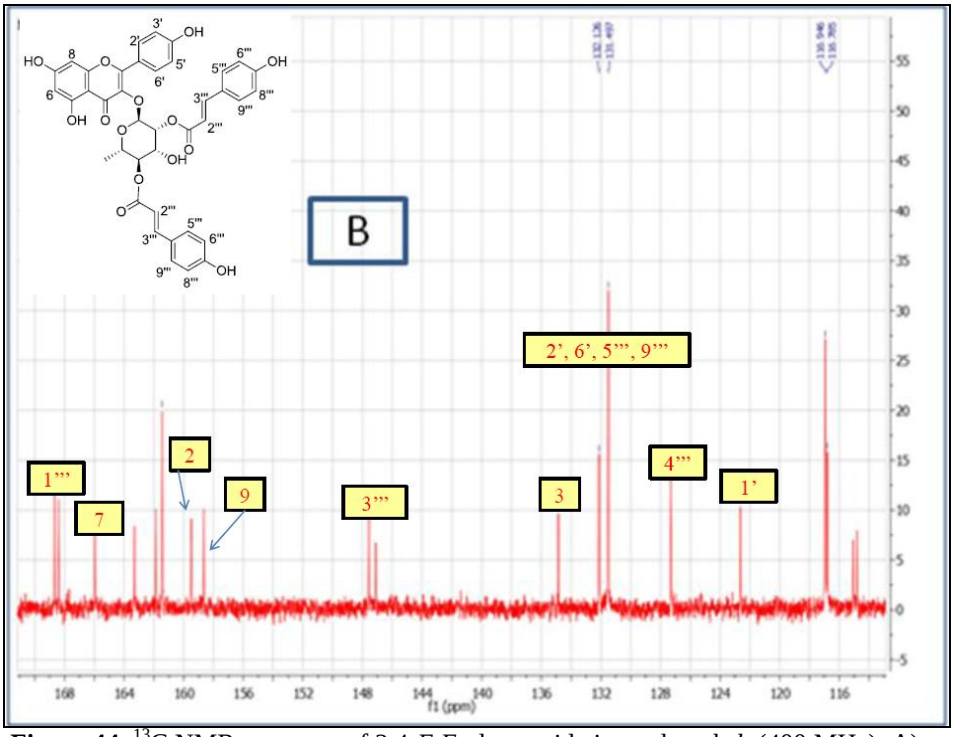

Figure 44. ^{13}C NMR spectrum of 2,4-*E*,*E*-platanoside in methanol-d_4 (400 MHz); A) the full spectrum, B) the downfield region

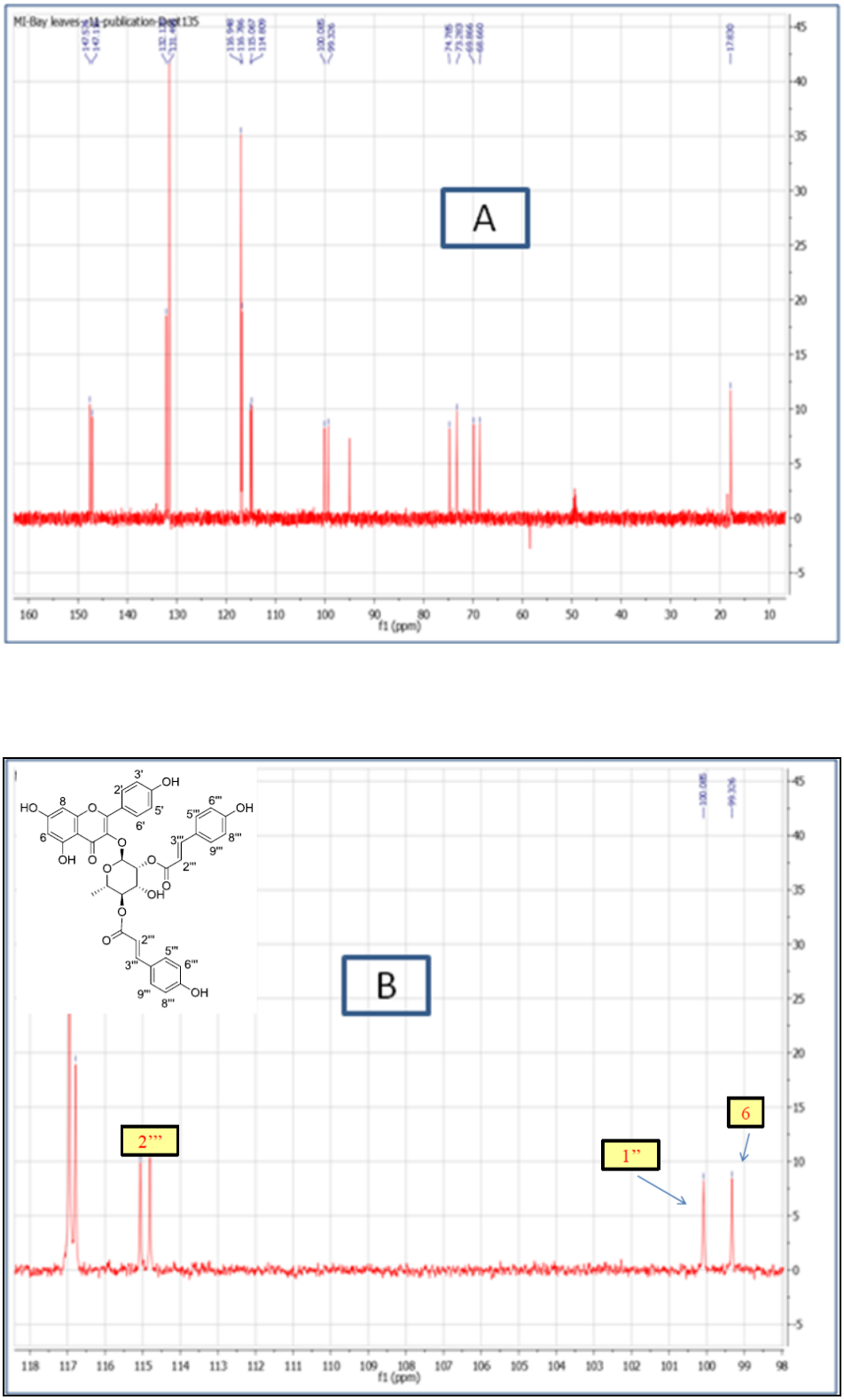

Figure 45. 135º DEPT spectrum of 2,4-*E*,*E*-platanoside in methanol-d_4 (400 MHz); A) the full spectrum, B) the downfield region

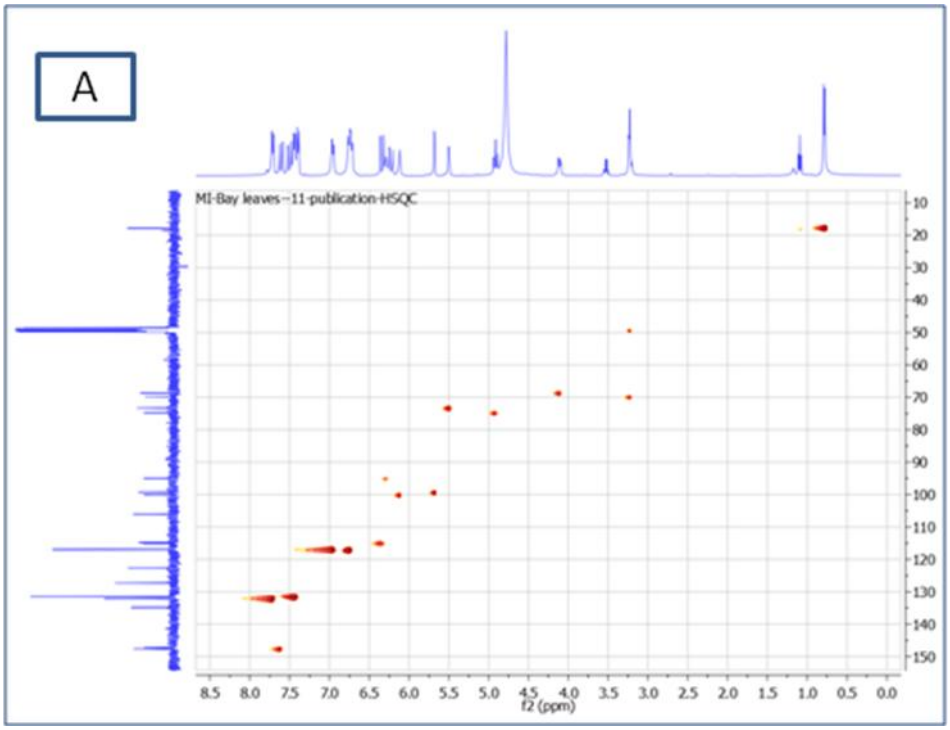

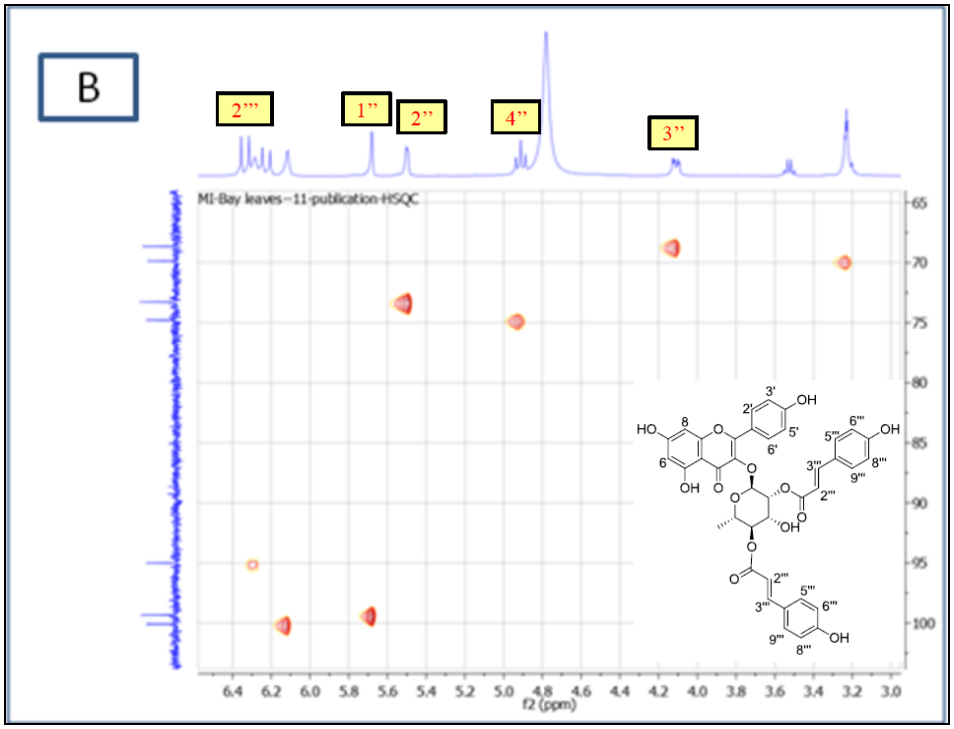

Figure 46. HSQC spectrum of 2,4-*E*,*E*-platanoside in methanol-d_4 (400 MHz); A) the full spectrum, B) the downfield region

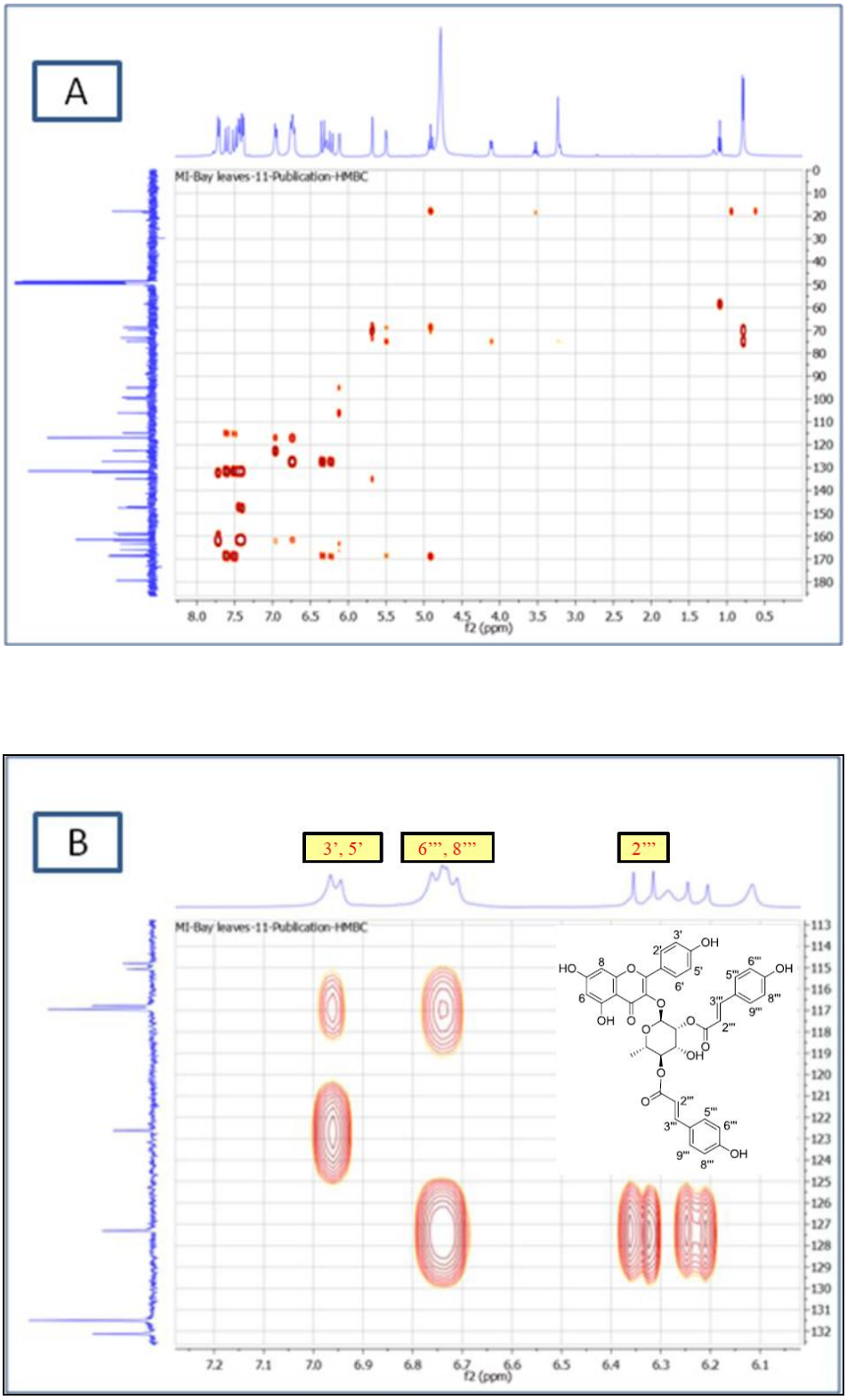

Figure 47. HMBC spectrum of 2,4-*E*,*E*-platanoside in methanol-d_4 (400 MHz); A) the full spectrum, B) the downfield region

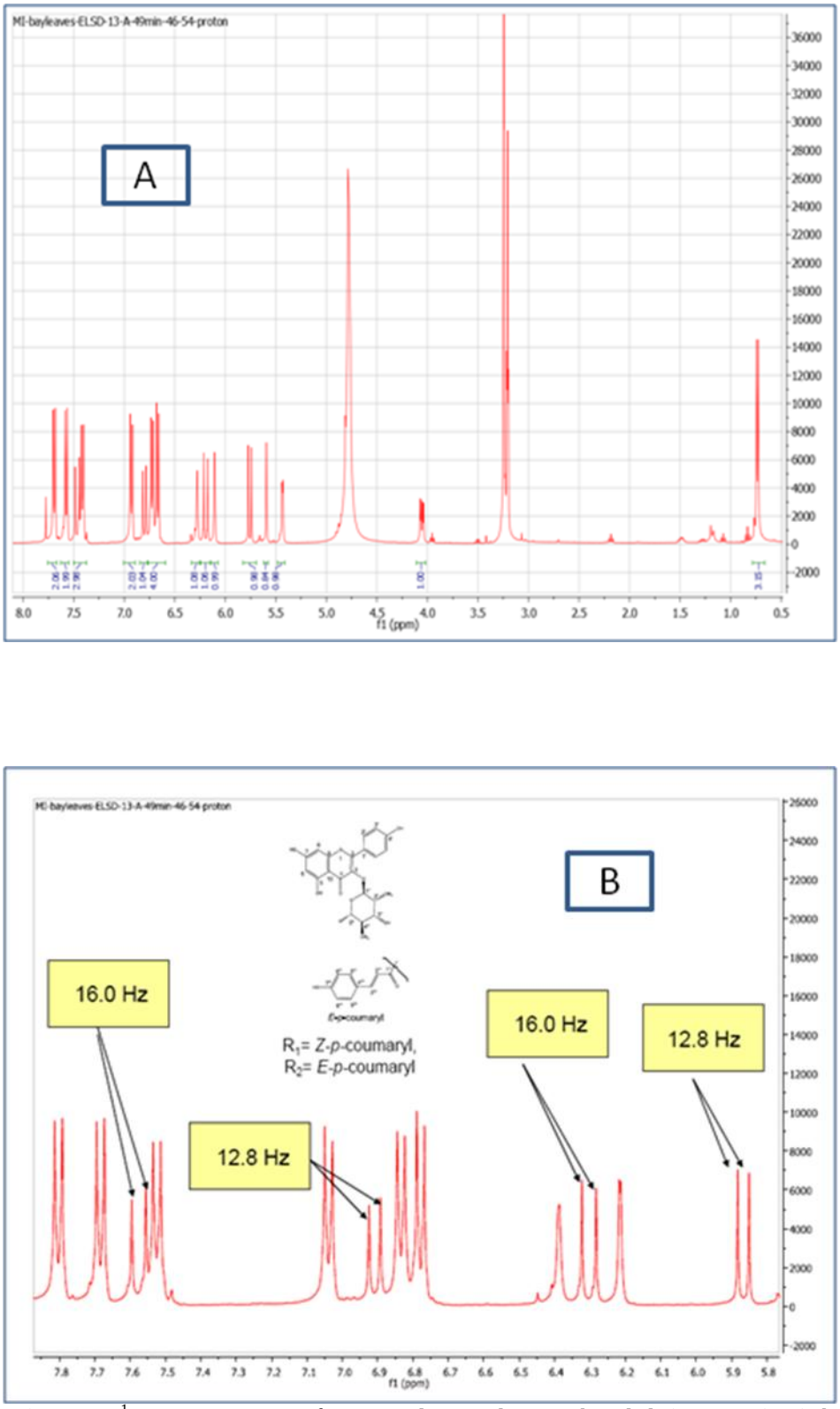

Figure 48. ^{1}H NMR spectrum of 2,4-*Z*,*E*-platanoside in methanol-d_4 (400 MHz); A) the full spectrum, B) the downfield region

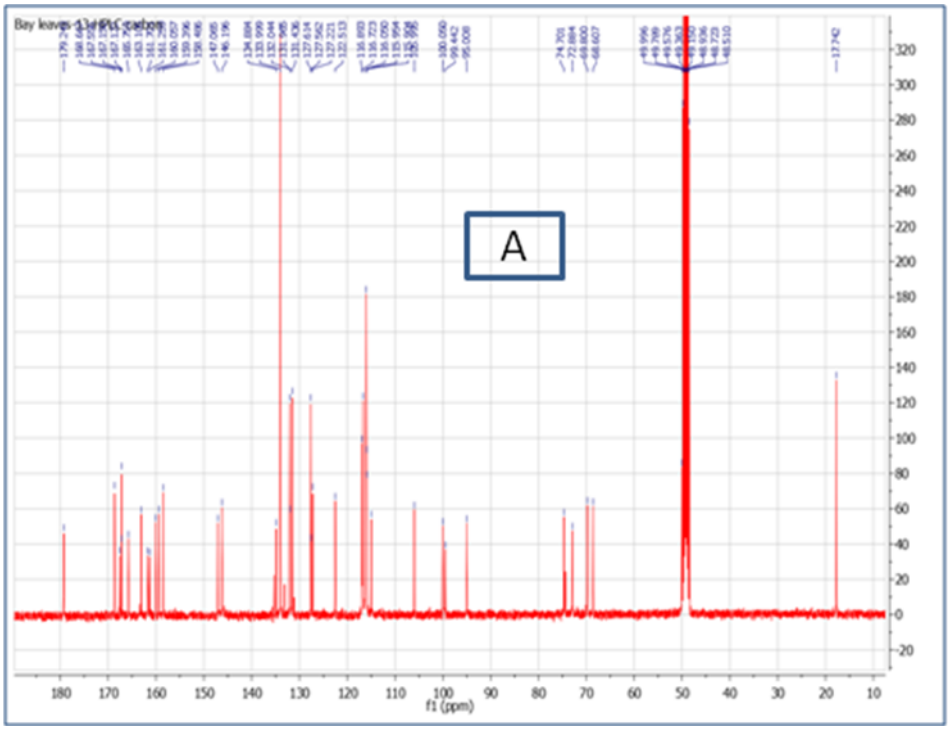

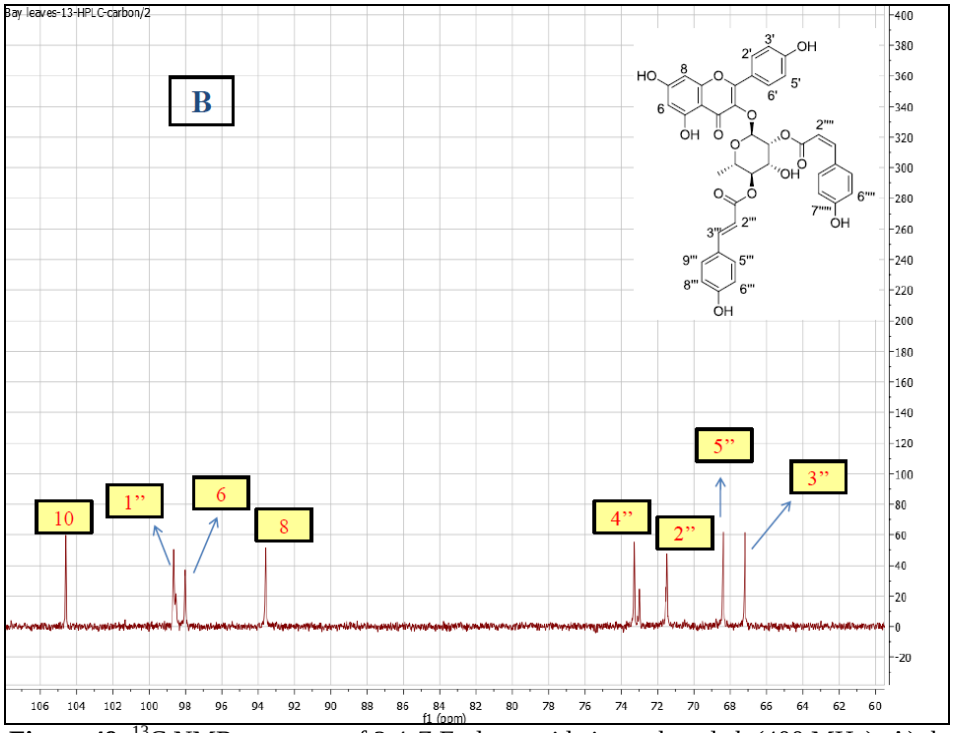

Figure 49. ^{13}C NMR spectrum of 2,4-*Z*,*E*-platanoside in methanol-d_4 (400 MHz); A) the full spectrum, B) the downfield region

Isomerization of *Z,Z*-Platanoside (4) in Aqueous Medium.

During the isolation process, we encountered some difficulties due to rapid isomerization of the most active metabolite, *Z,Z*-platanoside (**4**) in aqueous medium to the less active metabolites (**1**-**3**). This, in turn, agrees with what was reported by Leenders et al.[29] Leenders showed that the solvation of *p*-coumaric acid in water increases its polarization which in turn facilitates its isomerization rate. A similar trend was shown for *Z,Z*-platanoside (**4**), (Figure 3).

Alkylation of *E,E*-Platanoside (1).

We investigated the alkylation route as a possible method to disrupt the conjugation demonstrated in Figure 50 by decreasing the electron-flow that was assumed to cause *Z*- to *E*-isomerization in the most active *Z,Z*-platanoside (**4**) as well as a possible means to increase the activity of the less active isomer (**1**). Various alkylating agents were utilized, including methyltrifluoromethanesulfonate, without success.

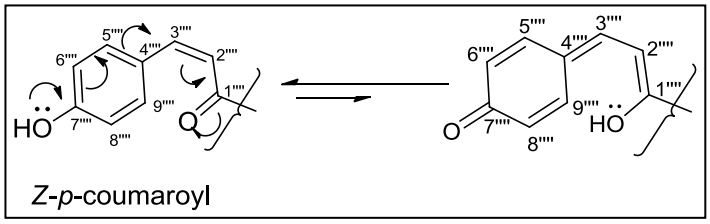

Figure 50. Possible conjugation in *Z,Z*-platanoside

Finally, utilizing methyl iodide in the presence of DMF containing K_2CO_3 and stirring at room temperature for 5-6 days yielded 10-15% alkylated product (Scheme 6). The purified methylated *E,E*-platanoside (**9**), (Figures 51-54), was shown by (+)-ESIMS to possess a mass with *m/z* 803.2; inferring the formula to be $C_{43}H_{40}O_{14}Na$ $[M+Na]^+$, matched with the introduction of four methyl groups. Structure assignment was confirmed by examination of 1D

^{1}H and ^{13}C NMR spectra as well as the 2D HSQC and HMBC data, where the four (*O*-methyl groups) show HMBC correlations to C-7, C-4' and the C-7''' (X2). The product, shown to be inactive in the MRSA assay, suggested the importance of the presence of free (OH-groups) groups at any or both of these positions for the MRSA activity.

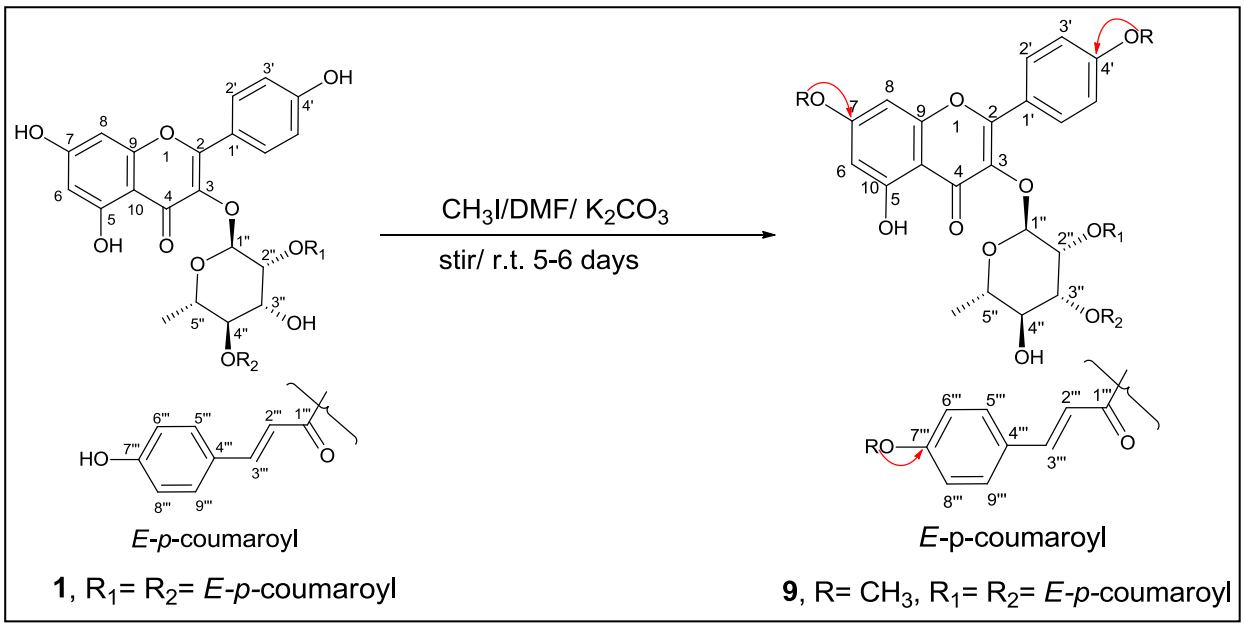

Scheme 6. Alkylation of *E*,*E*-platanoside

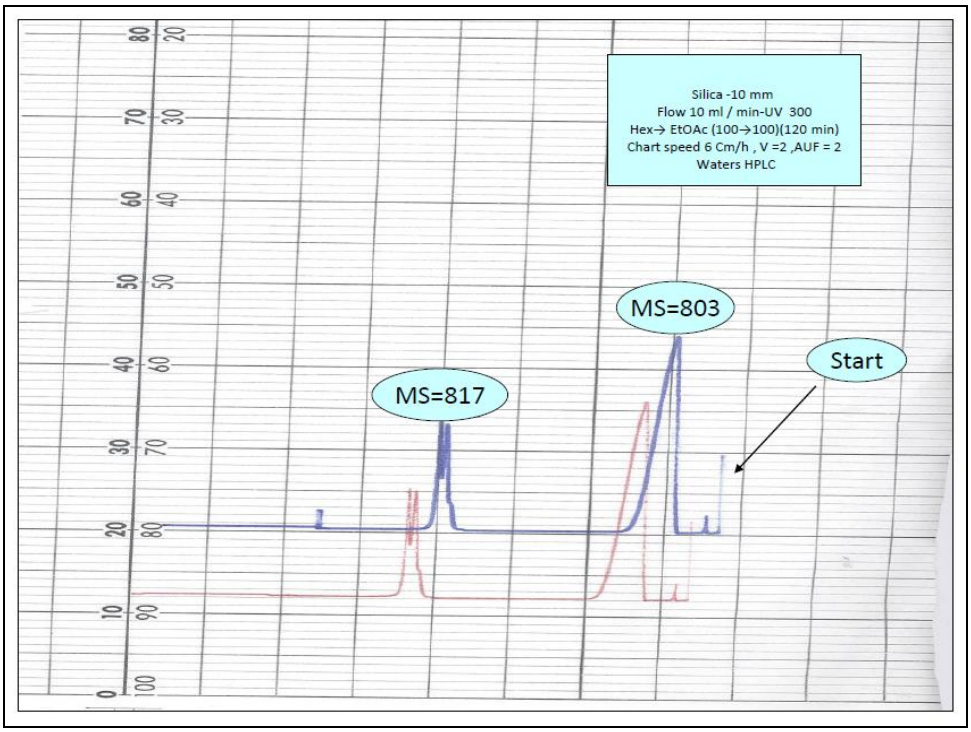

Figure 51. Purification of tetra-*O*-methyl-*E*,*E*-platanoside (**9**) on 250 x 10 mm Si HPLC column

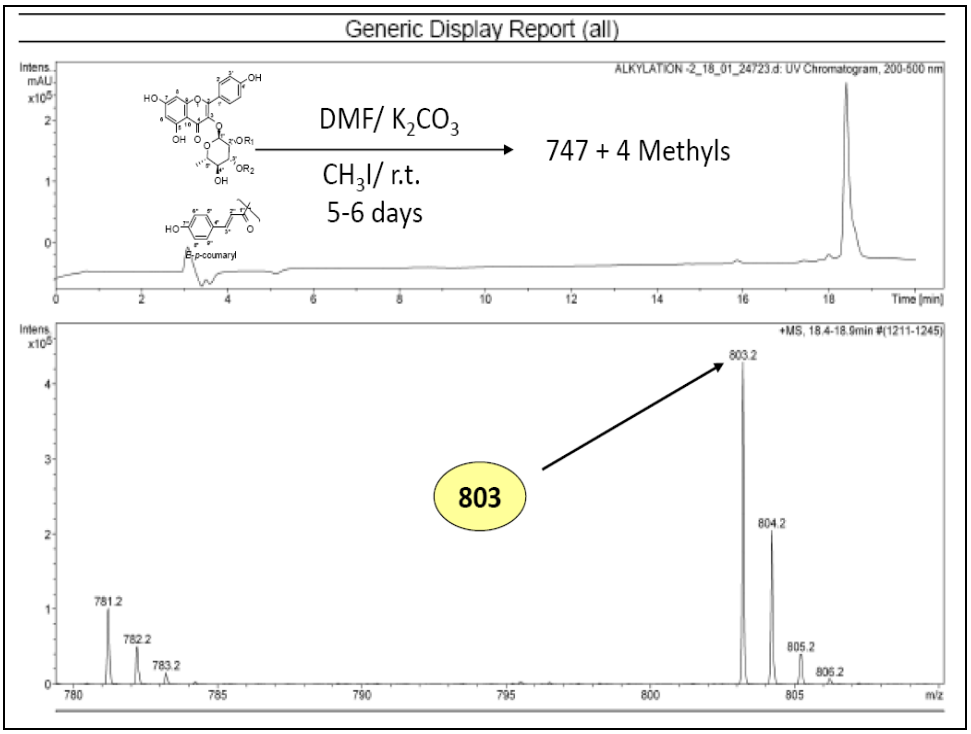

Figure 52. LC/MS chromatogram of tetra-*O*-methyl-*E*,*E*-platanoside (**9**)

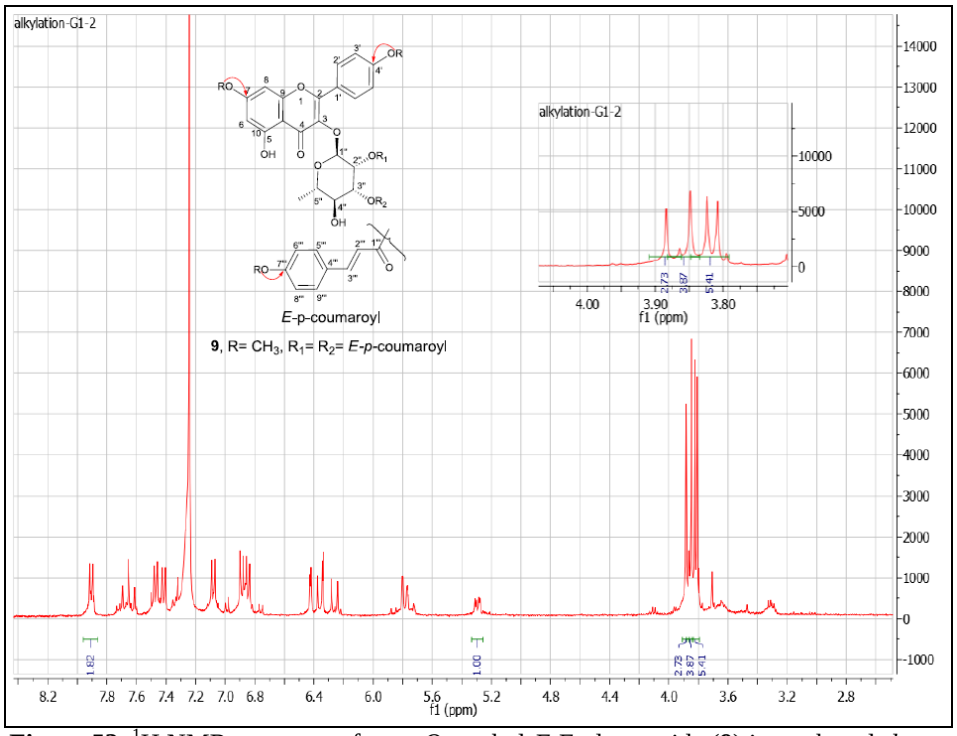

Figure 53. ^{1}H NMR spectrum of tetra-*O*-methyl-*E*,*E*-platanoside (**9**) in methanol-d_4 (400 MHz)

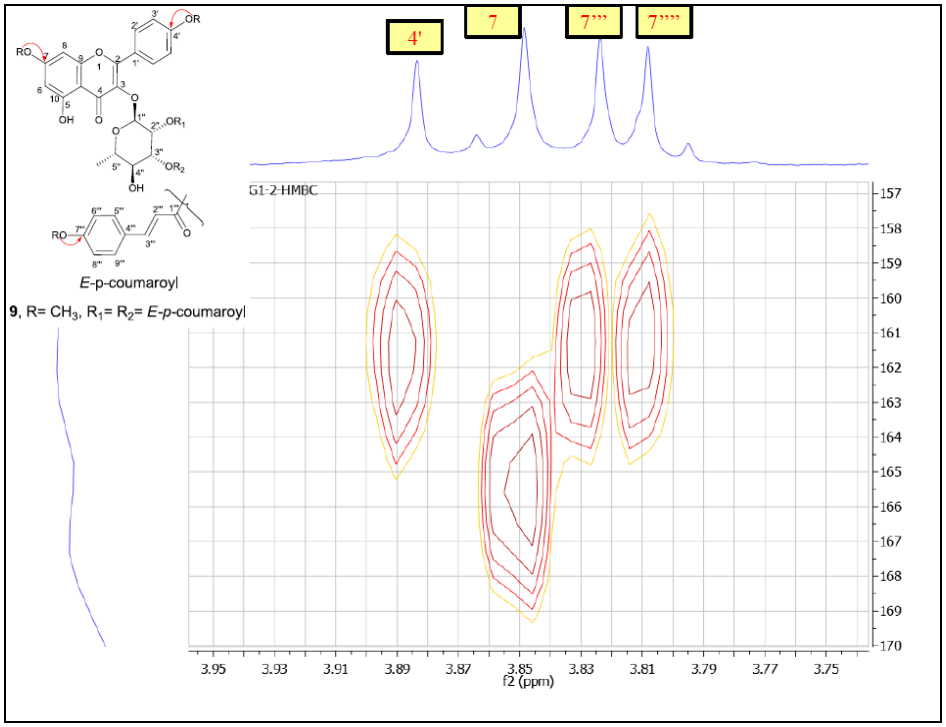

Figure 54. Selected HMBC correlations of tetra-*O*-methyl-*E*,*E*-platanoside (**9**) in methanol-d_4 (500 MHz)

Table 5. In vitro antimicrobial activity of compounds **1-9**

Compound	MRSA 33591			*Staph. aureus* 29213			*E. faecalis* 29212		
	IC_{50}	MIC	MBC	IC_{50}	MIC	MBC	IC_{50}	MIC	MBC
(1)	6.16	NA	NA	5.77	NA	NA	11.15	20	NA
(2)	1.93	8.33	NA	2.65	10.00	NA	3.38	10.00	NA
(3)	1.46	6.67	NA	2.85	10.00	NA	3.10	5.00	NA
(4)	0.75	2.08	NA	1.72	5.00	NA	2.67	5.00	NA
(5)	0.53	1.67	NA	0.46	1.25	NA	3.09	10.00	NA
(6)	0.73	1.67	NA	0.63	1.67	NA	3.25	6.67	NA
(7)	NA	NA	NA	NA	NA	NA	-	-	-
(8)	NA	NA	NA	NA	NA	NA	-	-	-
(9)	NA	NA	NA	NA	NA	NA	-	-	-
Methicillin	NA	NA	NA	0.43	1.56	1.56	20.52	50.00	50.00
Erythromycin	NA	NA	NA	0.16	0.63	1.25	3.85	5.00	5.00
Ciprofloxacin	0.12	0.58	0.67	0.09	0.33	0.42	0.41	0.83	NA

IC_{50} = the concentration that affords 50% inhibition of growth (µg/mL); MIC (Minimum Inhibitory Concentration µg/mL) is the lowest test concentration that allows no detectable growth; Minimum Bactericidal Concentration (MBC) is the lowest test concentration that kills the organism (µg/mL). NA = not active at the highest test concentration (20 µg/mL). (-), not tested.

Light-Activated Isomerization of *E,E*-Platanoside (1)

From the previous set of in vitro data, it is clear that the key transformation to improve the activity is to transform the less active *E*-isomer (**1**) to the most active *Z*-isomers (**2-4**). There was an urgent need for this transformation, especially after these compounds showed an impressive ability to inhibit MRSA growth on contaminated surfaces similar to those present in hospitals (a Thin Layer Chromatograpghy plate; TLC is used as a model surface) (Figure 55), which encouraged Triton Biopharma AG to file a patent for this group of metabolites for controlling MRSA.

Numerous trials were conducted to achieve this required isomerization utilizing commercially

available *E*-*p*-coumaric acid as a model compound, considering that the *Z*-*p*-coumaric is not available commercially. Finally we achieved a 10-20% yield of *Z*-*p*-coumaric acid using a simple green chemistry approach via UV irradiation at 365 nm / methanol-d_4 for 4-6 h. Applying the same procedure for the less active *E*,*E*-platanoside (**1**) enabled us to produce 10-15% of the most active isomers (**2**-**4**) after irradiation at 365 nm / methanol-d_4 for 12 h. The formation of the other three active metabolites may readily be detected by LC/MS spectrum (Figure 56). By extending the reaction time from 12 to 24 h, the yield of isomerization was improved by 20%.

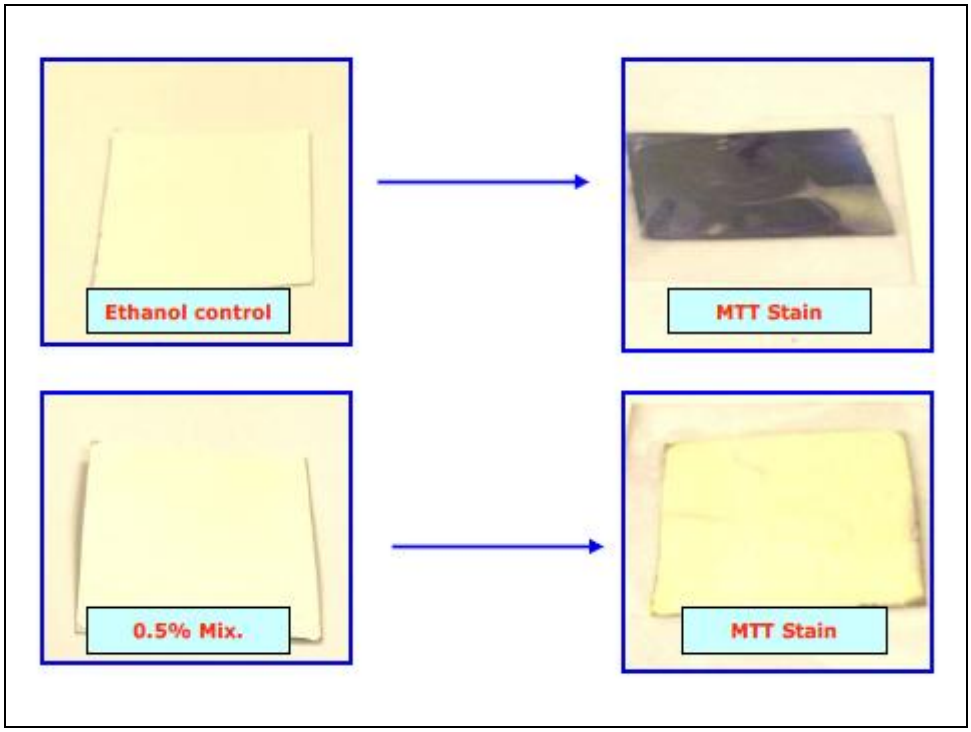

Figure 55. Application of 0.5% mixture platanosides (**1**-**4**) on TLC plates contaminated with MRSA

Chlorophyll has been shown previously to be a natural photosynthetizer.[30] One of our goals was to evaluate the role of chlorophyll in controlling the photoisomerization process. For this study, commercially available *E*-*p*-coumaric acid was used as a model, and chlorophylls (a, b) were isolated from American sycamore according to the simple approach reported by Iriyama et al.[31] Interestingly, UV-irradiation of a mixture of 90% *E*-*p*-coumaric and 10% chlorophylls (a, b) shows inhibition of the isomerization process with an overall yield of 4-6 % (Figure 57). The same result has been obtained by applying the same conditions to compound (**1**). This supports the hypothesis that the antioxidant properties of chlorophyll stabilize the equilibrium between the isolated isomers (**1-4**).

This "green" approach for increasing the activity was shown to be highly important as far as the amount of plant extract needed to produce the most active metabolites. Interestingly, these data supported the light mediated-biosynthetic formation of the *Z*-isomers (**2-4**) through two possible pathways. The first pathway involved UV-induced isomerization of *E*- to *Z*-*p*-coumaric acid, followed by acylation of the kaempferol glycoside. The second pathway involves UV irradiation of glycoside (**1**) or (**5**) to produce metabolites (**2-4**, and **6**); (Figure 58) without genetic modification.

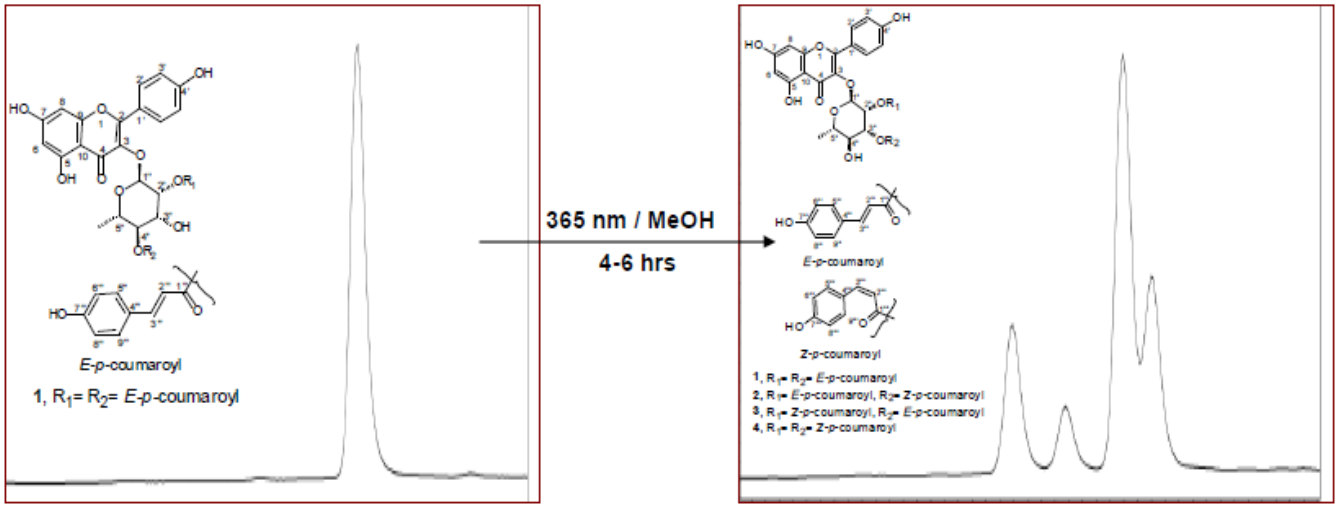

Figure 56. The formation of the three active metabolites (**2-4**) through UV irradiation of *E*,*E*-platanoside

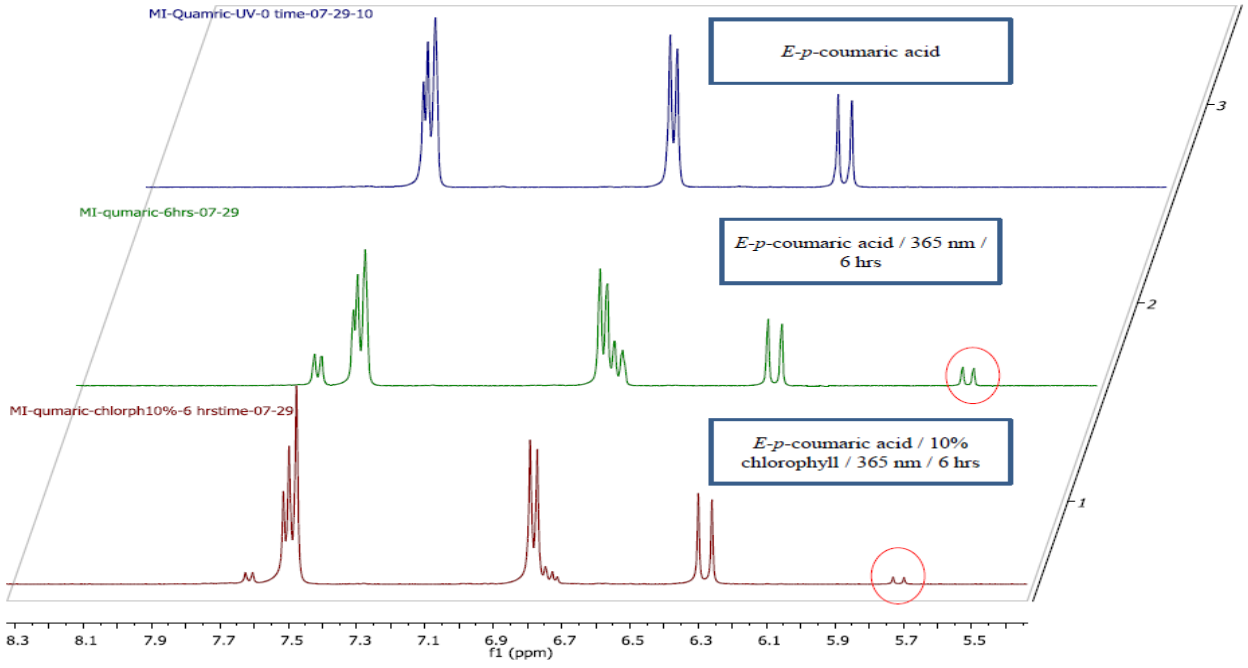

Figure 57. Effect of chlorophyll on the isomerization of *E*-*p*-coumaric acid, the *Z*-signal showed up at 5.5-5.7 ppm

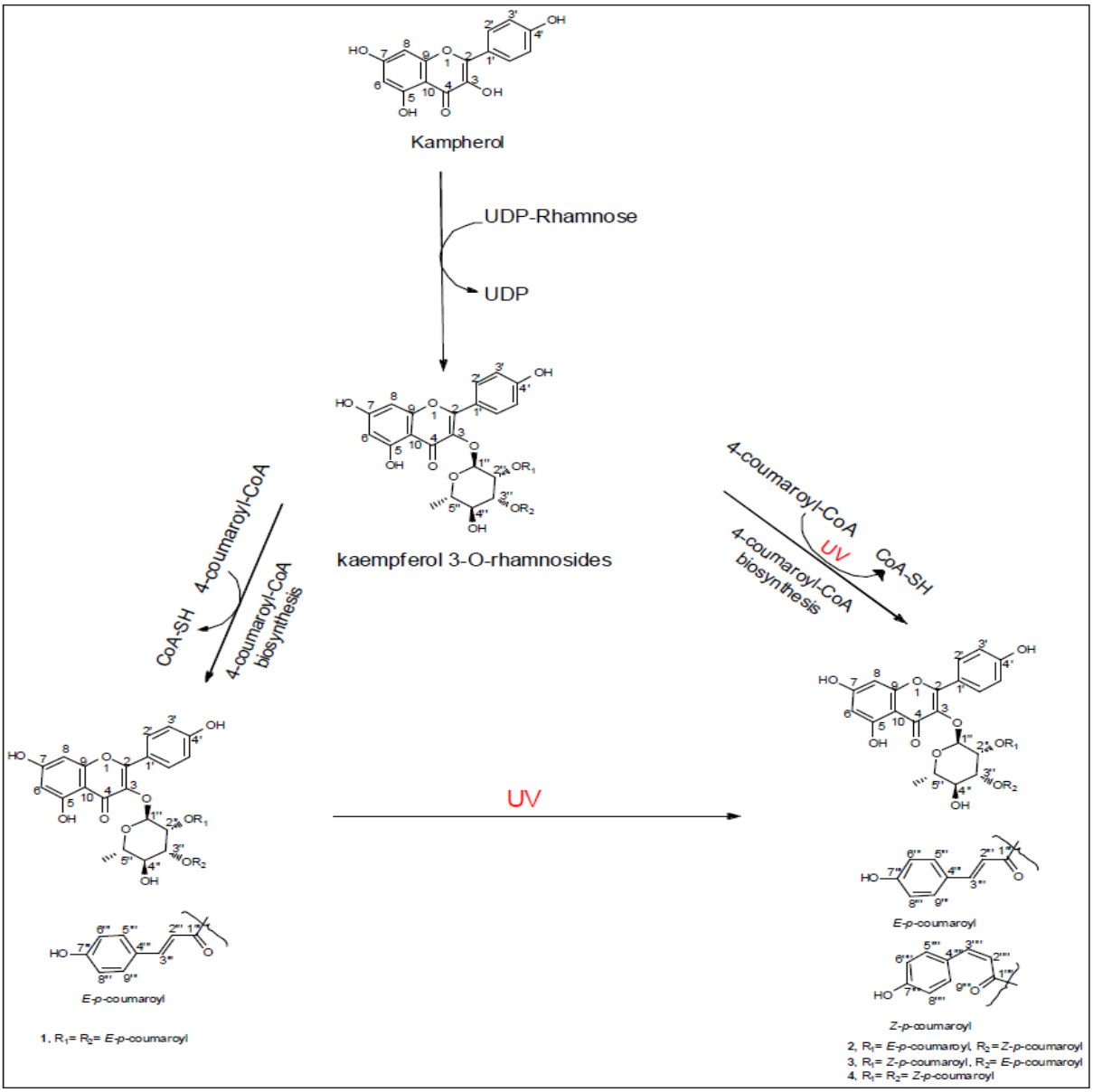

Figure 58. The suggested biosynthetic formation of the *Z*-metabolites (**2-4**)

The effect of solvent on the isomerization process was studied by conducting the isomerization in various protic and aprotic solvents (Figure 59). The results confirmed the importance of protic solvents for H-bond formation to facilitate the polarization of *E-p*-coumaric acid which in turn facilitates the isomerization process. These data are consistent with that reported in 2009 by Sigala et al.,[32] showing the hydrogen bond dynamics in the active site of photoactive yellow protein.

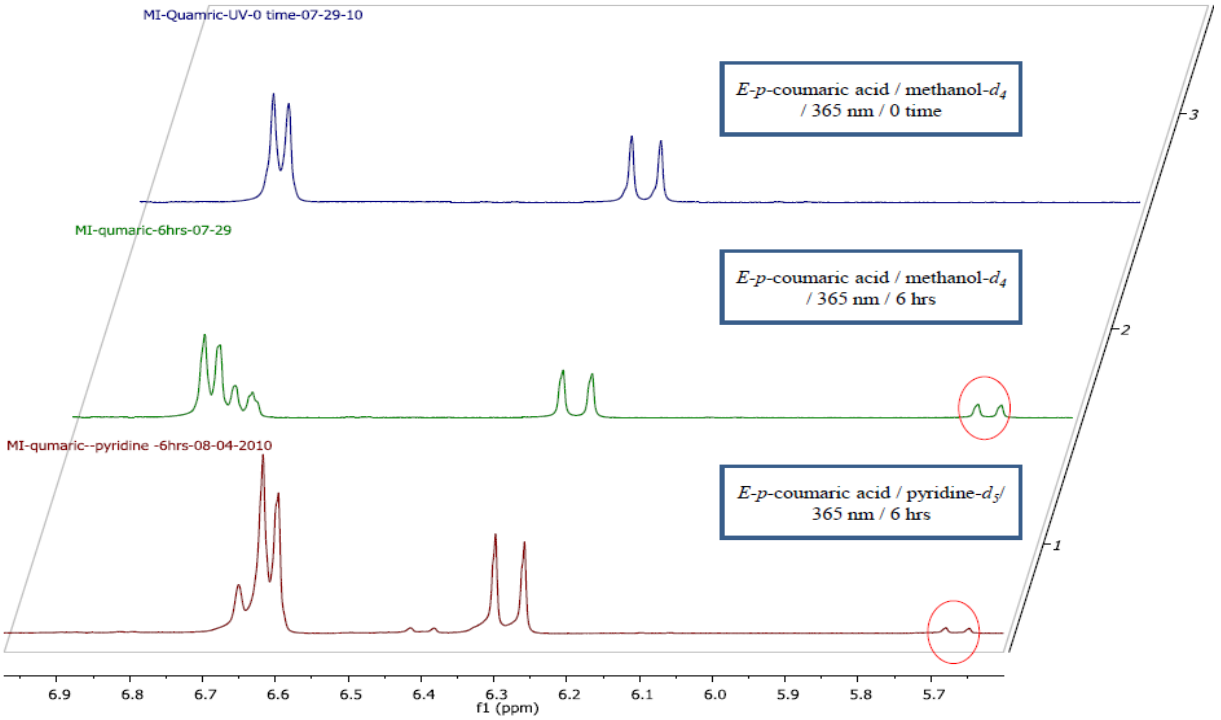

Figure 59. Effect of solvent (H-bonding) on the isomerization of *E-p*-coumaric acid, the *Z*-signal showed up at 5.5-5.7 ppm

The mechanism of the isomerization was tested for the presence of a radical intermediate utilizing butylated hydroxytoluene (BHT), a common radical capture compound. However, no radical species could be detected (Figure 60), suggesting the absence of a radical mechanism and the possibility of an sp^2-sp^3 carbon-interchange mechanism.

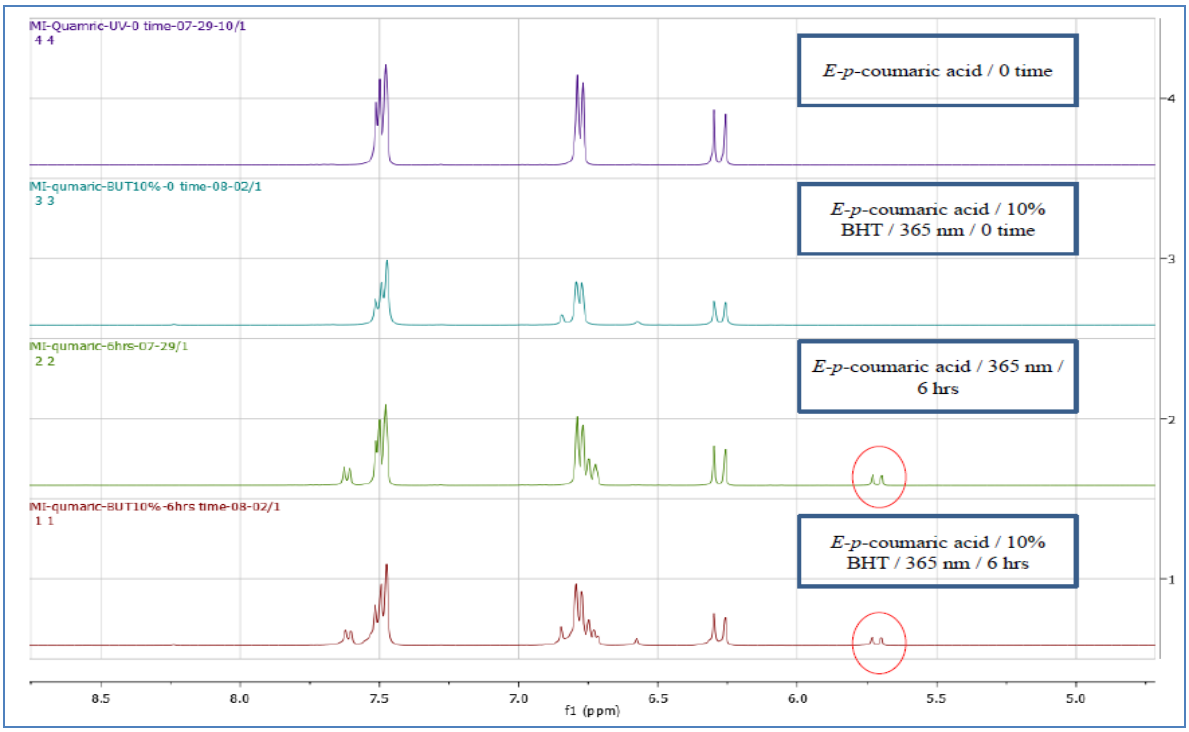

Figure 60. Effect of BHT on the isomerization of *E-p*-coumaric acid

Discussion

Platanosides have shown importance as drug leads with a high safety margin especially against methicillin-resistant *Staphylococcus aureus* (MRSA).[26] Table 5 shows the bacteriostatic activity of the isolated compounds (**1**-**6**) against MRSA. In addition, all metabolites were relatively inactive against other test organisms, including the Gram-negative bacteria *Escherichia coli* and *Pseudomonas aeruginosa*, as well as other microorganisms *Mycobacterium intracellulare*, *Candida albicans*, *Cryptococcus neoformans*, and *Aspergillus fumigatus* at maximum concentrations of 100 μg/mL, confirming the selectivity of this group of metabolites. In vitro Vero cell (kidney fibroblast cells) cytotoxicity was not observed up to the maximum dose of 100 μg/mL. The effect of changing the olefinic configuration in the *p*-coumaroyl units or changing the regiochemistry in the sugar moiety, was confirmed to be crucial for the *Staph.aureus* and MRSA activities. The rapid isomerization of the most active and least stable metabolites to the less active ones hampered the use of this group of compounds as drug candidates. We addressed these major obstacles, demonstrating a simple and clean approach to enhance the activity (5≈10 times) against MRSA that may improve the marketing of these compounds.

Methods

General Experimental Procedures. The 1D and 2D NMR spectra were measured on a Bruker AV NMR spectrometer (Bruker Biospin, Bruker Inc.) operating at 400 MHz, and the chemical shift (δ) values are expressed in ppm. Mass spectra were measured using a Bruker micrOTOF (Bruker Daltonics, Bruker Inc.) with an ESI ionization source. HPLC was carried out on a Waters Prep-LC with a 2487 dual absorbance detector.

Isolation and Purification of Metabolites (1-6). The leaves and stems of *P. occidentalis* were collected in August 2008 from the University of Mississippi Field Station, Oxford, MS. *Laurus nobilis*

leaves were purchased from American Mercantile Corporation in Memphis, TN. One kilogram of air-dried leaves of *P. occidentalis* was extracted at room temperature with EtOH (95%) yielding 50.0 g of extract residue. Fifty grams of the ethanolic extract were subjected to silica gel vacuum-liquid chromatography (VLC), yielding an active fraction from the EtOAc-MeOH (75:25) (7 g) eluate. Bioassay-guided fractionation and purification of this fraction utilized HPLC at room temperature, a Luna C_8 column (250 × 150 mm, Phenomenex, Inc.), using H_2O-CH_3CN (100→100, 90 min, λ 300 nm) in which the active fraction eluted with H_2O-CH_3CN (5:95, 85 min). Following this, a Luna NH_2 column (250 × 21.20 mm, Phenomenex, Inc.) was used with *n*-hexane-CH_2Cl_2 (100→100, 30 min) and then CH_2Cl_2-MeOH (100→100, 30 min, λ 300 nm), yielding three well-resolved signals. All of the signals eluted with 100% MeOH: the first at 65 min (**1**) (20 mg), the second representing two metabolites at 77 min (**2** and **3**) (10 mg), and the third at 101 min (**4**) (3 mg). Final purification of glycosides **2** and **3** was done using a PFP-2 (pentafluorophenyl) (250×10 mm, Phenomenex Inc.) column with CH_3CN-H_2O (0→100, 120, λ= 300 nm). Glycosides **2** and **3** eluted with CH_3CN-H_2O (50:50, λ= 300 nm) with retention times of 90 and 91 min, respectively. These four glycosides together represent 0.02-0.05% of leaf dry weight and the percentage of each individual glycoside is 65:25:3:7, respectively. A similar procedure was applied to 0.5 kg *Laurus nobilis* leaves, yielding the two metabolites (**5** and **6**) in about 20 mg and 15 mg respectively.

Antimicrobial Assays. The CLSI (formerly NCCLS) method[22] was used for the in vitro evaluation of the test samples. Duplicate samples were transferred to 96-well microplates after diluting with 0.9% saline. The microbial cell suspensions were added to the samples to give the target inocula after addition to the samples. Media and solvent controls were included in each assay. The IC_{50} values were calculated by plotting percent growth versus test concentration.[23]

Alkylation of *E,E*-Platanoside (1). Compound (**1**) (7.5 mg, 0.01 mmol) was treated with excess methyl iodide in DMF containing K_2CO_3 and the mixture stirred for 5-6 days at room temperature resulted in the formation of **9** in 10-15% yield. Purification was done via Si-HPLC column with *n*-hexane/ EtOAc (100→100, 120 min, λ 300 nm) and a flow rate of 10 mL/min. The major compound had a retention time of 40 minutes. The ^{1}H NMR spectrum shows the presence of four *O*-methyl groups at 3.82, 3.84, 3.86 and 3.91 ppm, with HMBC correlations to C-7, C-4' and the C- 7'"(X2).

TLC Demonstration of MRSA Activity of Mixture Glycosides (1-4). A 0.5% of mixture glycosides (**1-4**), (27% glycoside content by weight), was applied on TLC plates (4 cm x 4 cm) as model surfaces. The plates were dried overnight, the MRSA organism applied, incubated for 4-6 h, and stained with 3-(4,5-dimethylthiazol-2-yl)-2,5-diphenyltetrazolium bromide (MTT). The development of a purple color indicated growth.

Light-Activated Isomerization of Kaempferol *E,E*-Platanoside (1). Compound (**8**) was used as a model compound, where (16.4 mg, 0.01 mol) was dissolved in 200 µL methanol-d_4 and irradiated at 365 nm for 4-6 h to produce *Z-p*-coumaric acid in 20-30% yield. Compound (**1**) (7.5 mg, 0.01 mmol) was subjected to the same conditions. Follow up on the reaction was done by acquiring the LC/MS and ^{1} H NMR spectra every 2 hours. The formation of the most active metabolites (**2-4**) was shown with a 10-15% yield.

Isolation of Chlorophyll from American Sycamore. Fifty grams of fresh sycamore leaves were homogenized in 250.0 mL MeOH for 5.0 minutes. The resulting green extract was filtered through a cotton pad to remove coarse debris. The filtrate was centrifuged to remove any insoluble material. The green supernatant was mixed with dioxane (1:7 by volume) (35.0 mL). Distilled water was added dropwise under stirring until the mixture developed high turbidity. The mixture was placed in 0 ºC for one hour to promote precipitation. The thick dark green sediment at the bottom was collected by centrifugation. The crude

chlorophyll was dissolved in about 75.0 mL of methanol-dioxane mixture (7:1) by volume and re-precipitated by dropwise addition of water. The same procedure was repeated to achieve further purification.

Effect of Chlorophyll on the Isomerization Process. Compound (**8**) was used as a model compound whereby it (16.4 mg, 0.01 mol) was mixed with 10% chlorophyll and dissolved in 200 µL $CDCl_3$ and irradiated at 365 nm for 4-6 h to produce *Z-p*-coumaric acid in less than 10% yield. Compound (**1**) (7.5 mg, 0.01 mmol) was mixed with 10% chlorophyll and dissolved in 200 µL methanol-d_4 and irradiated at 365 nm for 12 h. Follow up of the reaction was achieved through acquiring the LC/MS and ^{1}H NMR spectra every 2 hours. The formation of the most active metabolites (**2-4**) was shown with around 5% yield.

CHAPTER III

LINKING THE DISCOVERY OF LEADS FOR DRUG RESISTANT HUMAN PATHOGENS TO THE GENERATION OF DISEASE RESISTANT STRAINS OF *PLATANUS OCCIDENTALIS* (AMERICAN SYCAMORE)

Platanus occidentalis (American sycamore) [family: Platanaceae] is fairly widespread throughout the eastern United States, from Texas to Nebraska, Iowa to Wisconsin and into southern Ontario, Canada, and the mountains of northeastern Mexico.[33] The tree can reach heights of 18-37 meters and diameters of 3-4 meters. Native Americans used sycamore for various medical purposes including cough and cold remedies, dietary supplements, gynecological, dermatological, and gastrointestinal aids. American sycamore is important to the forest products industry because it grows well in short-rotation plantations and is used mainly for pulp and fiberboard; sawlogs are used to make butcher's blocks, furniture, interior trim, boxes, and flooring.[33] The American sycamore is a fast growing tree with potential to be a dedicated biomass crop for fuel production. Howevere, the development, and thus the utility, of sycamore plantations for growing pulpwood, sawlogs, or biomass for biofuels is hampered by bacterial leaf scorch disease (BLS) caused by *Xylella fastidiosa*[33] that greatly impedes wood production. By the early 2000s because of concerns over BLS, most industrial forest companies in the southeastern U.S. began liquidating their American sycamore stands in favor of less disease-prone hardwood species. In one study in Mississippi, nine-year old BLS-diseased trees were reduced 26% in height and 27% in diameter growth compared to healthy trees; volumes of diseased trees were 74% less than healthy trees (T. Leininger, unpublished data), (Figure 61).[33]

Strains of *X. fastidiosa* cause various plant diseases such as phony peach disease (PPD), plum leaf scald (PLS), and Pierce's disease (PD) of grapevines, citrus variegated chlorosis (CVC), and leaf scorch of almond, oleander, pear, and several shade tree species such as American sycamore.[34a] These diseases are common in the southeastern United States but also occur in California, southern Ontario, and some southern midwestern states. In north Florida, PPD and PLS were shown to limit peach and plum orchard life.[34a] Bacterial leaf scorch (BLS) diseases have similar etiologies and share similar symptoms in plum, oak, sycamore, and many other woody species, where the leaves appear normal early in the season but later

develop a tan colored interveinal and/or marginal necrosis that spreads toward the base of the leaf. Leaf necrosis results as *X. fastidiosa* multiplies and the bacteria clog leaf xylem tracheary elements preventing water from reaching individual cells. Water transport to leaves, twigs, and branches is disrupted by the bacteria and their by-products causing water stress that leads to pathogenesis. The bacterial infection also causes tyloses to form in xylem elements causing further disruption to plant tissue water supply.

A typical symptomatic sycamore leaf has a narrow green zone of tissue (5-15 mm) with an uneven border surrounding the midrib and main veins while the rest of the leaf blade is necrotic (Figure 61).[34b] Initial foliar symptoms progress to branch dieback, which over a period of several years can lead to severe crown dieback, stem death and breakage, and eventual tree mortality. *X. fastidiosa* perennates in roots and moves yearly into the current year's xylem where it is transported to leaves.[34b] Thus, leaves of infected trees appear healthy in spring but begin to express symptoms in early to mid summer. Severe foliar symptoms and new twig and branch dieback are evident by late summer and early fall. While some reports claim that bacterial leaf scorch occurrence has increased dramatically to epidemic levels in the last ten to fifteen years in the middle-Atlantic states,[34a] BLS of American sycamore probably always has been common in the region. More likely, it became easier to identify BLS disease in the 1990's with the advent of a commercially available ELISA test that enabled clear detection of *X. fastidiosa* in diseased tissue. Furthermore, BLS of American sycamore may have become more common, especially in the southeastern U.S., when, beginning in the 1990's, forest products industries began planting large acreages for pulpwood.

Xylella fastidiosa (*Xf*) (Figure 62) grows slowly in culture and appears to to spread slowly up and down the xylem of the tree starting from the site of infection.[34a] The bacterium enters the plant through grafts or insects feeding on xylem sap. The major insect vector in the southeastern United States is most likely the glassy-winged sharpshooter, *Homalodisca vitripennis* (Figure 63), but other sharpshooters of the subfamily

Cicadellinae, or other xylem-feeding insects, including froghoppers, of the spittlebug family Cercopidae, are also known to transmit the disease. Within the last 10 years, grape production in California has been threatened by Pierce's disease because of the introduction of the glassy-winged sharpshooter, which is endemic to the southeastern U.S. Research into the ecological link between American sycamore tree health and platanoside content could potentially lead to remedies in controlling Pierce's disease and other *X. fastidiosa*-caused diseases.[34a]

Figure 61. A sycamore leaf expressing symptoms of bacterial leaf scorch[34a]

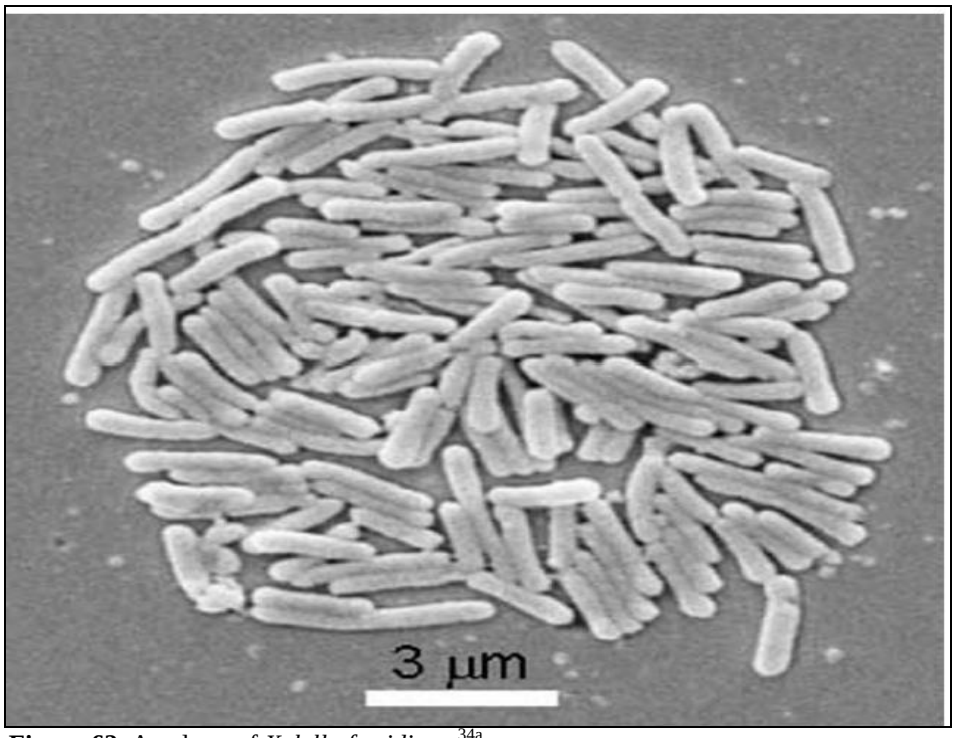

Figure 62. A colony of *Xylella fastidiosa* [34a]

Figure 63. *Homalodisca vitripennis*, the glassy-winged sharpshooter [34a]

Recently, we reported the isolation of a group of anti-MRSA metabolites from *Platanus occidentalis* (American sycamore). The four MRSA lead compounds are *E*,*E*-platanoside (**1**) (IC_{50} 2.0 µg/mL), *E*,*Z*-platanoside (**2**) (IC_{50} 0.8 µg/mL), *Z*,*E*-platanoside (**3**) (IC_{50} 0.7 µg/mL), and *Z*,*Z*-platanoside (**4**) (IC_{50} 0.4 µg/mL) Figure 64.[26] The ecological role of these metabolites was investigated in relation to bacterial leaf scorch caused by *X. fastidiosa* that reduces the productivity of American sycamore plantations and greatly curtailed its use for pulpwood by industry.

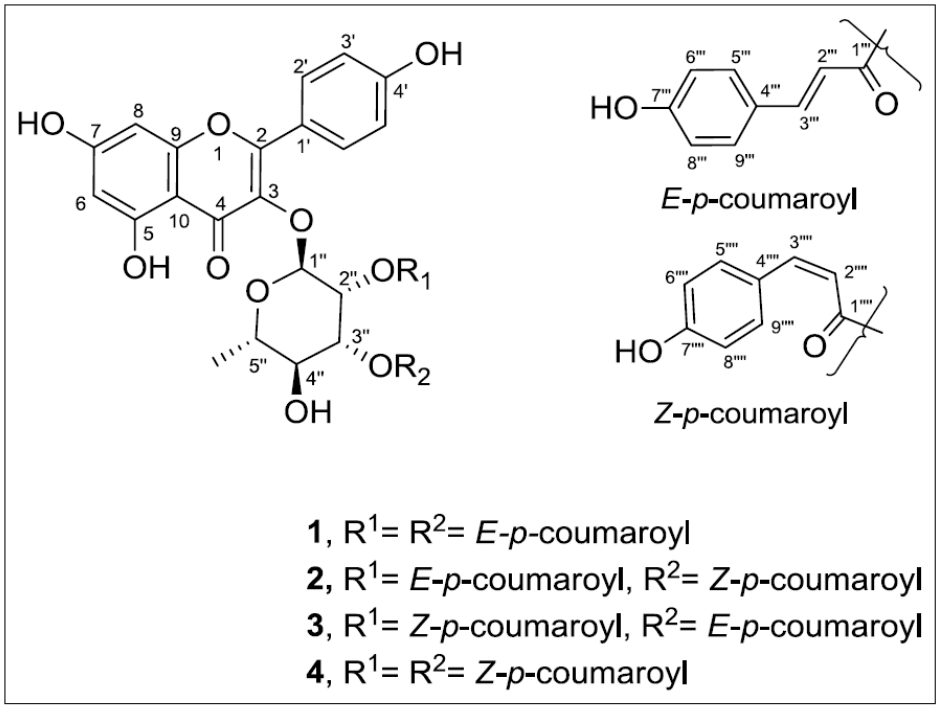

Figure 64. Anti-MRSA metabolites from *Platanus occidentalis* (American sycamore)[26]

A Standard Operating Procedure (SOP) for determination of rhamnose glycosides from American sycamore leaves by LC/MS was established, and the calibration curve was determined based on *E*,*E*-platanoside (**1**), Figure 65.

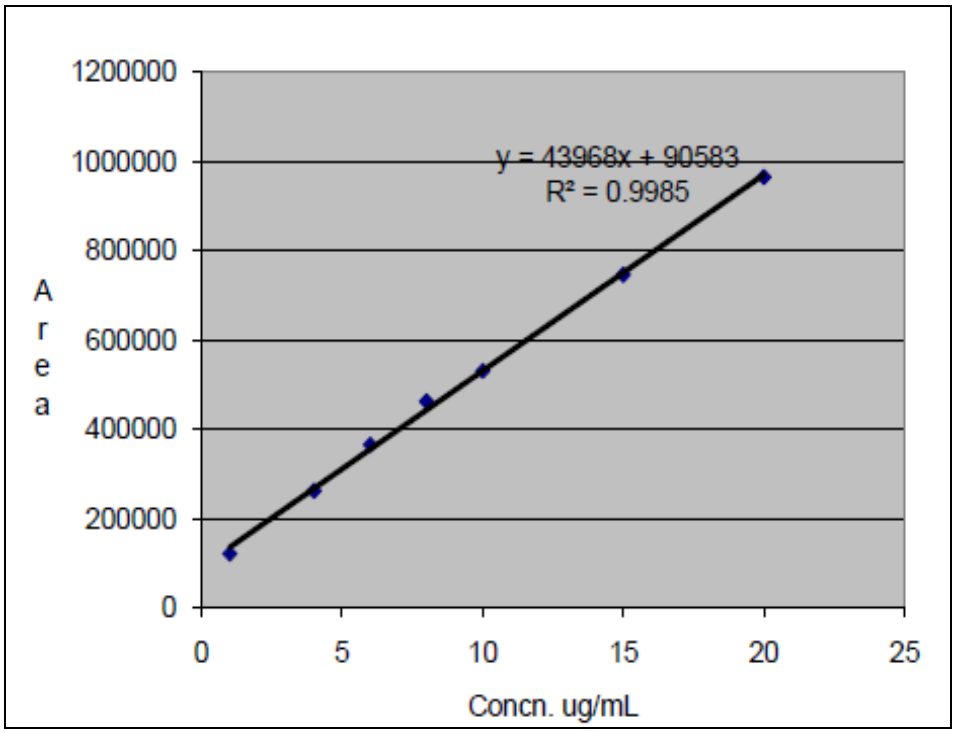

Figure 65. LC/MS calibration curve of *E*,*E*-platanoside

Seven leaf samples (composed of 5-7 mature leaves each) from leaf scorch asymptomatic trees and seven symptomatic trees were provided in August 2009 through the collaboration with Dr. Theodor D. Leininger, Project Leader, USDA Forest Service, Southern Research Station, Center for Bottomland Hardwoods Research, Stoneville, MS. These samples were evaluated for their glycoside content as shown in Table 6 and Figure 66.

Table 6. Percent glycosides in 7 asymptomatic and 7 symptomatic American sycamore trees

Tree Code	Health	% glycosides
4-11	0	0.39
14-5	0	0.27
11-11	0	0.20
17-11	0	0.28
17-19	0	0.21
9-17	0	0.31
14-19	0	0.19
6-17	1	0.17
8-13	1	0.24
16-19	1	0.14
4-5	1	0.23
12-19	1	0.14
18-12	1	0.14
17-6	1	0.17

"0"= leaf from leaf scorch asymptomatic tree; "1" = leaf from leaf scorch symptomatic tree

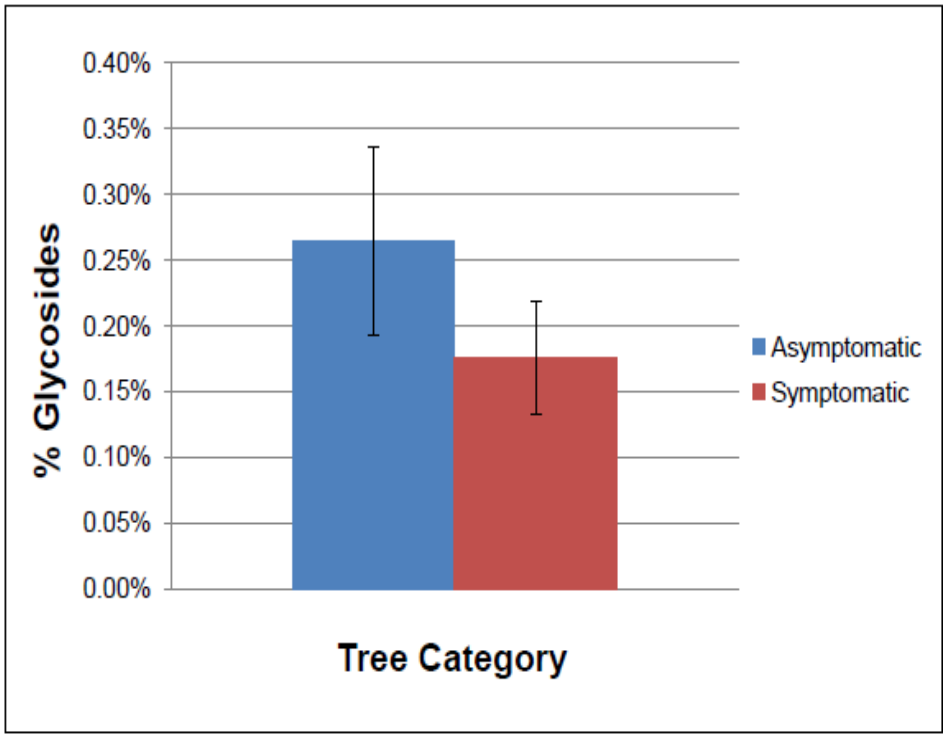

Figure 66. Percent glycosides in 7 asymptomatic and 7 symptomatic trees

Six samples were recollected in May 2010, re-assayed for their glycoside content, and the data were compared to those of August 2009 (Table 7).

Table 7. Glycoside content comparison between August 2009 and May 2010 for three asymptomatic and three symptomatic trees

Tree Code	Health	% glycosides (August 2009)	% glycosides (May 2010)
4-11	0	0.39	0.45
14-5	0	0.27	0.43
9-17	0	0.31	0.52
16-19	1	0.14	0.40
18-12	1	0.14	0.41
17-6	1	0.17	0.27

"0"= leaf from leaf scorch asymptomatic tree; "1" = leaf from leaf scorch symptomatic tree

As shown in Table 7, some trees are showing consistently low content (i.e., 17-6), while others show consistently high content, like 9-17, suggesting a possible ecological link between these metabolites and resistance to *X. fastidiosa*. Pictures of both trees (Figure 67) show the severe BLS-diseased condition of tree 17-6 with only one live basal shoot while tree 9-17 remains healthy.

Figure 67. Picture of the two American sycamore trees coded 17-6 (BLS-symptomatic) and 9-17 (BLS-asymptomatic)

An in vitro bacteriocidal evaluation of these metabolites against *X. fastidiosa* was completed using the bacterium was obtained from Ruth Donaldson at the Department of Plant Pathology, University of Georgia, Griffin, GA. Bacterial cultures were maintained using CS20 specific medium. Two sets of experiments were performed: a) various concentrations of a semi purified mixture of glycosides (purity ≥ 70% by LC/MS) were tested for their in vitro activity against *X. fastidiosa* and, b) the pure metabolites were evaluated for their in vitro activity against *X. fastidiosa* in the same Petri plates with the semi-purified mixture of glycosides (27% glycoside content by weight). Interestingly, glycoside mixture concentrations of 0.2%, 0.1%, and 0.025% prevented *X. fastidiosa* growth. The 0.005% concentration did not prevent *X.*

fastidiosa growth (MIC ≤ 0.05 μg/mL) Figures 68 and 69. The data showed similar SARs to those demonstrated for MRSA, where the in vitro antibacterial activity of the *Z,Z*-platanoside was more effective against *Xf* (MIC ≤ 17 nM) than was shown for the *E,E*-platanoside (MIC ≤ 67 nM), Figures 70-72. In view of the information presented in the previous chapter, these data suggest a possible photochemical defense mechanism of American sycamore against *X. fastidiosa* infections.

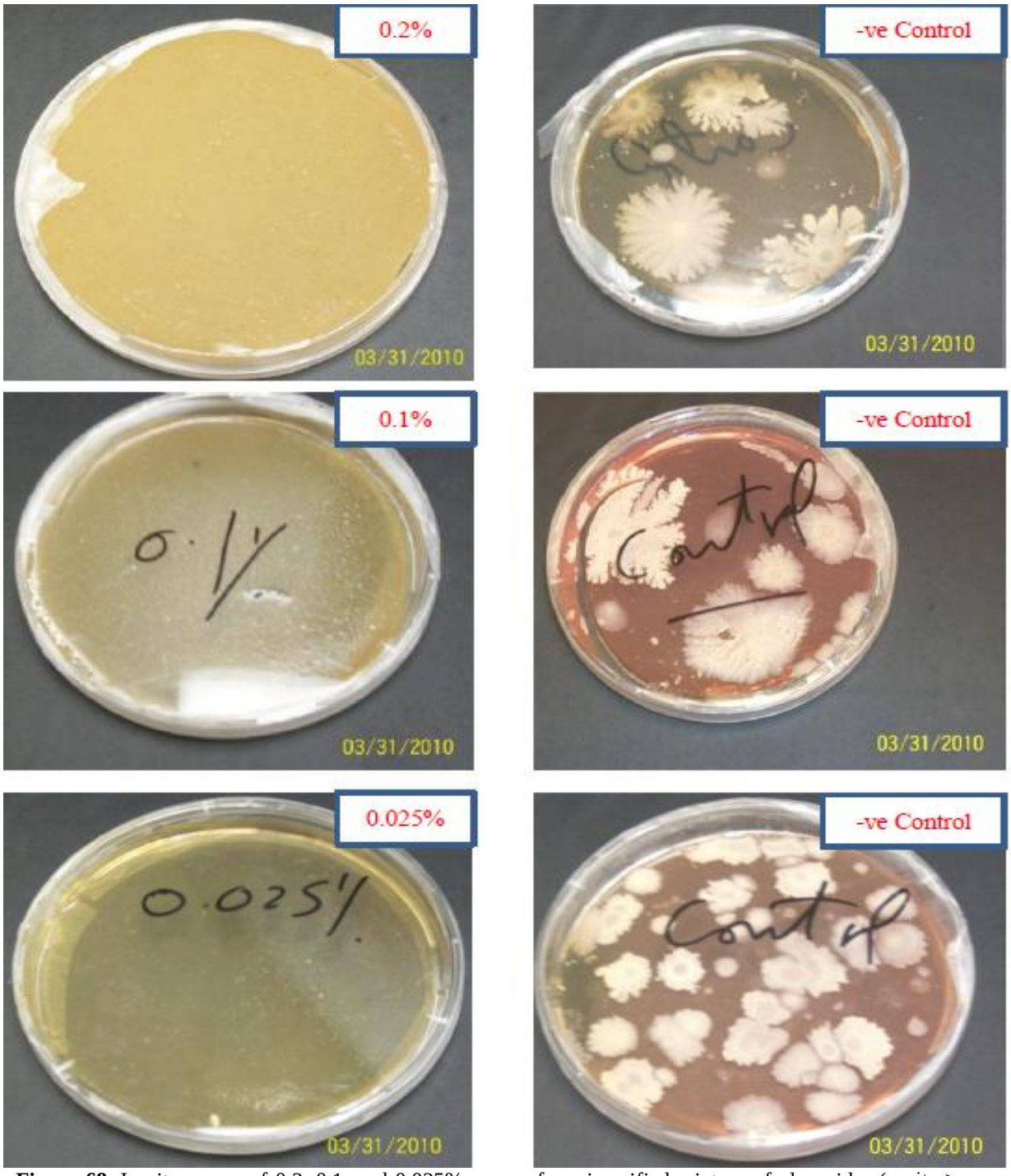

Figure 68. In vitro assay of 0.2, 0.1, and 0.025% range of semi purified mixture of glycosides (purity ≥ 70% by LC/MS) against *X. fastidiosa*

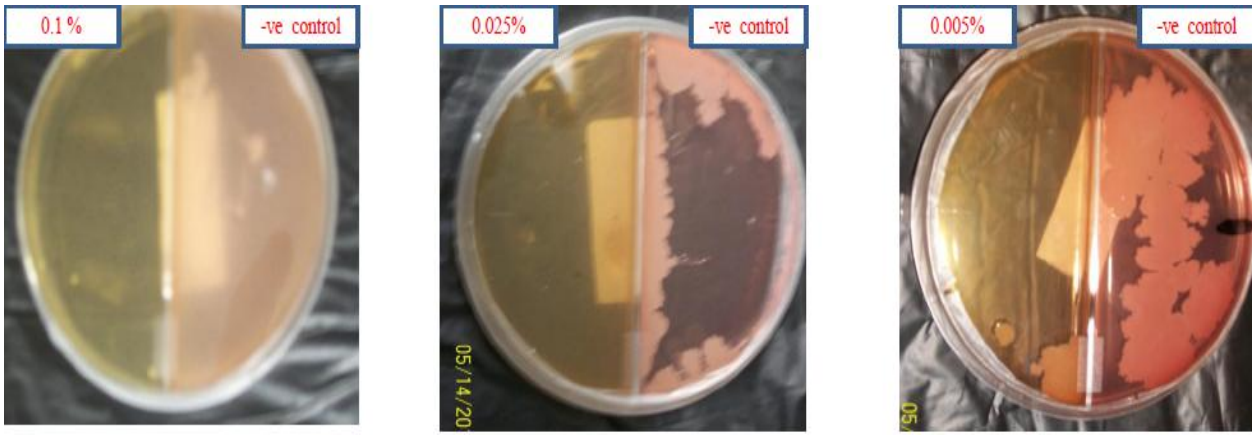

Figure 69. In vitro assay of 0.1, 0.025, and 0.005% range of semi purified mixture of glycosides (purity ≥ 70% by LC/MS) against *X. fastidiosa* in double compartment Petri plates (72 h)

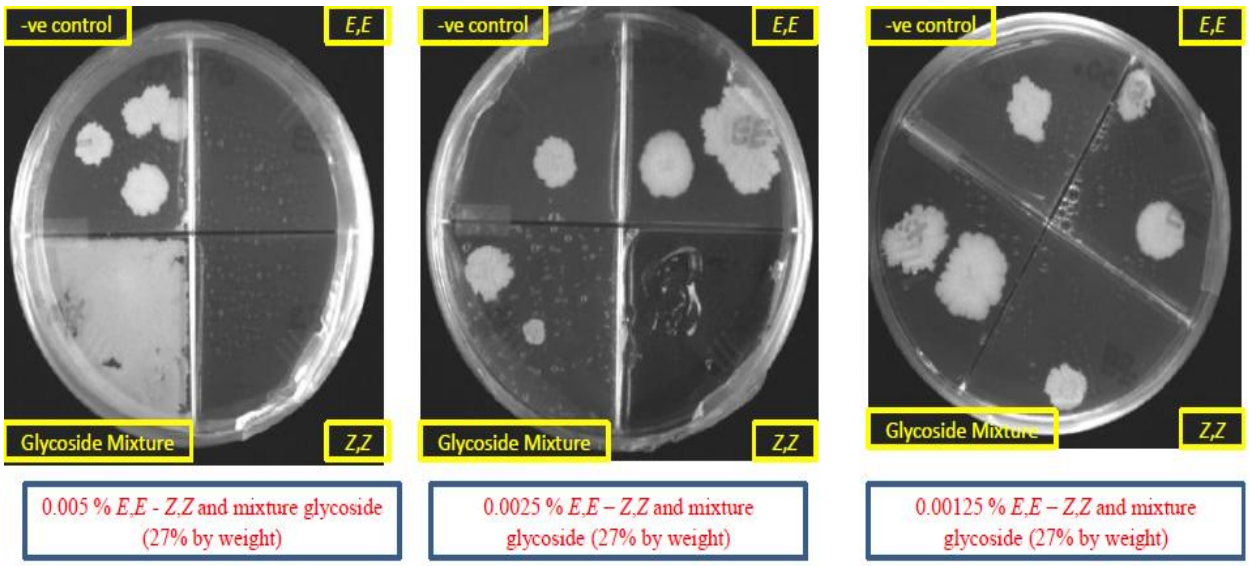

Figure 70. In vitro assay of 0.005-0.00125% of *E*,*E*-platanoside, *Z*,*Z*-platanoside, mixture of glycosides (27% purity by weight), and –ve control in four compartment Petri plates

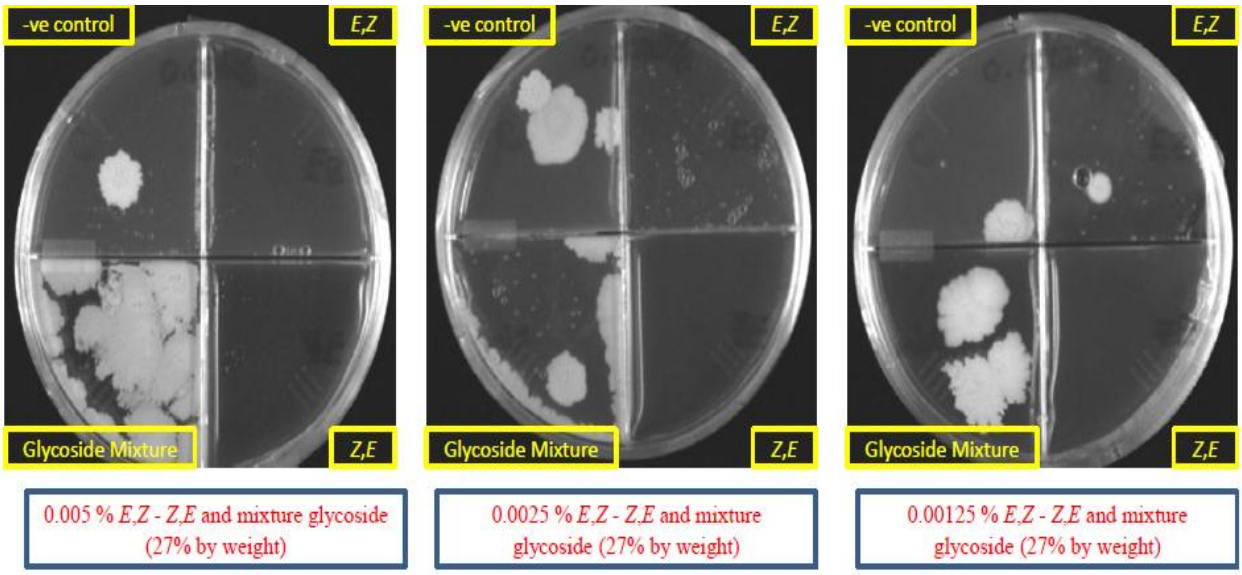

Figure 71. In vitro assay of 0.005-0.00125% of *E*,*Z*-platanoside, *Z*,*E*-platanoside, mixture of glycosides (27% purity by weight), and –ve control in four compartment Petri plates

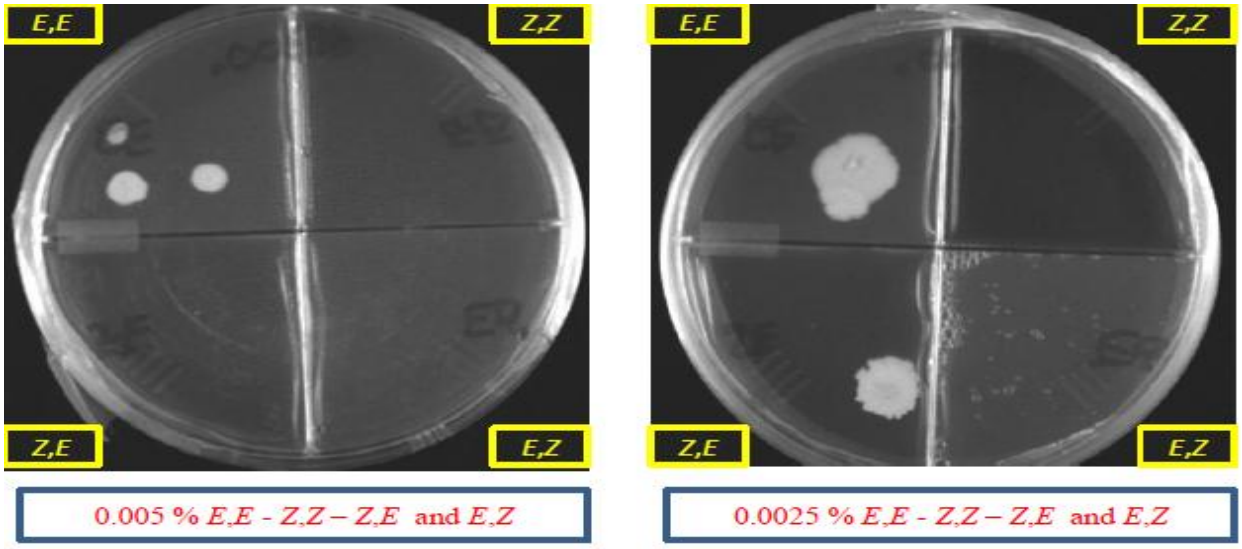

Figure 72. In vitro assay of 0.005-0.0025% of *E*,*E*-platanoside, *Z*,*Z*-platanoside, *Z*,*E*-platanoside, and *E*,*Z*-platanoside in four compartment Petri plates

Experimental Section:

General Experimental Procedures. The 1D and 2D NMR experiments were measured on a Bruker AV NMR spectrometer (Bruker Biospin, Bruker Inc.) operating at 400 MHz and the chemical shift (δ) values are expressed in ppm. The mass spectra were measured using the Bruker micrOTOF (Bruker Daltonics, Bruker Inc.) with an ESI ionization source. HPLC was carried out on a Waters Prep-LC with a 2487 dual absorbance detector.

Plant Material. The leaves of *P. occidentalis* were collected in August 2009 and May 2010 from the USDA Forest Service, Center for Bottomland Hardwoods Research, Stoneville, Mississippi and were dried under vacuum for about 2-4 h and then ground to small pieces by hand (particle size < 0.01 mm).

Extraction and Isolation. Air-dried leaves and petioles (1.0 g) were extracted with 25 mL of EtOH (95%)-H_2O (25:75) and shaken for 2 h to extract unwanted material. The active glycosides were extracted in 25 mL of EtOH (95%)-H_2O (75:25) by stirring for an additional 2 h. The active metabolite extraction was repeated three times. Finally, all the active extracts were combined. The solvent was evaporated using a rotavap at 40-45 ^oC, and the insoluble materials were removed by passing the extract solution through a 0.22 μm filter. The dried extract was dissolved in 20 mL MeOH. A 100 μL sample was placed in an LC/MS vial and a 20 μl sample was injected using the gradient in Table 8 at 35 ºC.

Table 8. LC/MS program for determination of rhamnose glycosides

Time (minute)	H_2O(0.05%)HCOOH	MeOH(0.05%)HCOOH	Flow rate (ml/min)
0	90	10	0.6
15	0	100	0.6
30	0	100	0.6

In Vitro Assay. *X. fastidiosa* was grown on a CS20 specific medium (soy peptone 2.0 g/L, bacto tryptone 2.0 g/L, $(NH_4)_2HPO_4$ 0.85 g/L, hemin Cl [(0.1%), 15.0 mL/L], KH_2PO_4 1.0 g/L, $MgSO_4.7H_2O$ 0.4g/L, L-glutamine 6.0 g/L, dextrose 1.0 g/L, starch (potato soluble) 2.0 g/L, L-histidine 1.0 g/L, phenol red

[(0.2%) 5.0 mL/L], and 14.0 g/L agar). The pH was adjusted to be in the range of 6.6-6.7. For experiment (a), the crude mixture of glycosides was subjected to semi purification [50-100 mg extract loaded on SPE, Strata C_{18}-E (55 µm, 70 A), (1000 mg/6 mL) - Phenomenex, eluted with H_2O-CH_3CN(100:0 → 0:100), 25% increment, 3 bed volumes each, the glycosides eluted mainly in H_2O-CH_3CN (25:75)], while for experiment (b), no further purification was applied to the crude mixture.

a) A 0.2-0.005% concentration range of the semi purified mixture of glycosides (purity ≥ 70% by LC/MS) was tested for efficacy against *X. fastidiosa* by mixing each concentration with 20 mL of media to overcome the poor diffusion properties of these metabolites. The mixture of media and glycosides was autoclaved, poured into Petri plates, and cooled. The bacterium was streaked onto the agar surface and the plates were incubated for 72 h at 37 ºC.

b) A 0.005-0.00125% concentration range of the mixture of glycosides (27% purity by weight) and the pure metabolites were tested for efficacy against *X. fastidiosa* by mixing each concentration with 15 mL autoclaved media, poured into Petri plates, and cooled. The bacterium was streaked onto the agar surface and the plates were incubated for 72 h at 37 ºC.

CHAPTER IV

2-(5-HALO-1*H*-INDOL-3-YL)-*N*,*N*-DIMETHYLETHANAMINES AS ANTIDEPRESSANT DRUG LEADS

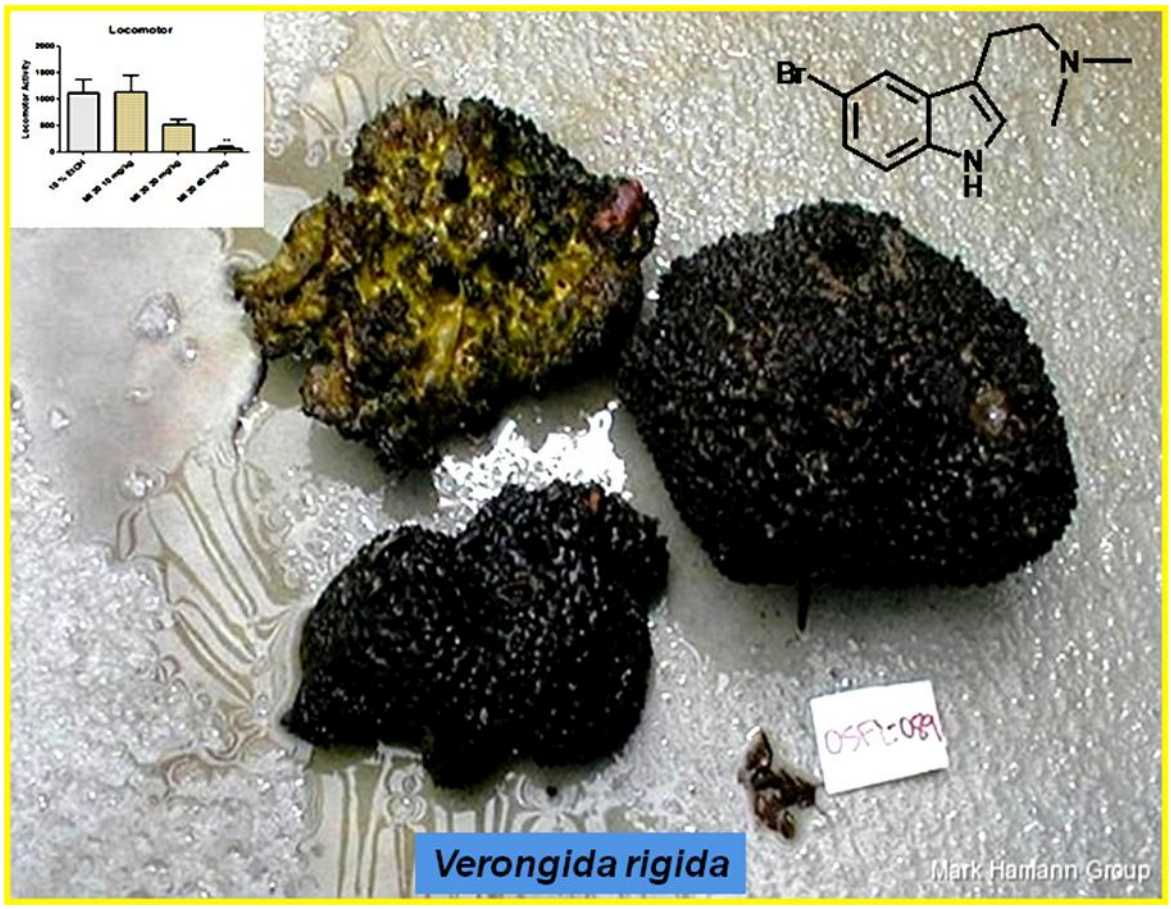

1. Introduction

Depression is the most common disease of the central nervous system, affecting approximately 17% of Americans each year.[35] According to National Institute of Mental Health (NIMH), about 40 million American adults suffer from anxiety disorders every year that frequently co-occur with other psychiatric illnesses, like depression.[36] Both disorders are often treated with antidepressant medications. All currently available antidepressant drugs enhance the monoaminergic transmitter mechanism by inhibiting the metabolism or reuptake of certain neurotransmitters (serotonin or adrenaline) and increasing their concentration in the brain. However, the clinically-used antidepressants suffer from serious side effects and take approximately six weeks before the patient is able to experience the full therapeutic effect. Anxiety disorders can be also treated with sedative medications, which can cause addiction and other side effects like drowsiness, dizziness, and headaches. There is a clear need for more effective and safer drugs for depression and anxiety disorders. Recently, various marine natural products were reported as valuable drug leads for neurological disorders.[37]

In previous studies, we isolated several marine indole alkaloids and evaluated them in the forced swim test (FST) and locomotor activity test, revealing their potentials to become new antidepressant and sedative drug leads.[37,38] Among the reported neurological active compounds, 5-bromo-*N*,*N*-dimethyltryptamine was found to exhibit strong sedative effect in the locomotor activity test.[37] Because of limited amounts of the natural product, a synthetic approach was adopted to prepare 5-bromo-*N*,*N*-dimethyltryptamine and its derivatives to study the structure activity relationships and complete the dose-response experiments. The current study describes the preparation of various derivatives of 2-(1*H*-indol-3-yl)-*N*,*N*-dimethylethanamine with different halogens in position 5 and the evaluation of their activity in two animal models, forced swim and locomotor activity tests. The forced swim test is a well established animal

model assessing the potential clinical antidepressant action of drug.[39-41] The locomotor activity test was used to confirm that the antidepressant action observed in the FST could not be attributed to a nonspecific stimulant activity of the tested compounds. A significant reduction in locomotor activity is usually predictive of a potential sedative action.

2. Methods

2.1. Subjects

Experiments were performed using eight week old mice. Male Swiss Webster mice (Harlan, IN, USA) weighing 24-31 grams at the time of testing were used for the automated forced swim test. The mice were housed in groups of five with a 12 h light/12 h dark cycle. Food and water were provided *ad libitum*. All mice were randomly selected for each treatment group. Procedures involving animals were performed according to the guidelines approved by the Institutional Animal Care and Use Committee.

2.2. Drugs

A series of 2-(5-halo-1*H*-indol-3-yl)-*N*,*N*-dimethyl-2-oxoacetamides and 2-(5-halo-1*H*-indol-3-yl)-*N*,*N*-dimethylethanamines (Scheme 7) were synthesized via a straightforward and efficient approach.[42] We have encountered problems associated with loosing the halogen in the last reduction step; however these can be eliminated by changing the solvent from THF, which is commonly used for these types of reactions, to DME and monitoring the reaction by either GC/MS or LC/MS.

The synthesis of the haloindoledimethylethanamines began by conversion of halo-substituted indoles to the corresponding oxoacetyl chlorides via portionwise addition of oxalyl chloride in anhydrous diethyl ether at 0 ^{o}C, followed by stirring for one hour under inert atmosphere to provide **2a-e** in (80-90%) yield as yellowish orange solids. The resulting oxoacetyl chlorides **2a-e** were treated with dimethylamine solution (40% in water) at 0 ^{o}C for 30 minutes, followed by stirring for additional two hours at room temperature.

After extraction of the product with DCM, the white solid residues were further purified by HPLC using reverse-phase C_8 column and H_2O-MeOH solvent system to afford oxoacetamides **3a-e** in (80-90%) yields. The final step of the synthesis was achieved by catalytic reduction of oxoacetamides **3** using $LiAlH_4$ solution in anhydrous DME with sequential stirring of the mixture at 0 ^oC for one hour, at room temperature for two hours, and at 80 ^oC for six hours, respectively. After work up, the resulting yellowish-brown precipitate was collected and subjected to further purification using an HPLC C_8 column and H_2O-MeOH solvent system to give the anticipated ethyldimethylamines **4a-e** in (65-75%) yields.

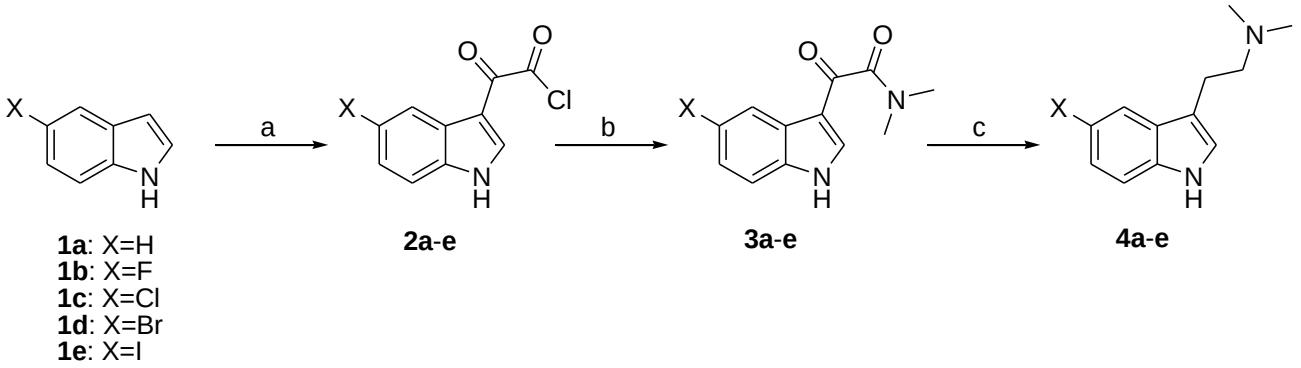

Scheme 7. The synthesis of 5-haloindoledimethylethanamines. Reagents and reaction conditions: (a) Oxalyl chloride, diethyl ether, 0 ^oC, 30-60 min, (80-90%); (b) Dimethylamine, 0 ^oC, 30 min, then rt, 2 h, (80-90%); (c) $LiAlH_4$, DME, 0 ^oC, 1 h, then rt, 2 h, then 80 ^oC, 2 h, (65-75%).

The structures of the synthesized compounds were established via 1D and 2D NMR experiments that were measured on a Bruker DRX NMR spectrometer operating at 400 MHz, and the chemical shift (δ) values are expressed in (ppm); (Figures 73-80). HPLC analysis was carried out on Waters instrument with a 2487 dual absorbance detector. The molecular structure of oxoacetamide **3a** in the solid state was confirmed by X-ray analysis. A suitable single crystal of non-halogenated compound **3a** was obtained by slow evaporation of a concentrated solution in methanol. The crystal structure and the crystallographic numbering are shown in Figure 81.

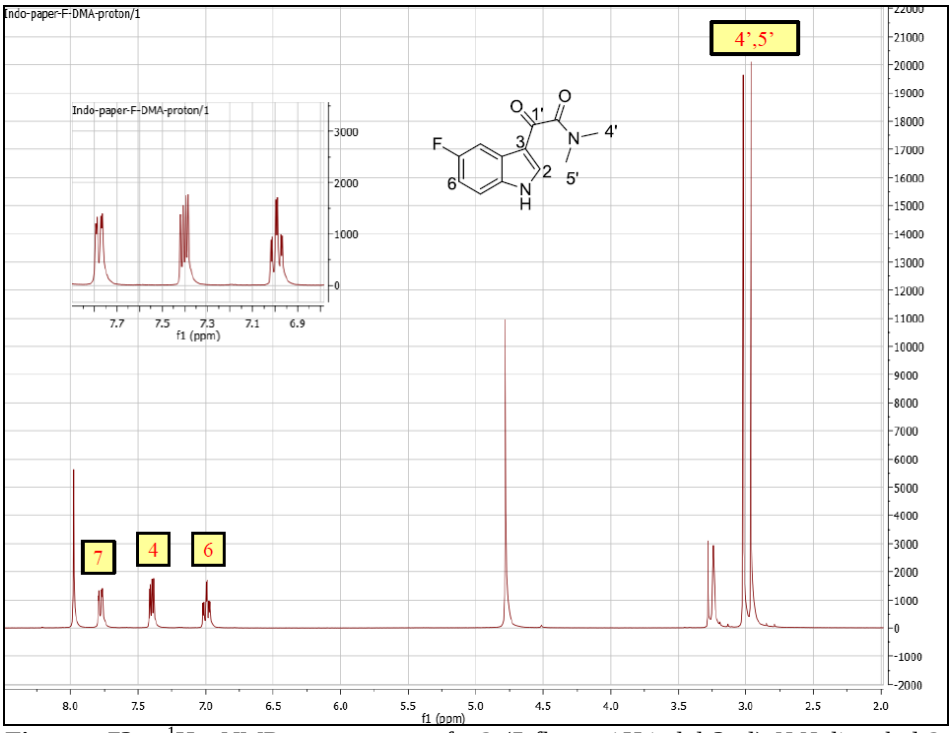

Figure 73. ^{1}H NMR spectrum of 2-(5-fluoro-1*H*-indol-3-yl)-*N*,*N*-dimethyl-2-oxoacetamide (**3b**) in methanol-d_4 (400 MHz)

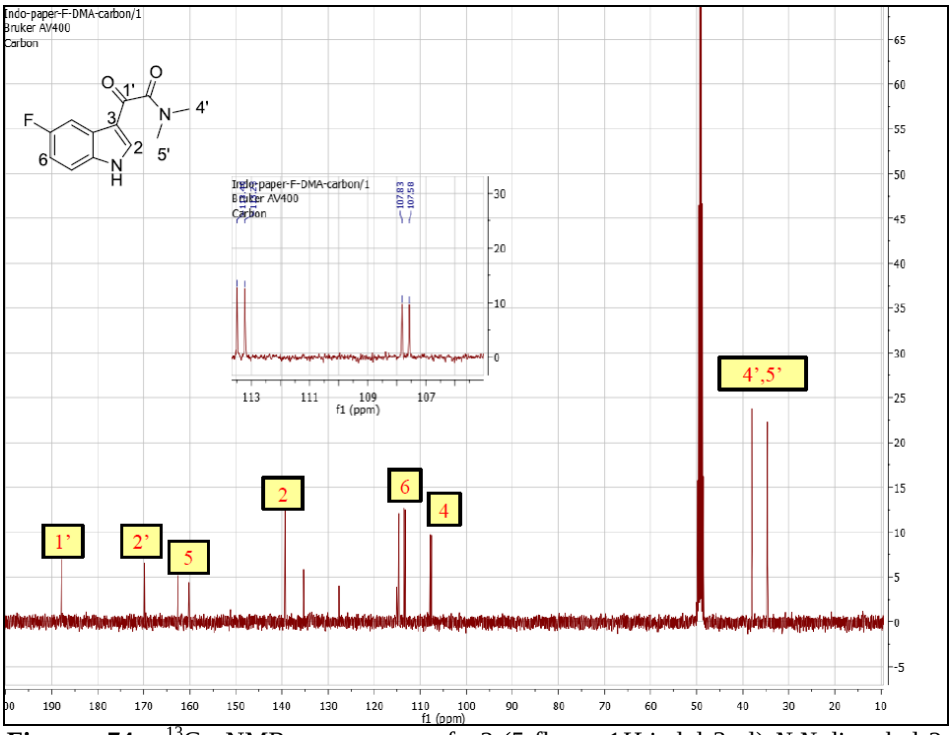

Figure 74. ^{13}C NMR spectrum of 2-(5-fluoro-1*H*-indol-3-yl)-*N*,*N*-dimethyl-2-oxoacetamide (**3b**) in methanol-d_4 (400 MHz)

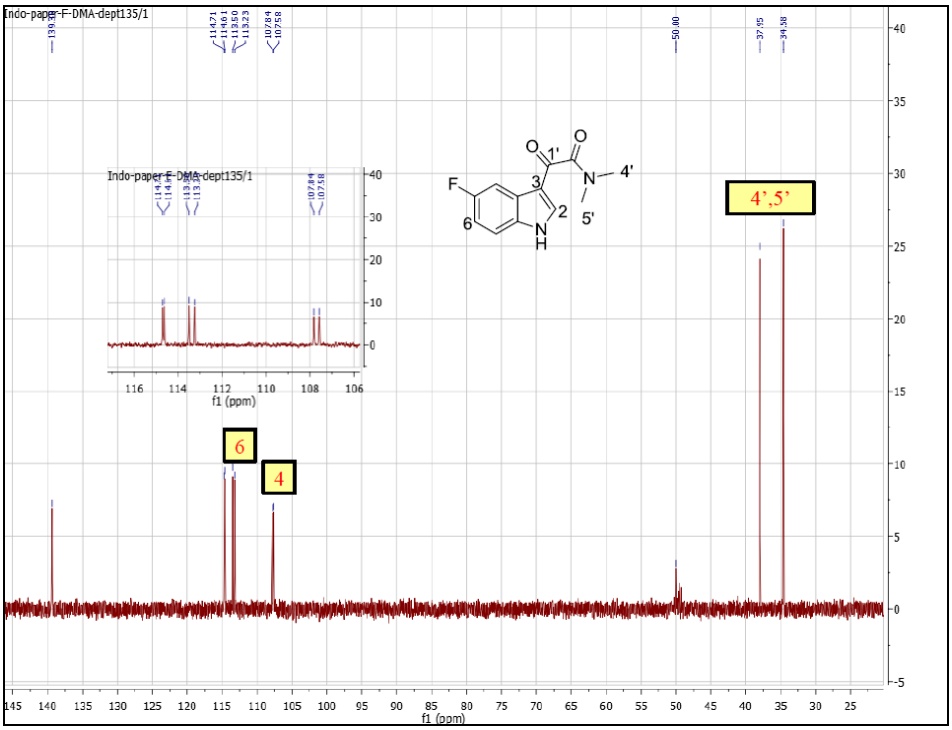

Figure 75. 135º DEPT spectrum of 2-(5-fluoro-1*H*-indol-3-yl)-*N*,*N*-dimethyl-2-oxoacetamide (**3b**) in methanol-d_4 (400 MHz)

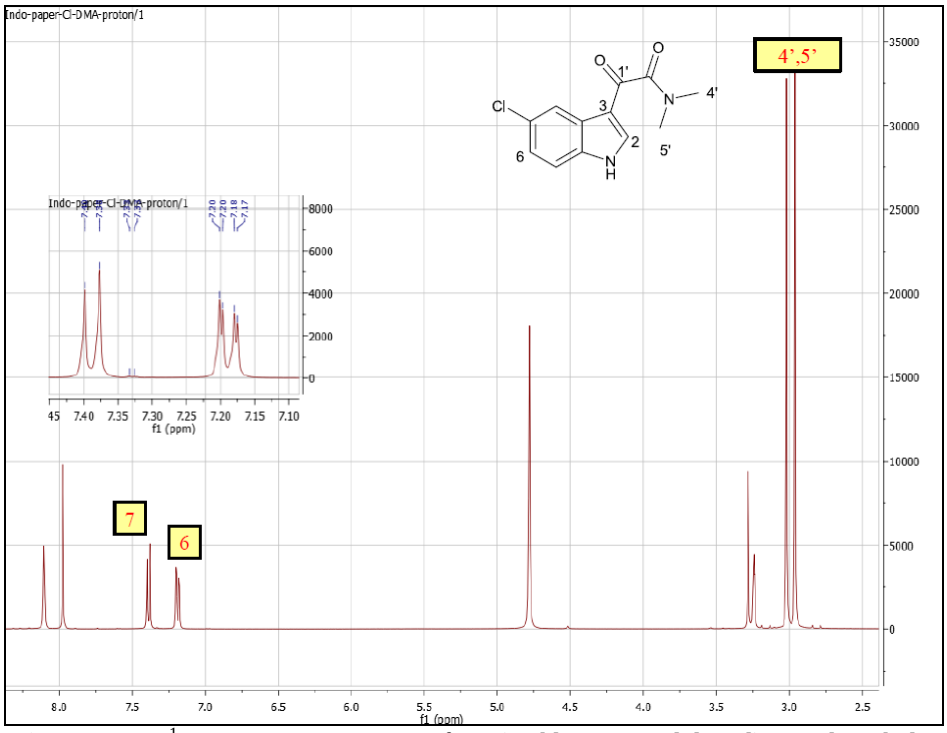

Figure 76. ^{1}H NMR spectrum of 2-(5-chloro-1*H*-indol-3-yl)-*N*,*N*-dimethyl-2-oxoacetamide (**3c**) in methanol-d_4 (400 MHz)

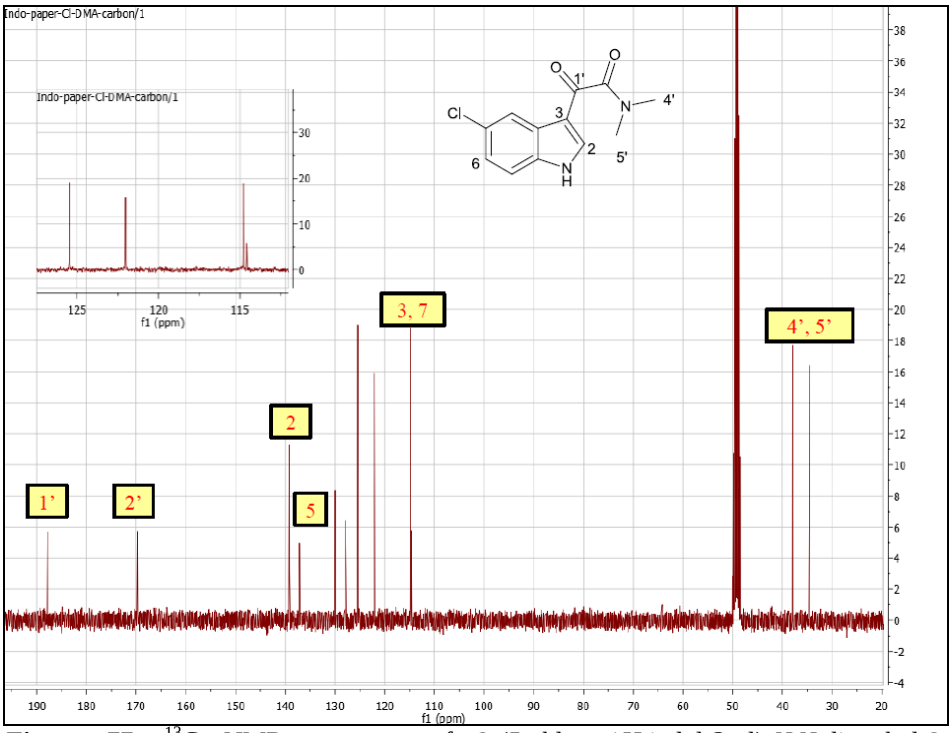

Figure 77. ^{13}C NMR spectrum of 2-(5-chloro-1*H*-indol-3-yl)-*N*,*N*-dimethyl-2-oxoacetamide (**3c**) in methanol-d_4 (400 MHz)

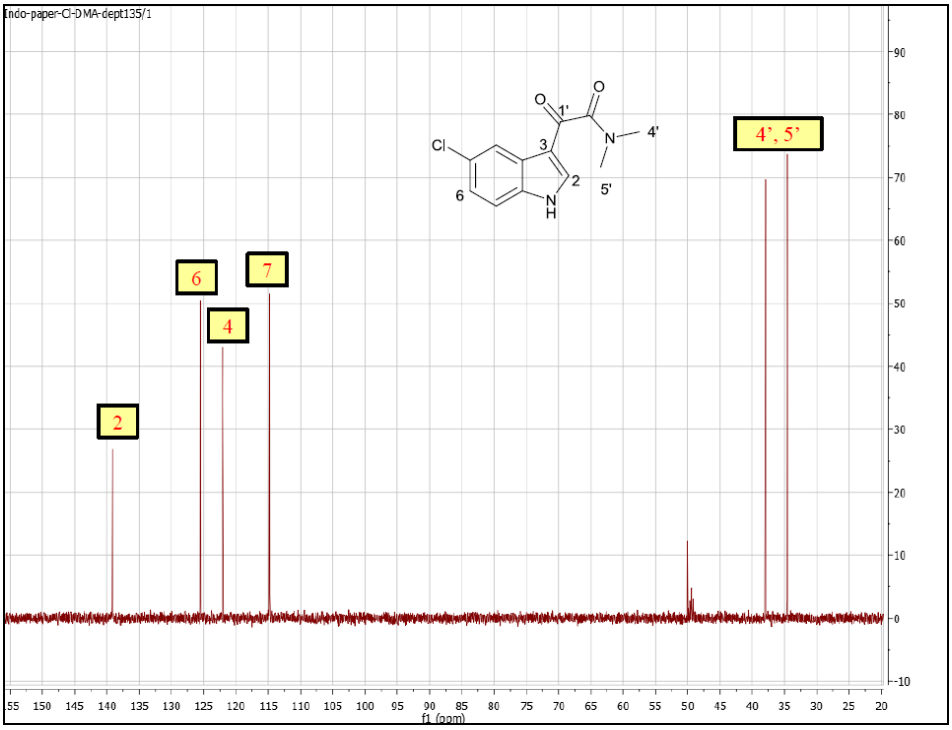

Figure 78. 135º DEPT spectrum of 2-(5-chloro-1*H*-indol-3-yl)-*N*,*N*-dimethyl-2-oxoacetamide (**3c**) in methanol-d_4 (400 MHz)

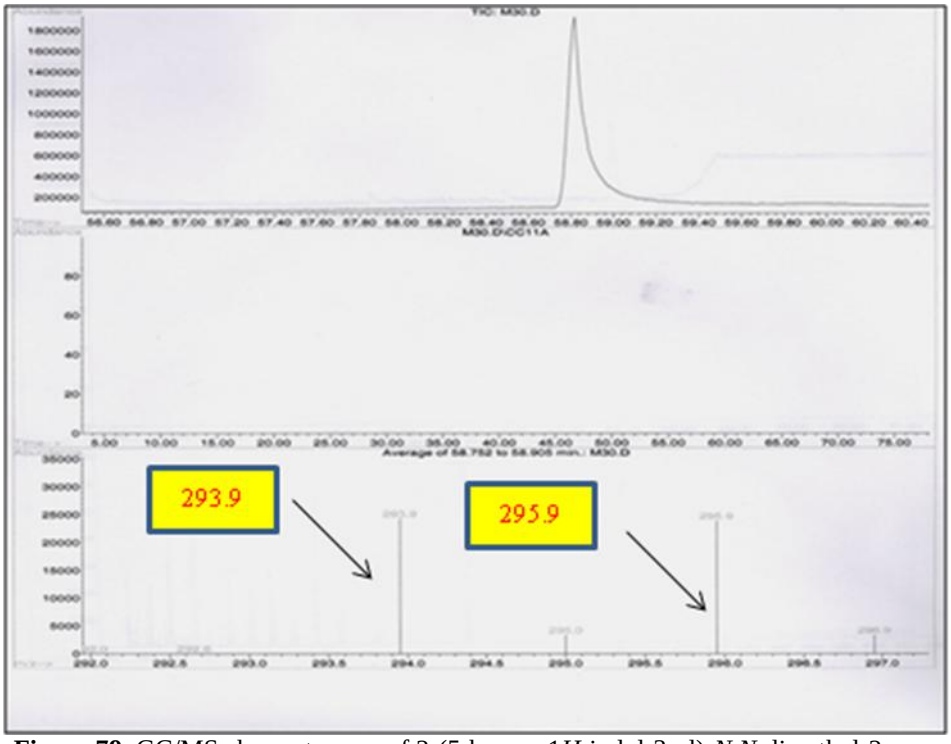

Figure 79. GC/MS chromatogram of 2-(5-bromo-1*H*-indol-3-yl)-*N*,*N*-dimethyl-2-oxoacetamide (**3d**)

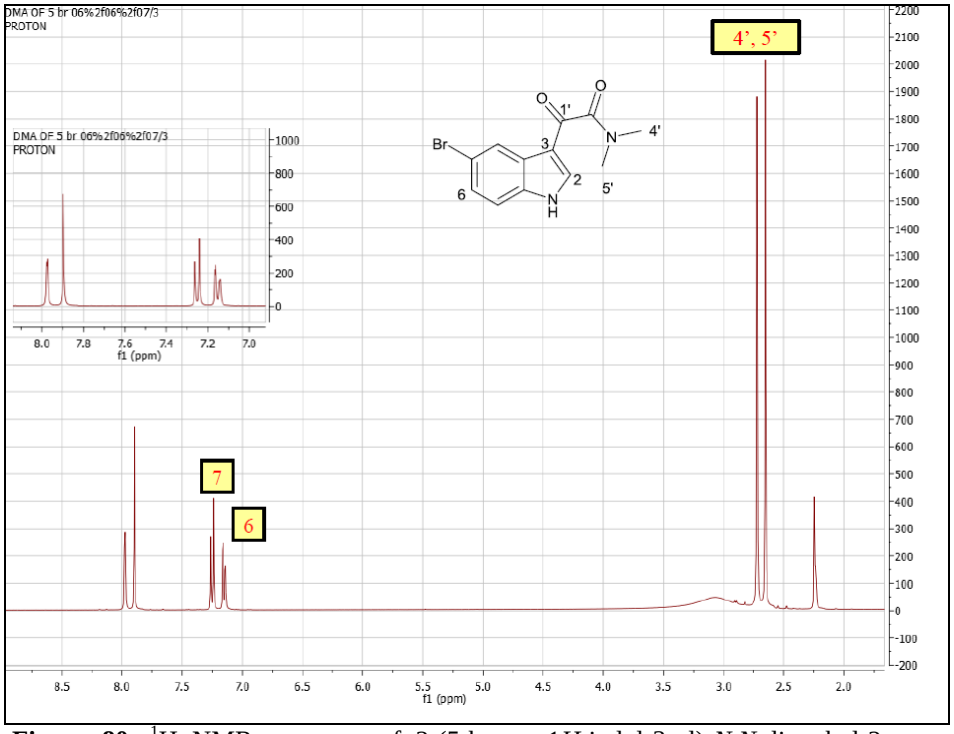

Figure 80. ^{1}H NMR spectrum of 2-(5-bromo-1*H*-indol-3-yl)-*N*,*N*-dimethyl-2-oxoacetamide (**3d**) in $CDCl_3$ (400 MHz)

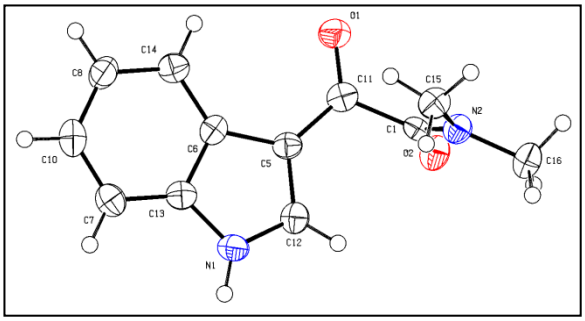

Figure 81. The X-ray crystal structure of compound 2-(1*H*-indol-3-yl)-*N*,*N*-dimethyl-2-oxoacetamide (**3a**)

The 2-(1*H*-indol-3-yl)-*N*,*N*-dimethylethanamine (**4a**); $C_{12}H_{16}N_2$, was purified as a brownish white precipitate, ^{1}H NMR (methanol-d_4), δ 1.61 (s, 6H), 1.99 (d, 2H), 2.35 (d, 2H), 6.41 (s, 1H), 6.56 (dt, 1H), 6.85 (d, 1H), 7.06 (d, 1H). ^{13}C NMR (methanol-d_4), δ 24.11 (t), 45.66 (q), 61.01 (t), 112.39 (d), 113.54 (s), 119.34 (s), 119.68 (d), 122.40 (d), 123.10 (d), 128.64 (s), 137.97 (s); (Figures 82-87). The 2-(5-fluoro-1*H*-indol-3-yl)-*N*,*N*-dimethylethanamine (**4b**); $C_{12}H_{15}N_2F$, was purified as a yellowish white precipitate, ^{1}H NMR (methanol-d_4), δ 1.79 (s, 6H), 2.97 (d, 2H), 3.12 (d, 2H), 6.74 (dt, 1H), 7.08 (s, 1H), 7.15 (m, 2H). ^{13}C NMR (methanol-d_4), δ 22.01 (t), 43.64 (q), 59.15 (t), 103.76 (d), 104.00 (s), 110.83 (s), 111.10 (d), 113.44 (d), 113.54 (d), 126.16 (s), 134.86 (s); (Figures 88-90). The 2-(5-chloro-1*H*-indol-3-yl)-*N*,*N*-dimethylethanamine (**4c**); $C_{12}H_{15}N_2Cl$, was purified as a yellowish white precipitate, ^{1}H NMR (methanol-d_4), δ 2.36 (s, 6H), 2.70 (d, 2H), 2.91 (d, 2H), 5.93 (t, 1H), 6.99 (s, 1H), 7.24 (d, 1H), 7.47(s, 1H). ^{13}C NMR (methanol-d_4), δ 22.48 (t), 43.67 (q), 59.67 (t), 110.83 (d), 111.60 (s), 117.69 (s), 118.21 (d), 120.96 (d), 121.83 (d), 127.15 (s), 136.79 (s); (Figures 91-95). The 2-(5-bromo-1*H*-indol-3-yl)-*N*,*N*-dimethylethanamine (**4d**); $C_{12}H_{15}N_2Br$, was purified as a yellowish white precipitate, ^{1}H NMR (methanol-d_4), δ 2.191 (s, 6H), 2.48 (d, 2H), 2.75 (d, 2H), 6.95 (s, 1H), 7.07 (d, 1H), 7.130 (d, 1H), 7.56 (s, 1H). ^{13}C NMR (methanol-d_4), δ 24.11 (t), 45.46 (q), 61.39 (t), 112.88 (d), 113.57 (s), 114.05 (s), 121.88 (d), 124.86 (d), 125.14 (d), 130.59 (s), 136.84 (s); (Figures 96-101). The 2-(5-iodo-1*H*-indol-3-yl)-*N*,*N*-dimethylethanamine (**4e**); $C_{12}H_{15}N_2I$,

was purified as a yellowish white precipitate, ^{1}H NMR (methanol-d_4), δ 2.21 (s, 6H), 2.53 (d, 2H), 2.82 (d, 2H), 6.93 (s, 1H), 6.99 (t, 1H), 7.22 (d, 1H), 7.42 (d, 1H). ^{13}C NMR (methanol-d_4), δ 24.29 (t), 46.0 (q), 61.80 (t), 112.41 (d), 113.66 (s), 119.30 (s), 119.77 (d), 122.42 (d), 123.22 (d), 128.75 (s), 138.25 (s); (Figures 102-104).

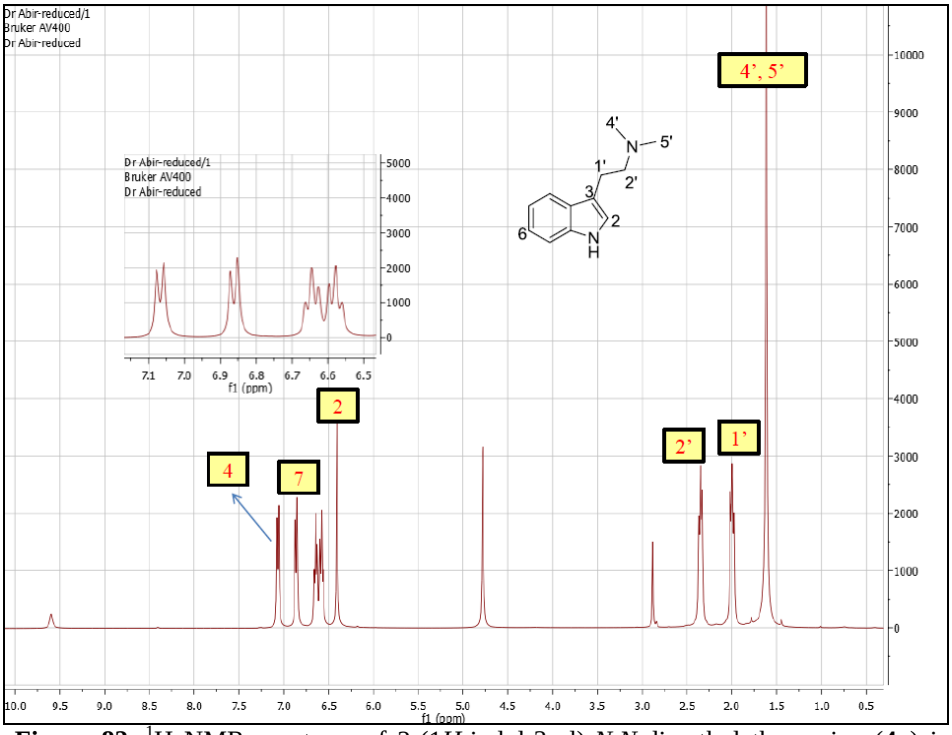

Figure 82. ^{1}H NMR spectrum of 2-(1*H*-indol-3-yl)-*N*,*N*-dimethylethanamine (**4a**) in methanol-d_4 (400 MHz)

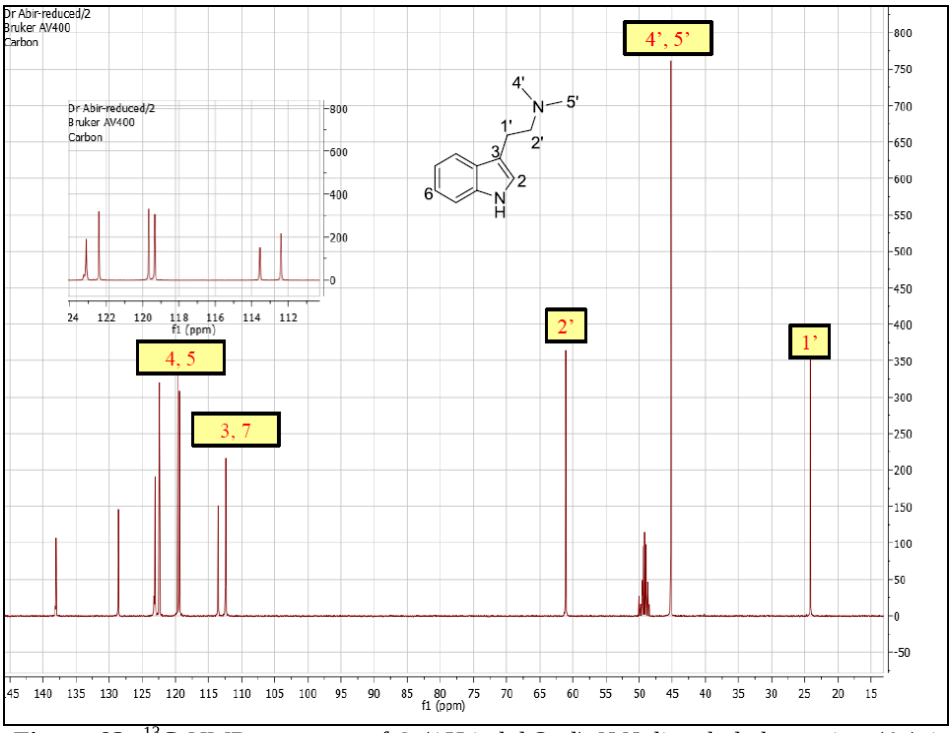

Figure 83. ^{13}C NMR spectrum of 2-(1*H*-indol-3-yl)-*N*,*N*-dimethylethanamine (**4a**) in methanol-d_4 (400 MHz)

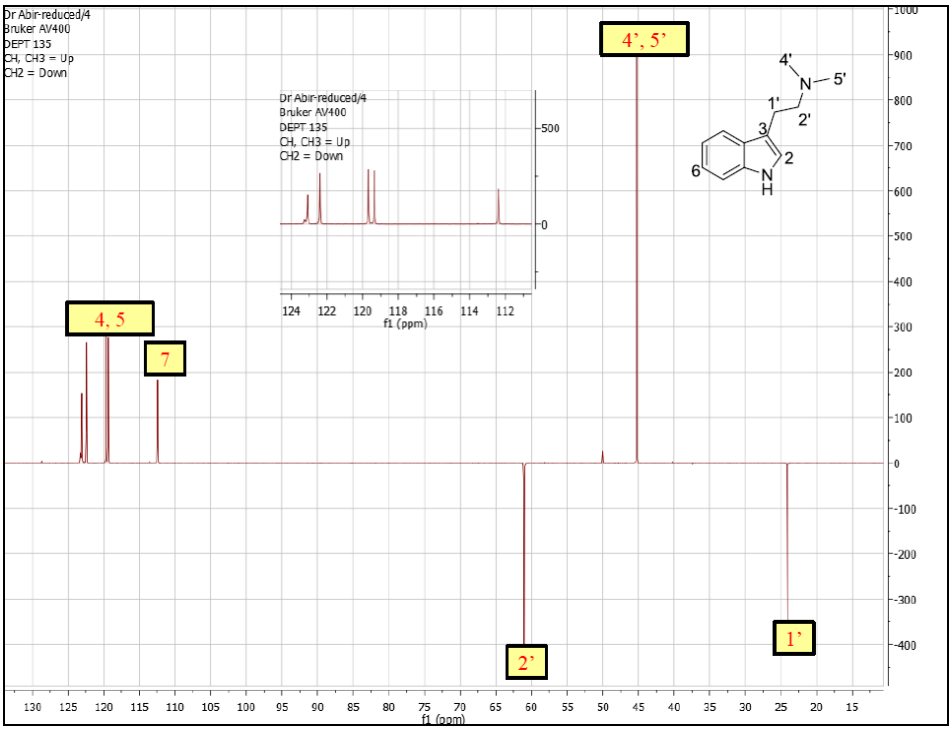

Figure 84. 135° DEPT spectrum of 2-(1*H*-indol-3-yl)-*N*,*N*-dimethylethanamine (**4a**) in methanol-d_4 (400 MHz)

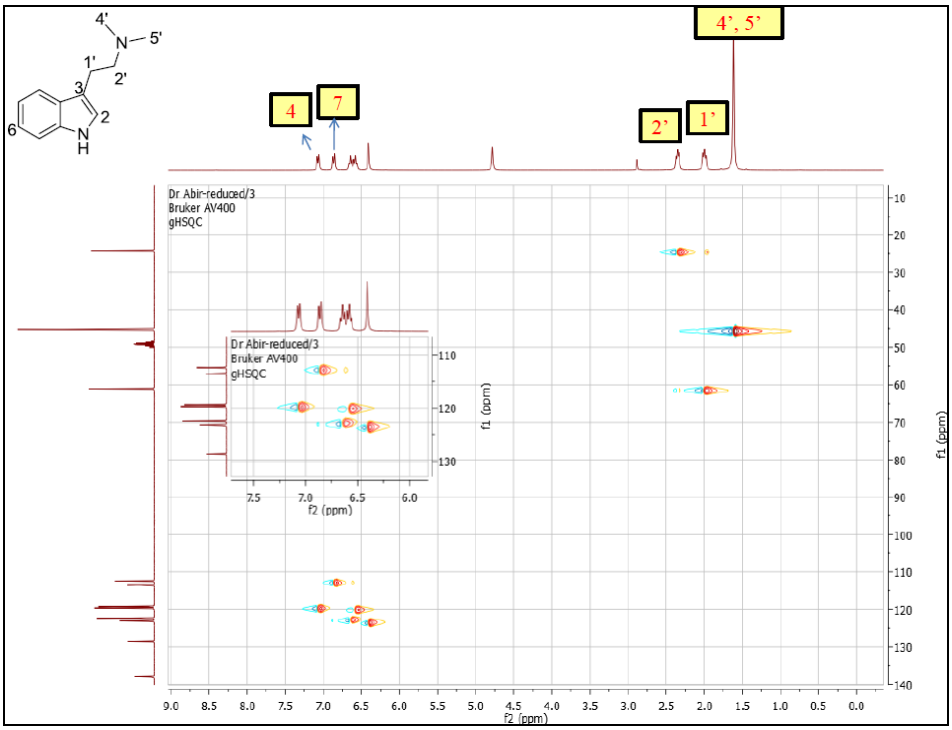

Figure 85. HSQC spectrum of 2-(1*H*-indol-3-yl)-*N*,*N*-dimethylethanamine (**4a**) in methanol-d_4 (400 MHz)

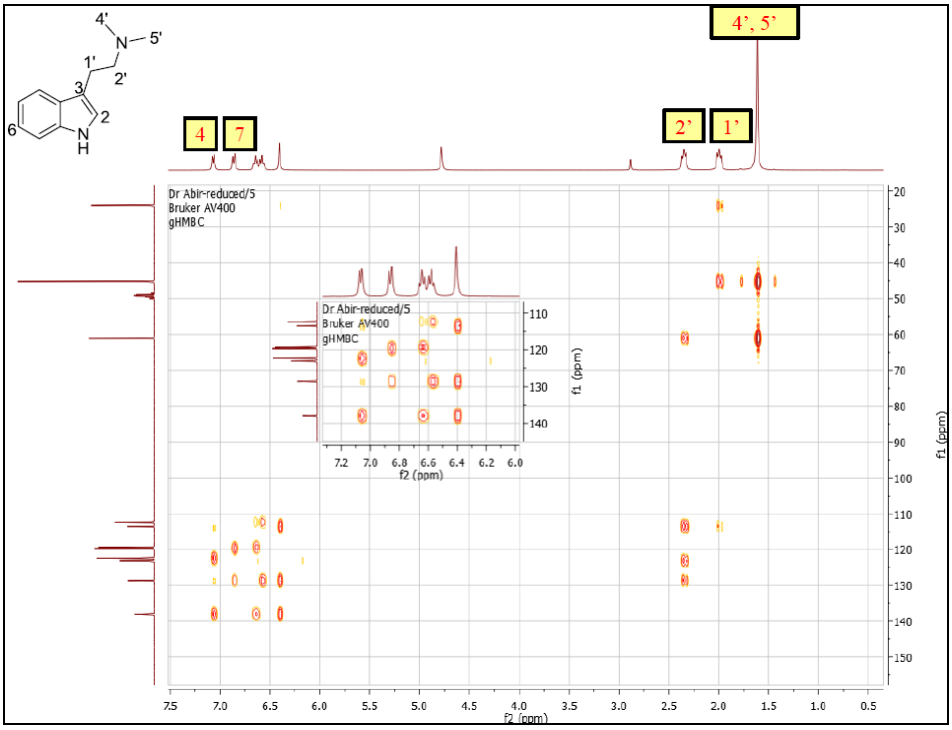

Figure 86. HMBC spectrum of 2-(1*H*-indol-3-yl)-*N*,*N*-dimethylethanamine (**4a**) in methanol-d_4 (400 MHz)

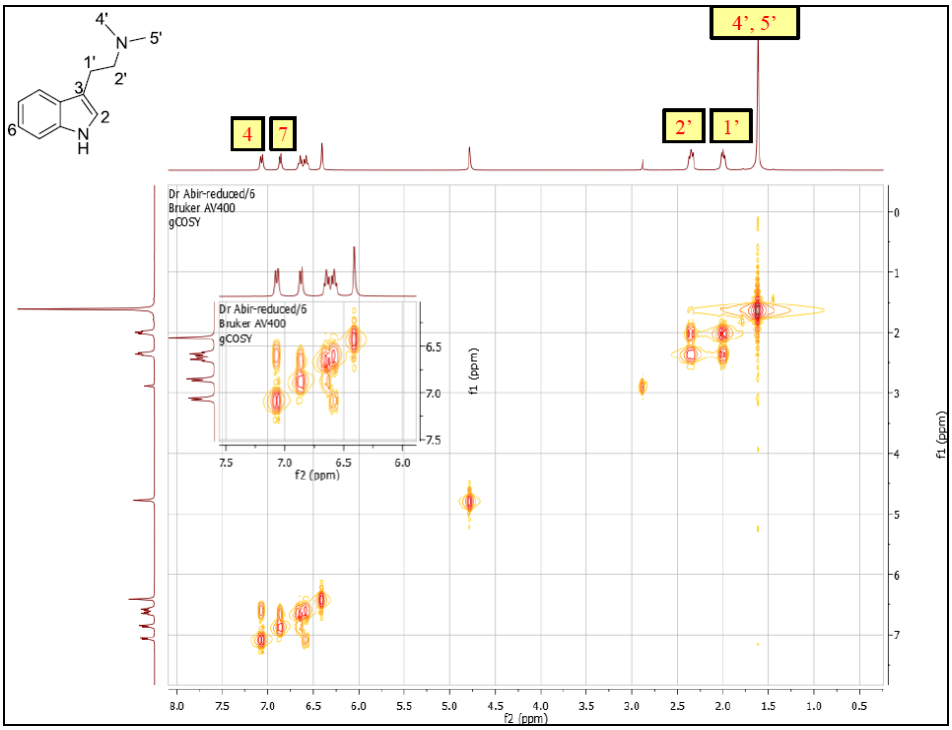

Figure 87. COSY spectrum of 2-(1*H*-indol-3-yl)-*N*,*N*-dimethylethanamine (**4a**) in methanol-d_4 (400 MHz)

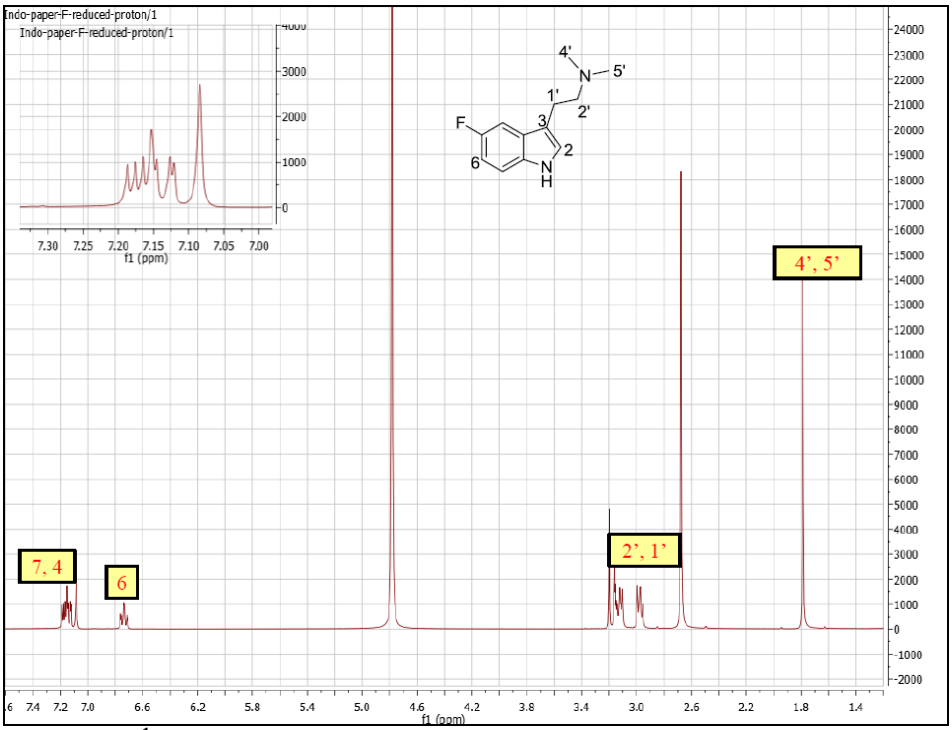

Figure 88. ^{1}H NMR spectrum of 2-(5-fluoro-1*H*-indol-3-yl)-*N*,*N*-dimethylethanamine (**4b**) in methanol-d_4 (400 MHz)

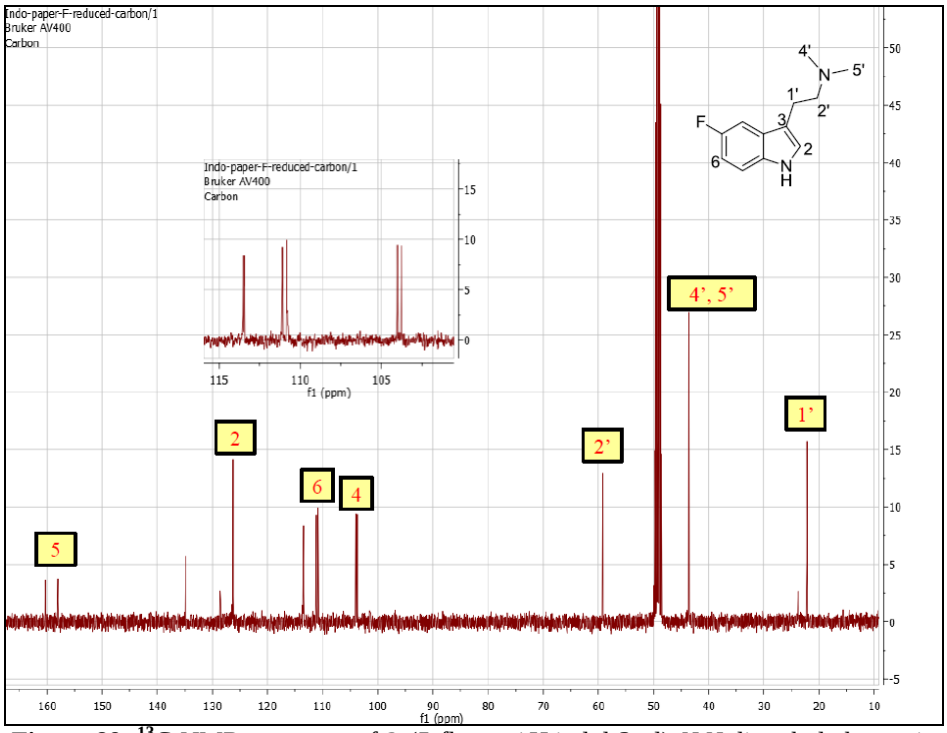

Figure 89. ^{13}C NMR spectrum of 2-(5-fluoro-1*H*-indol-3-yl)-*N*,*N*-dimethylethanamine (**4b**) in methanol-d_4 (400 MHz)

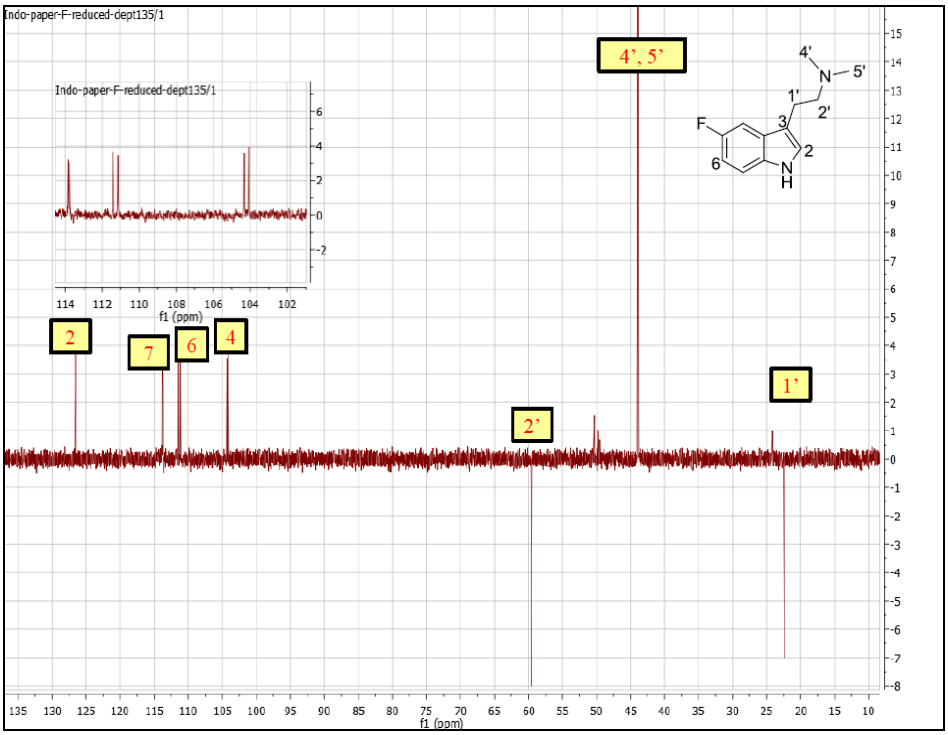

Figure 90. 135º DEPT spectrum of 2-(5-fluoro-1*H*-indol-3-yl)-*N*,*N*-dimethylethanamine (**4b**) in methanol-d_4 (400 MHz)

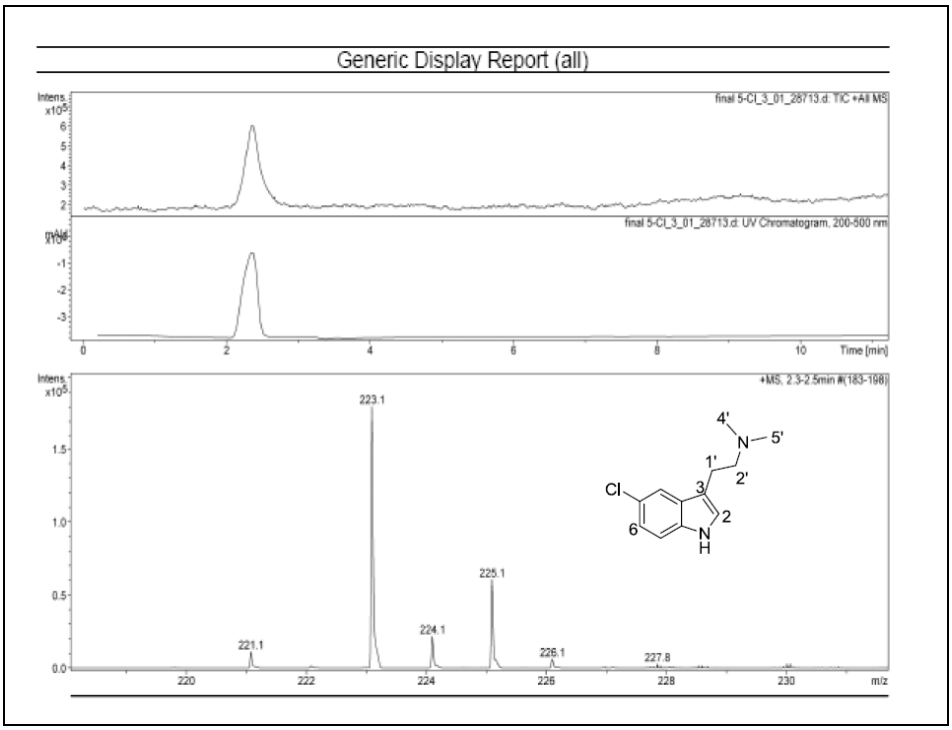

Figure 91. LC/MS chromatogram of 2-(5-chloro-1*H*-indol-3-yl)-*N*,*N*-dimethylethanamine (**4c**)

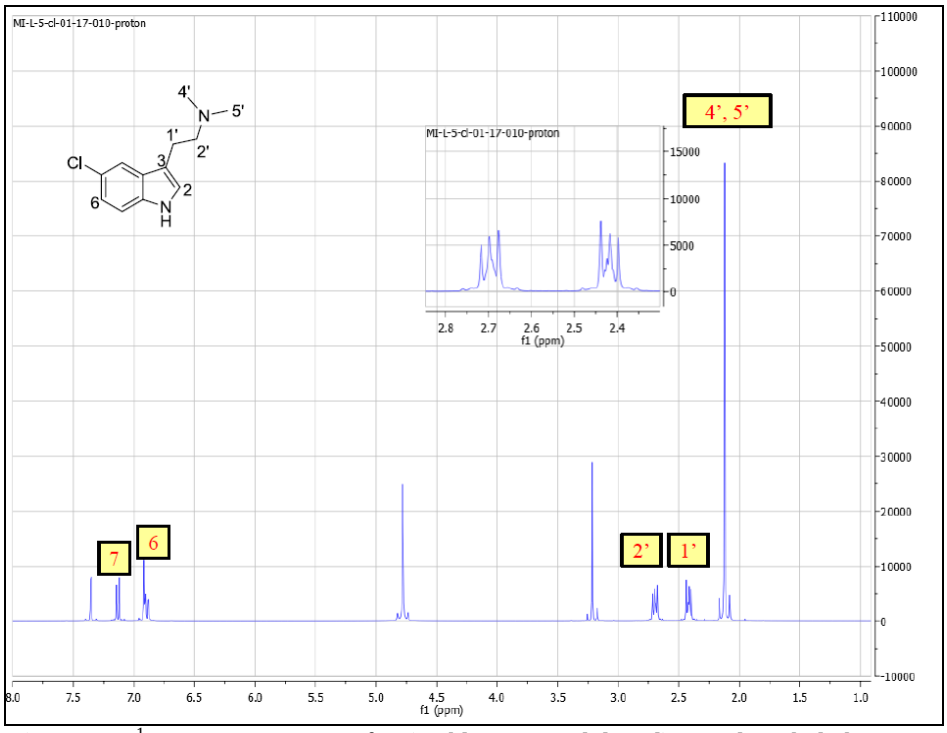

Figure 92. ^{1}H NMR spectrum of 2-(5-chloro-1*H*-indol-3-yl)-*N*,*N*-dimethylethanamine (**4c**) in methanol-d_4 (400 MHz)

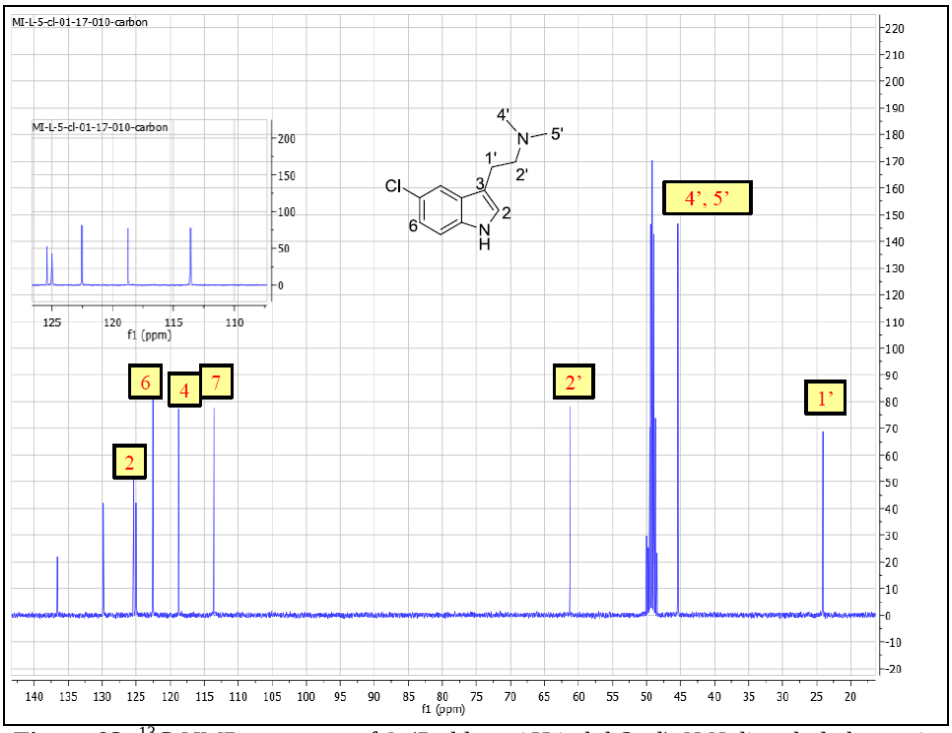

Figure 93. ^{13}C NMR spectrum of 2-(5-chloro-1*H*-indol-3-yl)-*N*,*N*-dimethylethanamine (**4c**) in methanol-d_4 (400 MHz)

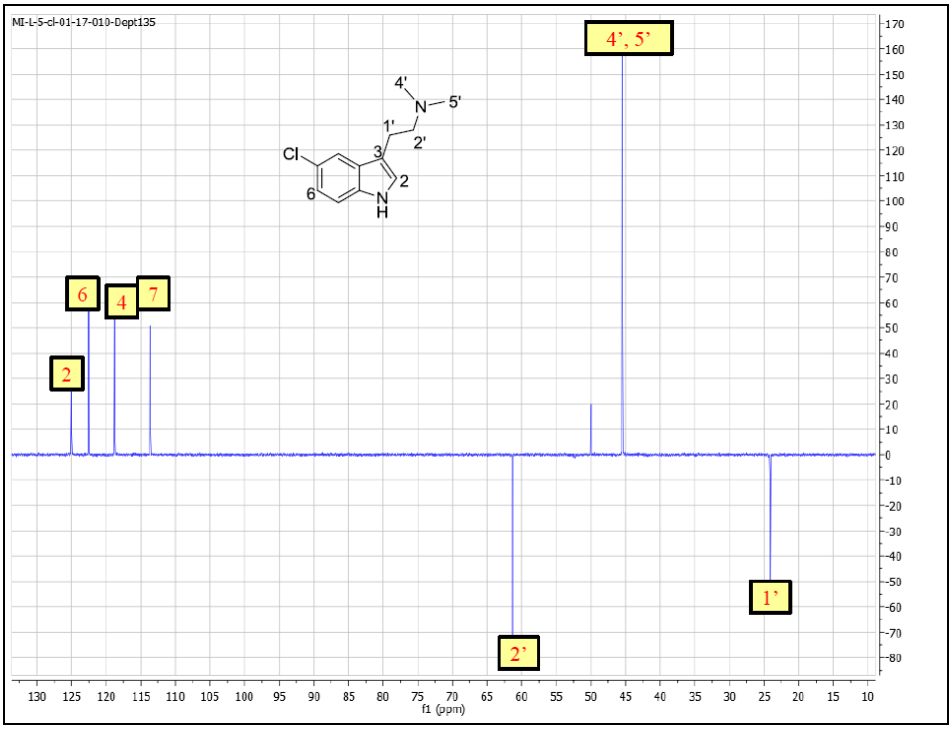

Figure 94. 135º DEPT spectrum of 2-(5-chloro-1*H*-indol-3-yl)-*N*,*N*-dimethylethanamine (**4c**) in methanol-d_4 (400 MHz)

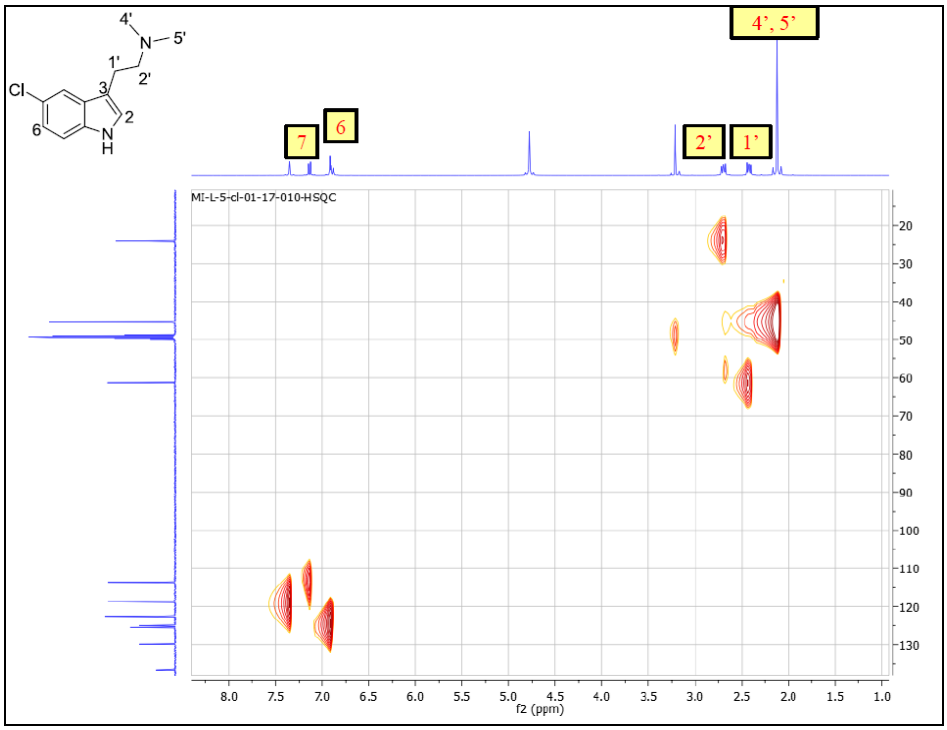

Figure 95. HSQC spectrum of 2-(5-chloro-1*H*-indol-3-yl)-*N*,*N*-dimethylethanamine (**4c**) in methanol-d_4 (400 MHz)

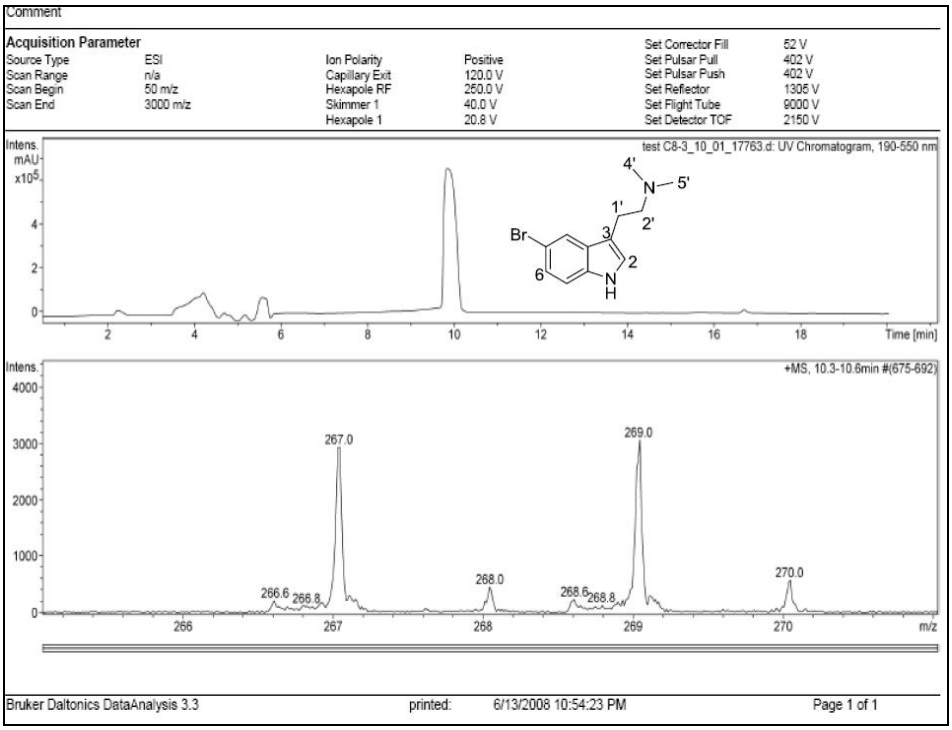

Figure 96. LC/MS chromatogram of 2-(5-bromo-1*H*-indol-3-yl)-*N*,*N*-dimethylethanamine (**4d**)

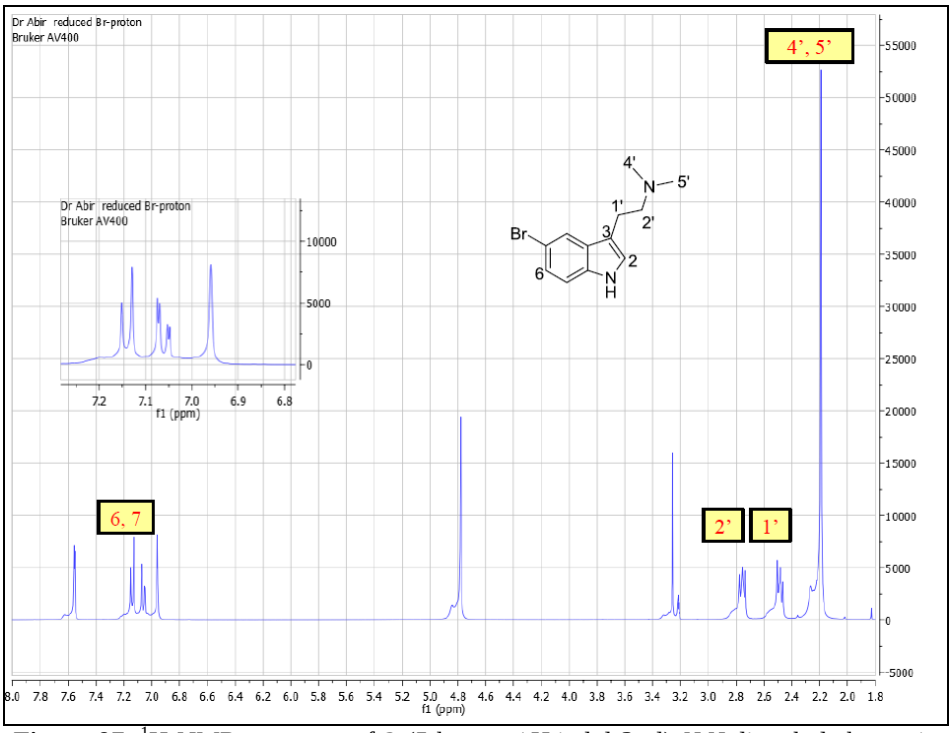

Figure 97. ^{1}H NMR spectrum of 2-(5-bromo-1*H*-indol-3-yl)-*N*,*N*-dimethylethanamine (**4d**) in methanol-d_4 (400 MHz)

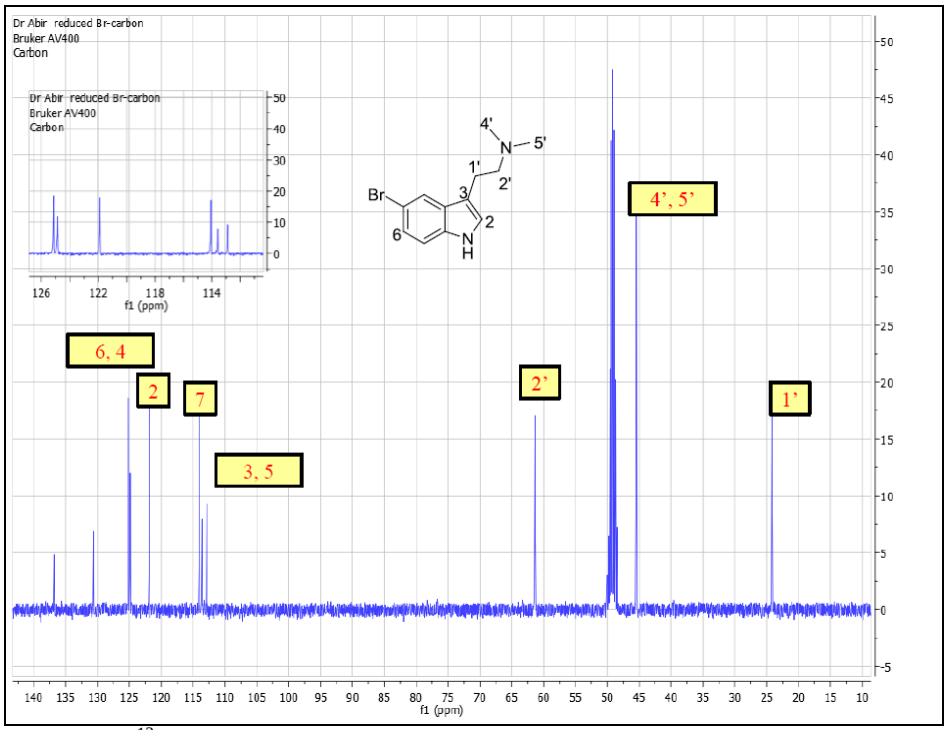

Figure 98. ^{13}C NMR spectrum of 2-(5-bromo-1*H*-indol-3-yl)-*N*,*N*-dimethylethanamine (**4d**) in methanol-d_4 (400 MHz)

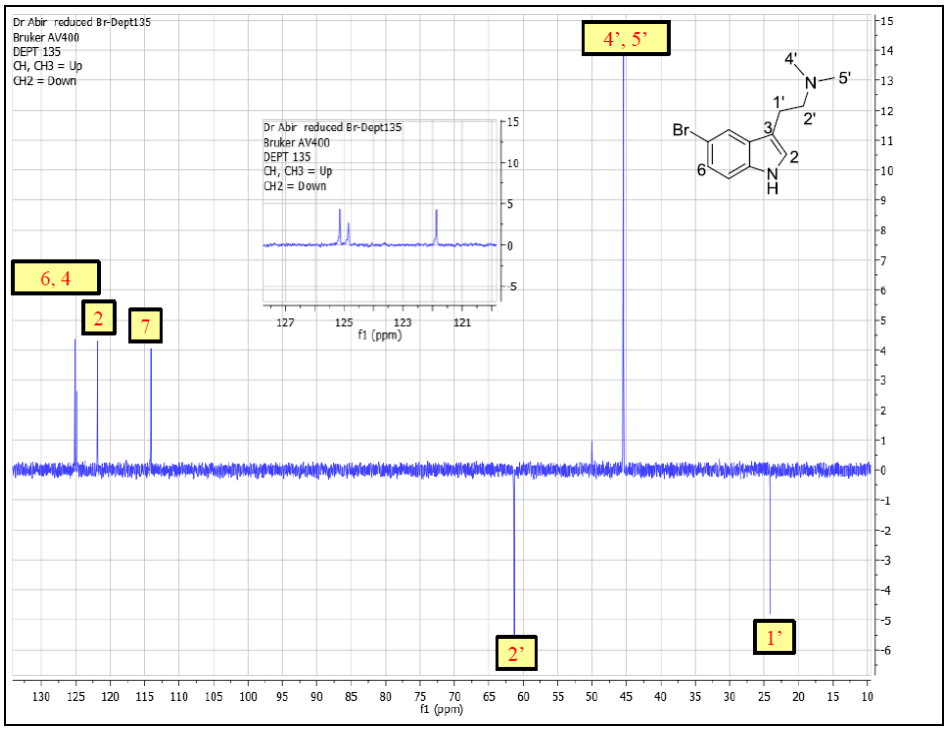

Figure 99. 135º DEPT spectrum of 2-(5-bromo-1*H*-indol-3-yl)-*N*,*N*-dimethylethanamine (**4d**) in methanol-d_4 (400 MHz)

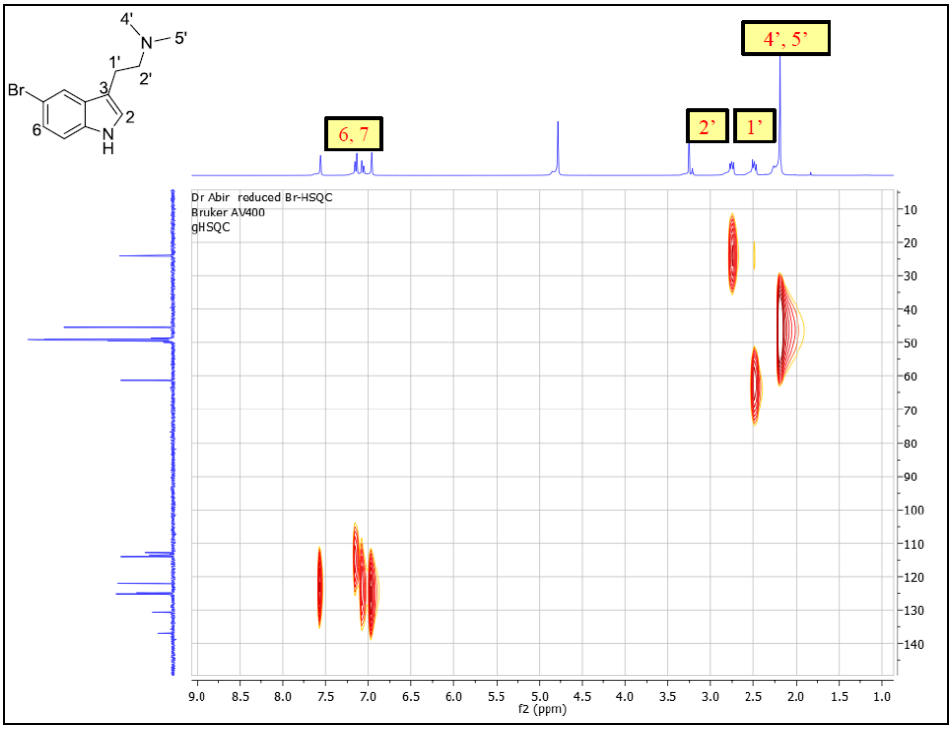

Figure 100. HSQC spectrum of 2-(5-bromo-1*H*-indol-3-yl)-*N*,*N*-dimethylethanamine (**4d**) in methanol-d_4 (400 MHz)

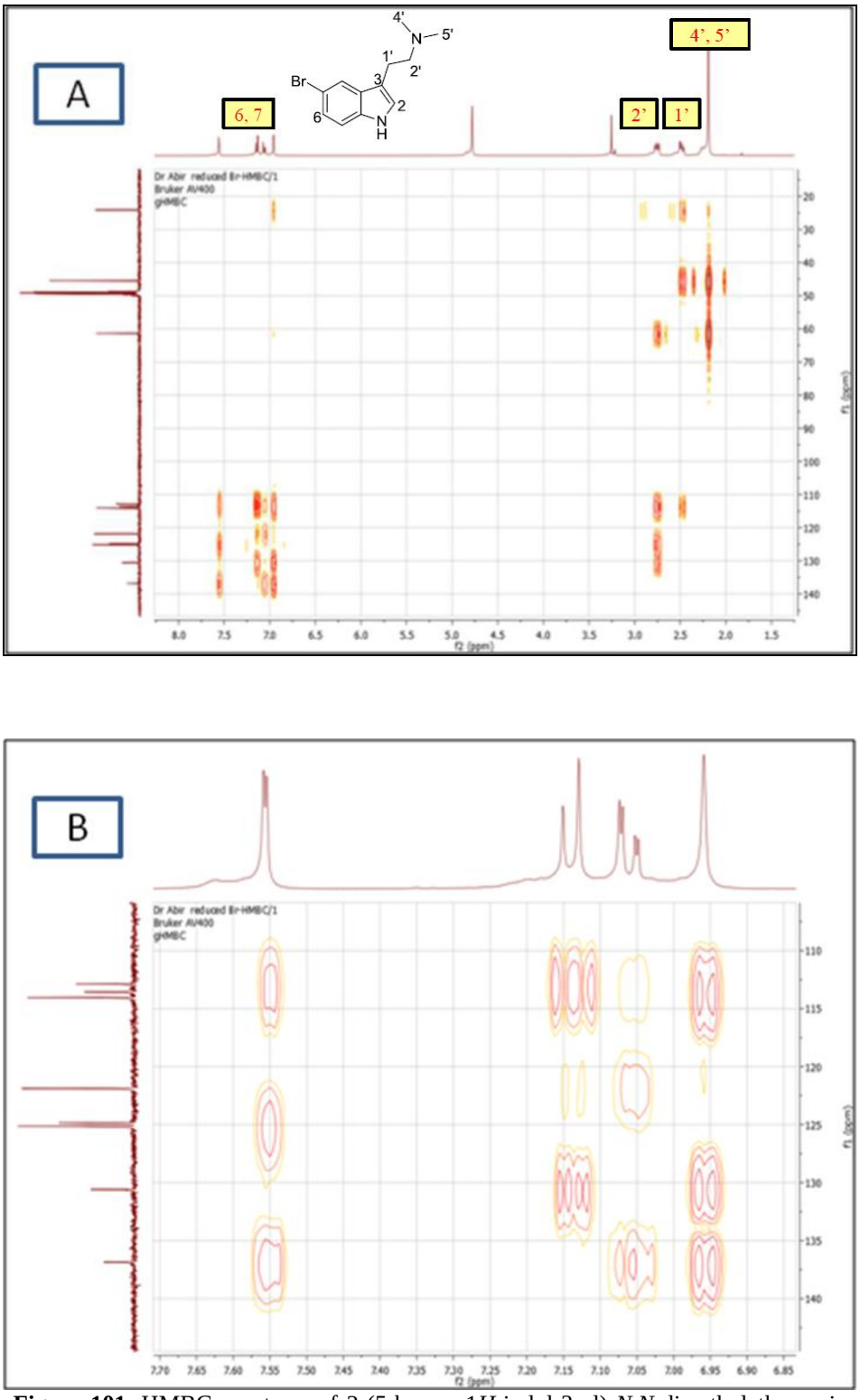

Figure 101. HMBC spectrum of 2-(5-bromo-1*H*-indol-3-yl)-*N*,*N*-dimethylethanamine (**4d**) in methanol-d_4 (400 MHz); A) the full spectrum, B) the high field region

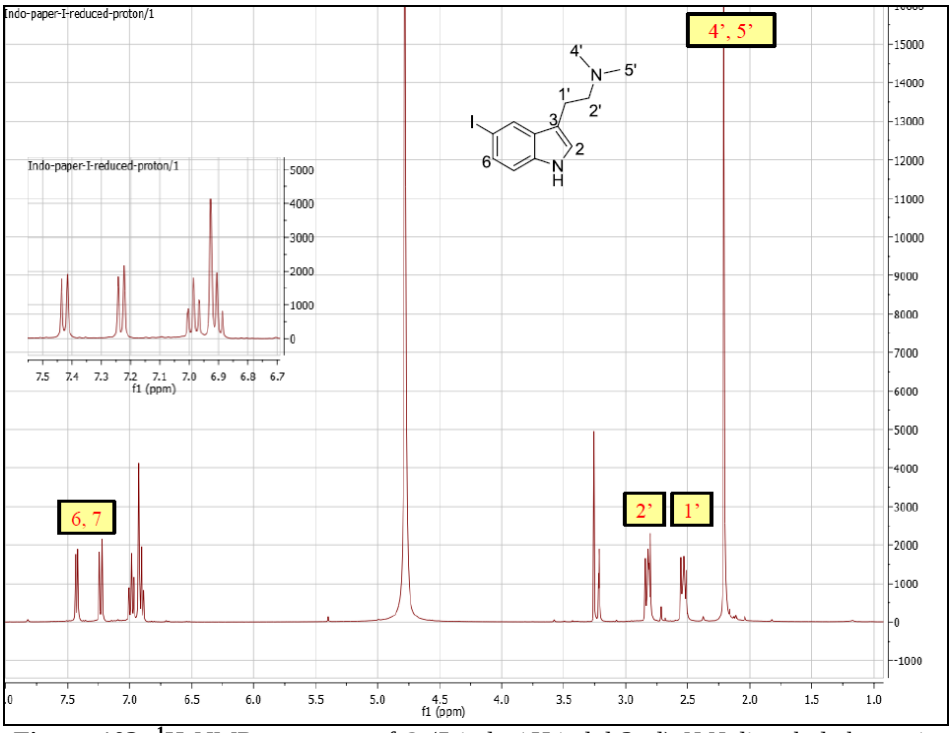

Figure 102. ^{1}H NMR spectrum of 2-(5-iodo-1*H*-indol-3-yl)-*N*,*N*-dimethylethanamine (**4e**) in methanol-d_4 (400 MHz)

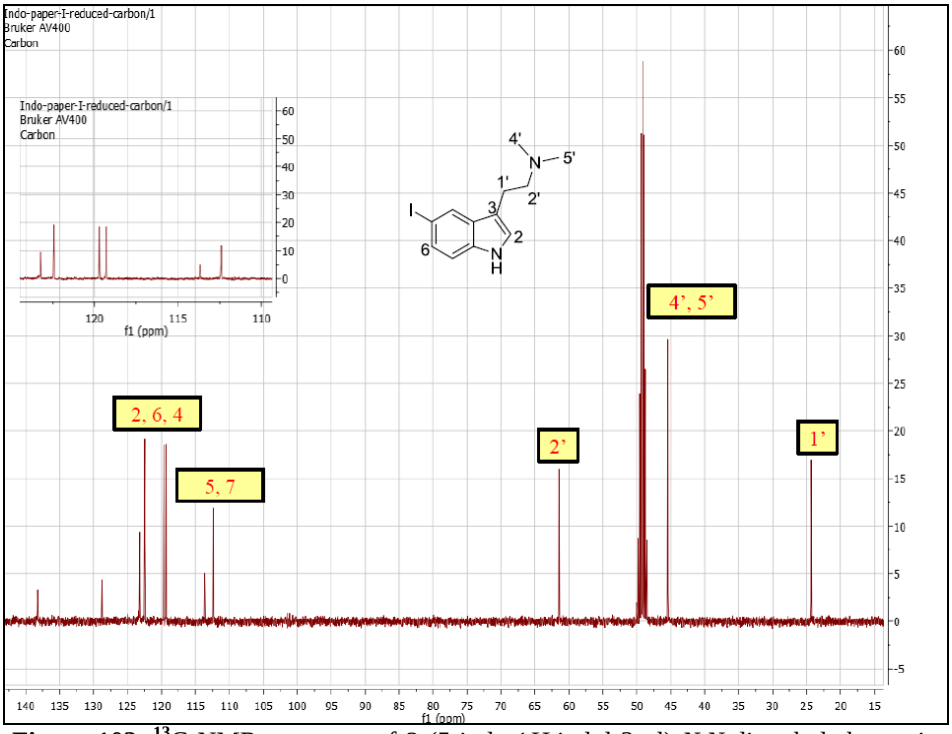

Figure 103. ^{13}C NMR spectrum of 2-(5-iodo-1*H*-indol-3-yl)-*N*,*N*-dimethylethanamine (**4e**) in methanol-d_4 (400 MHz)

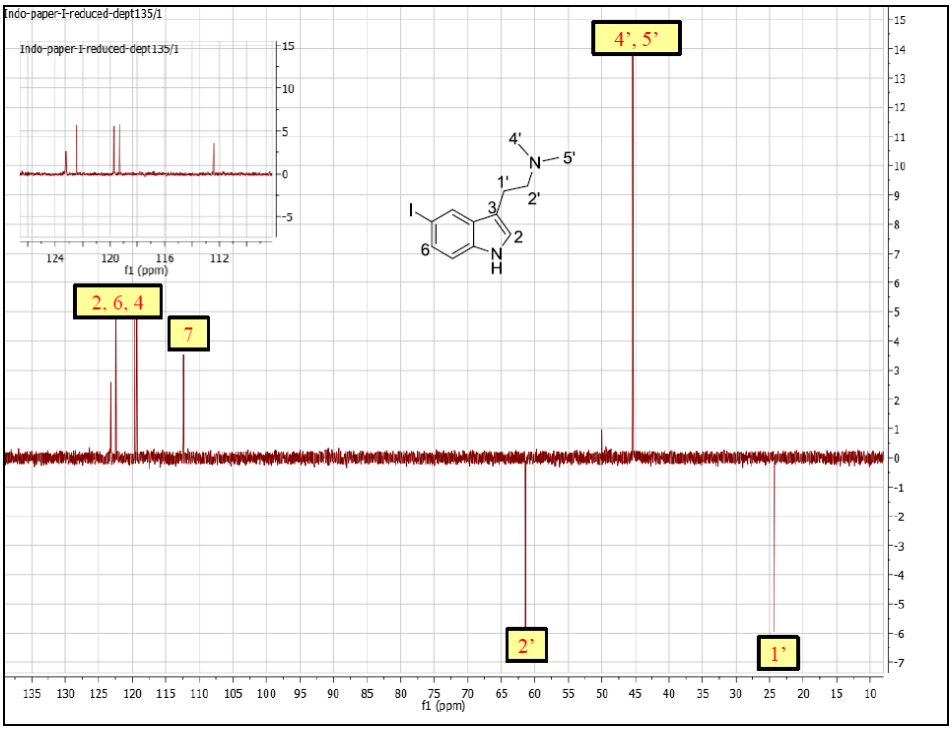

Figure 104. 135° DEPT spectrum of 2-(5-iodo-1*H*-indol-3-yl)-*N*,*N*-dimethylethanamine (**4e**) in methanol-d_4 (400 MHz)

2.3 Forced Swim Test (FST)

The FST is a model of behavioral despair whereby mice placed in an inescapable situation (in this case a cylinder of water) usually exhibit behavioral despair within two minutes of a six minute session. An antidepressant effect is elicited as a reduction in immobility duration and sustained escape attempts (swimming and climbing).[43] Swiss Webster mice were injected (i.p.) with the test compound, vehicle, or control antidepressant desipramine, bupropion, or fluoxetine (10-40 mg/kg, i.p.), *n*=7-10/group. The animals were immediately placed in individual locomotor chambers and their total activity was monitored for 30 minutes. The mice were then individually placed in clear plastic cylinders (height 23 cm, internal diameter 10 cm) filled with 8 cm of deionized water at 25 °C. Individual mice were videotaped for a total of six minutes. Digital video output was then analyzed using the SMART II Video Tracking System Software (San Diego Instruments, CA, USA). The software then determined immobility in the six minute session, but only

the data of the last four minutes was used to determine the effect. The immobility time was defined as the time spent by the mouse moving at a velocity below 2 cm/s. Such a threshold velocity was chosen based on previously published data and our validation of the automated system where this threshold produced immobility scores similar to those determined from manually scored tapes.[44]

2.4 Locomotor Activity

Coupled with the FST, the effect of the test compound on locomotor activity was monitored to avoid any false positives resulting from stimulant action, as well as to evaluate any potential sedative action of the compound. Locomotor activity was measured using an automated activity monitoring system (San Diego Instruments, CA, USA). Mice were acclimated to the testing environment for 30 minutes and then injected (i.p.) with the vehicle (10% ethanol), control antidepressant, or test compound. Each mouse was immediately placed in a Plexiglas enclosure and locomotor activity monitored for the next 30 minutes. Activity is recorded as interruptions of two sets of photo-beams. The data during the last ten minutes of the testing period was analyzed. Immediately following the locomotor measurements (equivalent to the 30 minutes pre-treatment time), the mice were subject to the FST as described above.

2.5 In Vitro Binding to Serotonin Receptors

Compounds **4a**, **4c**, **4d**, and **4e** were assayed in the NIMH Psychoactive Drug Screening Program which provides screening of pharmacological activity in the panel of cloned human and rodent receptors, channels, and transporters. For experimental details, please refer to the PDSP web site http://pdsp.med.unc.edu.

2.6. Data Analysis

All values were presented as mean ± S.E.M. with *n*= 7-10 animals /group. All data was analyzed using One Way ANOVA followed by Dunnett's post hoc test to determine significant difference from the

vehicle control at $p<0.05$.

3. Results

Compounds **3a-e** and **4a-e** were evaluated for their potential antidepressant activity in the forced swim test, (Figures 105A and 106A), which is a reliable and widely used animal model for antidepressant screening.[45] The compounds were initially evaluated at a dose of 20 mg/kg in comparison to the parent 2-(5,6-di-bromo-1*H*-indol-3-yl)-*N*,*N*-dimethylethanamine and 2-(5-bromo-1*H*-indol-3-yl)-*N*,*N*-dimethylethanamine derivatives previously showing significant antidepressant and sedative action at such a dose. A set of clinically used antidepressants (the tricyclic antidepressant desipramine, the selective serotonin reuptake inhibitor fluoxetine, and the dual dopamine and noradrenaline inhibitor bupropion) were used as positive controls.

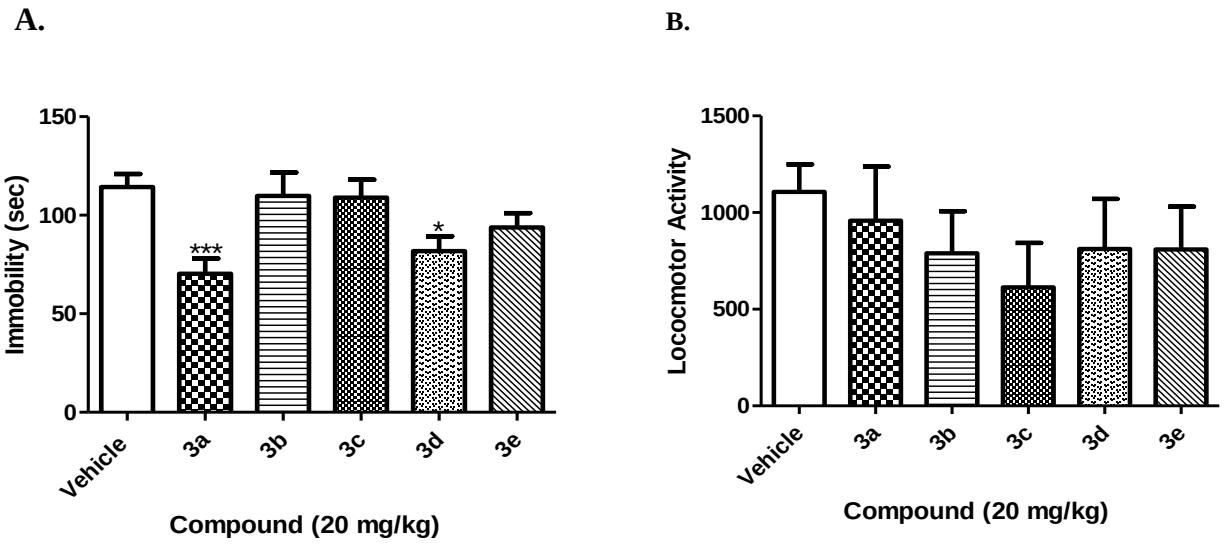

Figure 105. Effect of compounds **3a-e** (20 mg/kg, i.p.) in (A) the forced swim test and (B) locomotor activity. Data presented as the mean ± S.E.M. (n=7-10). Data were analyzed using One Way ANOVA followed by Dunnett's post-hoc test where *$p<0.05$ and ***$p<0.001$ were statistically different from the vehicle control.

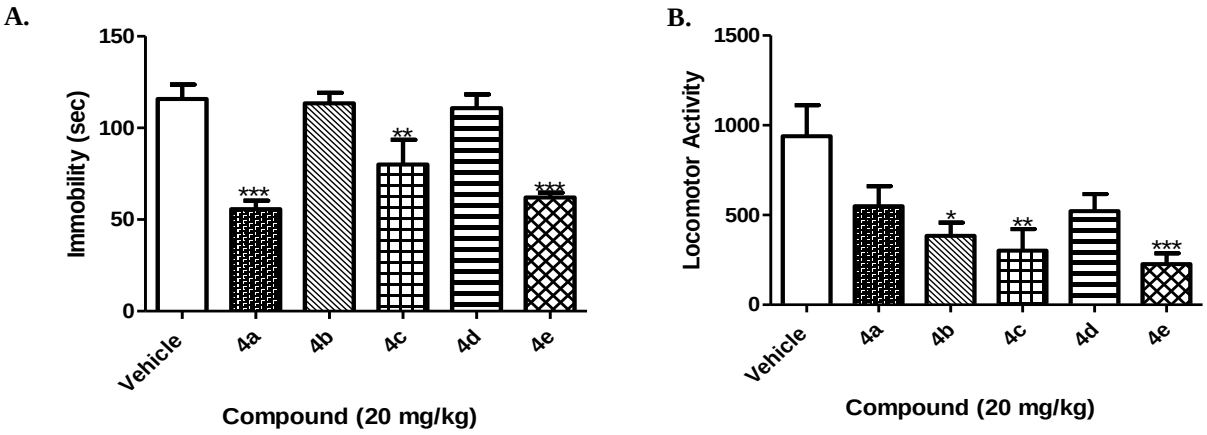

Figure 106. Effect of compounds **4a-e** (20 mg/kg, i.p.) in (A) the forced swim test and (B) locomotor activity. Data presented as the mean ± S.E.M. (*n*=7-10). Data were analyzed using One Way ANOVA followed by Dunnett's post-hoc test where ***p<0.01*, ****p<0.001* were statistically different from the vehicle control.

The effect on locomotor activity was also evaluated to eliminate any non-specific stimulating effect and to reveal any possible sedative activity. As shown in Table 9, the control antidepressants showed significant dose-dependent reduction in immobility consistent with their established antidepressant action. The effect on locomotor activity was different, whereby both desipramine and fluoxetine caused significant reduction in activity, while bupropion showed a significant locomotor stimulant effect. As shown in Figure 105A, the initial evaluation of analogs revealed that compounds **3a** and **3d** significantly reduced immobility in the FST (*p<0.001*, and *p<0.05*, respectively) at the tested 20 mg/kg. The compounds did not significantly alter locomotor activity at this dose (Figure 105B). Similarly, compounds **4a**, **4c**, and **4e** showed significant antidepressant-like action in the FST (*p<0.001*, *p<0.01*, and *p<0.001*, respectively) when administered at the 20 mg/kg dose (Figure 106A). Compound **4a** did not exert a significant effect on locomotor activity, while both compounds **4c** and **4e** had significant hypolocomotive action (*p<0.01*, and *p<0.001*, respectively). On the other hand, compound **4b** did not affect immobility in the FST but significantly reduced locomotor activity (*p<0.01*) as presented in Figure 106B.

Table 9. Effect of control antidepressants on immobility time in mouse forced swim test and total locomotor activity

Treatment	Immobility (sec)	Locomotor
Vehicle	121 ± 7.3	1618 ± 142
Bupropion 10 mg/kg	101 ± 10.5	2746 ± 298*
Bupropion 20 mg/kg	80 ± 7.1**	3564 ± 503***
Bupropion 40 mg/kg	58 ± 8.2 ***	5290 ± 544***
Fluoxetine 10 mg/kg	91 ± 10	1898 ± 132
Fluoxetine 20 mg/kg	90 ± 6.8	1293 ± 243
Fluoxetine 40 mg/kg	75.8 ± 12.9**	143 ± 34***
Desipramine 10 mg/kg	112 ± 6.6	763 ± 112**
Desipramine 20 mg/kg	81 ± 4.9**	776 ± 265**
Desipramine 40 mg/kg	70 ± 8.9***	117 ± 43***

*p<0.05, **p<0.01, ***p<0.001 (Dunnett's post-hoc test versus vehicle)

Full dose response studies for effects in FST, as well as locomotor activity were conducted for compounds **3a**, **3d**, **4a**, **4c**, **4d**, and **4e** (Figures 107-112A and 107-112B). Results revealed that, with the exception of compound **4d**, all the tested compounds show a U-shaped dose response effect in the FST. Compound **3a** shows only significant antidepressant-like action at the 20 mg/kg dose only ($p<0.01$) and a significant increase in locomotor activity at the 40 mg/kg dose ($p<0.01$). Compound **4c** showed a significant reduction in immobility time at the 10 ($p<0.01$) and 20 ($p<.001$) mg/kg doses and significant decrease in locomotor activity at both the 20 and 40 mg/kg doses ($p<0.01$). Similarly, compound **4e** had significant antidepressant-like effect in the FST at 10 and 20 mg/kg ($p<0.001$) that coincided with a significant hypolocomotive effect ($p<0.05$ at 10 mg/kg and $p<0.01$ at 20 mg/kg). Although compound **4d** did not show an antidepressant-like action in the initial evaluation studies, a significant reduction in immobility was observed at 40 mg/kg ($p<0.001$) accompanied by a significant decrease in locomotor activity at the same

dose (*p<0.01*).

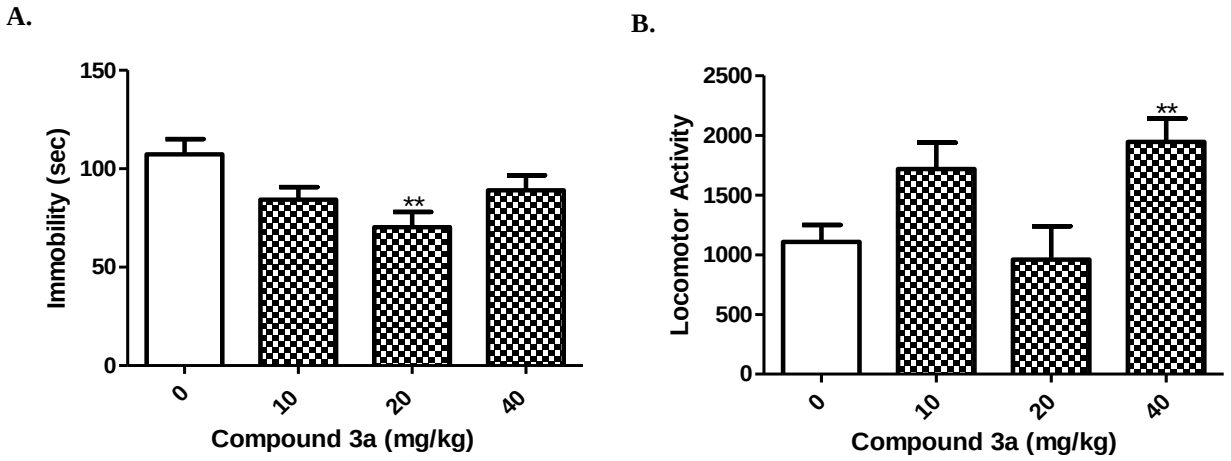

Figure 107. Dose response curves of compound **3a** in (A) the forced swim test and (B) locomotor activity. Data presented as the mean ± S.E.M. (*n*=7-10). Data were analyzed using One Way ANOVA followed by Dunnett's post-hoc test where ***p<0.01* was statistically different from the vehicle control.

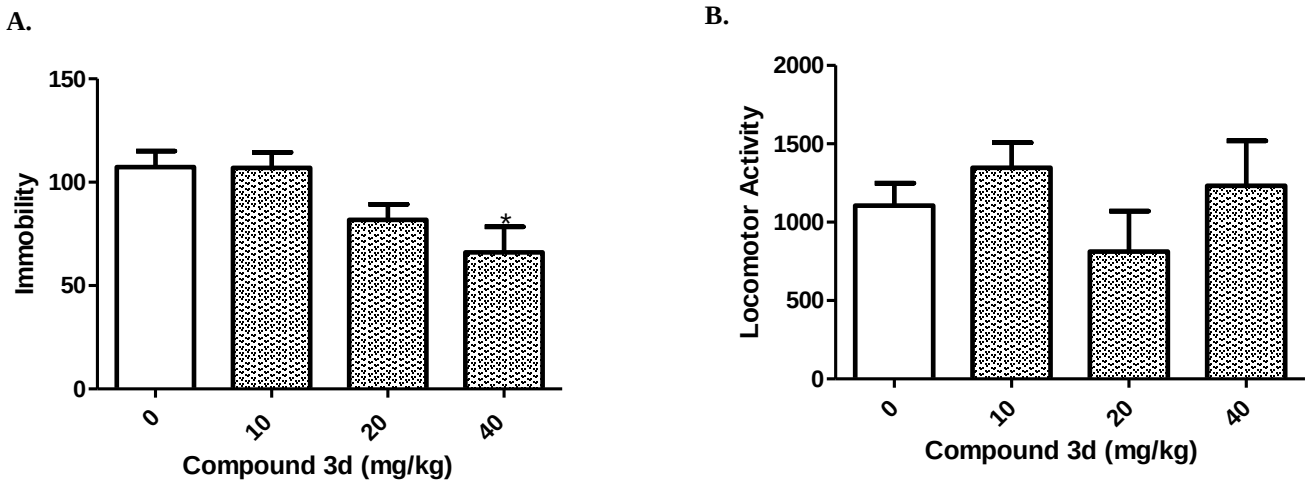

Figure 108. Dose response curves of compound **3d** in (A) the forced swim test and (B) locomotor activity. Data presented as the mean ± S.E.M. (*n*=7-10). Data were analyzed using One Way ANOVA followed by Dunnett's post-hoc test where **p<0.05* were statistically different from the vehicle control.

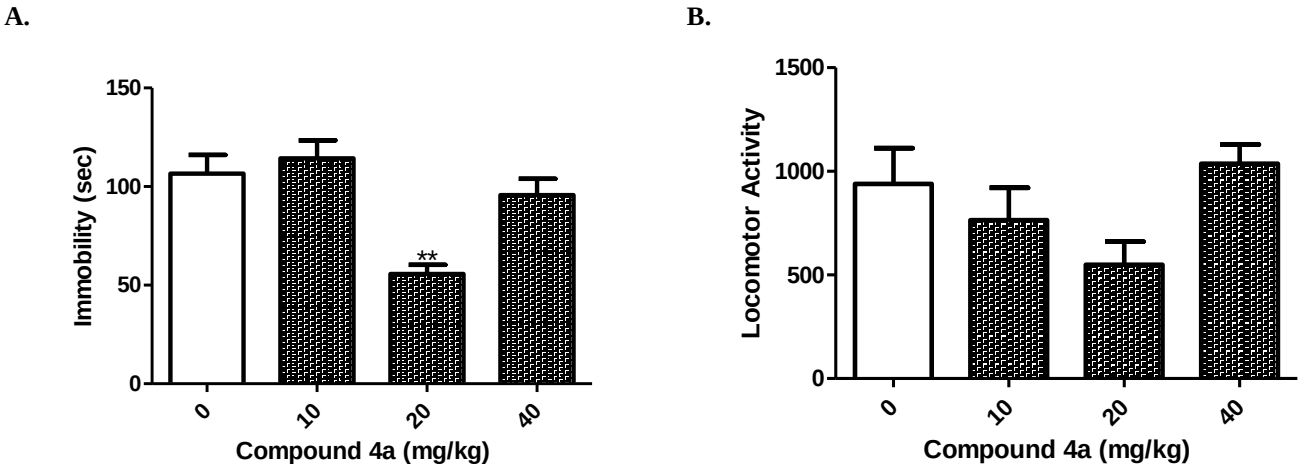

Figure 109. Dose response curves of compound **4a** in (A) the forced swim test and (B) locomotor activity. Data presented as the mean ± S.E.M. (*n*=7-10). Data were analyzed using One Way ANOVA followed by Dunnett's post-hoc test where ***p<0.01* was statistically different from the vehicle control.

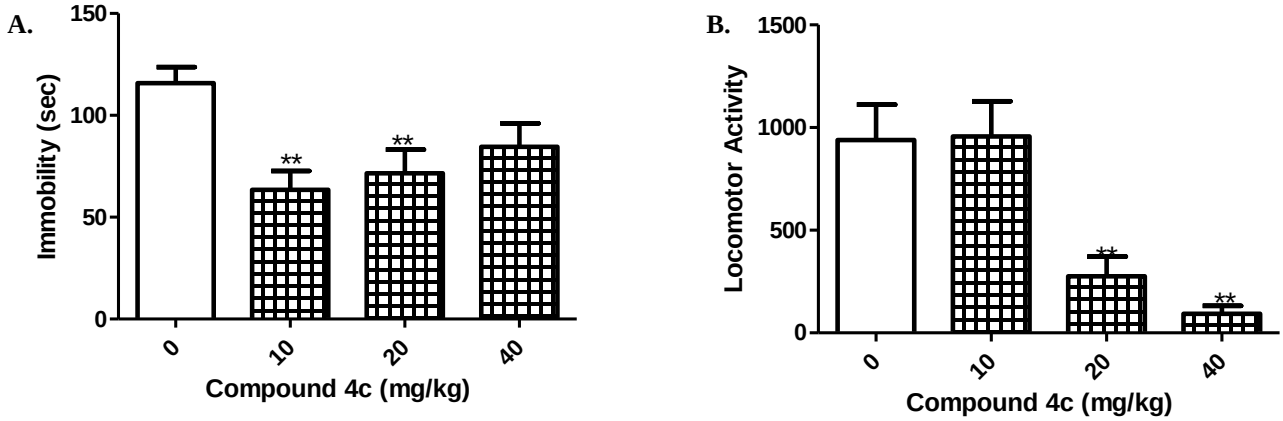

Figure 110. Dose response curves of compound **4c** in (A) the forced swim test and (B) locomotor activity. Data presented as the mean ± S.E.M. (*n*=7-10). Data were analyzed using One Way ANOVA followed by Dunnett's post-hoc test where ***p<0.01* was statistically different from the vehicle control.

.

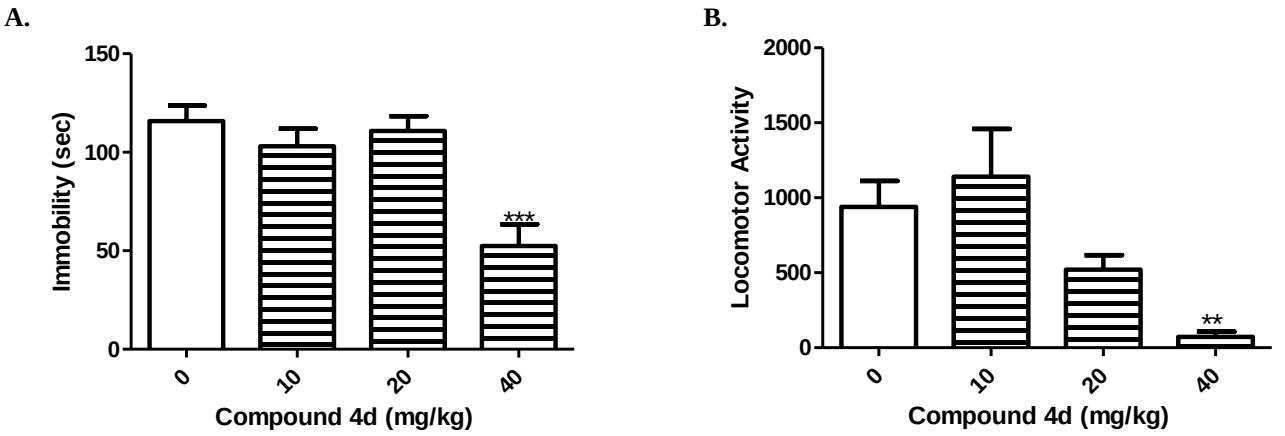

Figure 111. Dose response curves of compound **4d** in (A) the forced swim test and (B) locomotor activity. Data presented as the mean ± S.E.M. (*n*=7-10). Data were analyzed using One Way ANOVA followed by Dunnett's post-hoc test where ***p<0.01* and ****p<0.001* were statistically different from the vehicle control.

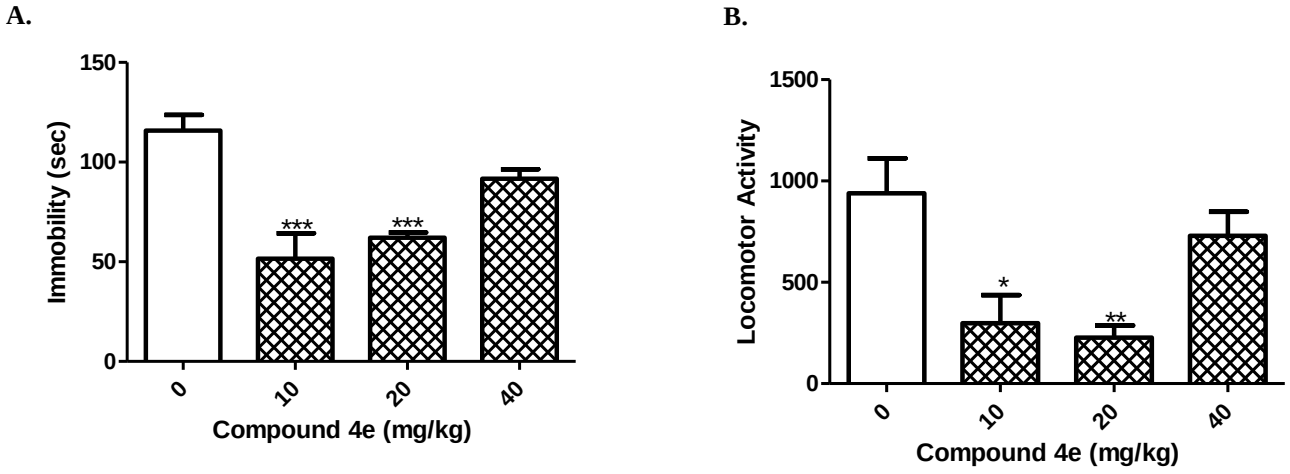

Figure 112. Dose response curves of compound **4e** in (A) the forced swim test and (B) locomotor activity. Data presented as the mean ± S.E.M. (*n*=7-10). Data were analyzed using One Way ANOVA followed by Dunnett's post-hoc test where *p<0.05, ***p<0.01, ****p<0.001* were statistically different from the vehicle control.

Compounds **4a, 4c, 4d**, and **4e** were assayed for their in vitro binding to serotonin receptors in the panel of cloned human and rodent receptors, channels, and transporters available in the NIMH Psychoactive Drug Screening Program. As shown in Table 10, compounds **4a**, **4c**, **4d**, and **4e** showed high nanomolar affinity to several serotonin receptor subtypes. Highest affinity was observed towards $5HT_{1A}$, $5HT_{1B/1D}$, $5HT_{2B}$, $5HT_6$, and $5HT_7$ subtypes; (Figures 113-124). In vitro Vero cell (kidney fibroblast cells) cytotoxicity of 4a, 4c, and 4d was not observed up to the maximum dose of 100 μg/mL.

Table 10. Binding affinities of **4a**, **4c**, **4d**, and **4e** towards serotonin receptors

Receptor	**Compound 4a** **Ki [nM]**	**Compound 4c** **Ki [nM]**	**Compound 4d** **Ki [nM]**	**Compound 4e** **Ki [nM]**	**Controls**	
					Ergotamine **Ki [nM]**	**Methysergide** **Ki [nM]**
$5HT_{1A}$	110.0 ± 17.0	5.5 ± 0.4	9.6 ± 1.1	130.0 ± 16.0	0.17	14.0
$5HT_{1B}$	66.0 ± 9.0	66.0 ± 5.0	19.0 ± 2.0	43.0 ± 5.0	0.3	2.5
$5HT_{1D}$	29.3 ± 3.7	14.0 ± 1.0	2.6 ± 0.32	8.5 ± 1.38	0.3	69.0
$5HT_{1E}$	>10,000	356.0 ± 34.0	398.0 ± 30.0	310.0 ± 33.0	19.0	237.0
$5HT_{2B}$	145.0 ± 13.0	7.8 ± 0.7	27.0 ± 1.0	98.0 ± 4.0	1.9	0.1
$5HT_3$	5,187 ± 883	1,325 ± 125	1,374 ± 212	4,486 ± 804	>10,000	>10,000
$5HT_{5A}$	>10,000	408.0 ± 54.0	1,038 ± 110	1,254 ± 197	-	>10,000
$5HT_6$	189.5 ± 32.5	30.0 ± 2.0.0	22.0 ± 2.0	198.0 ± 20.0	12.0	52.0
$5HT_7$	77.0 ± 16.0	7.2 ± 0.6	8.3 ± 0.9	116.0 ± 13.0	1,291	30.0

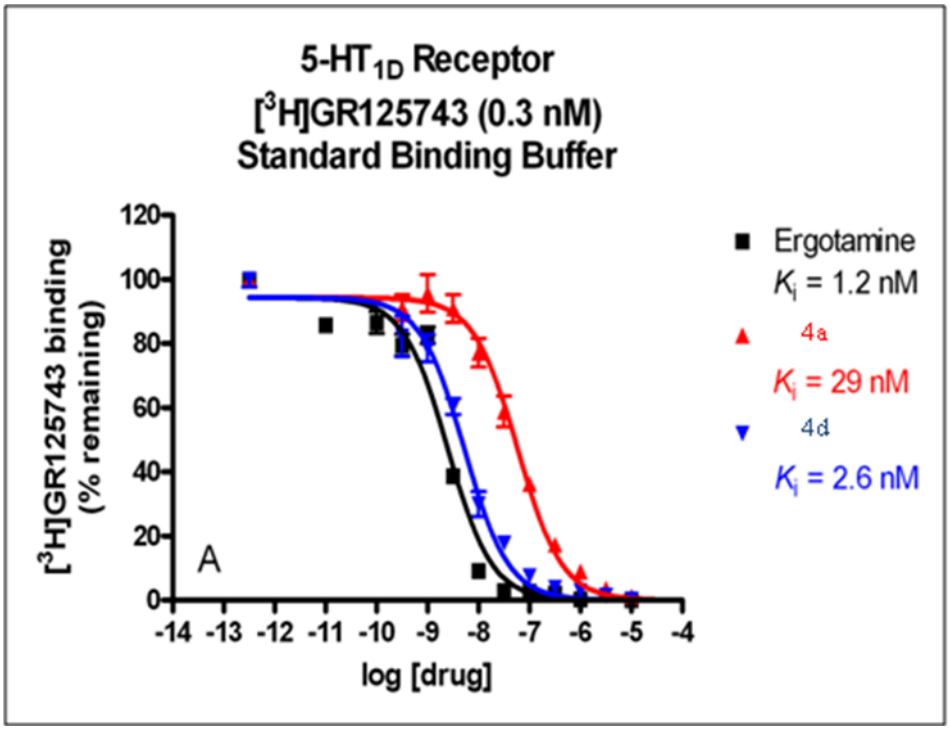

Figure 113. In vitro binding affinity of **4a** and **4d** towards 5-HT_{1D}

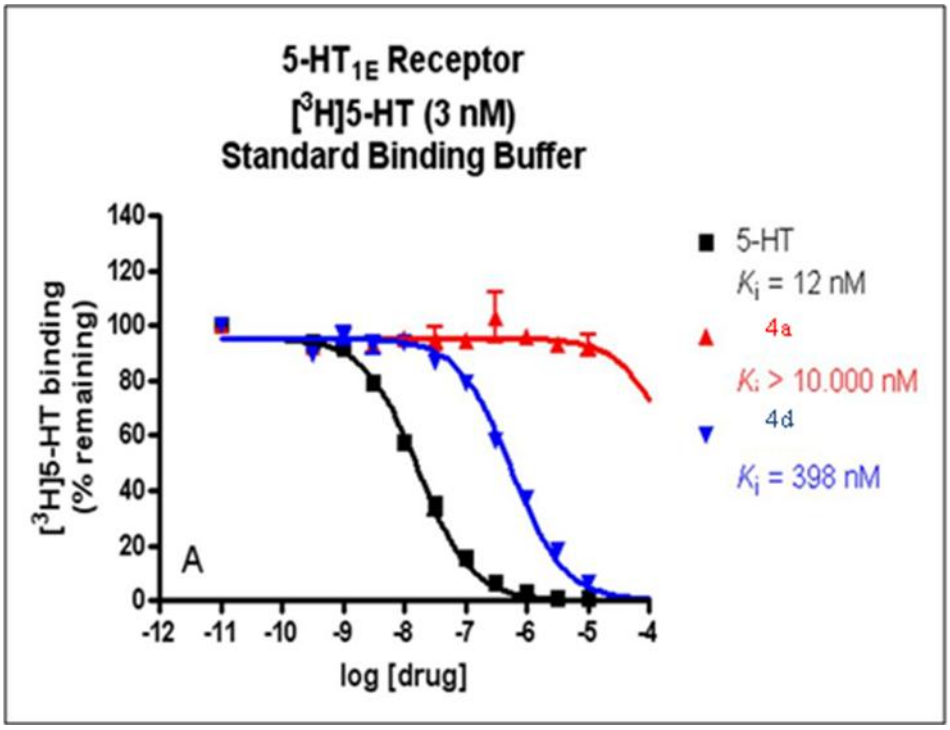

Figure 114. In vitro binding affinity of **4a** and **4d** towards 5-HT_{1E}

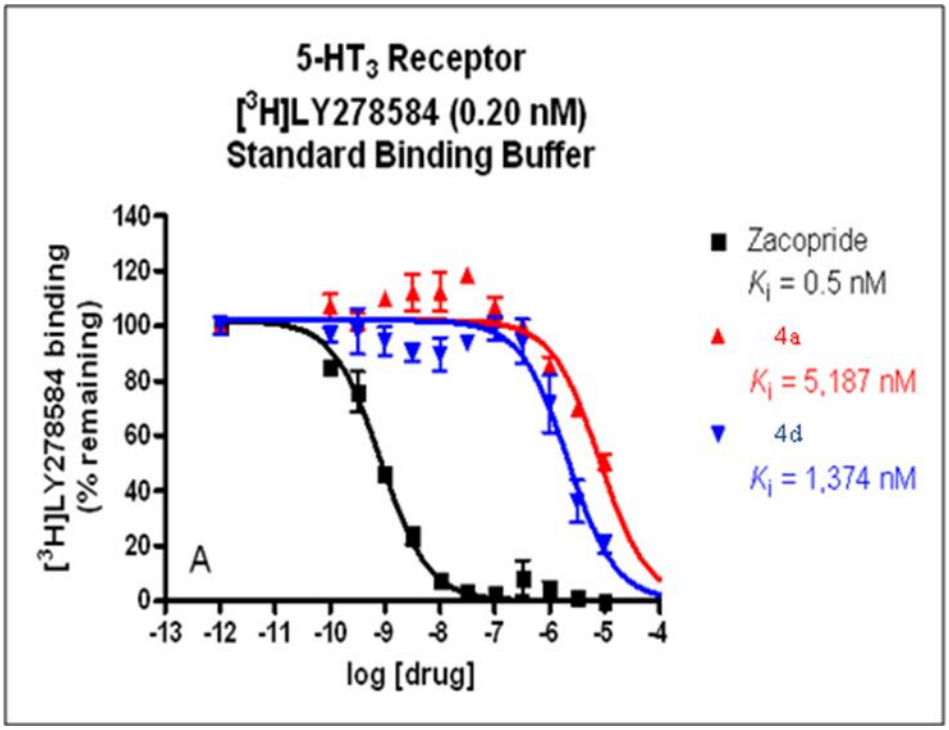

Figure 115. In vitro binding affinity of **4a** and **4d** towards 5-HT_3

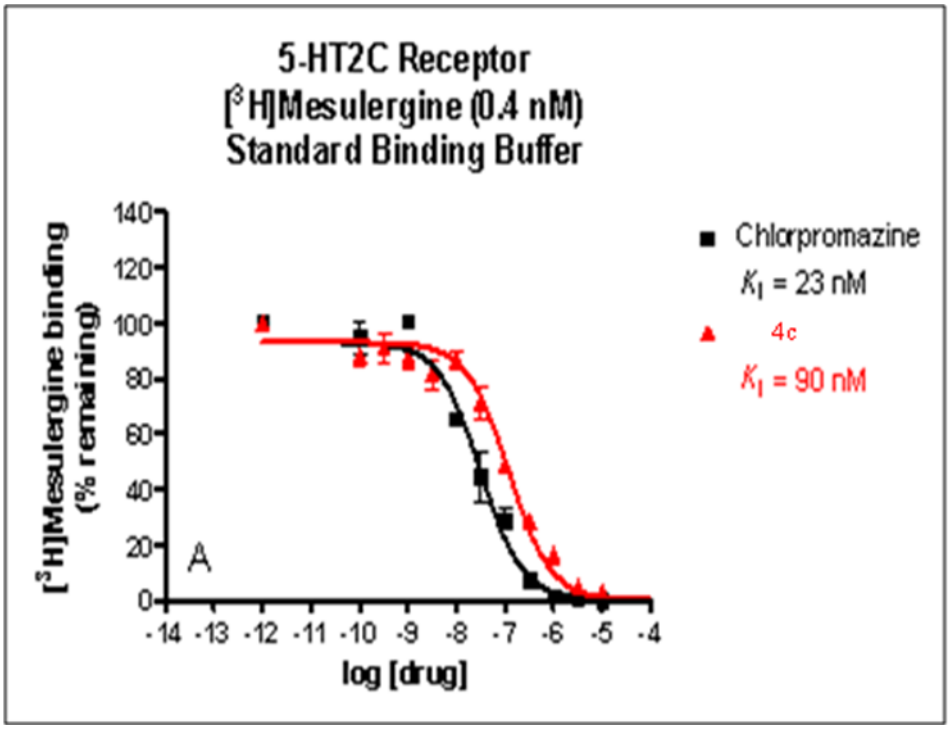

Figure 116. In vitro binding affinity of **4c** towards 5-HT_{2C}

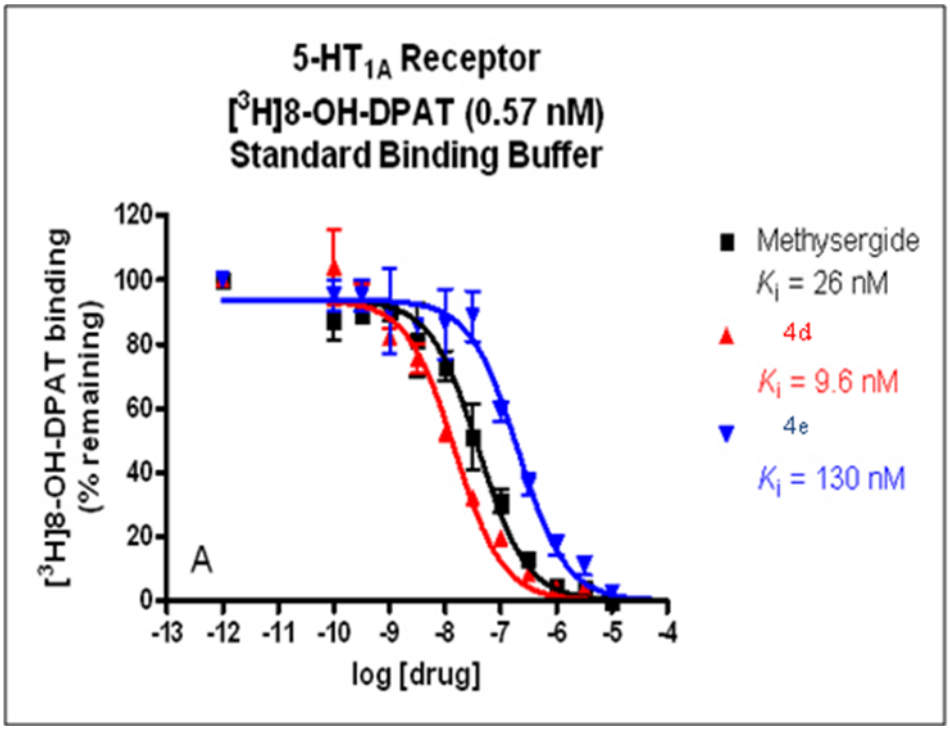

Figure 117. In vitro binding affinity of **4d** and **4e** towards 5-HT_{1A}

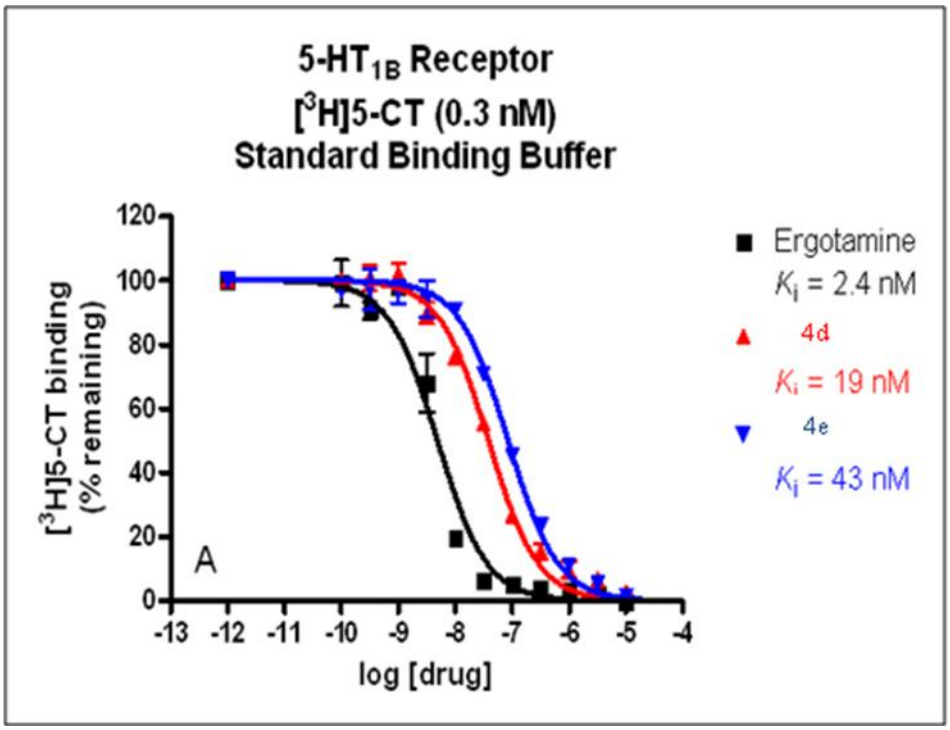

Figure 118. In vitro binding affinity of **4d** and **4e** towards 5-HT_{1B}

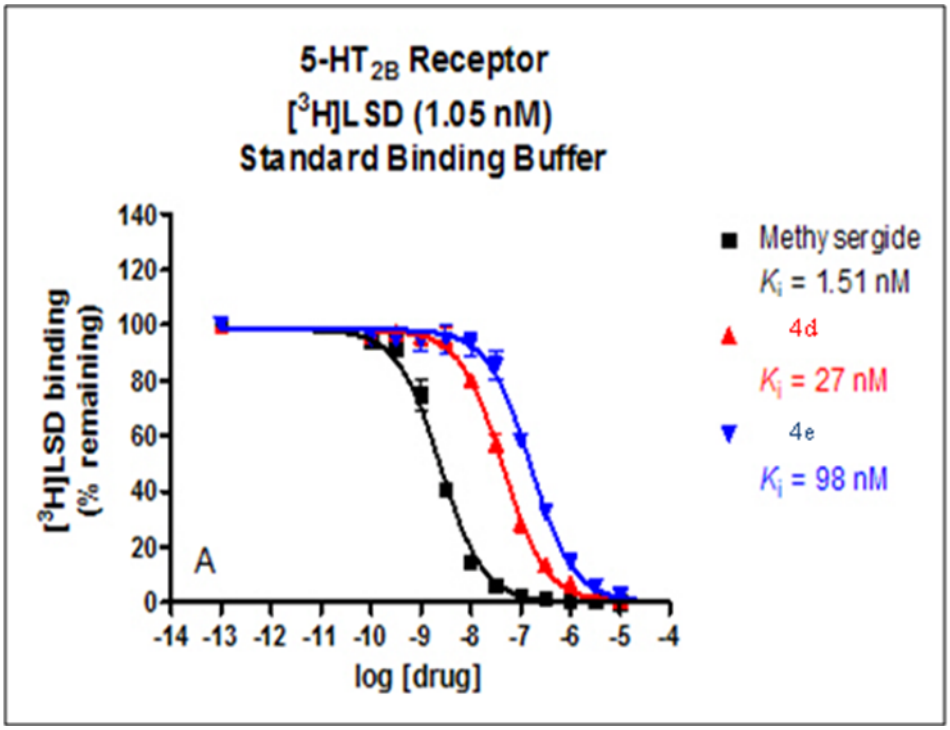

Figure 119. In vitro binding affinity of **4d** and **4e** towards 5-HT_{2B}

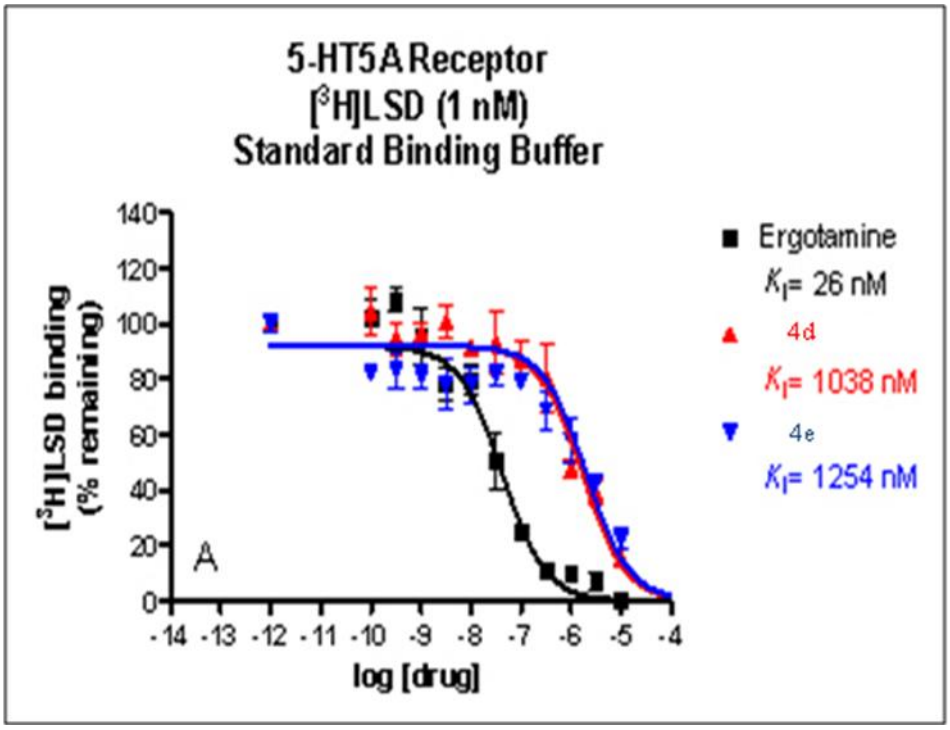

Figure 120. In vitro binding affinity of **4d** and **4e** towards 5-HT_{5A}

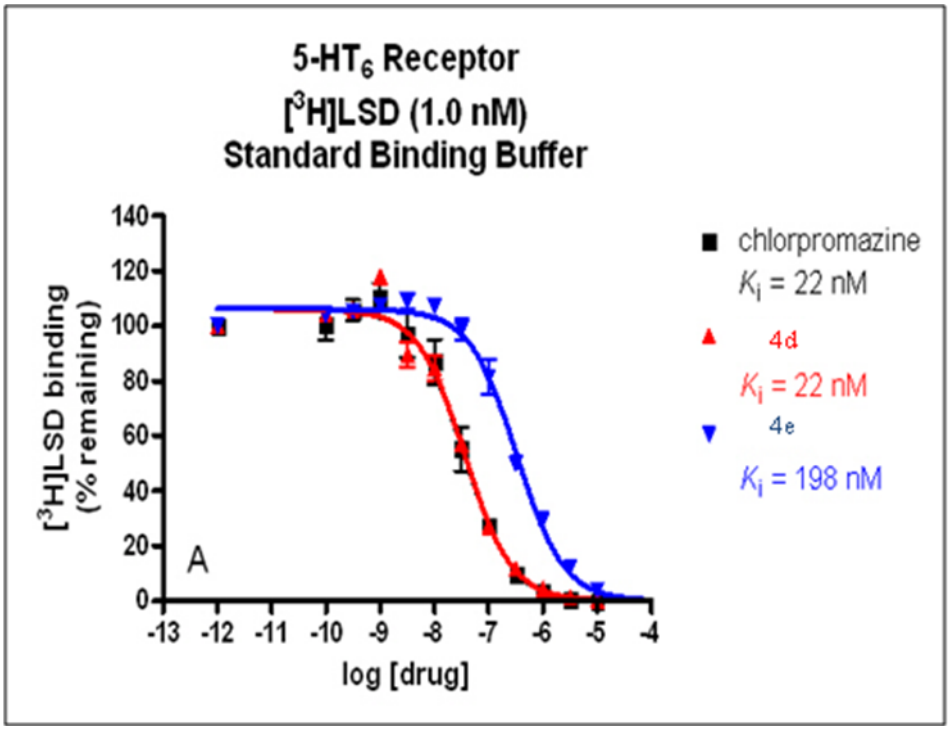

Figure 121. In vitro binding affinity of **4d** and **4e** towards 5-HT_6

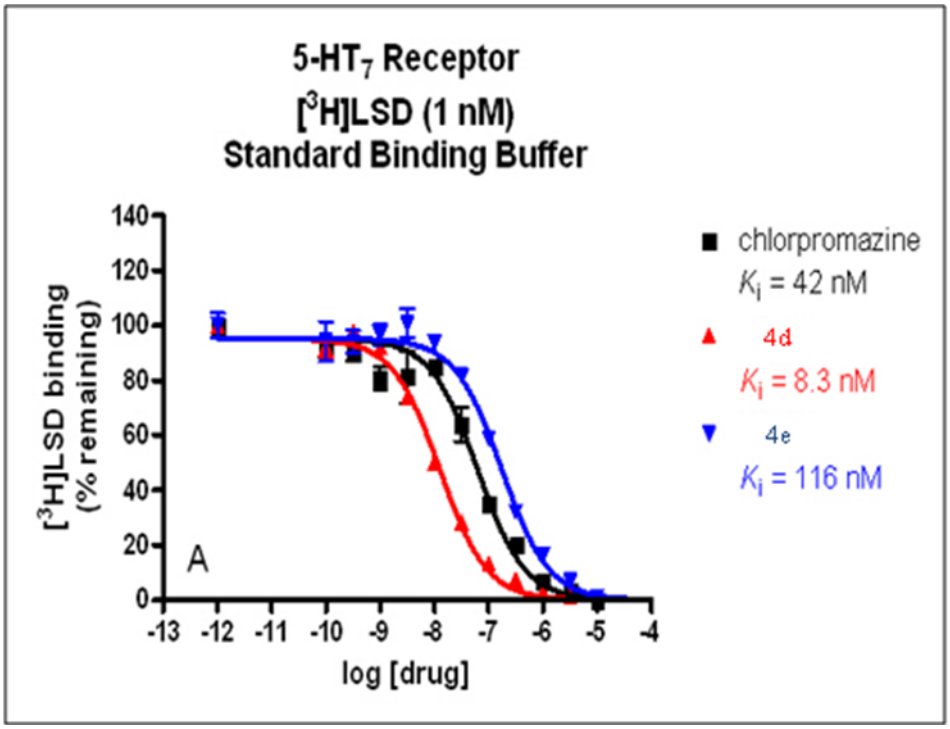

Figure 122. In vitro binding affinity of **4d** and **4e** towards 5-HT_7

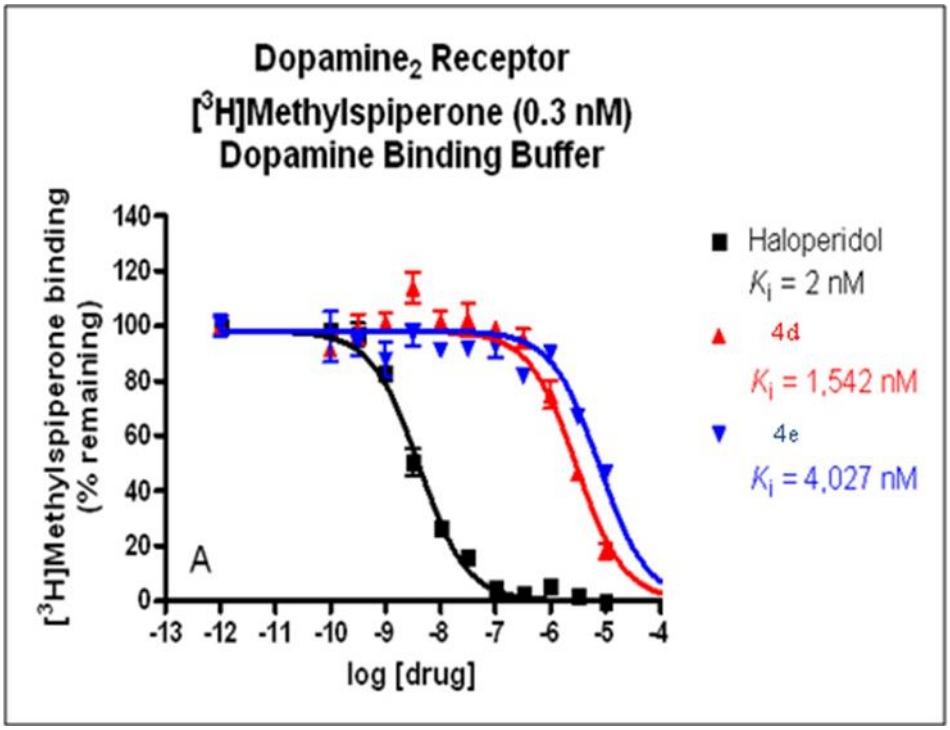

Figure 123. In vitro binding affinity of **4d** and **4e** towards dopamine 2 receptor

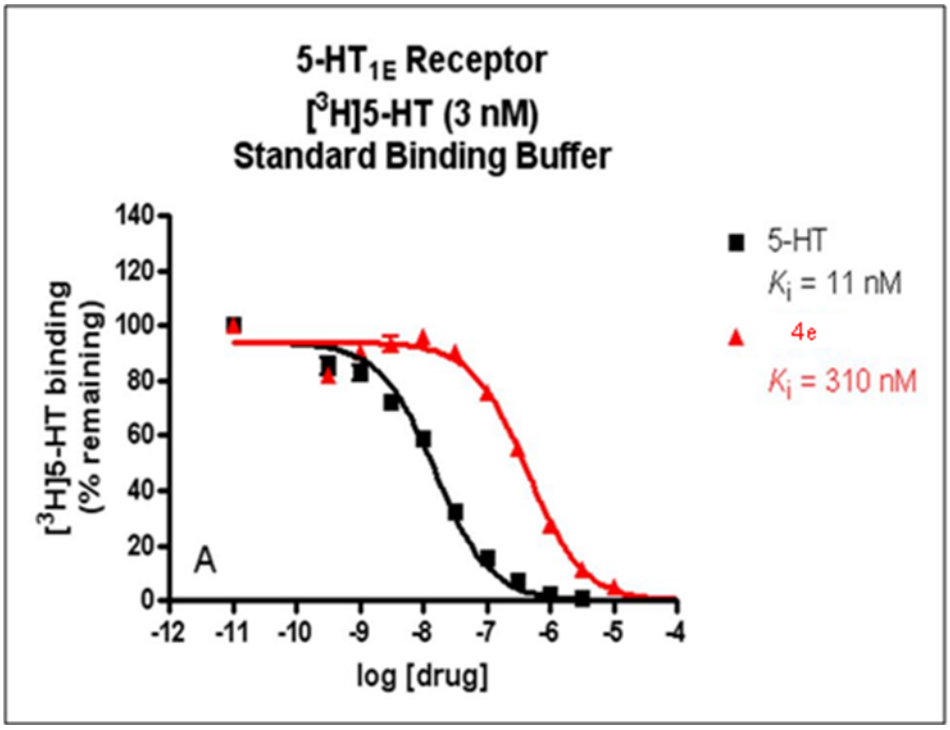

Figure 124. In vitro binding affinity of **4e** towards 5-HT$_{1E}$

4. Discussion

This study aimed at the synthesis of various derivatives of 2-(1*H*-indol-3-yl)-*N*,*N*-dimethylethanamine with different halogens at position 5 and evaluation of their activity both in vitro and in vivo for potential antidepressant and sedative actions.

As shown in Table 9, the tricyclic antidepressant desipramine, the selective serotonin reuptake inhibitor fluoxetine, the dual dopamine and noradrenaline inhibitor bupropion, all showed dose dependent reduction in immobility times in the FST. Such effects were previously established as a measure of antidepressant-like action. Both desipramine and fluoxetine caused significant reduction in locomotor activity indicative of their established sedative action. On the other hand, bupropion induced a significant stimulant effect. These trends are consistent with previously published literature.[46,47]

Compound **3a** exhibited significant ($p<0.001$) antidepressant-like activity in the FST at 20 mg/kg dose (Figure 105A). Similarly, compound **3d** caused significant ($p<0.05$) reduction in immobility, which is indicative of antidepressant action. Furthermore, such effect was not associated with any effect on the locomotor activity of the animals, as shown in Figure 105B. Such data indicates possible antidepressant action for both compounds without any possible sedative effect at the tested dose. Figure 106 shows the effect of compounds **4a-e** in the FST (Figure 106A) and on the locomotor activity of animals in an open field (Figure 106B). Compound **4a**; *N*,*N*-dimethyltryptamine (DMT) is a known hallucinogen found in psychoactive snuffs and teas used by native shamans of South America. DMT is also produced in mammalian organisms, and it was recently reported to be an endogenous sigma receptor ligand.[48] In our study, compound **4a** caused significant reduction in immobility ($p<0.001$) in the FST and a non-

significant reduction in locomotor activity. The compound did not cause any locomotor stimulant action usually associated with hallucinogenic effects at any of the tested doses. Compounds **4c** and **4e** exhibited significant antidepressant-like action in the FST ($p<0.01$, and $p<0.001$, respectively) at the 20 mg/kg dose. In addition, compounds **4b**, **4c,** and **4e** caused significant reduction in locomotor activity, suggesting potential sedative effect.

Full dose response studies for compound **3a** elicited U-shaped dose response antidepressant-like action (Figure 107A) with the 20 mg/kg dose significantly different from the vehicle control ($p<0.01$). A similar U-shaped response was observed in locomotor activity with a significant stimulant action evident at the 40 mg/kg dose ($p<0.01$). All tested compounds except compound **3d** exhibited such U-shaped antidepressant-like dose response curve (Figures 107, 109-112). In some cases, the lack of antidepressant action at the high dose can be partially explained by the severe sedative action observed in the locomotor activity (compound **4c**, Figure 110B). Such severe sedation can mask the antidepressant action by hindering the animal's ability to escape or move. Further studies are needed to examine the potential sedative action of this compound. In other cases (compounds **4a** and **4e**), the trend of the effect on locomotor activity does not correlate with the lack of antidepressant action (Figures 109 and 112). The observed U-shaped dose response could possibly be attributed to activation of a separate set of pathways through the action on multiple receptors at the high dose. Thus mechanistic studies are warranted to delineate the mechanisms underlying the observed antidepressant and sedative actions for these compounds. On the other hand, compound **3d** showed a typical dose dependent response curve with significant antidepressant-like action at the 40 mg/kg dose ($p<0.01$) and no significant effect on locomotor activity (Figure 108).

In vitro binding affinities data showed that compounds **4a**, **4c**, **4d**, and **4e** possessed nanomolar affinity to several serotonin receptor subtypes, particularly $5HT_{1A}$, $5HT_{1B/1D}$, $5HT_{2B}$, $5HT_6$, and $5HT_7$ subtypes. Previous research suggested the involvement of these serotonin receptor subtypes in depression, anxiety, and migraines.[49] The utilization of $5HT_{1A}$ knockout animals resulted in enhanced anxiety in several experimental paradigms as well as demonstrated significant increased baseline immobility in behavioral despair tests.[50,51] Moreover, selective $5HT_{1A}$ agonists showed antidepressant actions in preclinical as well as clinical testing.[52-55] The involvement of $5HT_{1B}$ receptors in mood disorders was also observed in knockout models. Such mice exhibited a decreased anxiety in open field, elevated plus maze, and tail suspension tests. On the other hand, the same mice displayed increased aggressive behavior.[56,57] Additionally $5HT_{1B}$ and $5HT_{1D}$ receptors are well known targets for antimigraine drugs. A number of studies examined the role of $5HT_{2B}$ receptors in mood regulation. These studies showed that direct injection of the selective $5HT_{2B}$ agonist, BW 723C86, into the medial amygdale resulted in anxiolytic effect in the rat social interaction test.[58] Recently, the attribution of $5HT_6$ and $5HT_7$ receptors in neuropsychiatric disorders drawn attention due to the pharmacological studies that demonstrated high affinity of several antipsychotic and antidepressant agents to these two receptor subtypes.[59,60] Thus the in vitro data suggested that the antidepressant action exerted by these compounds in vivo might be mediated via interaction with serotonin receptors. Further mechanistic studies are hence required to delineate the nature of such interaction and further establish the mechanism underlying the observed behavioral effects of these compounds.

CHAPTER V

2-*N*- MODIFICATIONS AND SAR STUDIES OF MANZAMINE A

Published in *Bioorganic & Medicinal Chemistry* **2008**, *16*, 6702-6706.

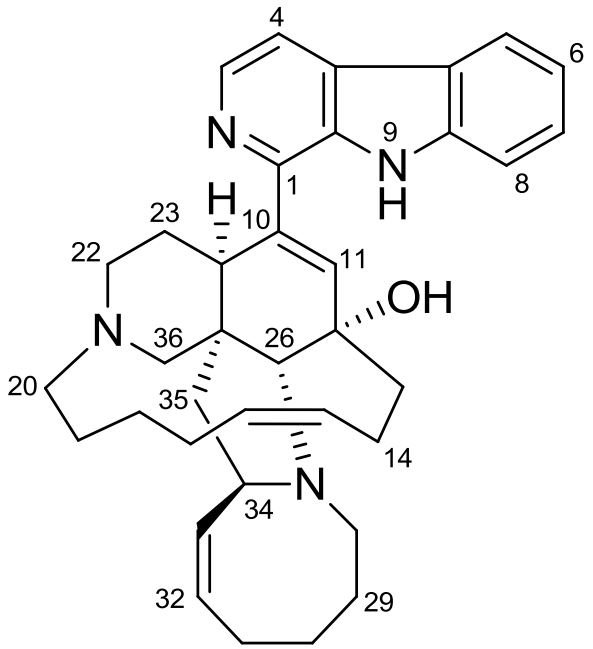

Manzamine A

Reproduced with permission from *Bioorganic & Medicinal Chemistry* **2008**, *16*, 6702-6706.

Copyright 2008 American Chemical Society

1. Introduction

Malaria, a major tropical infectious disease caused primarily by the protozoan parasite *Plasmodium falciparum*, is one of the most serious health problems worldwide and is responsible for the death of over 1.12 million individuals every year with more than 40 percent of the global population at risk.[61] β-Carboline alkaloids are widely distributed in a number of plant and animal species, as well as marine invertebrates. Some of these alkaloids such as manzamine A (**1**), akagerine, 10-hydroxycanthin-6-one and 4-methoxy-1-vinyl-β-carboline (MVC) (Figure 125), display a diverse array of biological activities including antiplasmodial efficacy.[62-64] Manzamine A, as a first representative of the manzamine alkaloids, bearing a unique multi-heterocyclic ring system coupled to a β-carboline moiety, was isolated from the sponge *Haliclona* sp. collected near Manzamo Island by Higa and co-workers in 1986.[65] Despite its potent in vitro activity as an antimalarial agent against *P. falciparum* the toxicity of manzamine A hampered its development as a drug candidate.[64, 66-68]

Recently, Ihara and co-workers have reported that the rhodacyanine family of compounds and the β-carboline system of MVC, owing in both cases to a π-delocalized lipophilic cationic (DLC) structure, display reasonable antimalarial and antileishmanial activities against *P. falciparum* and *Leishmania major*, respectively, with low cytotoxicity against mammalian cells.[69-73] The conceptual term, DLC, was originally proposed by Chen et al. in their studies related to anticancer agents.[74] It has been reported that several DLC compounds exhibit selective antitumor activity by accumulating in the mitochondria of carcinoma cells.[75-77] Vaidya and co-workers found that mitochondrial membrane potential collapse is an antimalarial mechanism of some drugs,[78] and many researchers concluded that DLCs could therefore represent a new

antiplasmodial class of drugs.

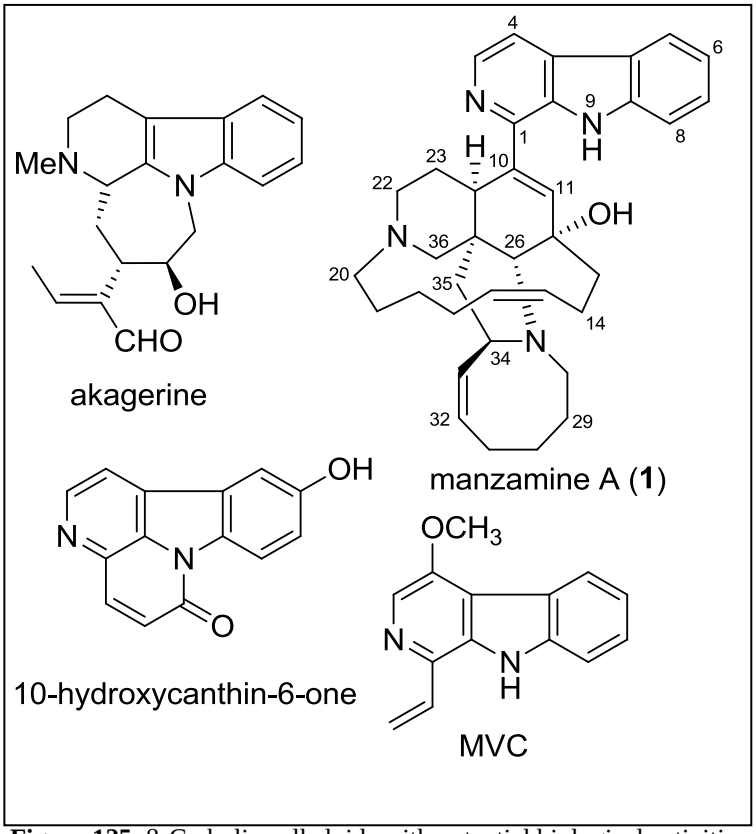

Figure 125. β-Carboline alkaloids with potential biological activities

Our goal was to synthesize manzamine A analogs with decreased toxicity and improved therapeutic index for antimalarial efficacy and continuing structure-activity relationship studies. The rationale for the modification of the β-carboline moiety through quarternization of the pyridine nitrogen to form β-carbolinium salts is based on previous work that showed reduced toxicity and increased antimalarial activity of DLC's formed upon transformation with either alkyl tosylates or alkyl halides as a correlation to the π–delocalization of the cationic species.[70,71,79]

Recently, we found that manzamine A inhibits GSK-3β with an IC_{50} value of 10.2 μM so inhibition of this multifunctional serine/threonine kinase may in part be the reason for various

therapeutic activities of manzamine A analogs.[80] Since, the crystal structure of GSK-3β is available, we initiated structure-based drug design paradigm of manzamine A analogs using molecular docking coupled with molecular dynamics. Quaternization of the neutral pyridine nitrogen to the desired quaternary ammonium cation was challenging but could finally be accomplished by methylation of manzamine A in the presence of methyl trifluoromethanesulfonate to afford three methylated products (**2-4)** in varying yields depending upon reaction conditions. The structures of **2**, **3**, and **4** were confirmed using HRESIMS, as well as ^{1}H, ^{13}C NMR, HMQC, and HMBC data. The in vitro antimalarial and antimicrobial activity in addition to cytotoxicity versus mammalian cells of analogs **2-4** were evaluated.

2-*N*-Methylmanzamine A (**2**), 2-*N*,12-*O*-dimethyl manzamine A (**3**) trifluoromethanesulfonate, and 9-*N*-methylmanzamine A (**4**) (Scheme 8) are generated from the treatment of the β-carboline moiety with methyl trifluoromethanesulfonate to afford the mono- and di-methylated products.[71,79]

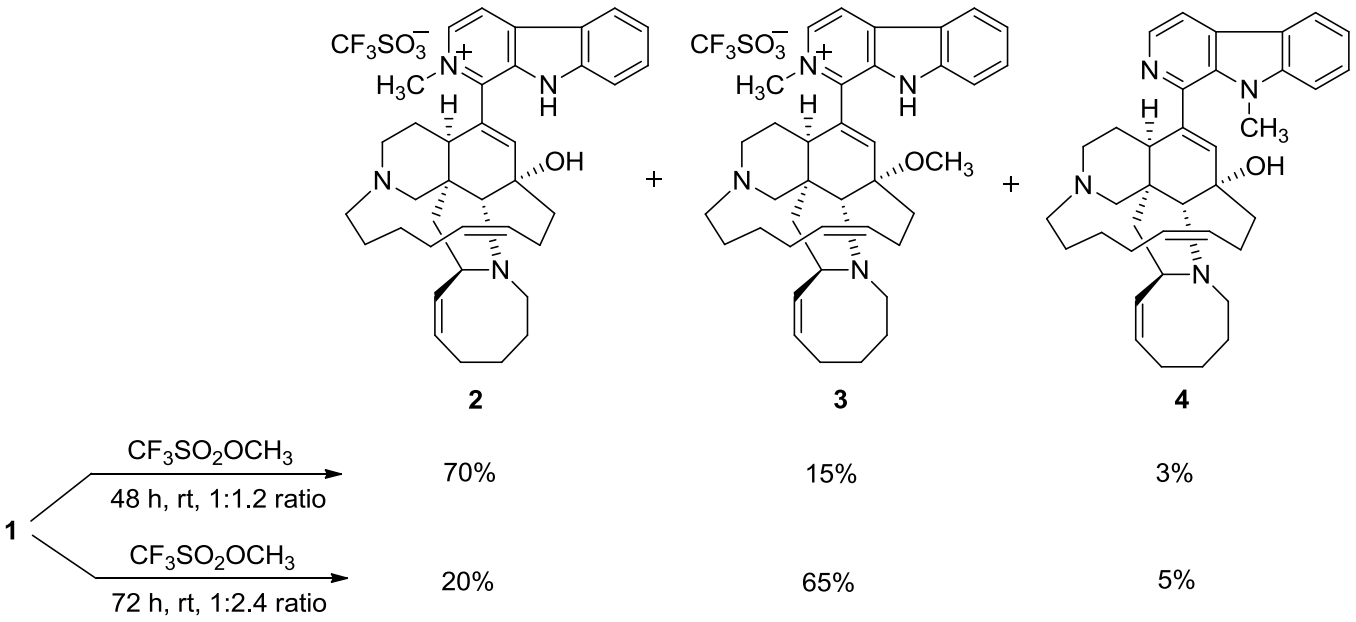

Scheme 8. Synthesis of 2-*N*-methylmanzamine A (**2**), 2-*N*,12-*O*-dimethylmanzamine A (**3**) trifluoromethanesulfonate, and 9-*N*-methylmanzamine A (**4**)

According to our previous unpublished work showing that *N*-methylation of the secondary amine of the β-carboline moiety drastically decreases antimalarial potency, along with the low yield of **4**, we were not interested to pursue further evaluation of this compound. Using methyl iodide as the alkylating agent furnished the non-preferential analogue **4** in higher yield.

The structures of analogues **2** and **3** were confirmed with spectroscopic and MS techniques. The (+)-HRESIMS of analog **2** showed the $[M+H]^+$ ion signal with *m/z* 563.36747 in positive mode, in accordance with its molecular formula $C_{37}H_{47}N_4O$. The ^1H NMR spectrum of **3** in methanol-d_4 in 400 MHz clearly indicated the presence of a new singlet methyl group at 4.57 (s, 3H, NCH_3) ppm. This finding was confirmed by a new methyl singlet at 45.3 ppm in the ^{13}C NMR spectrum. The HMBC spectrum of **2** supported the methylation of the pyridinium nitrogen as shown by a correlation between the CH_3 singlet at 4.57 ppm and both adjacent aromatic carbon signals at 134.6 ppm (C-3) and 138.8 ppm (C-1) (Figure 126).

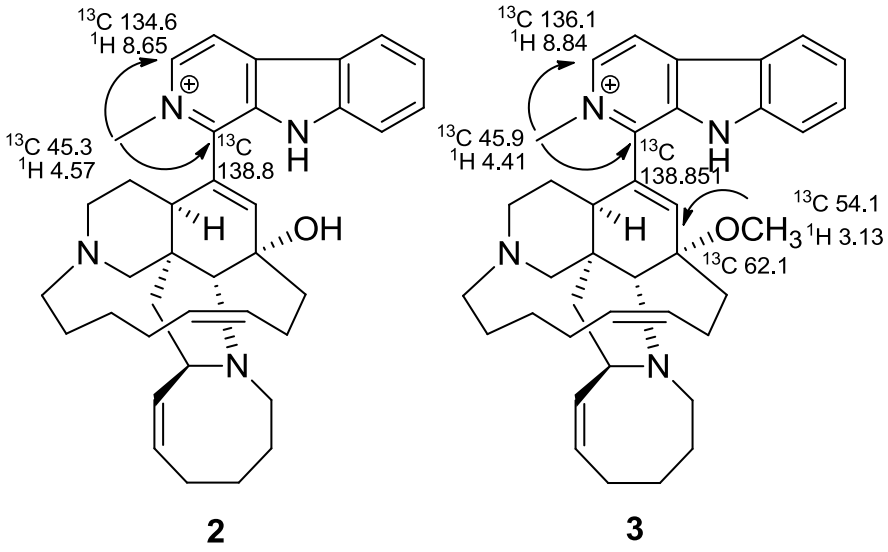

Figure 126. Selected HMBC correlations 2-*N*-methylmanzamine A (**2**), and 2-*N*,12-*O*-dimethylmanzamine A (**3**) trifluoromethanesulfonate

High-resolution TOF-ESIMS of analog **3** provided a molecular mass of $[M+H]^+$ with *m/z* 577.4245, corresponding to the addition of two methyl mass units, in comparison with the parent molecule. The ^1H and ^{13}C NMR spectra of compound **3** in DMSO-d_6 contained two methyl proton signals at 4.41 (s, 3H, NCH_3) and 3.13 ppm (s, 3H, OCH_3) along with corresponding carbon resonances at 45.9 and 54.1 ppm, respectively, in agreement with the structure of analog **3** (Figure 126). In addition, HMBC spectrum revealed an unambiguous correlation between the methoxy protons at 3.13 ppm and neighboring quaternary C-12 at 62.1 ppm. These findings are consistent with the fact that we observed the NH group at position 9 of the β-carboline moiety still intact at 11.4 (s, 1H, NH), which in turn indicates that secondary amine group is not involved in the methylation.

2. Biological Evaluation

All synthetic analogues were evaluated for in vitro antimalarial and antimicrobial activity as well as cytotoxicity against mammalian cells.

Antimalarial activity was determined against chloroquine-sensitive (D6) and chloroquine-resistant (W2) strains of *P. falciparum.* As shown in Table 11, compound **2** showed antimalarial activity with IC_{50} values of 0.7 and 1.0 μM for D6 and W2 strains, respectively. Compounds **3** and **4** were inactive. None of the synthesized analogs (**2**-**4**) showed any cytotoxicity to mammalian kidney fibroblasts (Vero cells) while manzamine A was cytotoxic (IC_{50} 0.5 μM). Although antimalarial activity of **2** was much less potent than manzamine A, the selectivity index of **2** remained comparable to manzamine A due to the loss of cytotoxicity. These results indicated that quarternization of the β-carboline moiety resulted in reduced toxicity but still retained antimalarial efficacy in the case of **2**. However, further methylation of **2** (to generate **3**) resulted in loss of antimalarial activity. Methylation of the indoline nitrogen of manzamine A (**4**) resulted in the loss of both antimalarial activity and cytotoxicity.

Manzamine A and some of its analogs are known to inhibit *Homo sapiens* glycogen synthase kinase-3β (GSK-3β).[80] Based on the assumption that the antimalarial activity of these analogs may be due to kinase inhibition of *P. falciparum*, we used the crystal structure of HsGSK-3β (PDB: 1gng)[81] for docking studies to predict the optimal binding positions and relative binding propensities of **1**-**3**. Based on the evidence that **1** was found to be an ATP-noncompetitive inhibitor of GSK-3β,[80] we attempted to dock **1**-**3** into a pocket located in the vicinity of the activation pocket formed by three basic residues, Arg96, Arg180 and Lys205. We used the GOLD 3.1.1 docking program[82] with the scoring function ChemScore,[83] to compare the

difference in binding affinity between the ligands and to compare with the experimental in vitro antimalarial activity. The co-crystallized ligands in 1gng, namely 2-amino-2-hydroxymethyl-propane-1,3-diol and sulfate ions, were removed before docking. The active site was defined as any atom that lay within a 15 Å radius of the δN of Arg96. The geometry of **1** was optimized using MMFF94 in Sybyl 7.2, starting from the published X-ray crystal structure of manzamine A.[65] **2** and **3** were built from the crystal structure of **1** followed by geometry optimization using the same force field. ChemScore is a dimensionless fitness function which is a measure of the free energy of a ligand binding to a protein. Since GOLD uses a genetic algorithm to dock ligands, consecutive docking runs do not give exactly the same fitness scores. To address this issue of inherent randomness of GOLD docking, we performed 3 consecutive docking runs to obtain average ChemScores for each ligand, which are given in Table 11 for **1**-**3**.

Table 11. In vitro antimalarial activity, selectivity index, cytotoxicity to Vero cells and docking scores of manzamine A (**1**), 2-*N*-methylmanzamine A (**2**), 2-*N*,12-*O*-dimethylmanzamine A (**3**) trifluoromethanesulfonate, and 9-*N*-methylmanzamine A (**4**)

Compound	*P. falciparum* D6		*P. falciparum* W2		Cytotoxicity to Vero cells	Docking Score
	IC_{50} (μM)	S.I.	IC_{50} (μM)	S.I.	IC_{50} (μM)	ChemScore[a]
1	0.017	29.4	0.020	25.23	0.501	24.9 (±1.0)
2	0.736	>24	1.011	>17.5	NC	22.3 (±0.6)
3	NA	–	NA	–	NC	20.6 (±0.8)
4	NA	–	NA	–	NC	–
Chloroquine	0.013	>1000	0.135	>100	NC	–
Artemisinin	0.0063	>2700	0.0045	>3700	NC	–

NA= No antimalarial activity up to 8 μM; NC = No cytotoxicity up to 17 μM: Selectivity Index (S.I.) = IC_{50} (Vero Cells) / IC_{50} (*P. falciparum*). [a]GOLD ChemScore was an average over 3 runs. Standard deviation in parentheses.

Docking scores agree with the in vitro antimalarial activity data and show that **1** > **2** > **3**. This is consistent with the experimental findings that the first methylation on the tertiary nitrogen of the β-carboline ring (**2**) and the second methylation on the 12-hydroxy group (**3**) each

decrease the antimalarial activity a step compared to having free tertiary nitrogen on the β-carboline ring and a 12-hydroxy group in manzamine A (**1**) (Table 11).

The predicted binding positions of **1**-**3** within the ATP-noncompetitive binding pocket (as identified by the Lee and Richards solvent accessible molecular surface)[84] are shown in Figure 127.

Compounds **1** and **3** have the same binding mode, whereas the binding position of **2** is different. The polar and hydrophobic interactions of **1** are shown in Figure 128. Manzamine A (**1**) shows a strong hydrogen bonding of its 12-hydroxy group with the backbone carbonyl of Arg92. Also, the hydrophobic β-carboline ring interacts with the side chains of Lys94, Asn95 and Arg96. The NH of the β-carboline ring is pointing towards Phe93 indicating a probable steric clash if any substitution is made at this position. In comparison to **1**, **2** adopts a binding mode in a different region of the ATP-noncompetitive binding pocket, leading to less favorable hydrogen bonding and hydrophobic interactions. The crucial interactions for **2** are also shown in Figure 128. The 12-hydroxy group of **2** forms a hydrogen bond, but it is with Gln89, unlike that of **1** with Arg92. The hydrogen bonding between the NH_2 of Gln89 and the 12-hydroxy of **2** is weaker (more distant) than the interaction seen in **1**. Also, **2** shows hydrophobic interactions with the side chain of Phe67. **3** adopts a binding position similar to **1,** and **3** does not show any hydrogen bonding interaction, due to the second methylation at the 12-hydroxy group. Thus the docking scores are in good agreement with the antimalarial results indicating their utility in the rational design of more active analogs from this class.

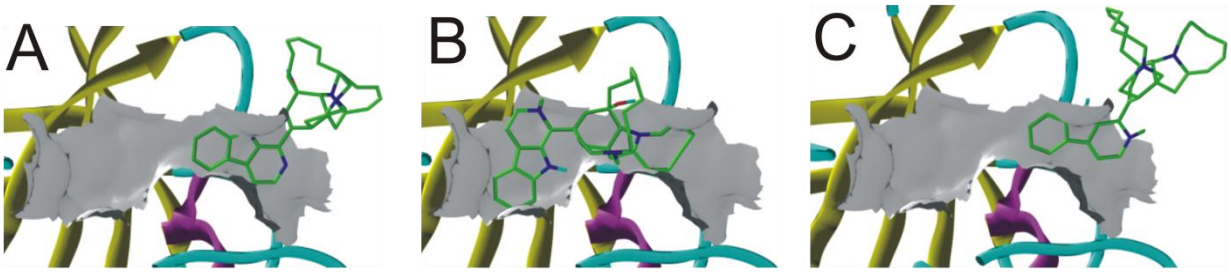

Figure 127. Binding positions of manzamine A (**1**), 2-*N*-methylmanzamine A (**2**), and 2-*N*,12-*O*-dimethylmanzamine A (**3**) trifluoromethanesulfonate within the ATP-noncompetitive binding pocket of GSK-3β (A: **1**, B: **2**, C: **3**). Ligands **1**-**3** are shown with green carbon; the protein is in ribbon format colored according to secondary structures; the binding pocket interior surface (as detected with the Lee/Richards molecular surface) is in white.

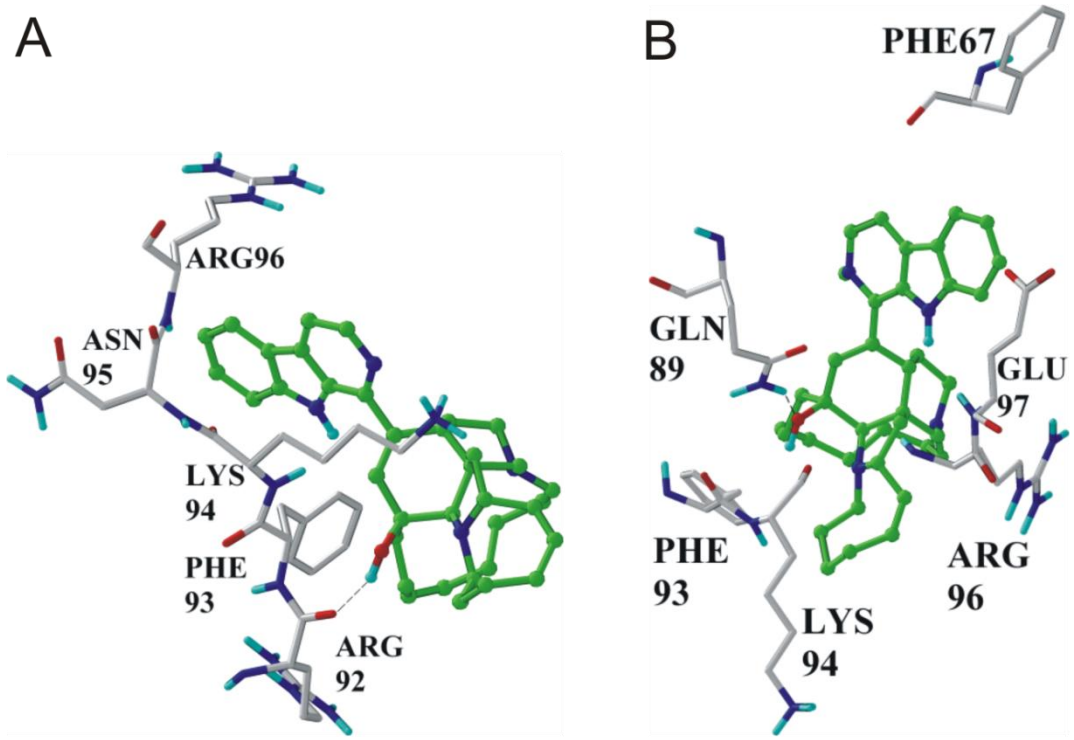

Figure 128. Interactions of manzamine A (A) and 2-*N*-methylmanzamine A trifluoromethanesulfonate (B) with the GSK-3β ATP-noncompetitive binding pocket residues.

Antimicrobial activity was determined against a panel of human pathogenic bacteria and fungi (Table 12). Compounds **1** to **4** were inactive against the Gram-negative bacteria *Escherichia coli* and *Pseudomonas aeruginosa*, in addition to the opportunistic filamentous

fungus *Aspergillus fumigatus* (data not shown). Moreover, compound **4** was inactive against all species tested, indicating that quaternarization of the secondary amine decreases bioactivity in general. Among compounds **1-3**, manzamine A (**1**) remains the most potent with strong activity against the opportunistic yeast *Cryptococcus neoformans*, methicillin-resistant *Staphylococcus aureus* (MRSA) and *Mycobacterium intracellulare*, with bioactivity against the latter microorganism rivaling the positive control Ciprofloxacin. Results indicated that the conversion of hydroxyl group to a methoxy in compound **3** also decreases in vitro antimicrobial activity. In summary, derivatization of either the pyridine or secondary amine of the β-carboline moiety, along with methylation of the C-12 hydroxy group of manzamine A decrease in vitro activity against several pathogenic microorganisms. Also anti-HCV activity for compound 2 was evaluated (Table 13).

Table 12. In vitro antimicrobial activity for manzamine A (**1**), 2-*N*-methylmanzamine A (**2**), 2-*N*,12-*O*-dimethylmanzamine A (**3**) trifluoromethanesulfonate, and 9-*N*-methylmanzamine A (**4**), (all values in μM)

Compound	*C. albicans*			*C. neoformans*			MRSA			*M. intracellulare*		
	IC_{50}	MIC	MFC	IC_{50}	MIC	MFC	IC_{50}	MIC	MBC	IC_{50}	MIC	MBC
1	16.4	-	-	2.7	5.7	23	0.18	-	-	0.18	0.36	2.84
2	-	-	-	71.1	-	-	44.5	89	89	17.8	44.5	44.5
3	-	-	-	52	87	87	-	-	-	-	-	-
4	-	-	-	-	-	-	-	-	-	-	-	-
Amphotericin B	0.3	0.68	1.35	0.8	1.35	1.35	NT	NT	NT	NT	NT	NT
Ciprofloxacin	NT	NT	NT	NT	NT	NT	0.3	1.5	-	1.1	1.5	3

IC_{50}, the concentration that affords 50% inhibition of growth; minimum inhibitory concentration (MIC) is the lowest test concentration that allows no detectable growth; minimum fungicidal/bactericidal concentration (MFC/MBC) is the lowest test concentration that kills the organism

"-", not active at the highest test concentration of 91, 89, 87, 89, 5.4 and 3.0 for samples **1**, **2**, **3**, **4**, Amphotericin B, and Ciprofloxacin, respectively; NT, not tested.

Amphotericin B and ciprofloxacin are used as positive antifungal and antibacterial controls, respectively.

Table 13. Anti-HCV activity of 2-*N*-methylmanzamine A trifluoromethanesulfonate (**2**) in the Huh-7 replicon assay

Compounds	**ΔCt HCV**	**ΔCt rRNA**	% Inhibition	
			HCV	rRNA
2	9.56	15.74	99.87	100.00
RS-446[a]	7.48	-0.25	99.43	-19.22

2'-C-methylcytidine; [a] RS-446 (2′-C-Me-C) was used as the control. The compound and the control are tested at 10 μM in triplicate immediately after seeding.

In conclusion, the preliminary structure–activity relationship study in regards to the first and second methylation showed that the introduction of the first methyl group at the pyridine nitrogen in the β-carboline moiety of manzamine A significantly decreases the cytotoxicity but also reduced the antimalarial activity of manzamine A. Introduction of a second methyl group at 12-OH completely eliminated the antimalarial activity indicating that the OH group is an essential pharmacophore for the antimalarial activity of the manzamine class of alkaloids. The docking studies of these analogs on GSK-3β delineated the ability of manzamine A (1) to form a stronger hydrogen bond than **2** and the inability of **3** to interact favorably with the ATP-noncompetitive site amino acids of GSK-3β, because **3** lacks a complementary donor atom at its C-12-OH position.

3. Experimental Section

3.1. General Preparation of Compounds 3-4.

Treatment of manzamine A (54.8 mg, 0.1 mmol) with methyl trifluoromethanesulfonate (135.5 μL, 1.2 mmol) in a molar ratio of 1 to 1.2 in dry methylene chloride while stirring for 48 h at ambient temperature resulted in the formation of major product **2** in 70% yield in addition to two minor products **3** in 15%, and **4** in 3% yield. Purification was completed via HPLC using a reverse-phase C_8 column with a mobile phase gradient of H_2O-CH_3CN and a flow rate of 10

mL/min. The major compound appears at a retention time of 40 minutes.

By increasing the molar ratio of methyl trifluoromethanesulfonate from 1.2 to 2.4 and stirring for 72 h, compound **3** was generated in 65% yield alongside the minor products **2** in 20%, and **4** in 5% yield. The resultant yellow solid was washed with diethyl ether and purified using the method above affording compound **3** at a retention time of 30 minutes.

3.1.1. 2-*N*-Methylmanzamine A trifluoromethanesulfonate (2); (Figures 129-136)

$[\alpha]^{25}_{D}$ +57.5 (*c* = 0.08, MeOH); UV λ_{max} (MeOH) 260, 310, 375 nm; IR ν_{max} ($CHCl_3$) 3207 (NH), 3073, 3011, 2928, 2855, 1671, 1628, 1577, 1520, 1415, 1296, 1198, 1030 cm^{-1}; ^1H NMR (methanol-d_4) δ 8.65 (2H, m), 8.43 (1H, d), 7.87 (2H, m), 7.52 (1H, t), 6.27 (1H, s), 5.68 (2H, m), 5.53 (1H, t), 4.71 (1H, m), 4.57 (3H, s, NCH_3), 4.43 (1H, m), 3.89 (1H, s), 3.65 (1H, m), 3.48 (1H, t) and 3.35-0.90 (complex); ^{13}C NMR (methanol-d_4) δ 144.8, 141.8, 138.8, 135.4, 135.2, 134.6, 132.6, 132.2, 132.0, 126.9, 122.7,122.1, 119.9, 116.3, 113.1, 74.8, 69.7, 68.7, 66.6, 56.9, 53.1, 48.7, 48.4, 46.8, 45.3, 43.2, 40.1, 39.7, 33.0, 28.4, 26.4, 25.4, 24.9, 24.3 and 20.8; (+)-HRESIMS *m*/*z* calcd for $C_{37}H_{47}N_4O$ $[M+H]^+$ 563.3750, found 563.3674.

3.1.2. 2-*N*,12-*O*-Dimethylmanzamine A trifluoromethanesulfonate (3); (Figures 137-141)

$[\alpha]^{25}_{D}$ +25.7 (*c* = 0.14, MeOH); UV λ_{max} (MeOH) 225, 260, 314, 380 nm; IR ν_{max} ($CHCl_3$) 3443 (NH), 3331, 3258, 2981, 2935, 1679, 1606, 1527, 1457, 1391, 1365, 1250, 1157, 1051 cm^{-1}; ^1H NMR (DMSO-d_6) δ 11.40 (1H, s, NH), 8.84 (2H, m), 8.48 (1H, d), 8.23 (1H, d), 7.72 (1H, t), 7.42 (1H, t), 5.88 (1H, s), 5.52 (1H, m), 5.40 (2H, m), 5.22(1H, m), 4.41 (3H, s, NCH_3), 4.01 (2H, m), 3.81 (1H, d), 3.56 (2H, m), 3.32 (5H, m), 3.20 (2H, m), 3.13 (3H, s, OCH_3), 2.89 (3H, m), 2.74 (1H, m) and 1.43-2.19 (complex); ^{13}C NMR (DMSO-d_6) δ 145.4, 145.1, 141.8, 138.8, 137.2, 136.1, 135.3, 133.4, 131.9, 129.6, 129.3, 125.8, 123.6, 121.9, 119.8,

117.2, 114.6, 74.1, 62.9, 62.1, 61.5, 59.1, 58.2, 54.1, 50.4, 45.9, 45.0, 43.8, 43.0, 36.7, 27.6, 26.4, 25.8, 25.4, 25.0, 24.2, 23.2 and 18.7; (+)-HRESIMS *m*/*z* calcd for $C_{38}H_{49}N_4O$ $[M+H]^+$ 577.3906, found 577.4245.

3.1.3. 9-*N*-Methylmanzamine A (4); (Figures 142-145)

$[\alpha]^{25}_D$ +18.6 (*c* = 0.07, MeOH); UV λ_{max} (MeOH) 260, 310, 375 nm; IR ν_{max} ($CHCl_3$) 3648 (NH), 3294, 3011, 2924, 2838, 1675, 1628, 1519, 1443, 1329, 1199, 1017 cm^{-1}; ^1H NMR (methanol-d_4) δ 8.63, (1H, br s), 8.40 (1H, d), 7.78 (1H, d), 7.53 (1H, d), 7.40 (1H, dd), 6.40 (1H, s), 5.91 (1H, br s), 5.62 (1H, q), 5.52 (1H, td), 5.26 (1H, t), 4.31 (1H, br s), 3.92 (3H, s, NCH_3), 3.50 (1H, d), 3.08 (2H, m), 2.78 (1H, m), 2.56 (2H, m), and 1.2-2.5 (complex); ^{13}C NMR (methanol-d_4) λ 154.2, 143.5, 139.9, 138.2, 137.4, 135.1, 134.5, 134.2, 132.3, 129.9, 129.2, 128.5, 122.2, 118.3, 117.2, 113.3, 112.5, 103.5, 75.1, 70.0, 68.7, 56.0, 55.0, 53.5, 50.9, 49.6, 47.1, 44.7, 40.9, 40.3, 32.7, 31.7, 28.1, 26.8, 26.0, 25.7, and 21.7; (+)-HRESIMS *m*/*z* calcd for $C_{37}H_{47}N_4O$ $[M+H]^+$ 563.3750, found 563.3764.

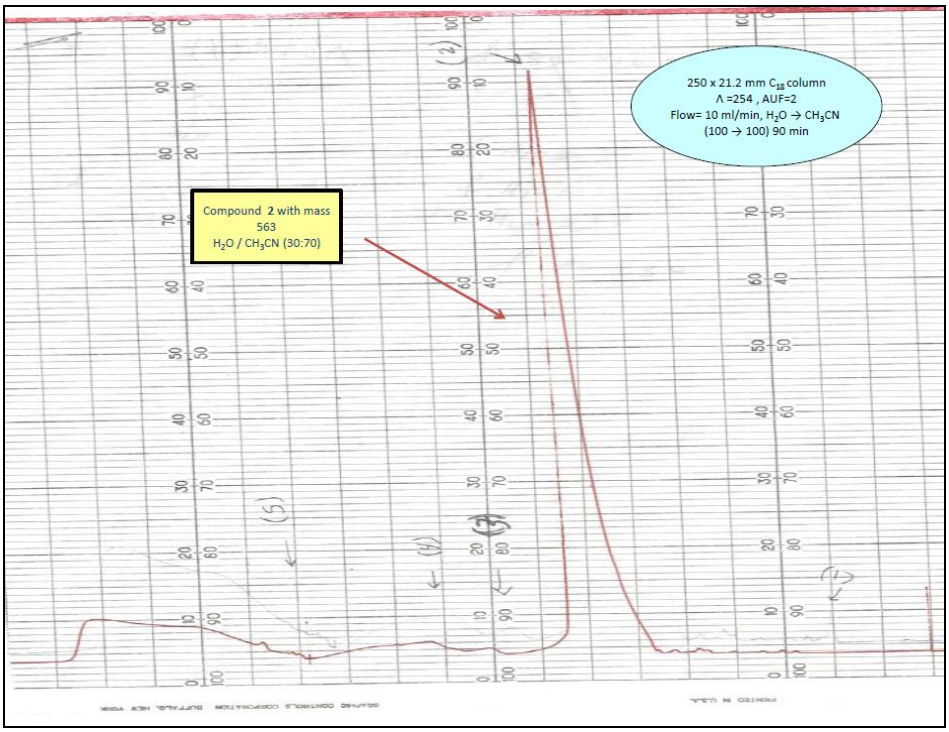

Figure 129. Purification of 2-*N*-methylmanzamine A trifluoromethanesulfonate **2** on 250 x 21.20 C_{18} column

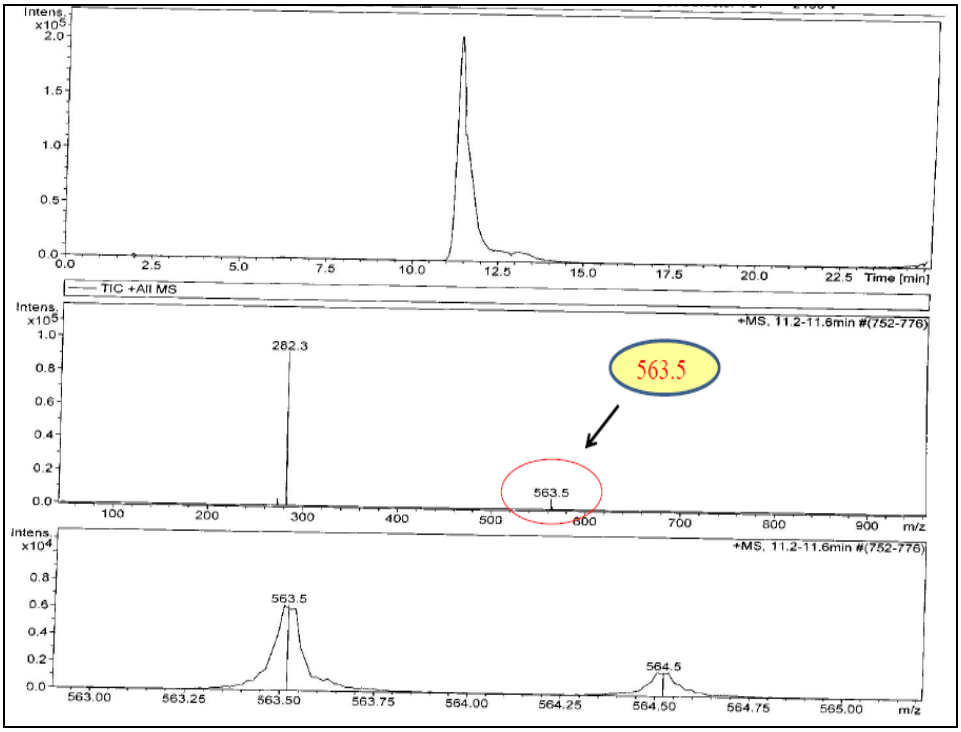

Figure 130. LC/MS chromatogram of 2-*N*-methylmanzamine A trifluoromethanesulfonate **2**

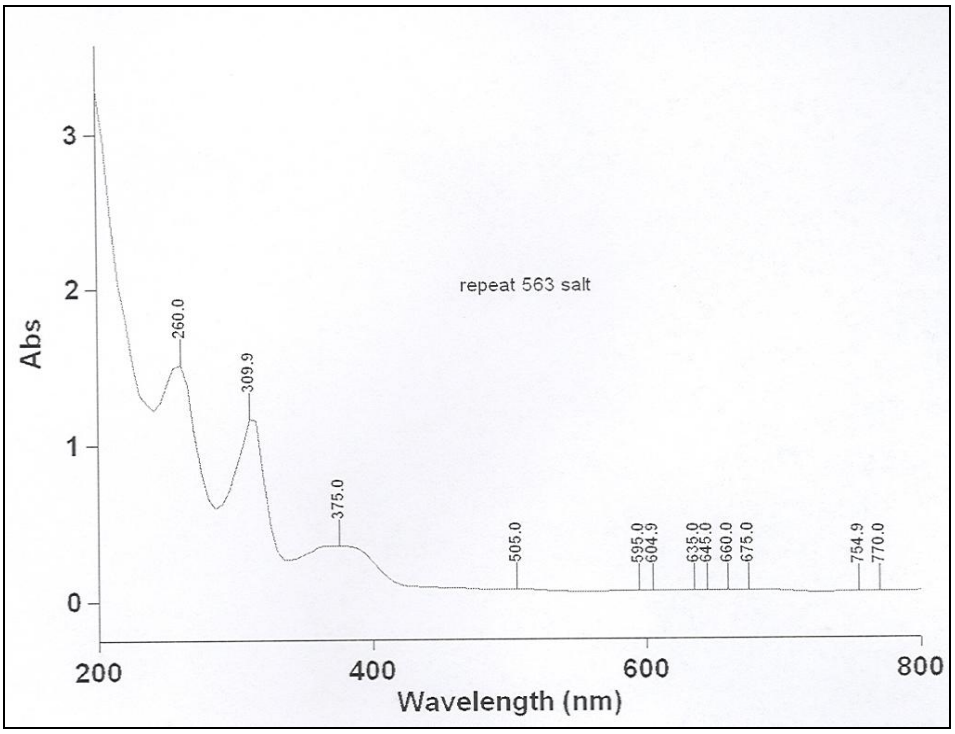

Figure 131. UV spectrum of 2-*N*-methylmanzamine A trifluoromethanesulfonate **2**

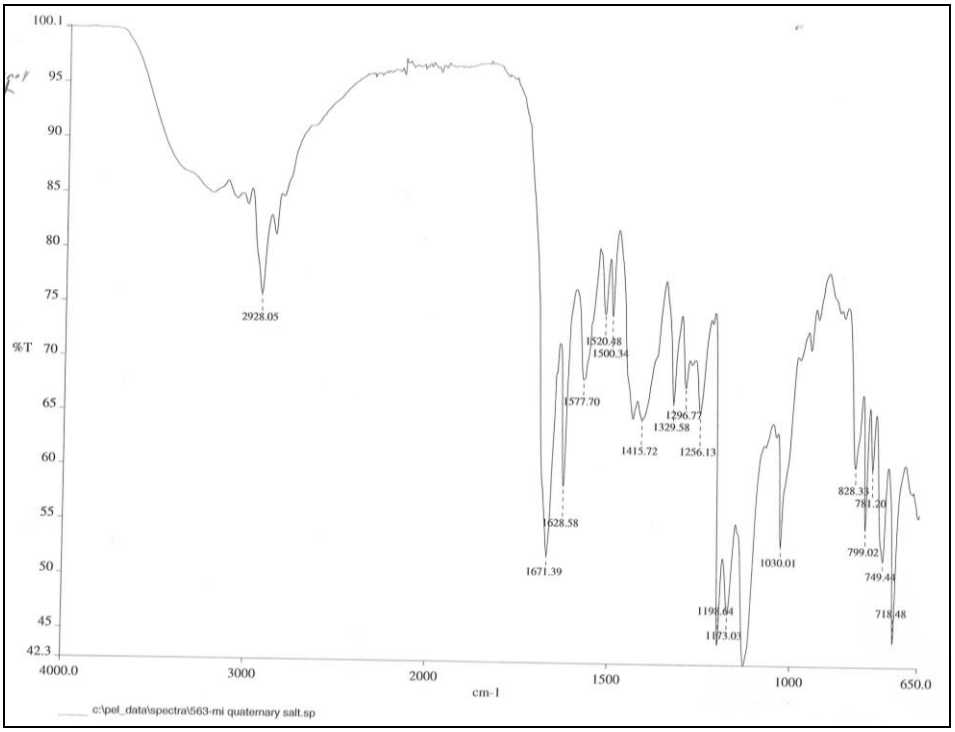

Figure 132. IR spectrum of 2-*N*-methylmanzamine A trifluoromethanesulfonate **2**

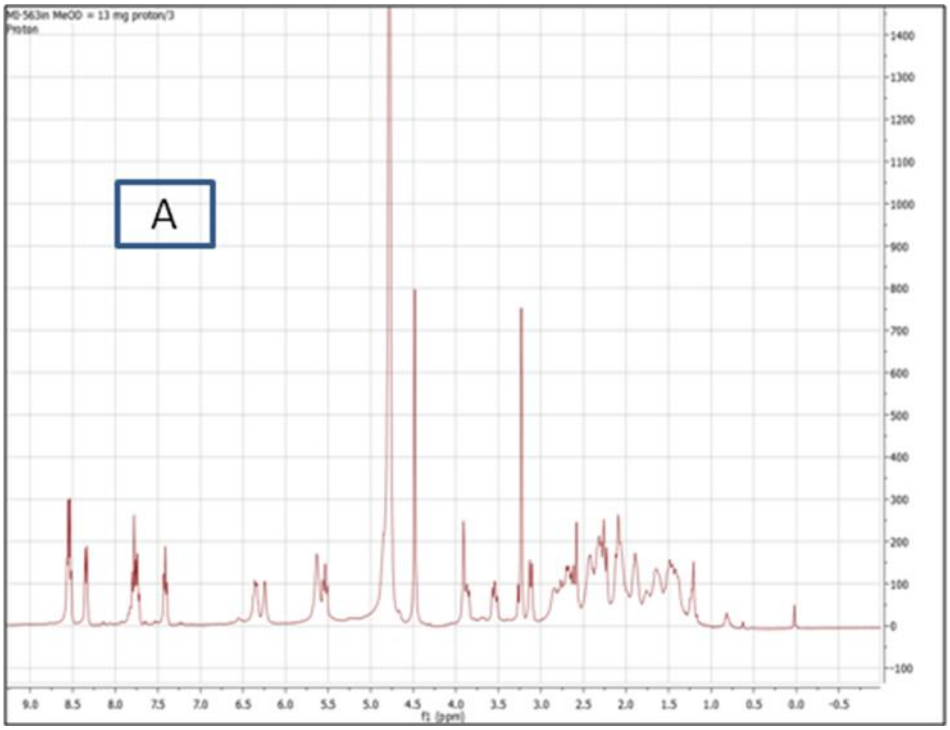

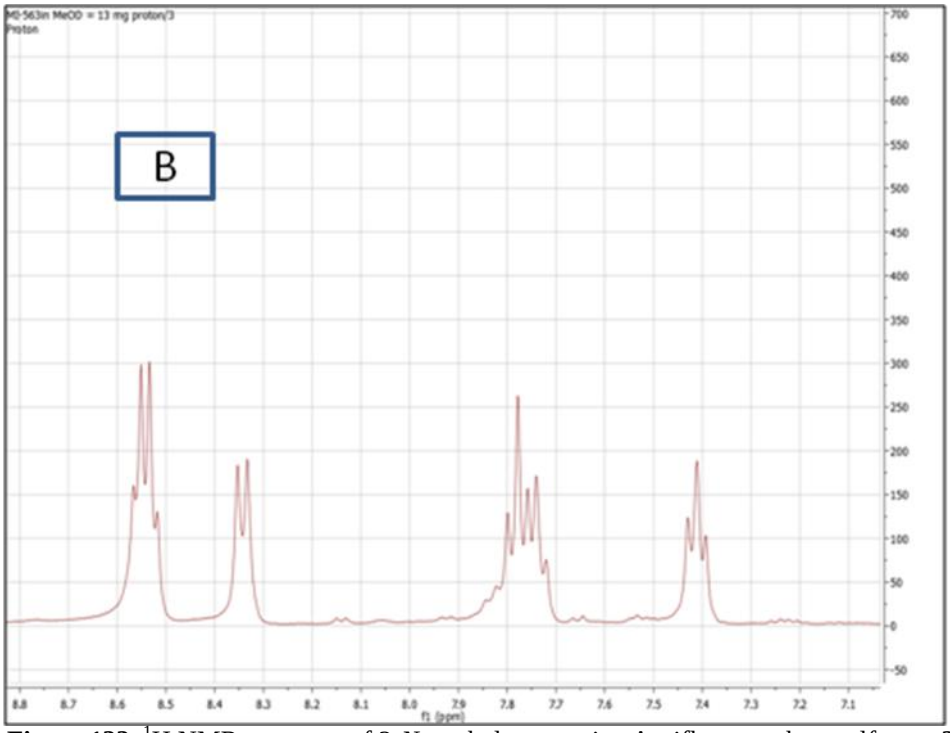

Figure 133. ^{1}H NMR spectrum of 2-*N*-methylmanzamine A trifluoromethanesulfonate **2** in methanol-d_4 (400 MHz); A) the full spectrum, B) the downfield region

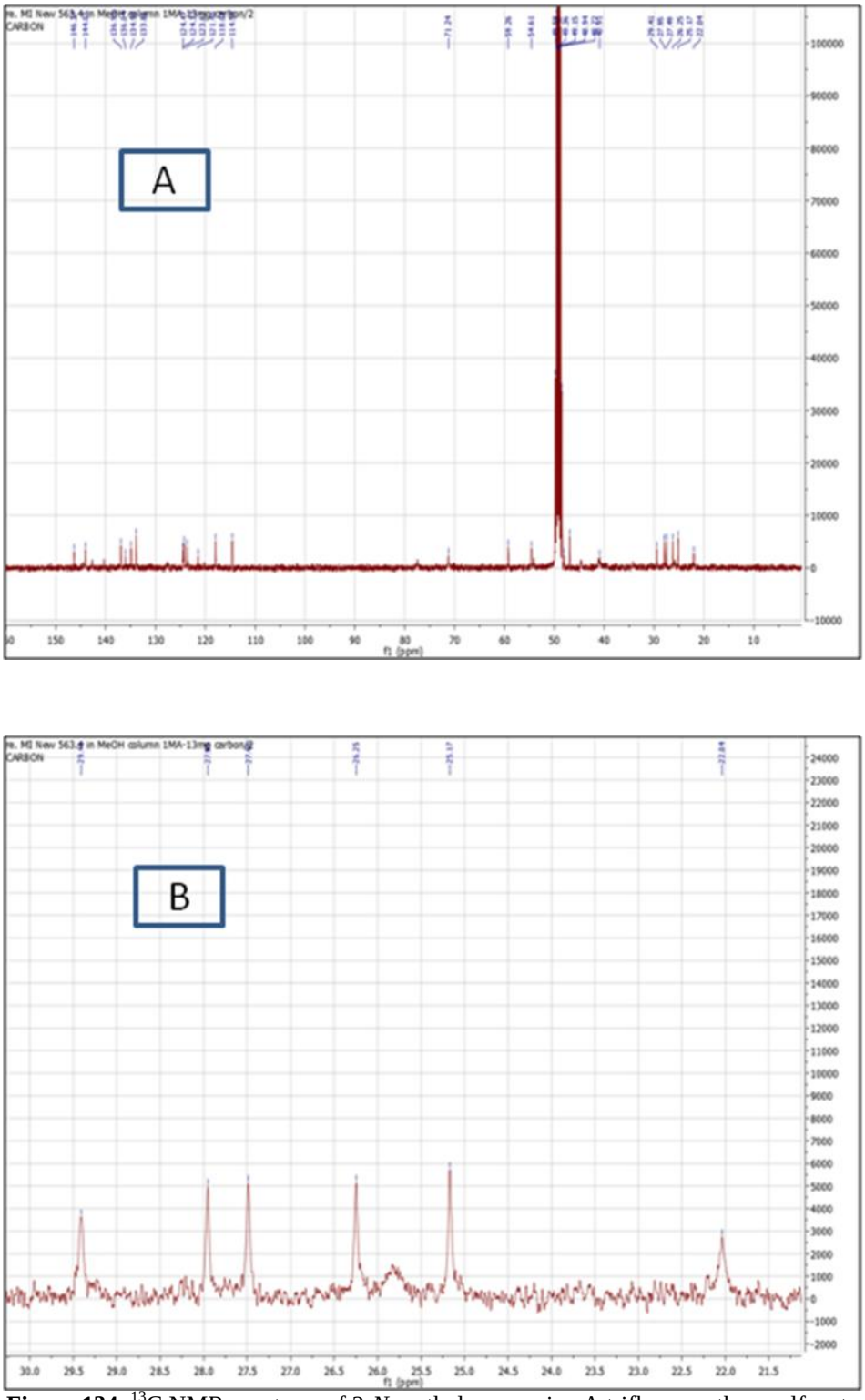

Figure 134. ^{13}C NMR spectrum of 2-*N*-methylmanzamine A trifluoromethanesulfonate **2** in methanol-d_4 (400 MHz); A) the full spectrum, B) the upfield region

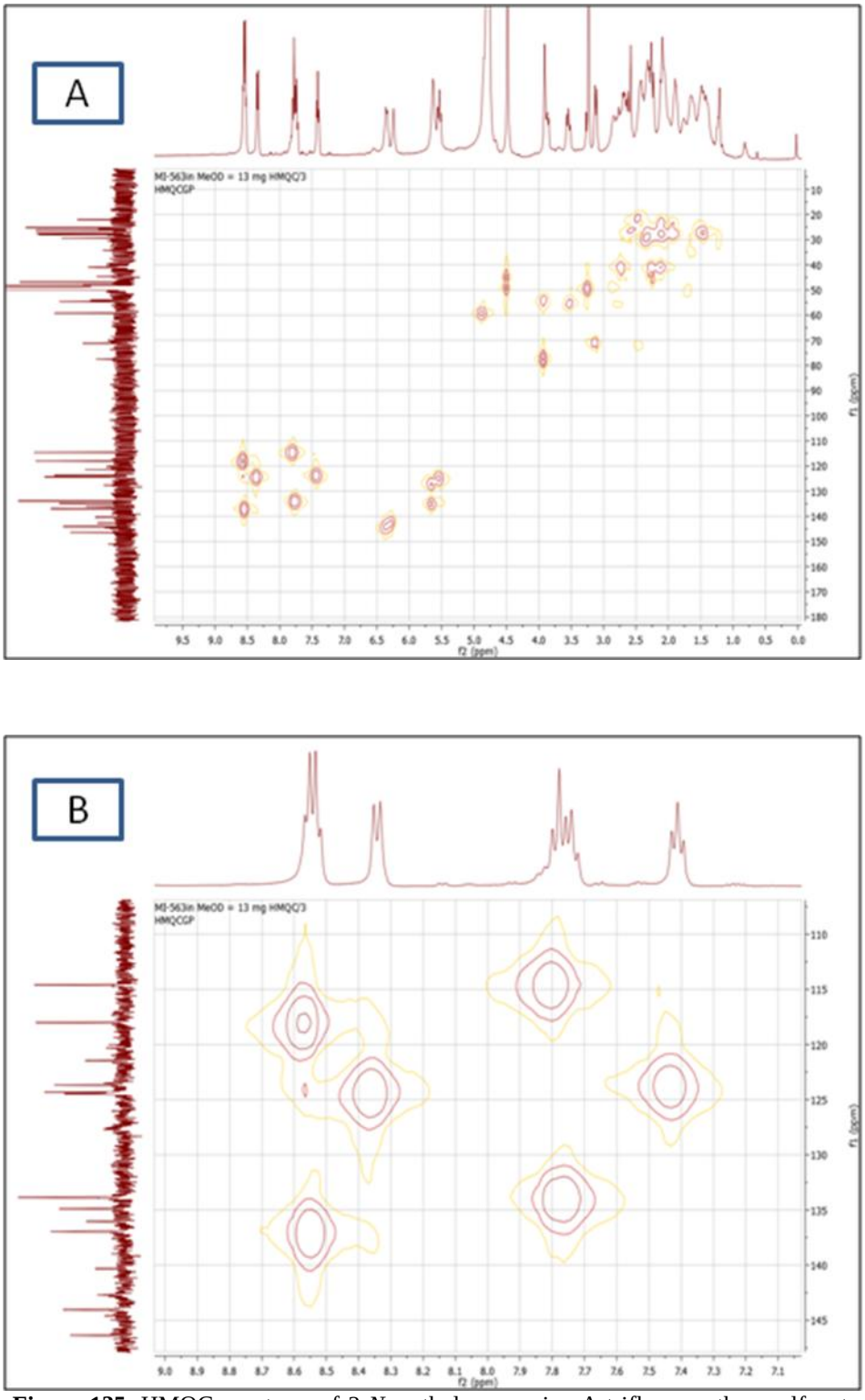

Figure 135. HMQC spectrum of 2-*N*-methylmanzamine A trifluoromethanesulfonate **2** in methanol-d_4 (400 MHz); A) the full spectrum, B) the downfield region

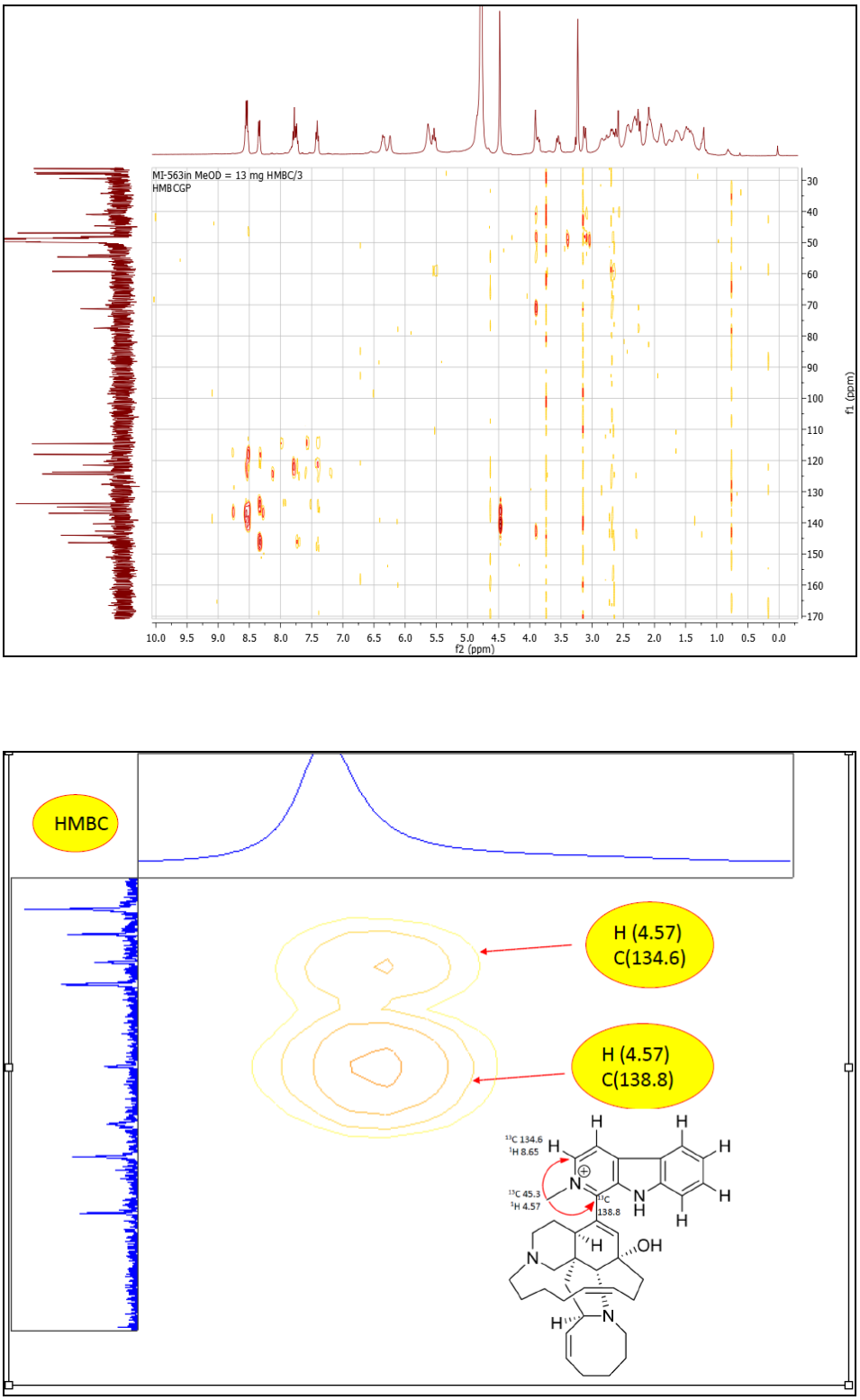

Figure 136. HMBC spectrum of 2-*N*-methylmanzamine A trifluoromethanesulfonate **2** in methanol-d_4 (400 MHz)

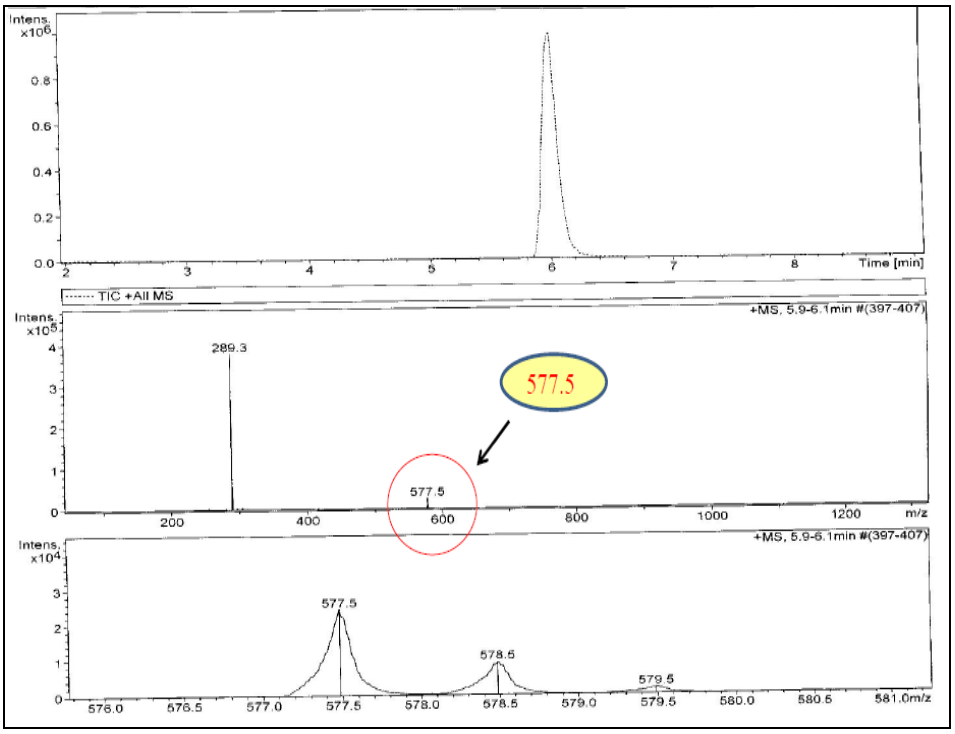

Figure 137. LC/MS chromatogram of 2-*N*,12-*O*-dimethylmanzamine A (**3**) trifluoromethanesulfonate

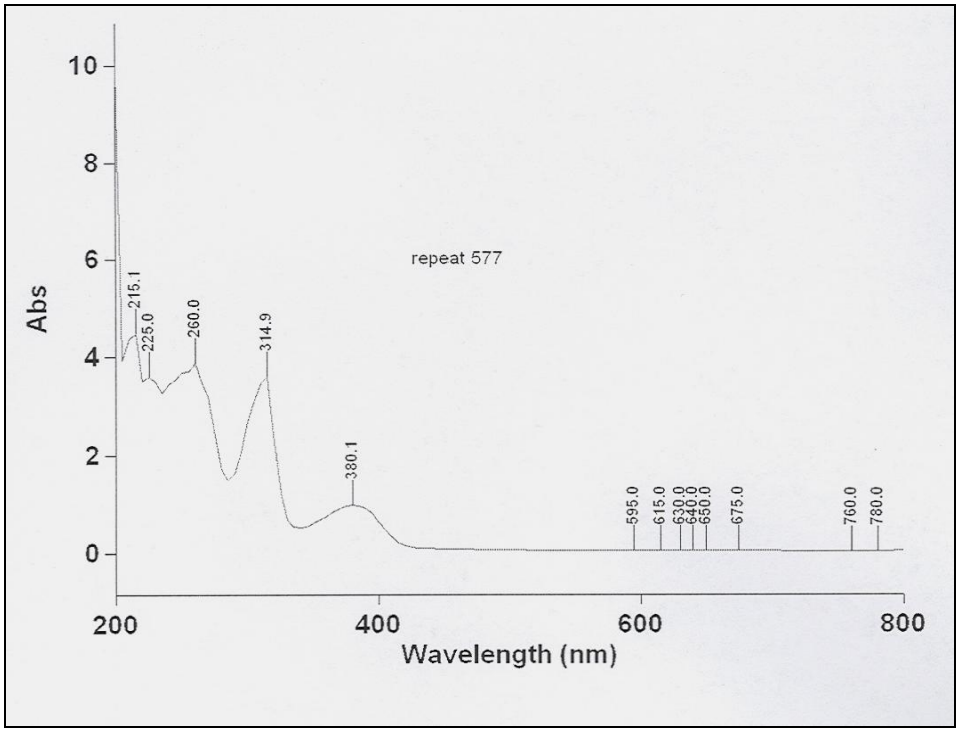

Figure 138. UV spectrum of 2-*N*,12-*O*-dimethylmanzamine A (**3**)

trifluoromethanesulfonate

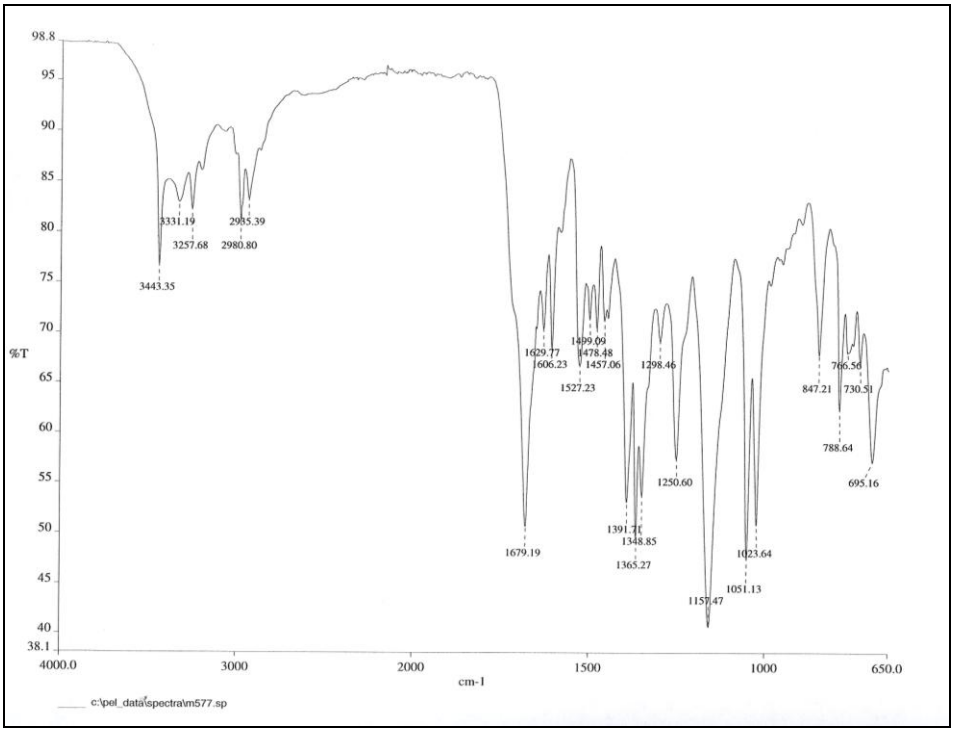

Figure 139. IR spectrum of 2-*N*,12-*O*-dimethylmanzamine A (**3**) trifluoromethanesulfonate

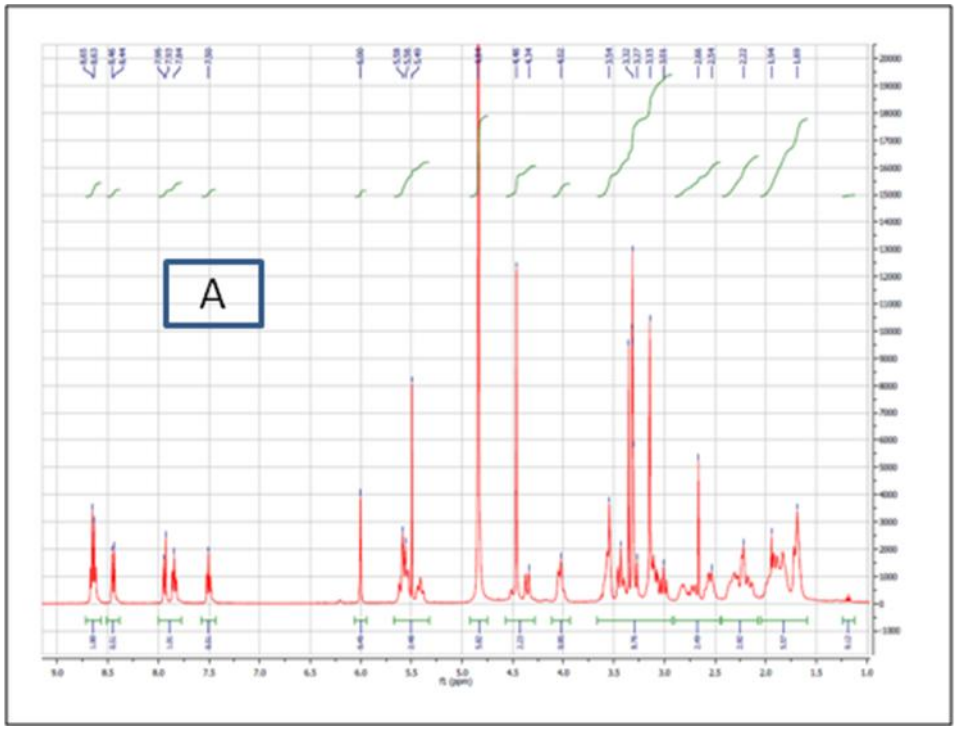

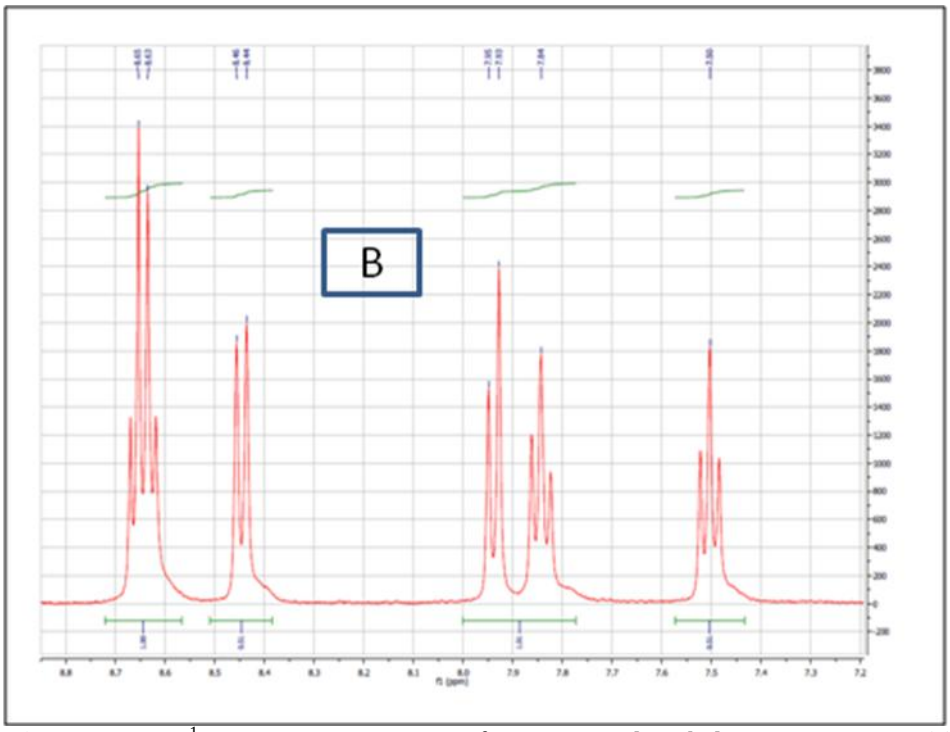

Figure 140. ^{1}H NMR spectrum of 2-*N*,12-*O*-dimethylmanzamine A (**3**) trifluoromethanesulfonate in methanol-d_4 (400 MHz); A) the full spectrum, B) the downfield region

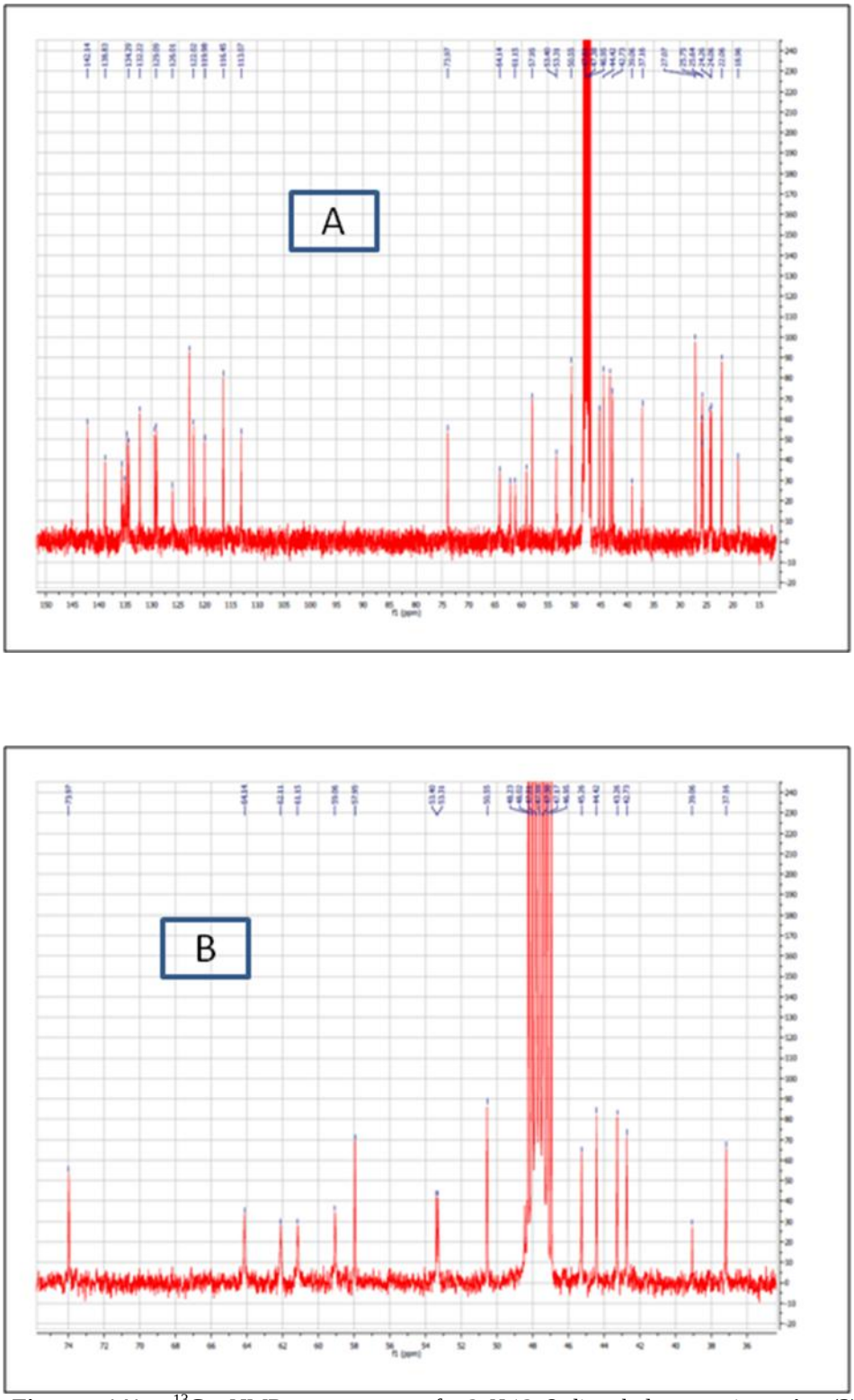

Figure 141. ^{13}C NMR spectrum of 2-*N*,12-*O*-dimethylmanzamine A (**3**) trifluoromethanesulfonate in methanol-d_4 (400 MHz); A) the full spectrum, B) the upfield region

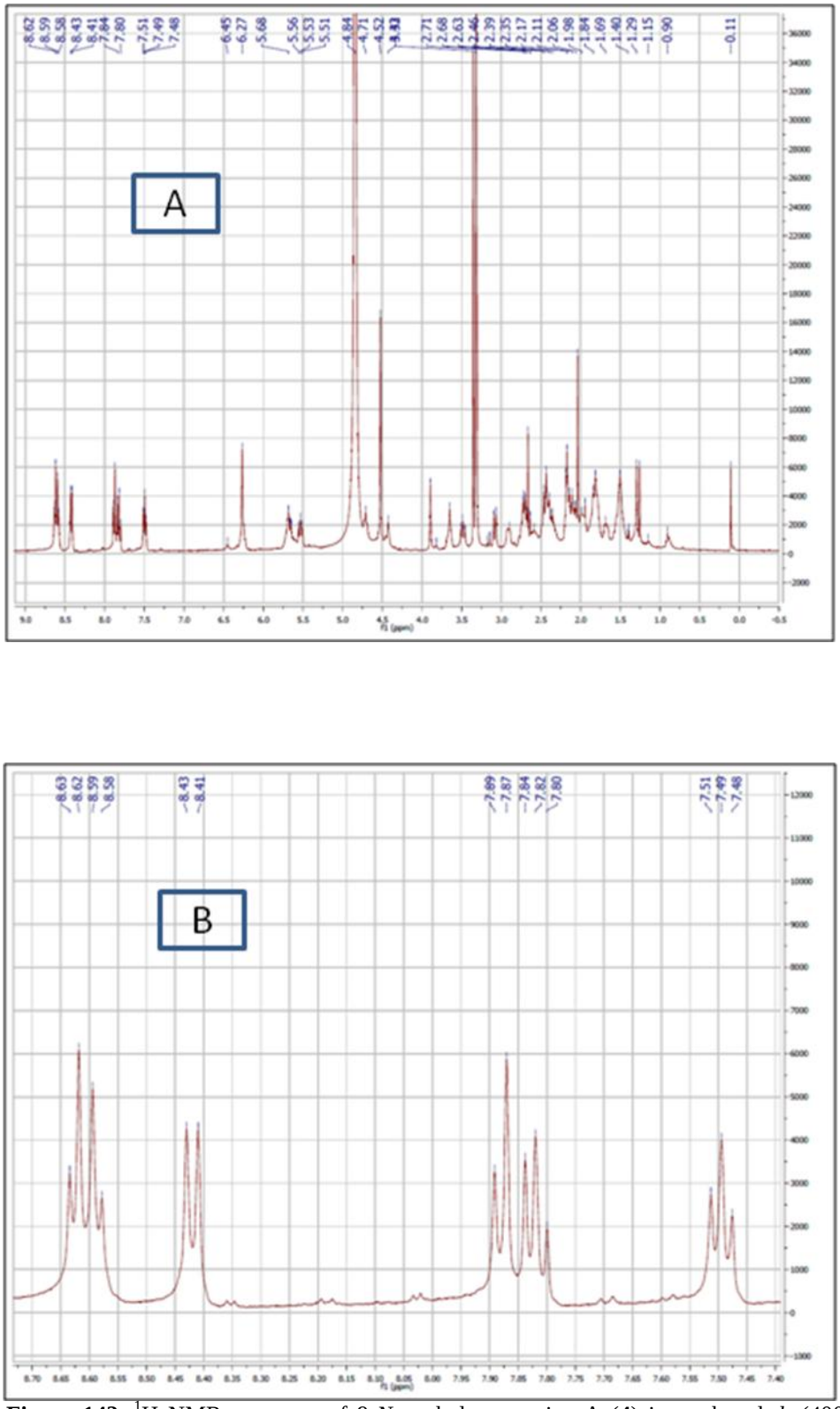

Figure 142. ^{1}H NMR spectrum of 9-*N*-methylmanzamine A (**4**) in methanol-d_4 (400 MHz); A) the full spectrum, B) the downfield region

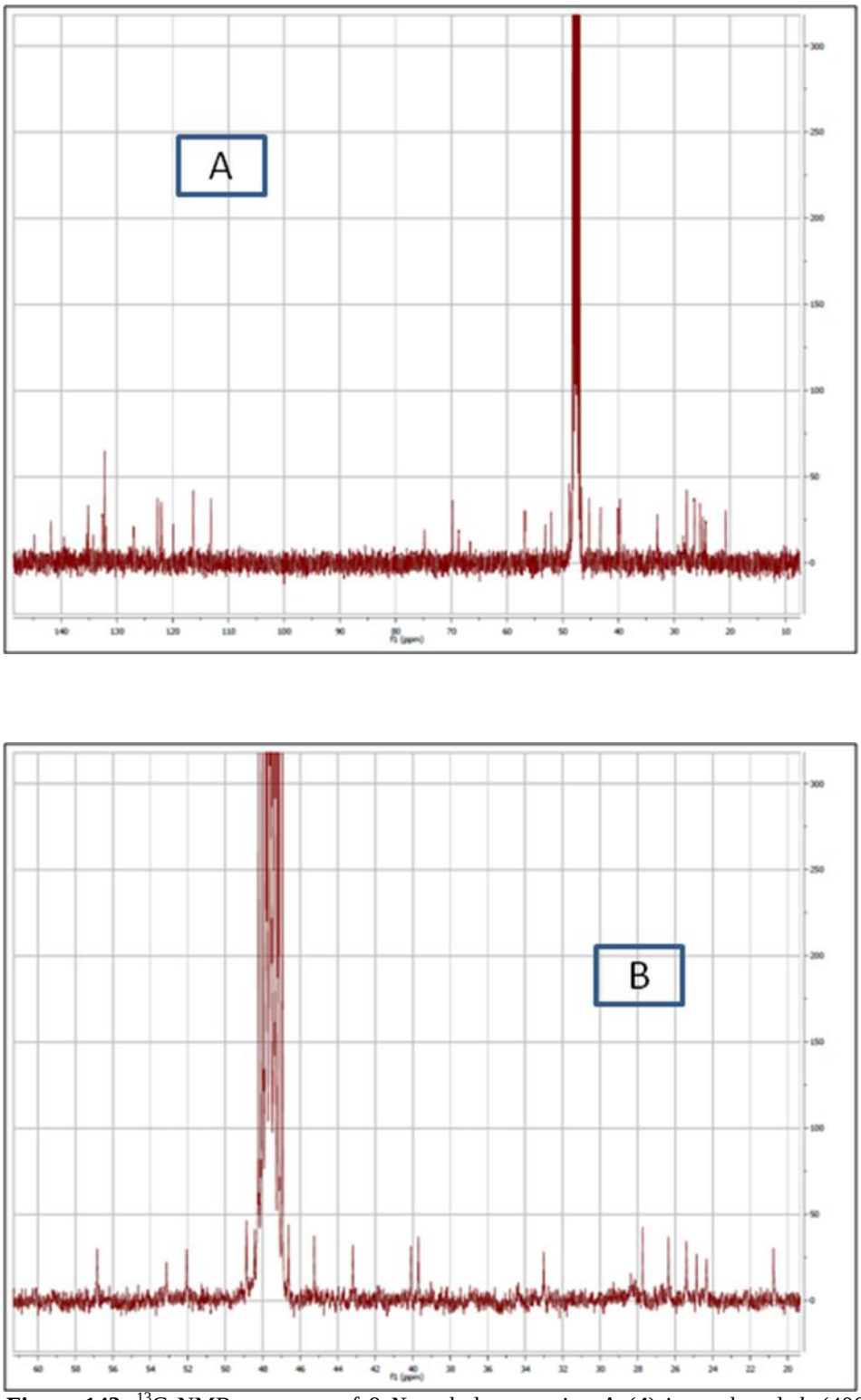

Figure 143. ^{13}C NMR spectrum of 9-*N*-methylmanzamine A (**4**) in methanol-d_4 (400 MHz); A) the full spectrum, B) the upfield region

3.2. Assay for in Vitro Antimalarial Activity and Cytotoxicity

A 200 µL suspension of red blood cells infected with D6 or W2 strain of *P. falciparum* (2% parasitemia and 2% hematocrit in RPMI 1640 medium supplemented with 10% human serum and 60 µg/mL Amikacin) was added to the wells of a 96-well plate containing 10 µL of serially diluted samples. The plate was flushed with a gas mixture of 90% N_2, 5% O_2, and 5% CO_2 and incubated at 37 ºC, for 72 h in a modular incubation chamber (Billups-Rothenberg, CA). Parasitic LDH activity was determined by using Malstat™ reagent (Flow Inc., Portland, OR) according to the procedure of Makler and Hinrichs.[85] The incubation mixture (20 µL) was mixed with 100 µL of the Malstat™ reagent and incubated at room temperature for 30 min followed by addition of 20 µL of a 1:1 mixture of NBT/PES (Sigma, St. Louis, MO) and further incubation in the dark for 1 hr. The reaction was stopped by the addition of 100 µL of 5% aq. acetic acid. The plate was read at 650 nm. Artemisinin and chloroquine were included as the drug controls. IC_{50} values were computed from the dose response curves to determine the selectivity index of antimalarial activity of the compounds. The in vitro cytotoxicity to mammalian cells was also determined. The assay was performed as described earlier.[86] Vero cells (monkey kidney fibroblasts) were seeded to the wells of 96-well plate at a density of 25,000 cells/well and incubated for 24 h. Samples at different concentrations were added and plates were again incubated for 48 h. The number of viable cells was determined by Neutral Red assay. IC_{50} values were obtained from dose response curves. Doxorubicin was used as a positive control.

3.3. Assay for Antimicrobial Activity

All organisms are obtained from the American Type Culture Collection (Manassas, VA)

and include the fungi *Candida albicans* ATCC 90028, *Cryptococcus neoformans* ATCC 90113, and *Aspergillus fumigatus* ATCC 90906 and the bacteria methicillin-resistant *Staphylococcus aureus* ATCC 43300 (MRS), *Escherichia coli* ATCC 35218, *Pseudomonas aeruginosa* ATCC 27853, and *Mycobacterium intracellulare* ATCC 23068. Susceptibility testing is performed using a modified version of the CLSI (formerly NCCLS) methods.[87-90] *M. intracellulare* is tested using a modified method of Franzblau et al.[91] Samples are serially-diluted in 20% DMSO/saline and transferred in duplicate to 96 well flat bottom microplates. Microbial inocula are prepared by correcting the OD630 of microbe suspensions in incubation broth to afford final target inocula. Drug controls [ciprofloxacin (ICN Biomedicals, Ohio) for bacteria and amphotericin B (ICN Biomedicals, Ohio) for fungi] are included in each assay. All organisms are read at either 630 nm using the EL-340 Biokinetics Reader (Bio-Tek Instruments, Vermont) or 544ex/590em, (*M. intracellulare*, *A. fumigatus*) using the Polarstar Galaxy Plate Reader (BMG LabTechnologies, Germany) prior to and after incubation. Minimum fungicidal or bactericidal concentrations are determined by removing 5 µL from each clear well, transferring to agar and incubating. The MFC/MBC is defined as the lowest test concentration that kills the organism (allows no growth on agar).

CHAPTER VI

HCV LEADS FROM THE SOUTH AMERICA ENDANGERED PLANT *DIPLOSTEPHIUM RHODODENDROIDES*

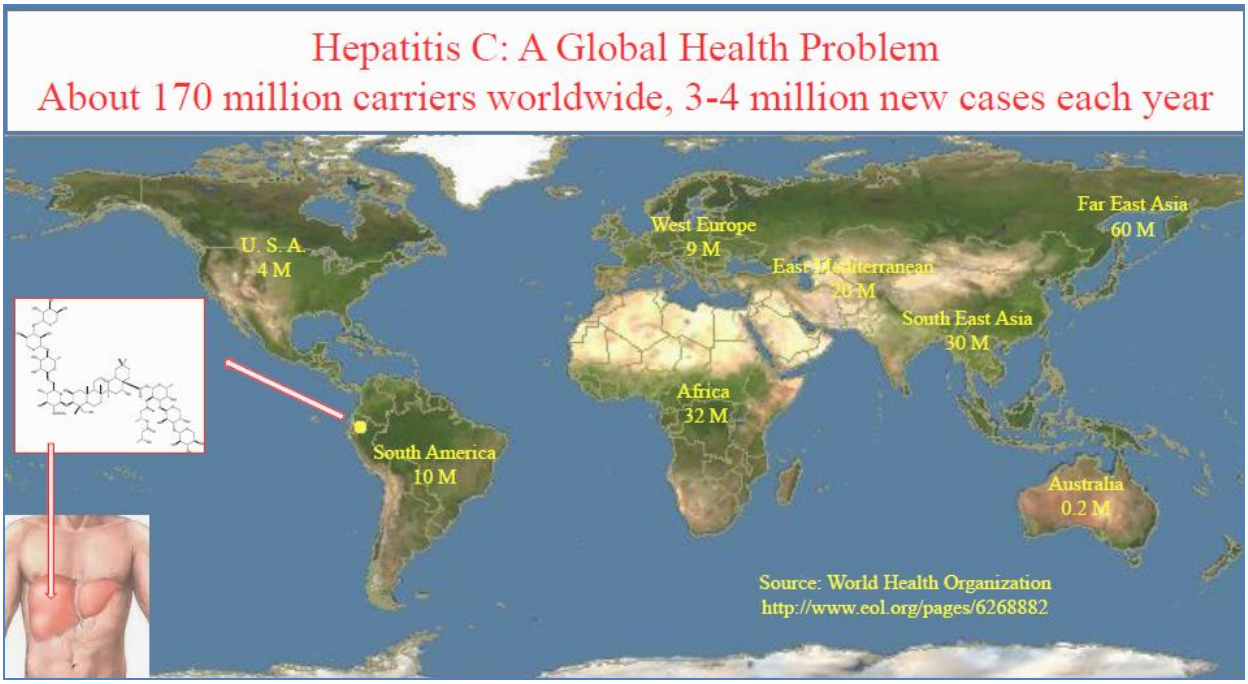

World distribution of *Diplostephium rhododendroides* and hepatitis C carriers

Although plants and marine organisms represent crucial sources in the field of drug discovery, little attention has been given to endangered and rare plant species. However, threatened plant species may provide drug leads for serious diseases that kill a large number of the population each year and if these opportunities are missed they may be gone forever. In 2009, the UK-Plantlife reported that about 15,000 of the 50,000 wild medicinal plants are at risk and headed for extinction.[92] Gilbert et al. reported in 2010 that more than 17,000 species of fauna and flora were at risk of extinction in 2009 and over half of all medicinal plants in Africa face extinction.[93] This causes serious concern, as the World Health Organization estimates that 80% of the world's population relies on traditional plant derived medicines for their pharmacopeia. The U.S. Fish & Wildlife Service declared that 795 plant species are at risk of extinction throughout the United States. According to Gordon Cragg, former director of the natural products branch of the NCI, over 60% of cancer therapeutics were derived from naturally-occurring products.[94] Various examples have been reported, like extracts from *Catharanthus roseus* (*Rosy periwinkle*) used to treat Hodgkin's disease and leukemia,[95] digitalis from *Digitalis purpurea* (foxglove) for the treatment of heart disease,[96] galantamine from *Galanthus caucasicus* (snowdrops) used for the treatment of Alzheimer's disease[97] and paclitaxel, the anti-cancer drug Taxol™, from the bark of the Pacific yew tree.[98] Though habitat loss and climate change[99] are the primary cause of species endangerment, other biological factors such as competition and invasion;[100] non-native fungi,[101] viruses or exotic arthropods,[102] can also drive plant species to extinction. For example, the Florida torreya (*Torreya taxifolia*) suffered a tragic decline due primarily to the fungus *Pestalotiopsis microspora* residing in its inner bark, triggering pathogenic activity on the host.[103]

Is it possible that rare plants can provide promising HCV treatments similar to the anti-cancer drug, Taxol?

Hepatitis epidemics were first recorded as early as 2000 B.C. but it wasn't until 1989 that hepatitis C virus (HCV) was identified[104] in tissue samples of chimpanzees.[105]

As many as four million individuals in the United States and 200-300 million worldwide are infected with HCV.[106] According to the CDC, there were up to 18,000 new HCV infections in the United States in 2008 and HCV is responsible for 12,000 deaths annually. According to The Hepatitis Central, HCV accounts for 20% of acute hepatitis cases, 70% of chronic hepatitis, 40% of end-stage cirrhosis, 60% of hepatocellular carcinoma, and 30-40% of liver transplants. The CDC estimates that in the next two decades, chronic HCV will be a major burden on the health care system. The direct medical costs of chronic HCV infection are estimated to exceed $10.7 billion, $54.2 billion for the societal cost of premature mortality, and $21.3 billion for the cost of disability due to HCV infections. According to Hepatitis Central statistics, there will be a 60% increase in the incidence of cirrhosis, a 68% increase in hepatoma incidence, a 279% increment in the incidence of hepatic decompensation, a 528% increase in the need for transplantation, and a 223% increase in liver death rates from HCV in the next 10-20 years.

HCV is a spherical, enveloped, single-stranded RNA virus (family Flaviviridae) that can replicate in the trillions at steady state.[107] The RNA-dependent RNA polymerase generates a large number of mutant viruses known as quasi-species, presenting a major challenge in the control of HCV.[108] Of the six major HCV genotypes, genotype 1 is the most common in the United States. Genotype 1 is associated with more severe liver diseases and a higher risk of

hepatocellular carcinoma.[109] The classified genotype 1b does not respond to therapy as well as genotypes 2 and 3.[109] Genotype 4 is the most prevalent genotype in Egypt, while genotype 5 is found in South Africa and genotype 6 in Southeast Asia. HCV encodes a single polyprotein of 3011 amino acids that is processed into 10 structural and regulatory proteins (Figure 144). This includes the core and two envelope proteins, E1 and E2 with a high rate of mutation.[110]

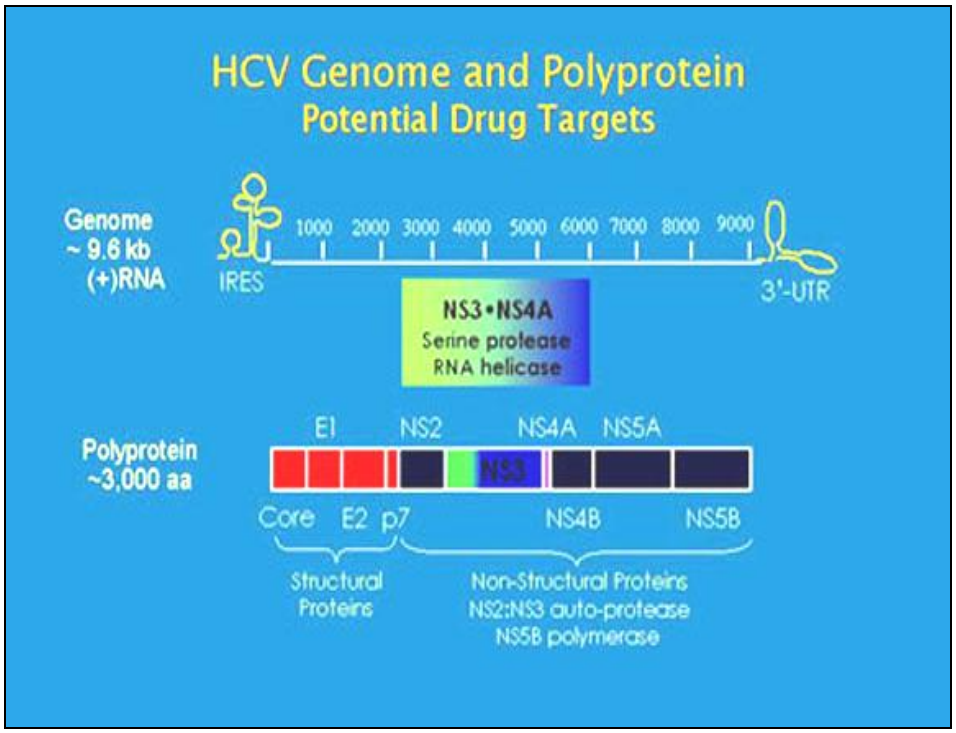

Figure 144. HCV genome and polyprotein potential drug target

According to Murray and Rice,[111] HCV replicates using a series of enzymes, including the two proteases (NS2-3 and NS3-4A), a helicase (NS3), and a polymerase (NS5B) (Figue 145). Of these, NS3-4A and NS5B have attracted the most attention as drug targets. In 2010, Gao et al. reported a potent NS5A inhibitor, BMS-790052 that is under evaluation in combination with other drugs, and this has stimulated studies targeting proteins with lack of intrinsic enzymatic or receptor functionality.[112]

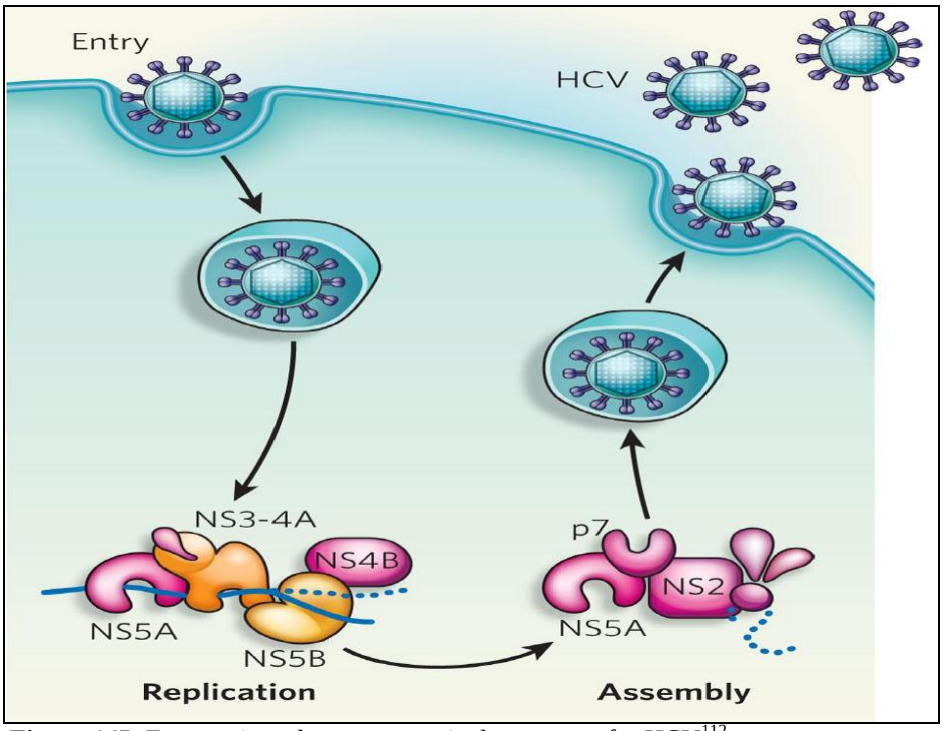

Figure 145. Enzymatic and non enzymatic drug targets for HCV[112]

High throughput HCV screening programs were used to identify potential drug leads, various natural products and extracts were tested for their HCV activity. For example, the well absorbed celgosivir (Figure 146) is a valuable oral prodrug of the natural product castanospermine that inhibits α-glucosidase I, an enzyme that plays an important role in viral maturation by initiating the *N*-linked oligosaccharides of the viral envelope glycoproteins.[113] However, most of the agents are not effective as a monotherapy for the treatment of HCV, but demonstrated a synergistic effect in combination with the current standard of care pegylated α-interferon (IFN). The most frequently used treatment involves a weekly injection of a combination of (IFN) and ribavirin (Figure 146), which are only 50% effective and have serious side effects including depression and influenza-like symptoms in more than 60% of the patients.[114] An herbal medicine (Mao-to) in combination with natural IFN-β was tried for

eighteen Japanese patients with chronic HCV characterized by a high serum viral load (1 meq/mL) and genotype-1b who seem to be resistant to interferon (IFN) therapy. Sixteen of the 18 patients (89 %) tested negative for serum HCV RNA at the end of treatment, but only two of them (11%) remained negative for the viral RNA at the six month of follow-up studies.[115] Recently various natural glucosidases inhibitors were reported such as deoxynojirimycin (Figure 146) and its derivatives.[116] In addition, a non-immunosuppressive derivative of cyclosporine A, NIM811 (Figure 146), was shown to possess anti-HCV activity through binding to cyclophilin.[116] More recently, Telaprevir and Bocepravir were approved by the FDA, but even these potent protease inhibitors are effective at most 80% of the time when combined with standard of care (IFN) (Figure 146).

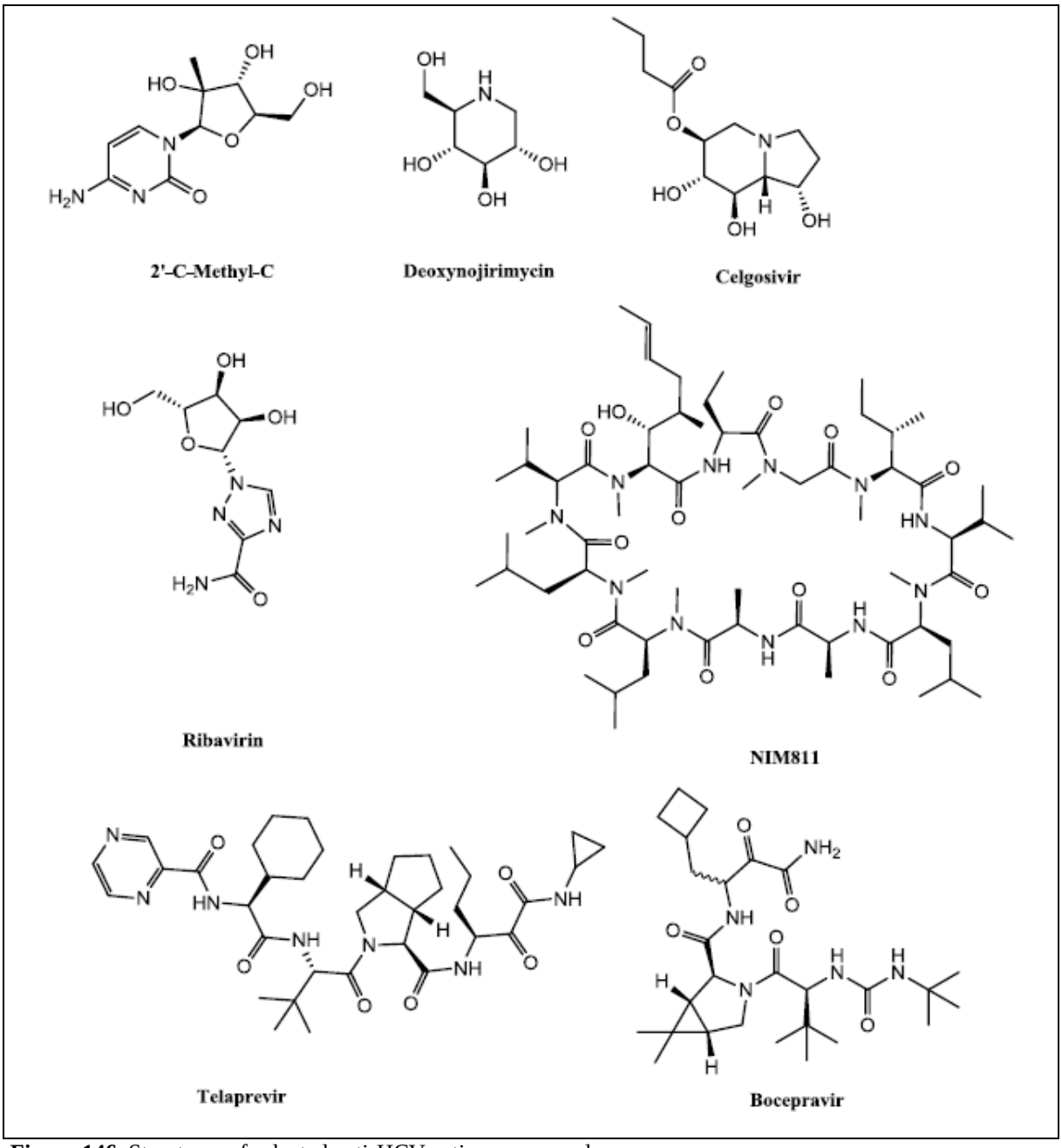

Figure 146. Structures of selected anti-HCV active compounds

Recently, we began to evaluate the anti-HCV properties of rare Latin American plant extract provided by Newman of the Natural Products Branch of the National Cancer Institute (repository #77951); collected from Ecuador; longitude: 77 055.02 W latitude: 046.98 N) under a specific Material Transfer Agreement (MTA) that protects the rights of Ecuador. *Diplostephium*

rhododendroides (family Asteraceae) found in Ecuador and Colombia and it is no surprise that this species has not been subjected to any major phytochemical screening. *Diplostephium* (Figure 147) is a genus composed of approximately 110 species. Colombia has 63 species and *Diplostephium* is the third most diverse genus on the paramos at the border between Colombia and Ecuador.[117]

Figure 147. Selected species from the genus *Diplostephium*

The HCV inhibitory guided evaluation of the *rhododendroides* extract led to the isolation and identification of a group of unique and complicated oleanane-triterpene glycosides rhododendrosaponins **I-III** with *m/z* of 1722-1764. The isolation of the active metabolites was challenging due to the limited amount of extract and the absence of additional fresh plant material. The extraction started with a rapid solvent elution utilizing MeOH-DCM, where the active metabolites were extracted in DCM-MeOH (25:75) (Scheme 9), followed by HPLC on

250 × 21.2 mm C_{18} column with MeOH-H_2O, where the active material eluted off the column as a broad signal by the end of the elution (Scheme 10, Figure 148). The material representing this broad signal was subjected to 250 × 21.2 mm NH_2 column with $CHCl_3$-MeOH to yield three UV inactive metabolites (Scheme 11, Figure 149). The three resolved metabolites were further subjected to 250 × 4.6 mm NH_2 (Figure 150), and the co-injection of metabolites **2** and **3** on 250 × 4.6 mm NH_2 column was also completed (Figure 151). The complete 1D and 2D NMR data sets of rhododendrosaponins **I-III** were gathered (Figures 152-180). Evaluation of ^{1}H and ^{13}C NMR data of the rhododendrosaponins **I-III** permitted the validation of the basic skeletons of the oleanane-type triterpenes [polygalacic acid; (2β,3β,4α,16α)-2,3,16,23-tetrahydroxyolean-12-en-28-oic acid] with one characteristic double bond (Figure 181), [118] where H-12 (5.34 Hz) shows an HMBC correlation to C-14 (40.9 Hz); H-23 shows HMBC correlations to C-3 (84.0 Hz), C-4 (43.1 Hz), C-5 (48.3 Hz) and C-24 (65.6 Hz);. H-25 (1.22 Hz) shows HMBC correlations to C-1 (44.4 Hz), C-5 (48.3 Hz), C-9 (48.2 Hz) and C-10 (37.6 Hz); H-26 (0.72 Hz) shows HMBC correlations to C-7 (33.8 Hz), C-8 (42.9 Hz), C-9 (48.2 Hz) and C-14 (40.9 Hz); H-27 (1.31 Hz) shows HMBC correlations to C-8 (42.9 Hz), C-13 (144.8 Hz), C-14 (40.9 Hz) and C-15 (36.4 Hz); H-30 (0.81 Hz) shows HMBC correlations to C-19 (48.2 Hz), C-21 (35.5 Hz) and C-29 (25.0 Hz). In addition mild hydrolysis using dioxane containing HCl followed by GC/MS analysis, showed the presence of 3-hydroxybutanoate (Figure 182). This was confirmed by HMBC correlations of the 3-hydroxybutanoate dimer, where H-2′ (2.83 Hz) shows HMBC correlations to C-1′ (171.5 Hz), C-3′ (68.8 Hz), and C-4′ (20.8 Hz), while H-2″ (2.52 Hz) shows HMBC correlations to C-1″ (172.6 Hz), C-3″ (65.6 Hz), and C-4″ (23.6 Hz) (Figure183).

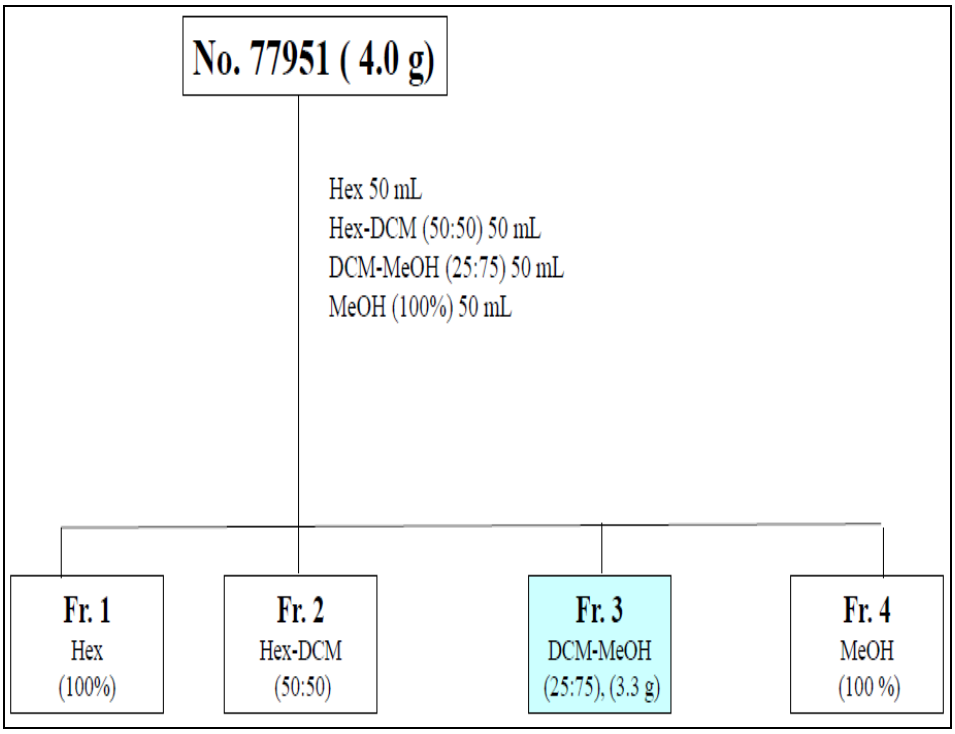

Scheme 9. Fractionation of *Diplostephium rhododendroides* extract via solvent extraction, blue color indicated the presence of the Rhododendrosaponins **I-III**

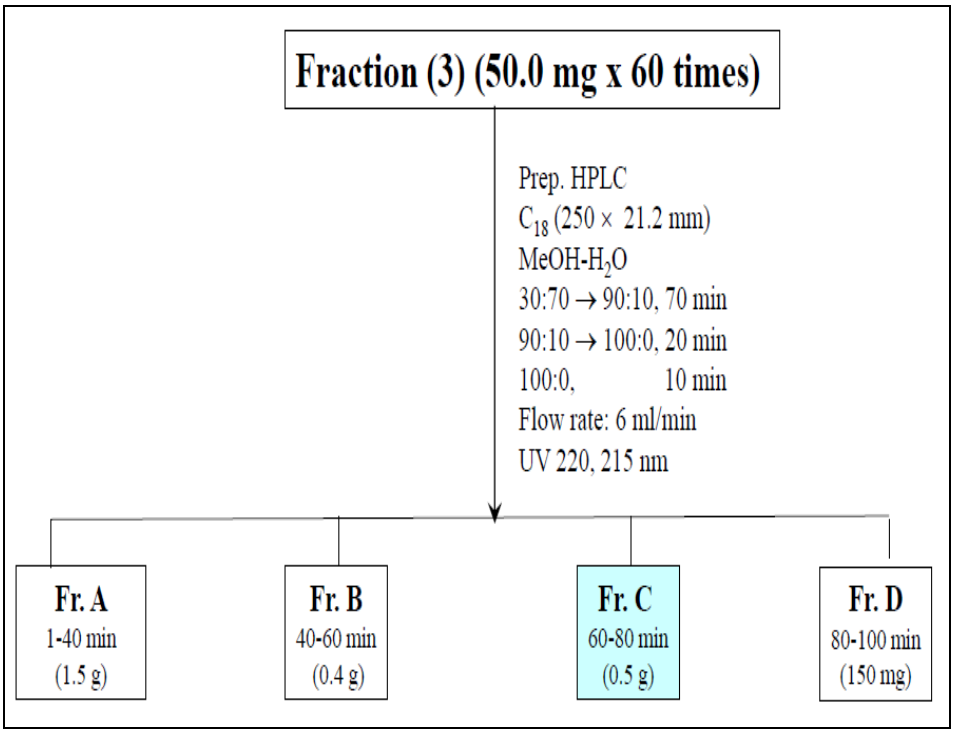

Scheme 10. Fractionation of Fr. **3**; DCM-MeOH (25:75), on 250 x 21.2 mm C_{18} column, blue color indicated the presence of the rhododendrosaponins **I-III**

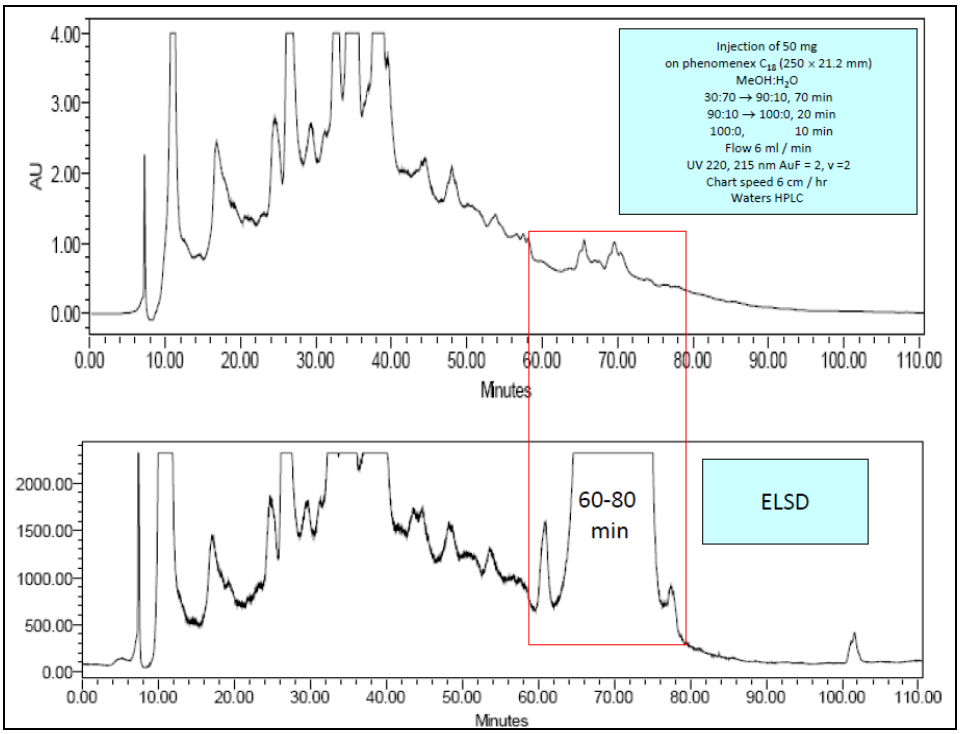

Figure 148. HPLC chromatogram of Fr. **3**; DCM-MeOH (25:75), on 250 x 21.2 mm C_{18} column

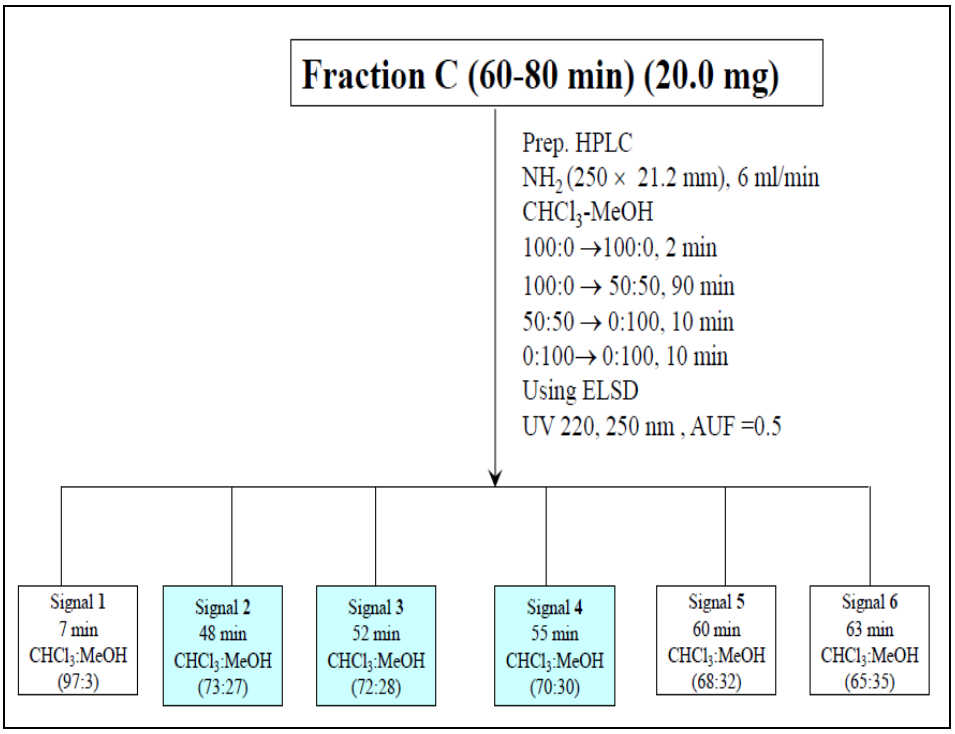

Scheme 11. Fractionation of Fr. **C**; (60-80 min off C_{18}), on 250 x 21.2 mm NH_2 column, blue color indicated the presence of the rhododendrosaponins **I-III**

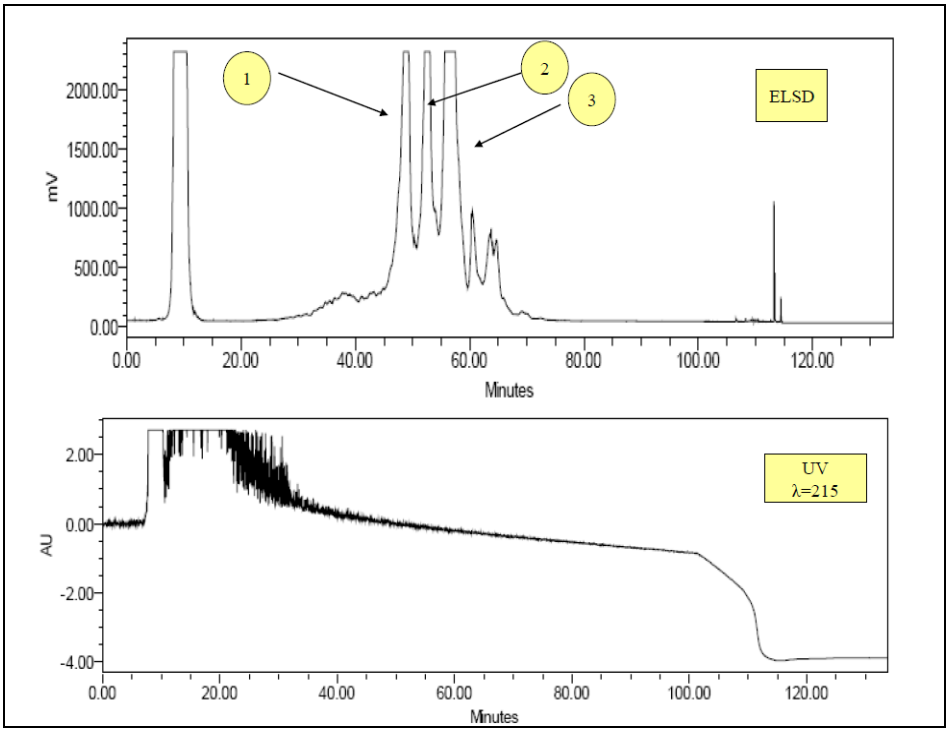

Figure 149. HPLC chromatogram of Fr. **C**; (60-80 min off C_{18}), on 250 x 21.2 mm NH_2 column, signals 1-3 indicated the presence of the rhododendrosaponins **I-III** in similar order.

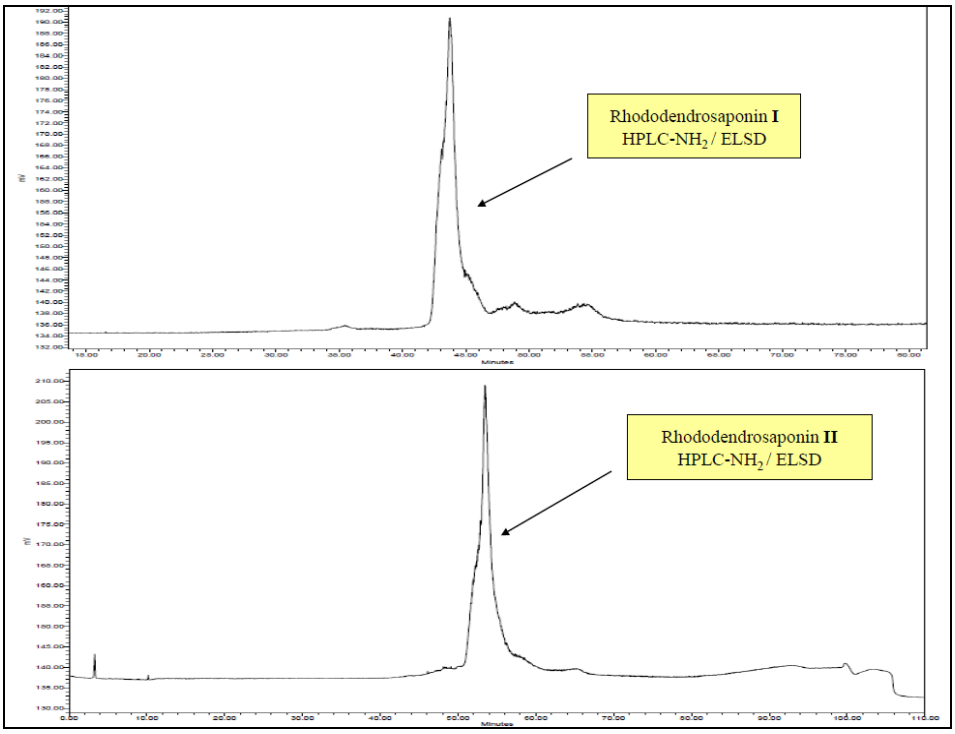

Figure 150. Re-injection of rhododendrosaponins **I** and **II** on 250 × 4.6 mm NH_2 column

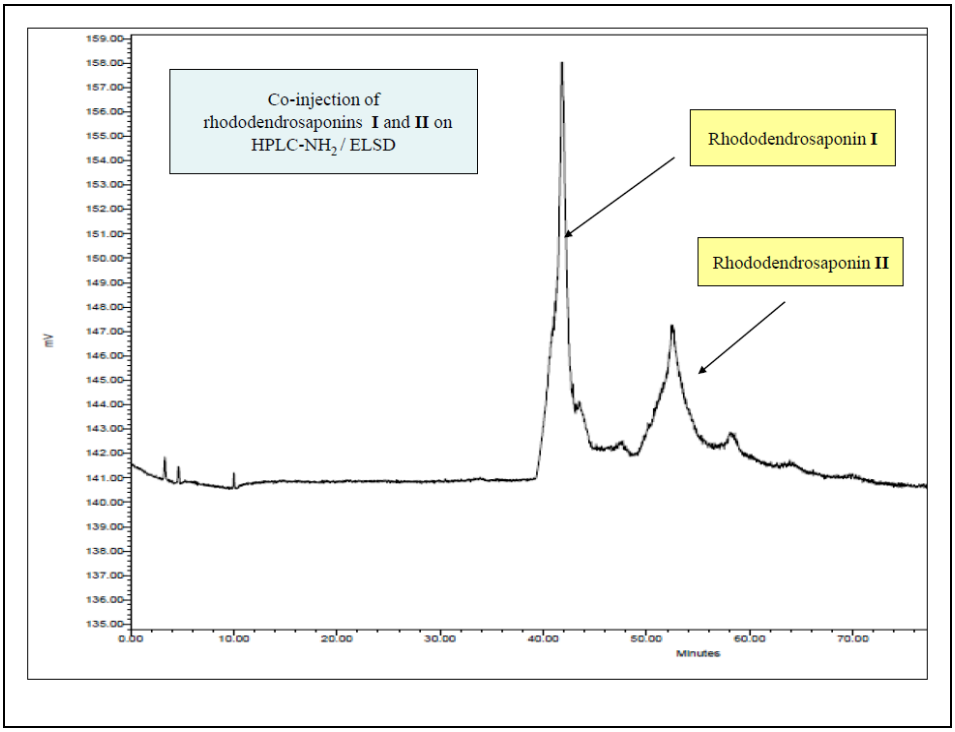

Figure 151. Co-injection of rhododendrosaponins **I** and **II** on 250 × 4.6 mm NH_2 column

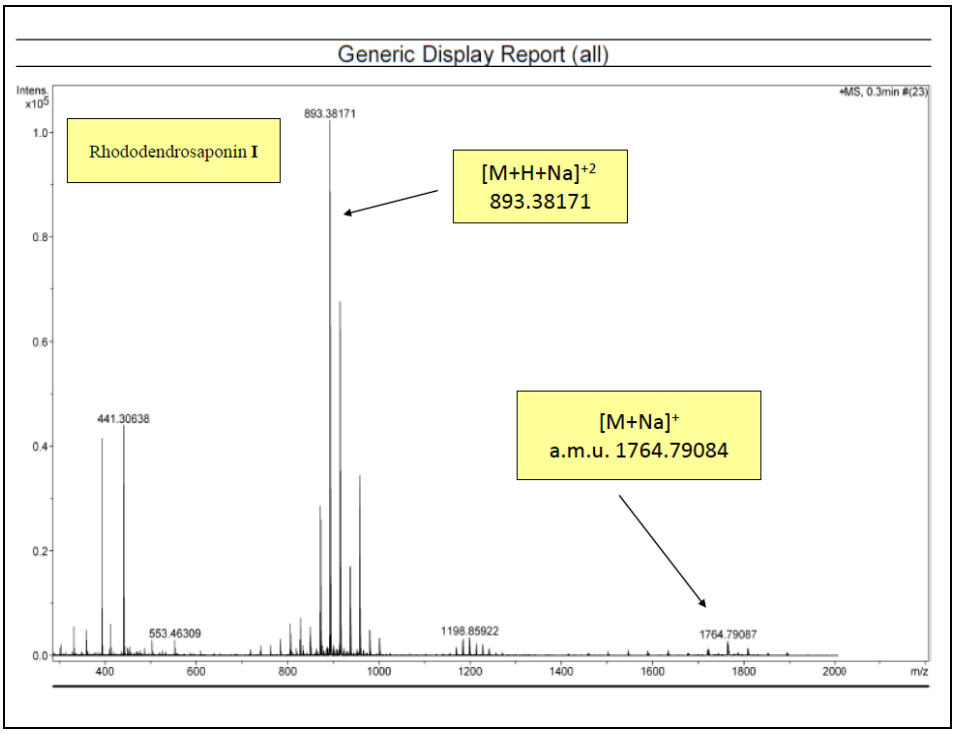

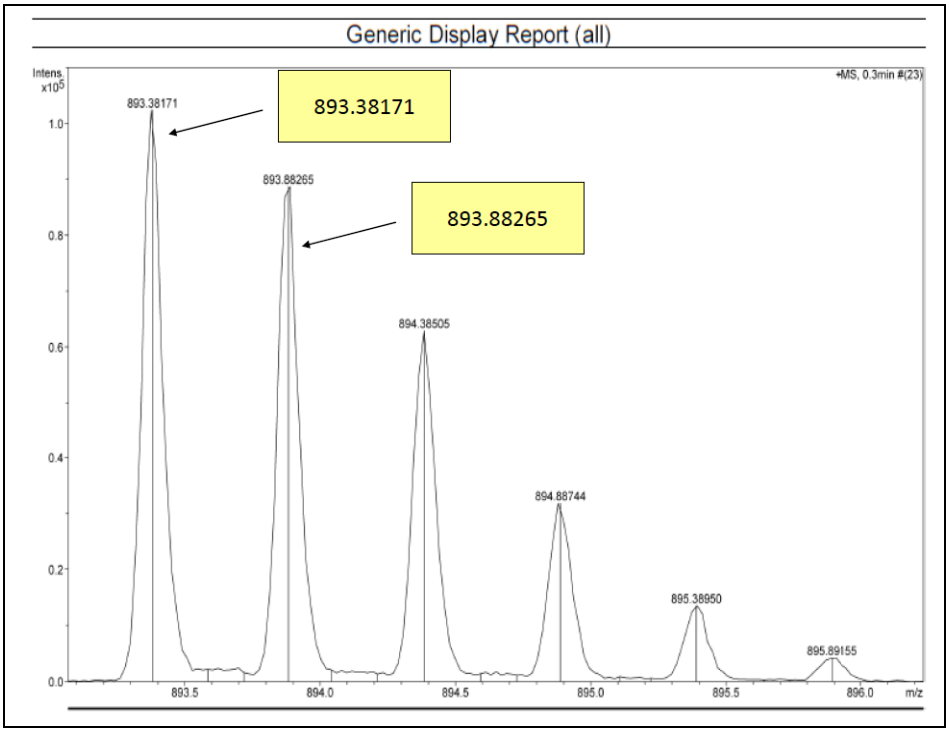

Figure 152. (+)-HRESIMS spectrum of rhododendrosaponin **I**

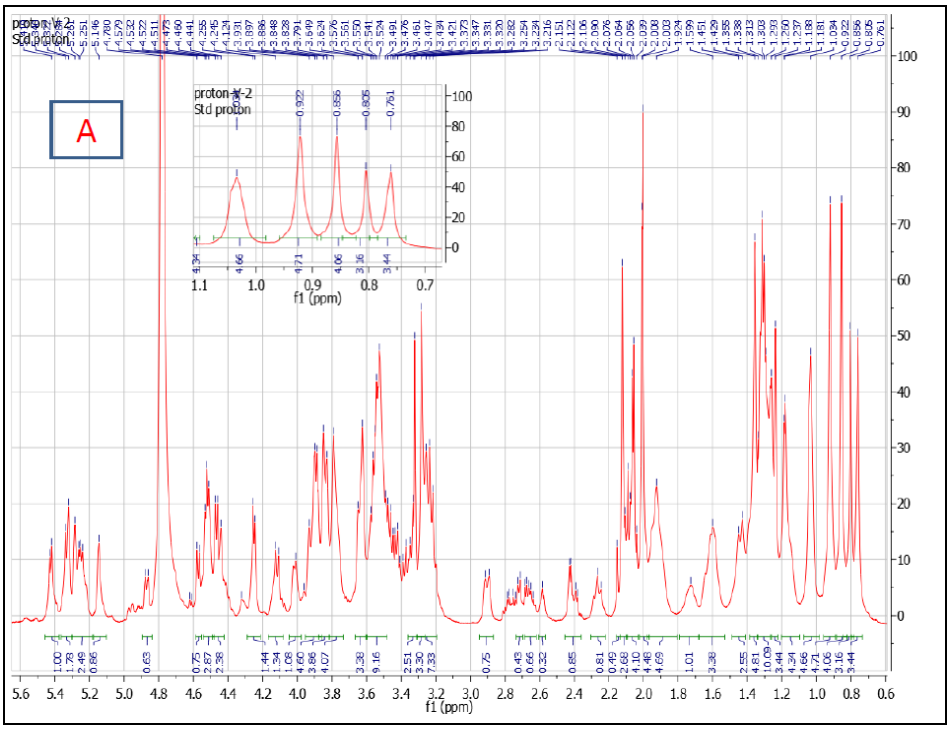

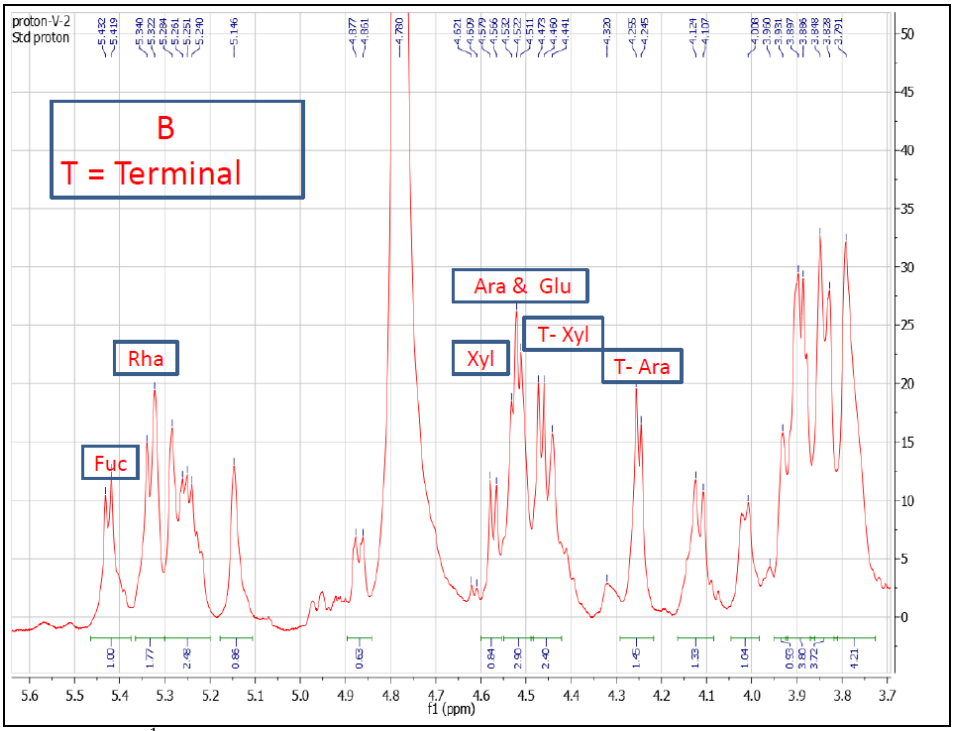

Figure 153. [1]H NMR spectrum of rhododendrosaponin **I** in methanol-d_4 (600 MHz); A) the full spectrum, B) the downfield region

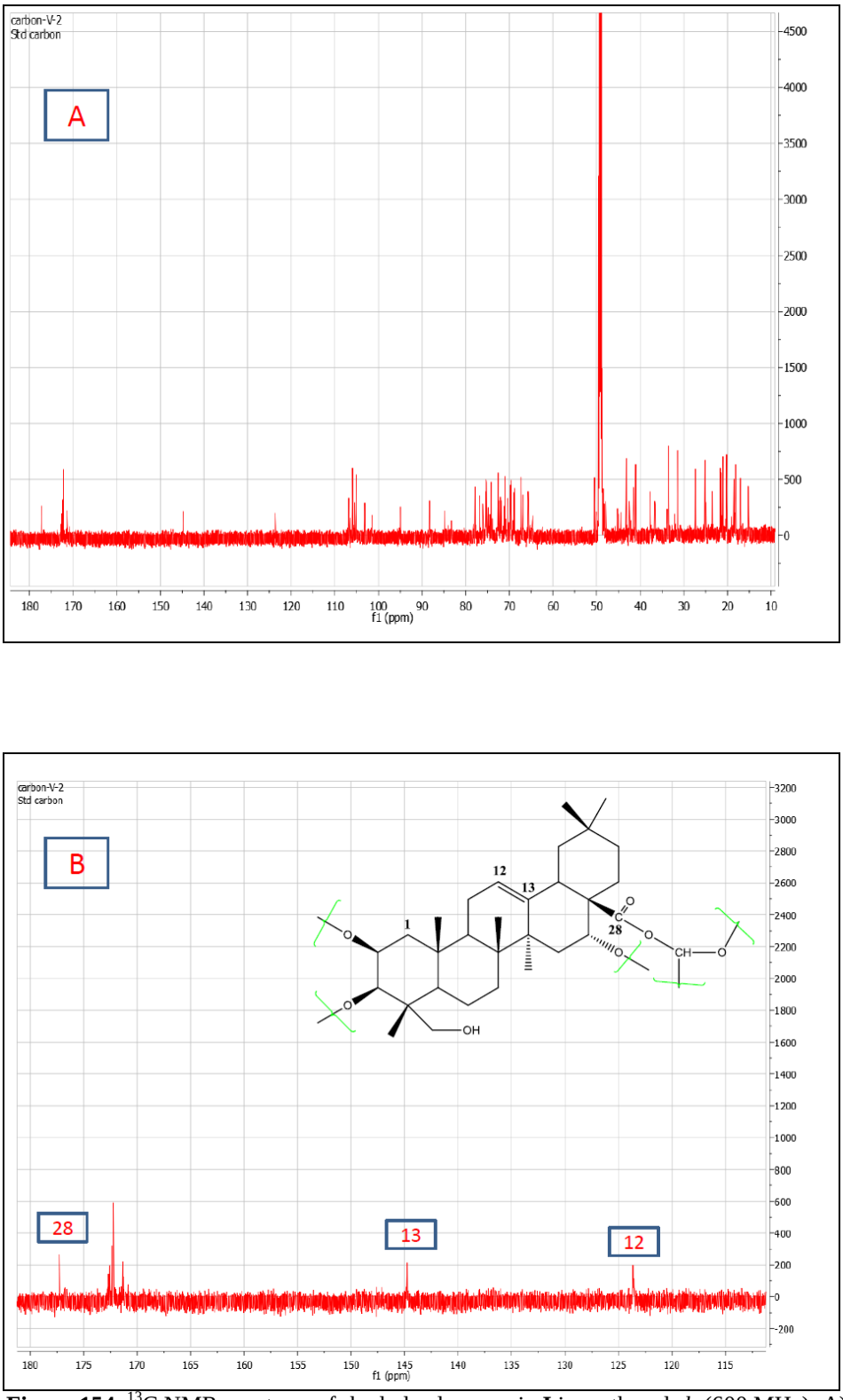

Figure 154. ^{13}C NMR spectrum of rhododendrosaponin **I** in methanol-d_4 (600 MHz); A) the full spectrum, B) the downfield region

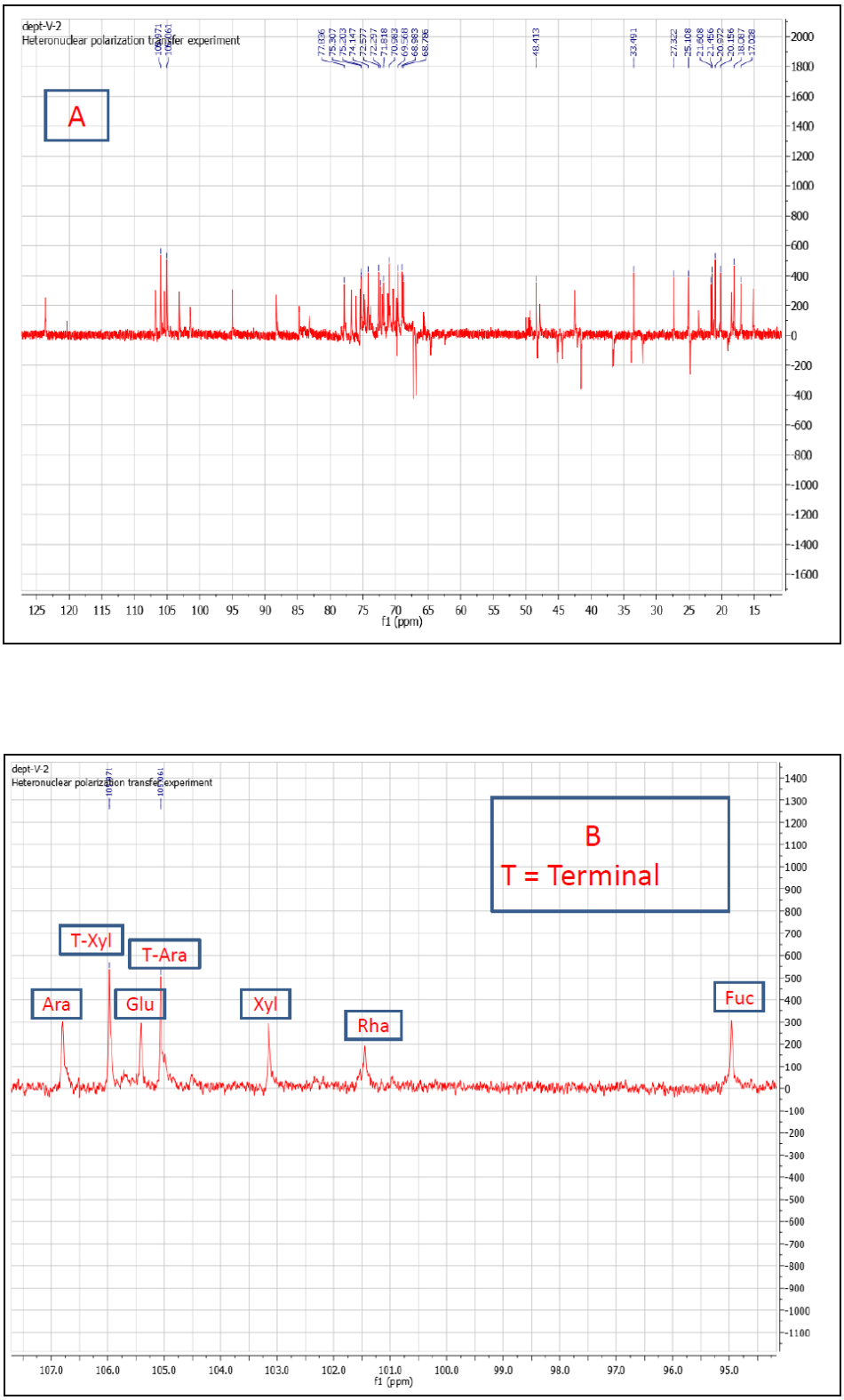

Figure 155. 135º DEPT spectrum of rhododendrosaponin **I** in methanol-d_4 (600 MHz); A) the full spectrum, B) the downfield region

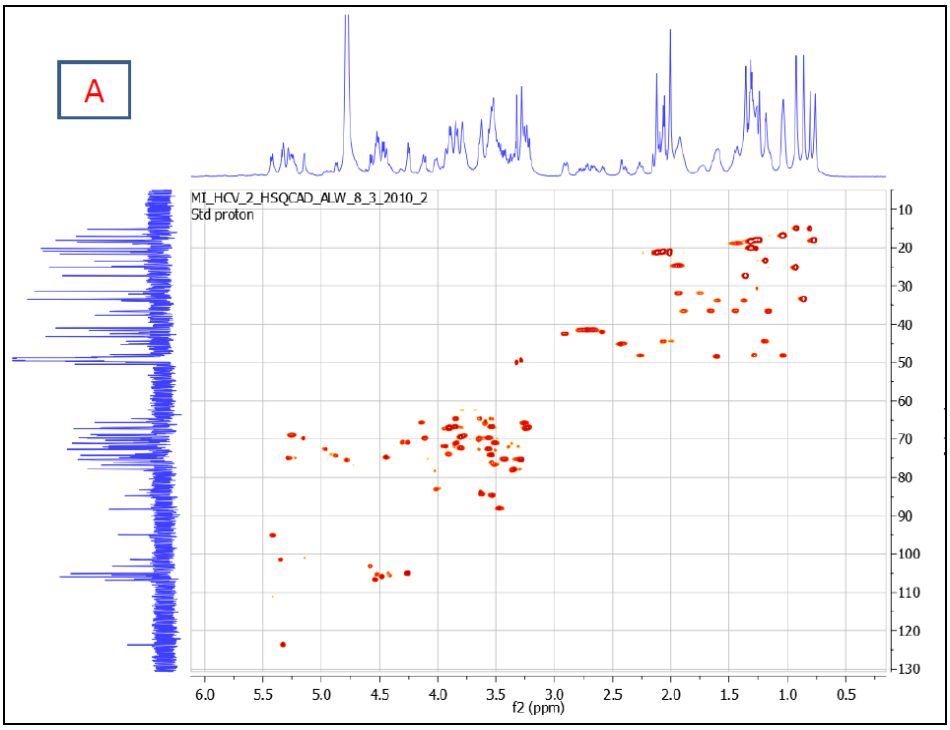

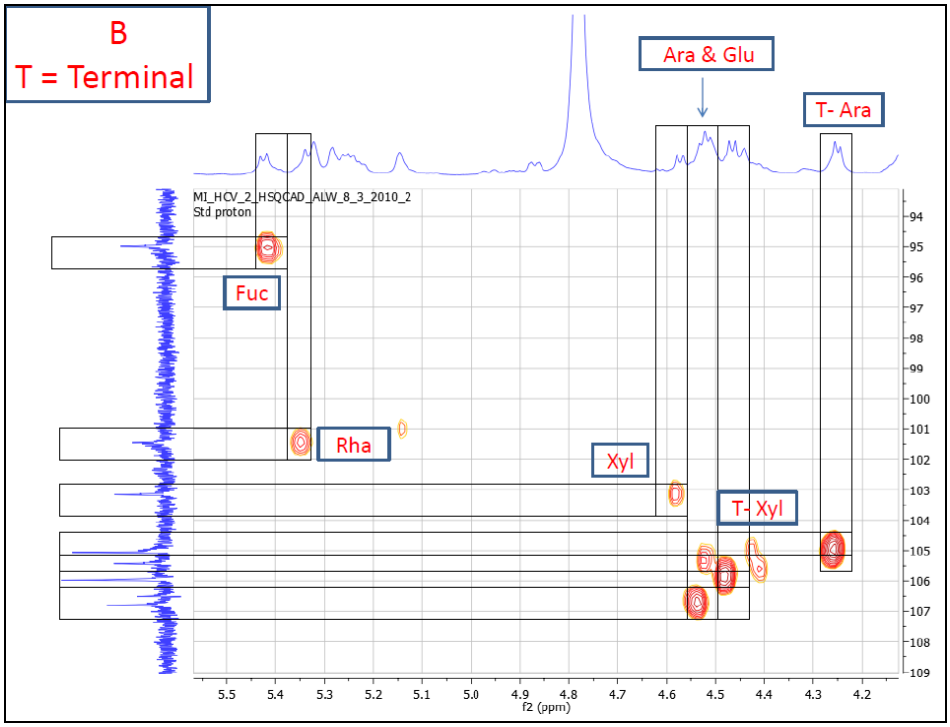

Figure 156. HSQC spectrum of rhododendrosaponin **I** in methanol-d_4 (600 MHz); A) the full spectrum, B) the downfield region

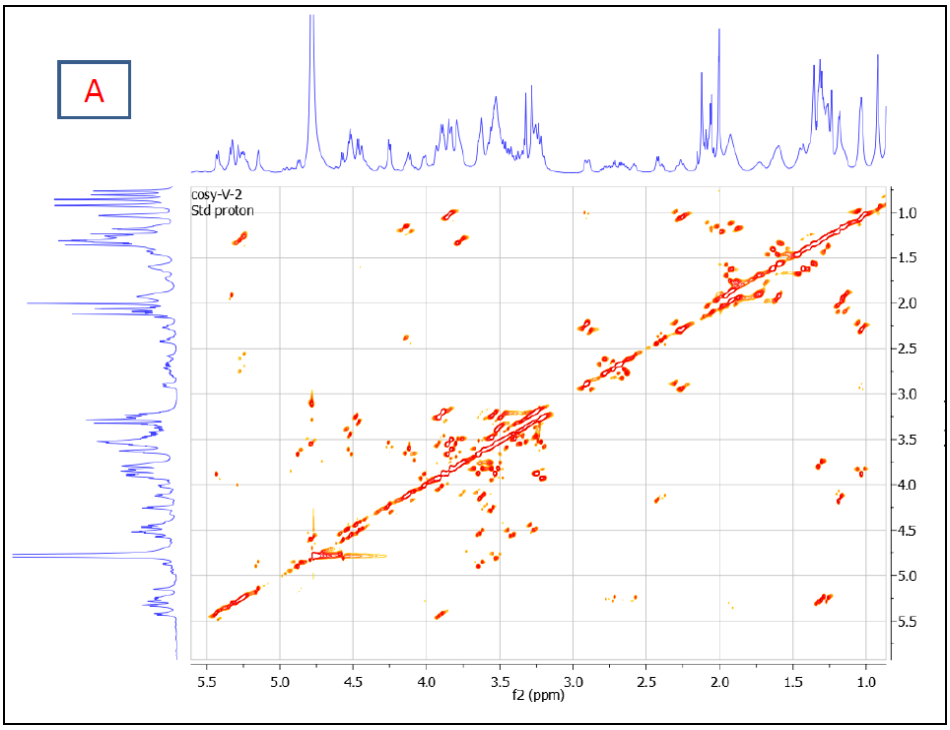

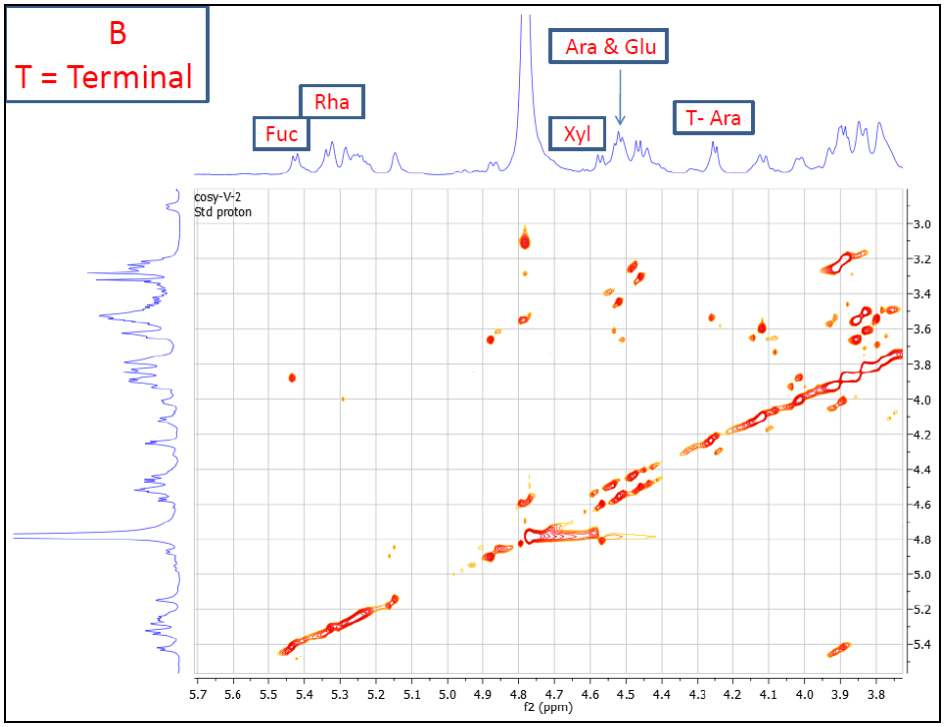

Figure 157. COSY spectrum of rhododendrosaponin **I** in methanol-d_4 (600 MHz); A) the full spectrum, B) the downfield region

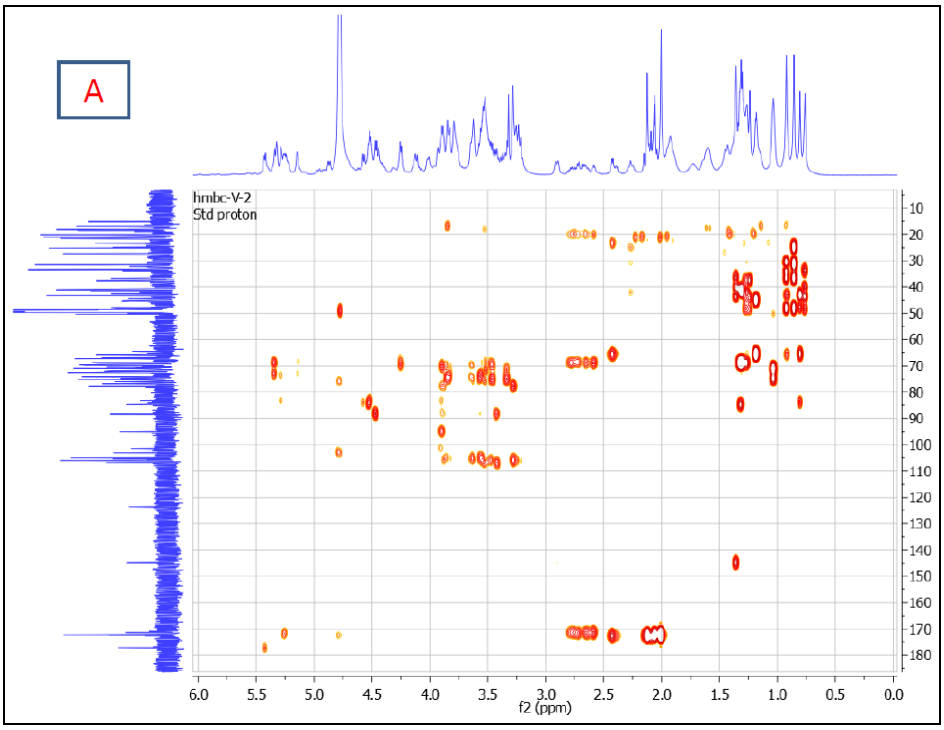

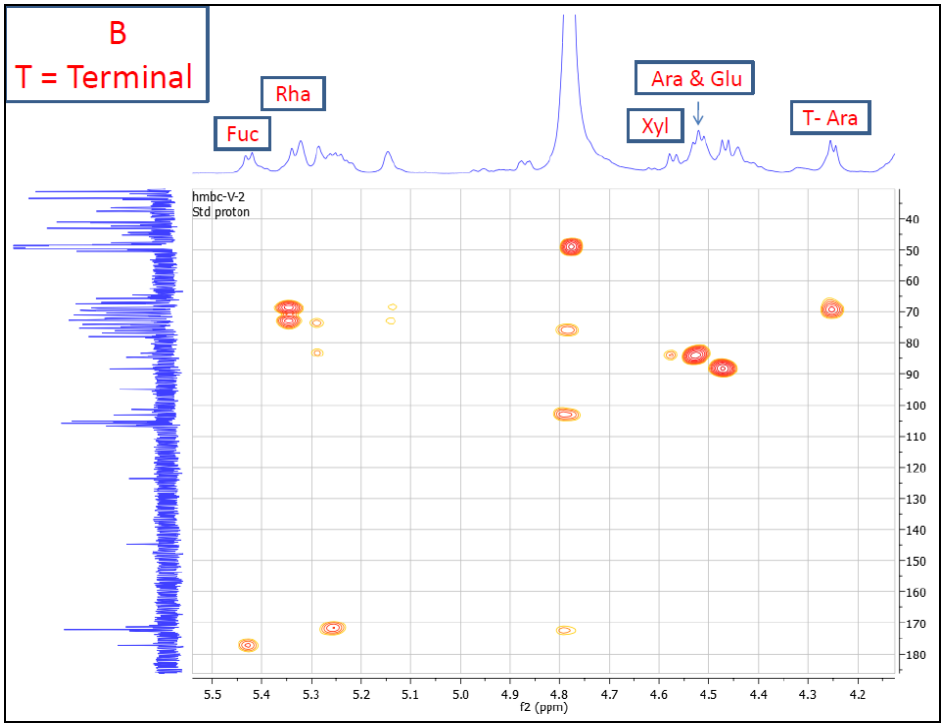

Figure 158. HMBC spectrum of rhododendrosaponin **I** in methanol-d_4 (600 MHz); A) the full spectrum, B) the downfield region

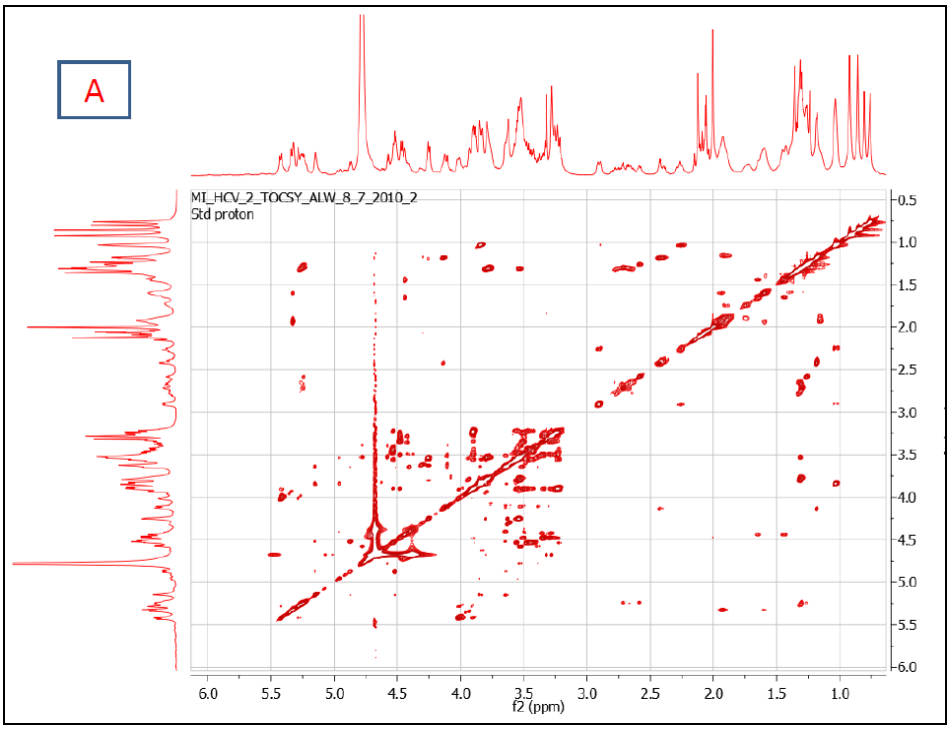

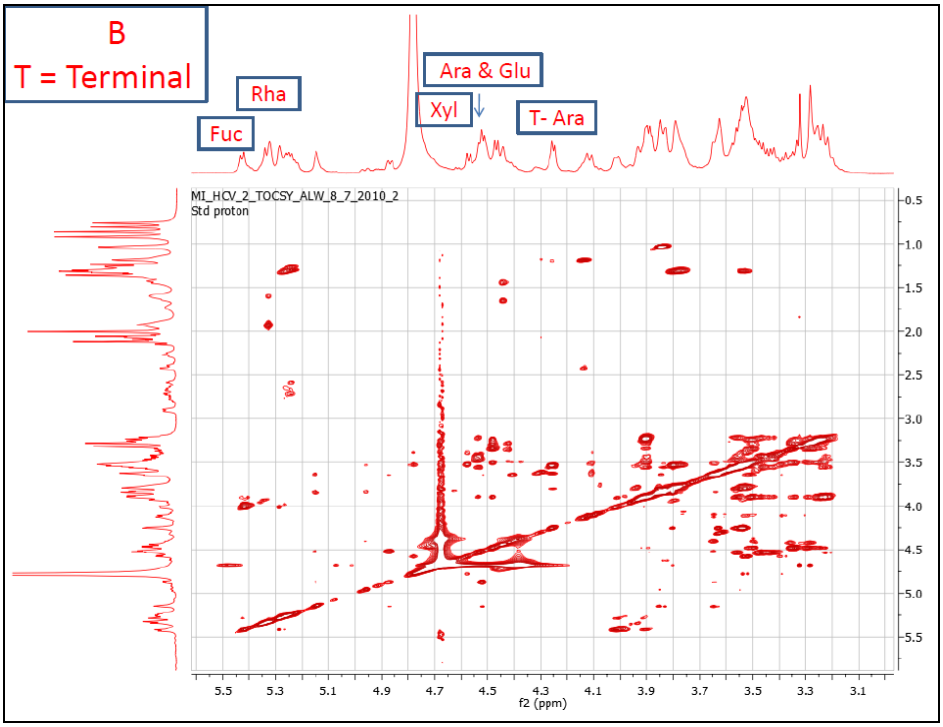

Figure 159. TOCSY spectrum of rhododendrosaponin **I** in methanol-d_4 (600 MHz); A) the full spectrum, B) the downfield region

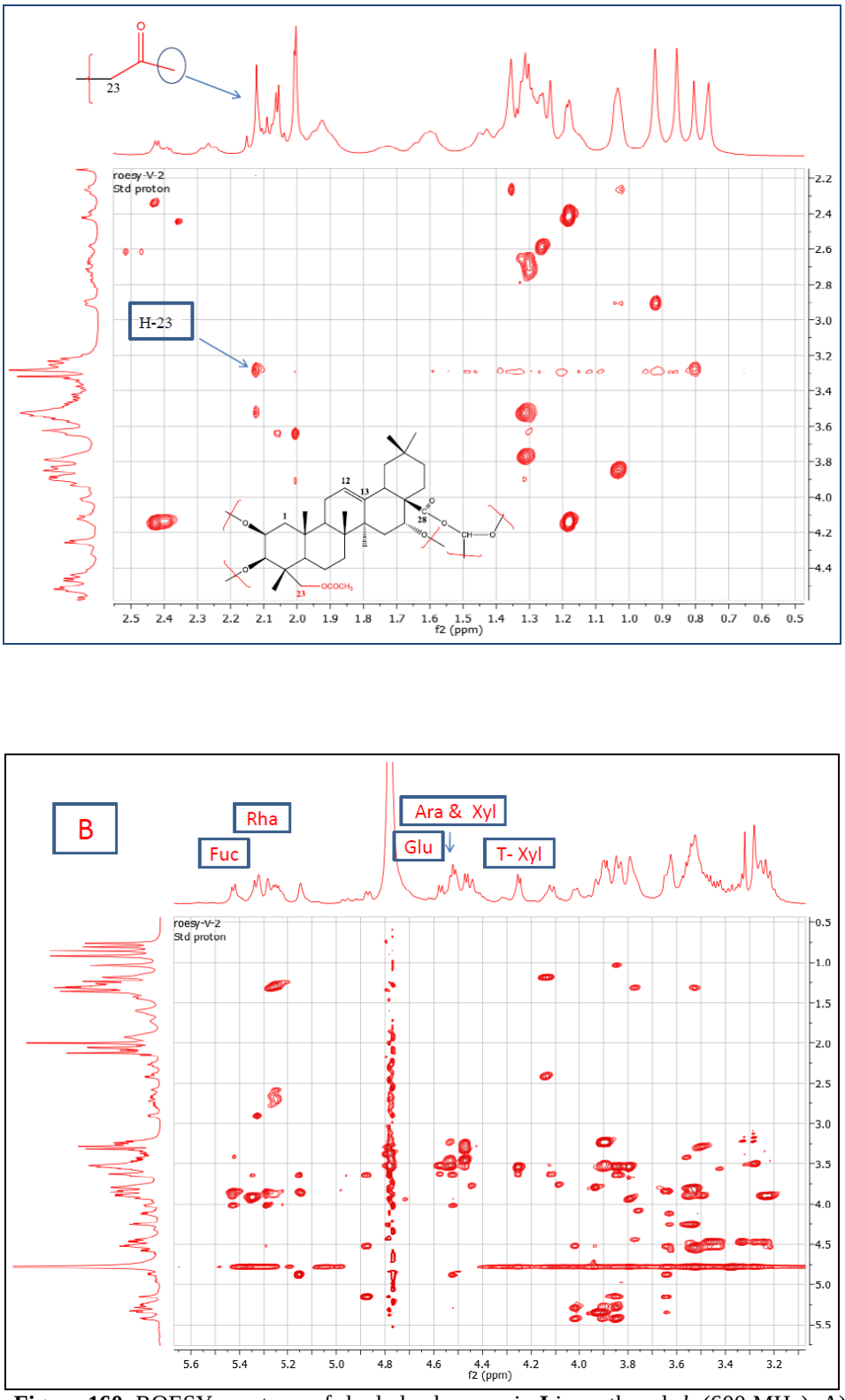

Figure 160. ROESY spectrum of rhododendrosaponin **I** in methanol-d_4 (600 MHz); A) the upfield region, B) the downfield region

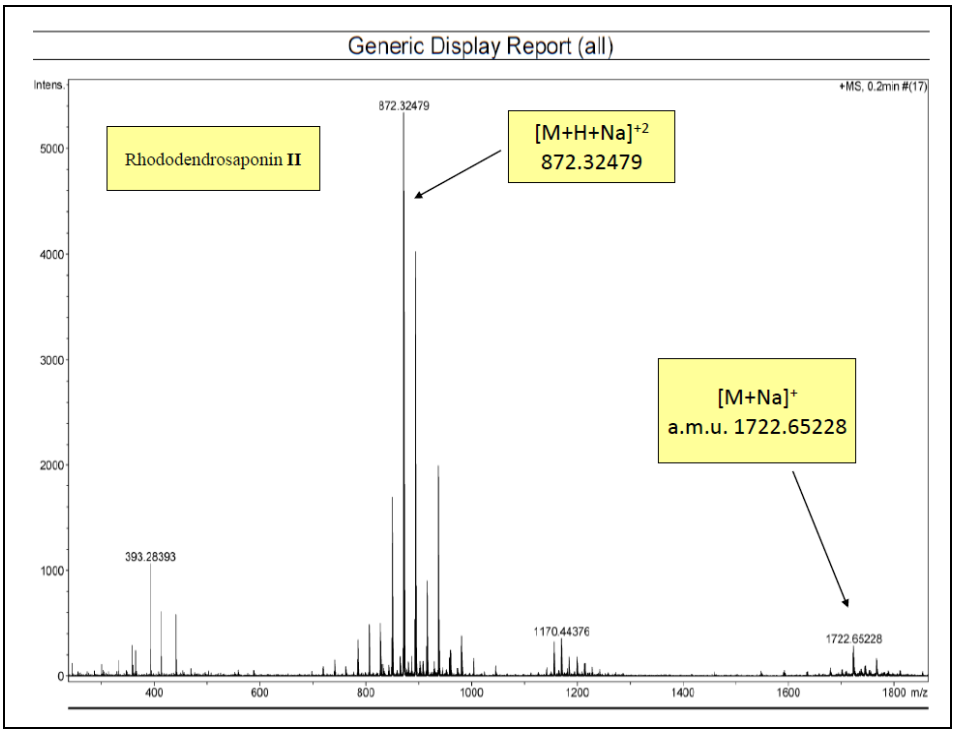

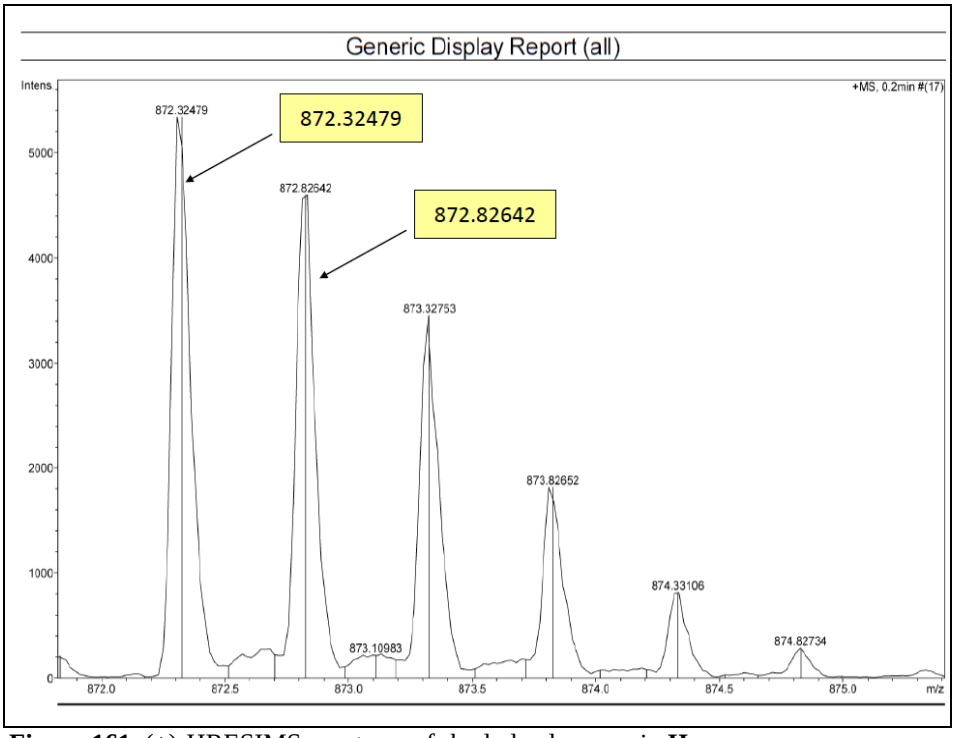

Figure 161. (+)-HRESIMS spectrum of rhododendrosaponin **II**

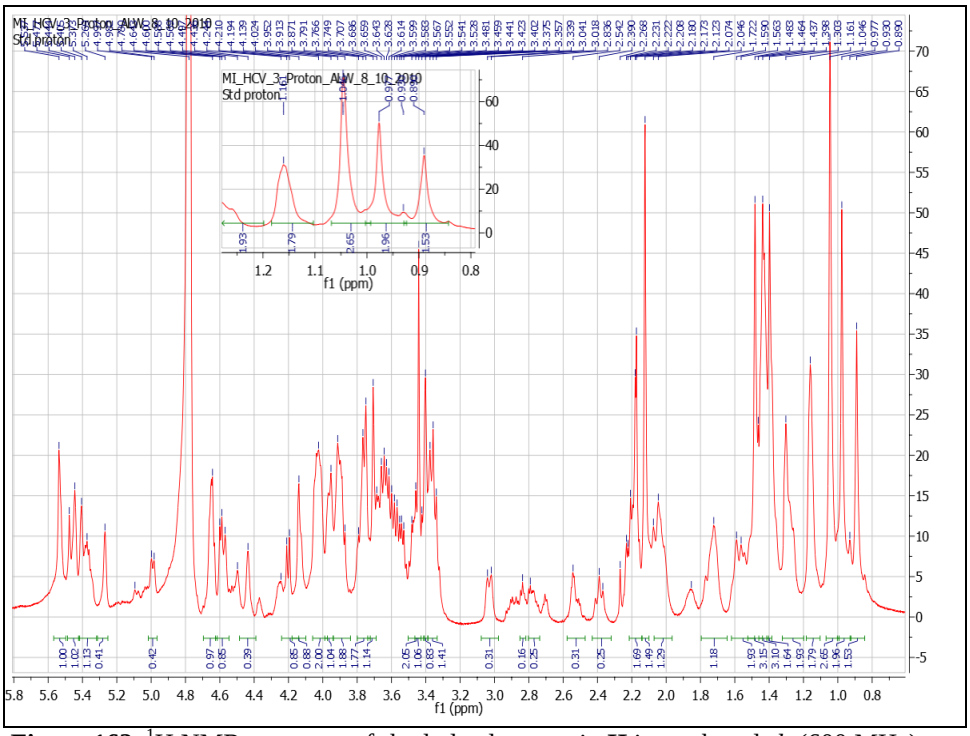

Figure 162. ^{1}H NMR spectrum of rhododendrosaponin **II** in methanol-d_4 (600 MHz)

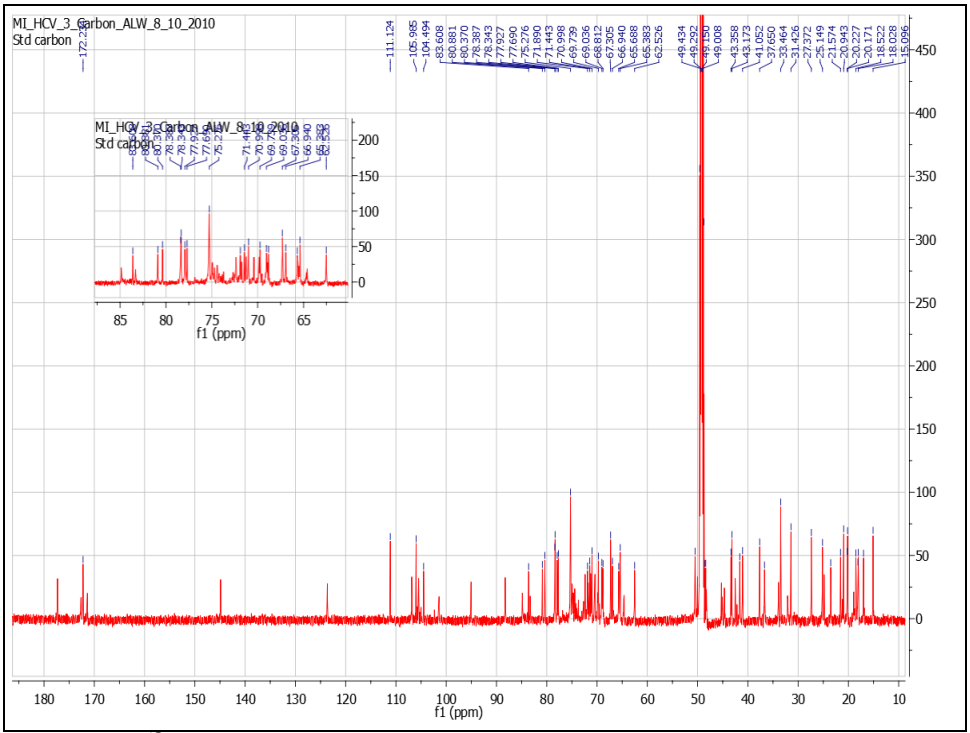

Figure 163. ^{13}C NMR spectrum of rhododendrosaponin **II** in methanol-d_4 (600 MHz)

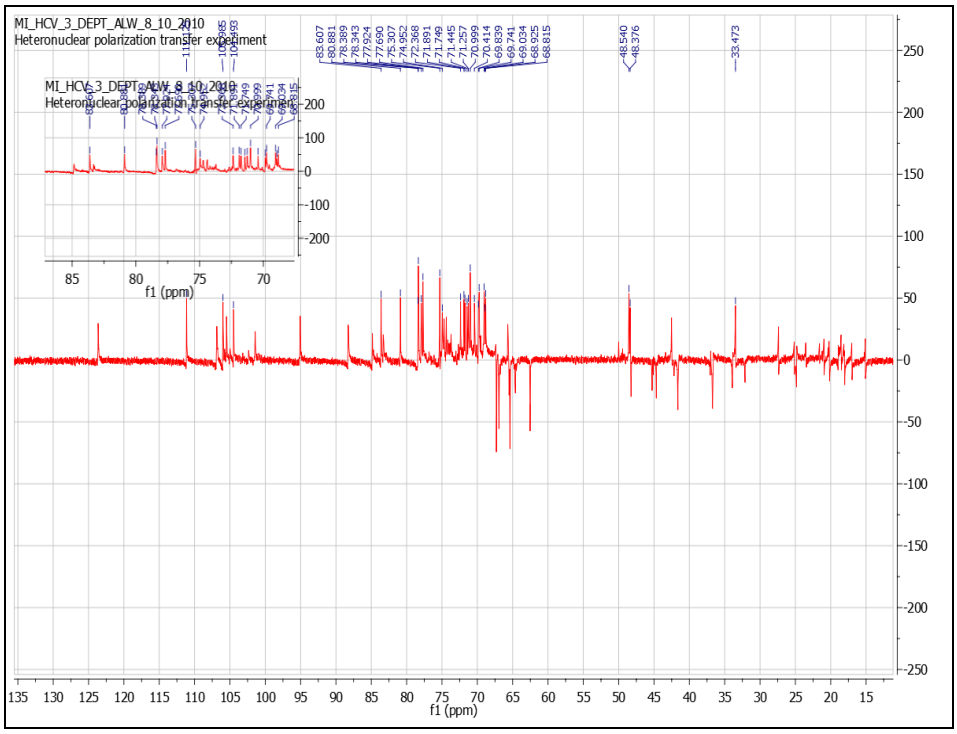

Figure 164. 135º DEPT spectrum of rhododendrosaponin **II** in methanol-d_4 (600 MHz)

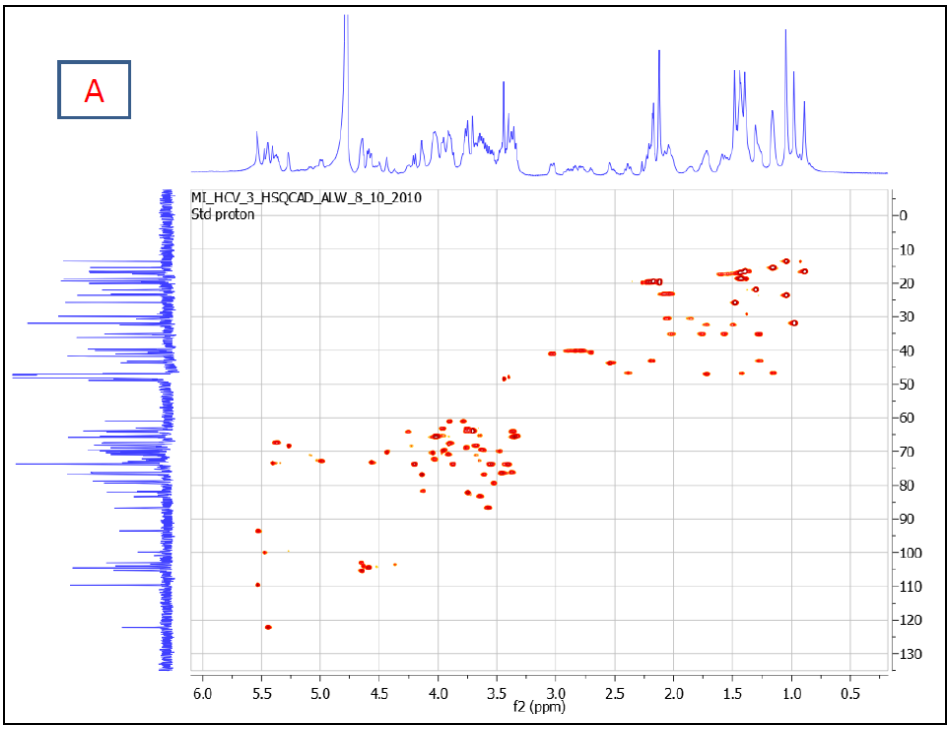

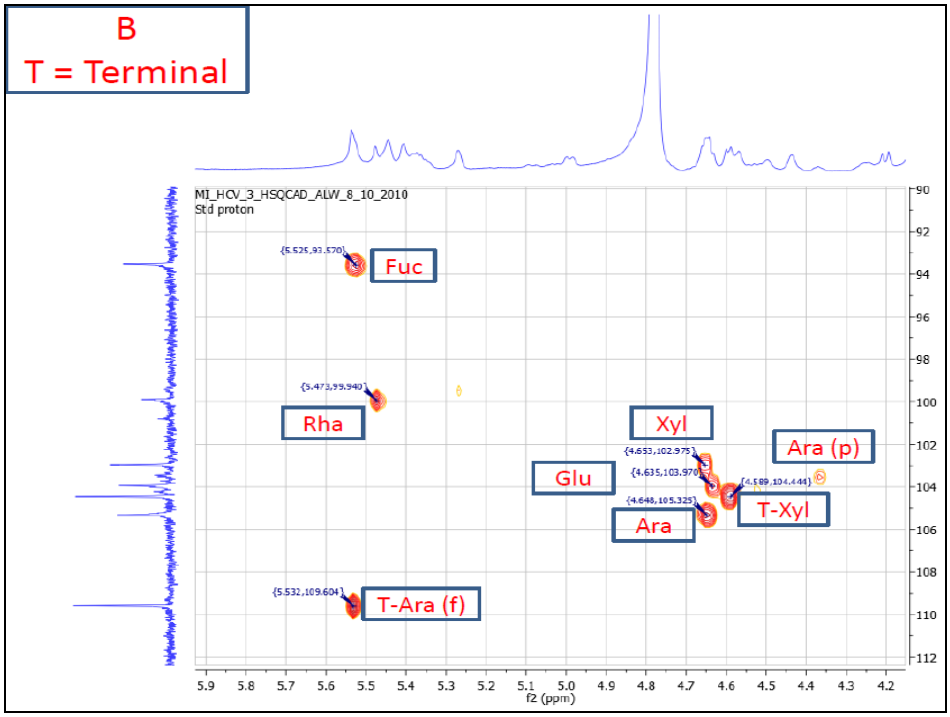

Figure 165. HSQC spectrum of rhododendrosaponin **II** in methanol-d_4 (600 MHz); A) the full spectrum, B) the downfield region

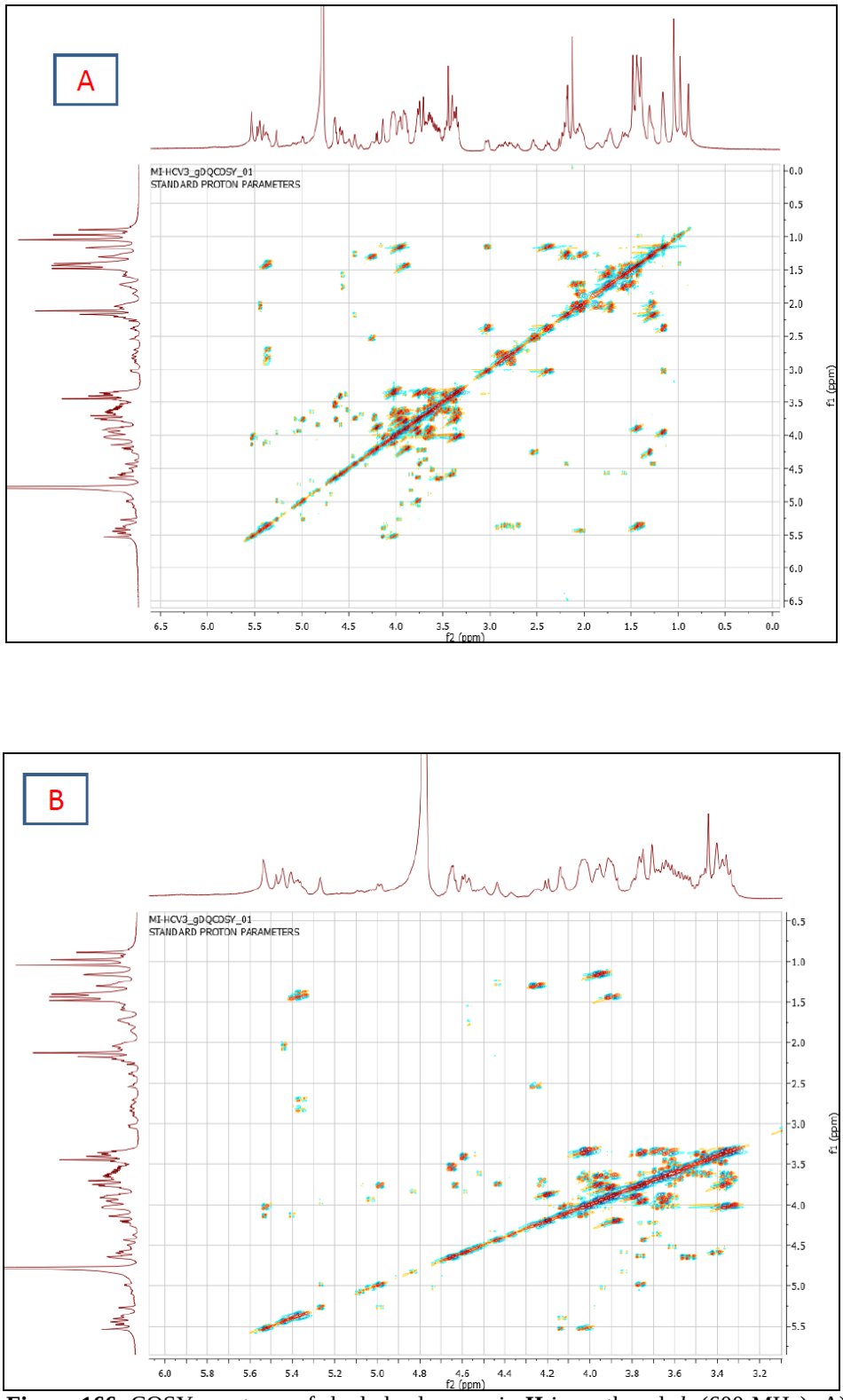

Figure 166. COSY spectrum of rhododendrosaponin **II** in methanol-d_4 (600 MHz); A) the full spectrum, B) the downfield region

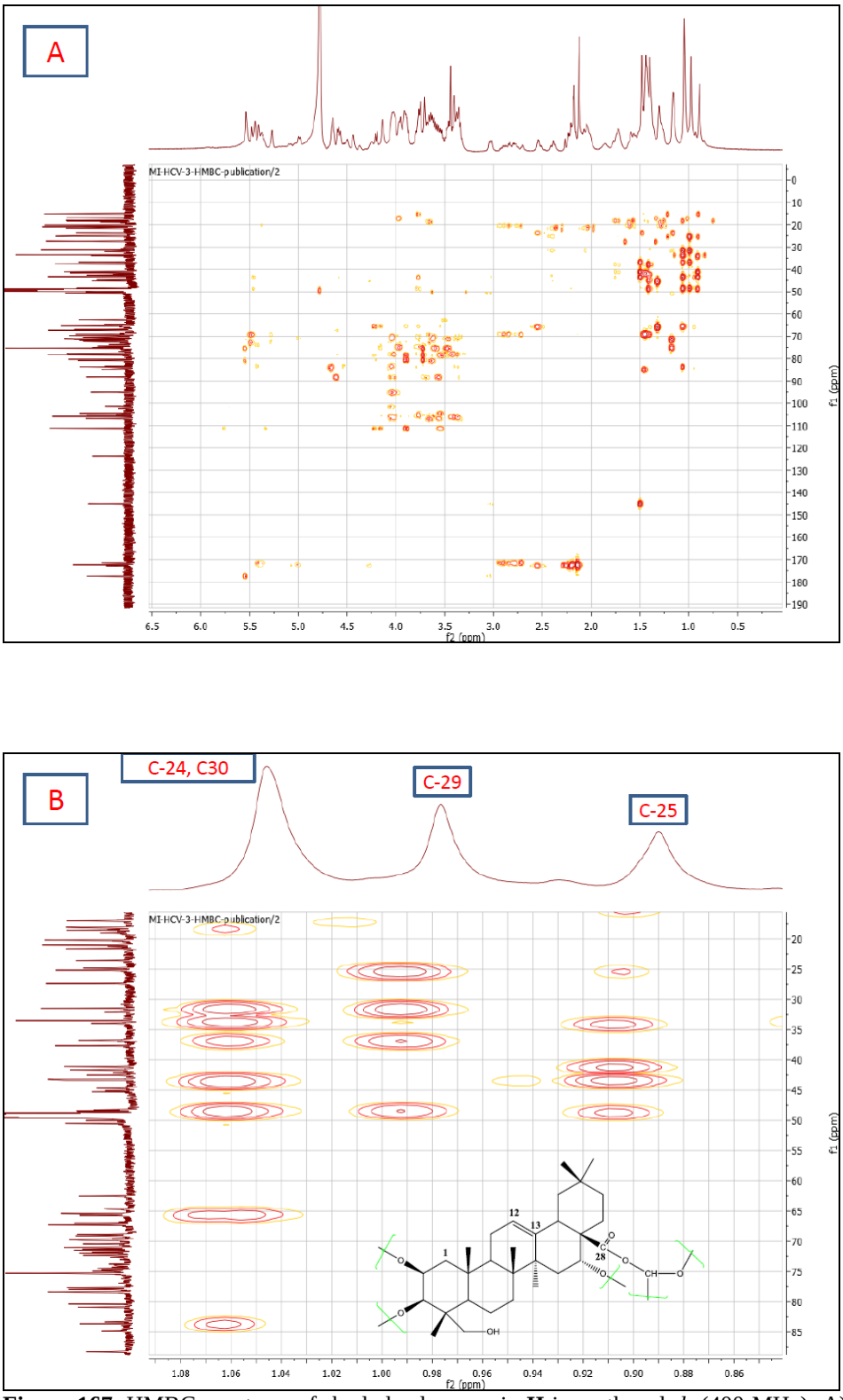

Figure 167. HMBC spectrum of rhododendrosaponin **II** in methanol-d_4 (400 MHz); A) the full spectrum, B) the upfield region

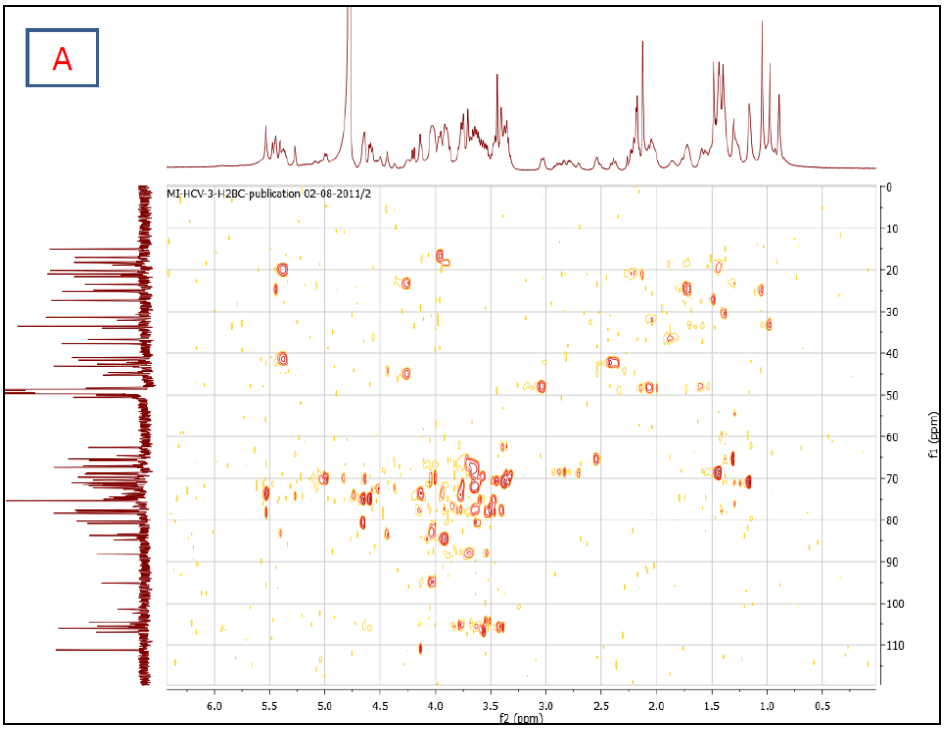

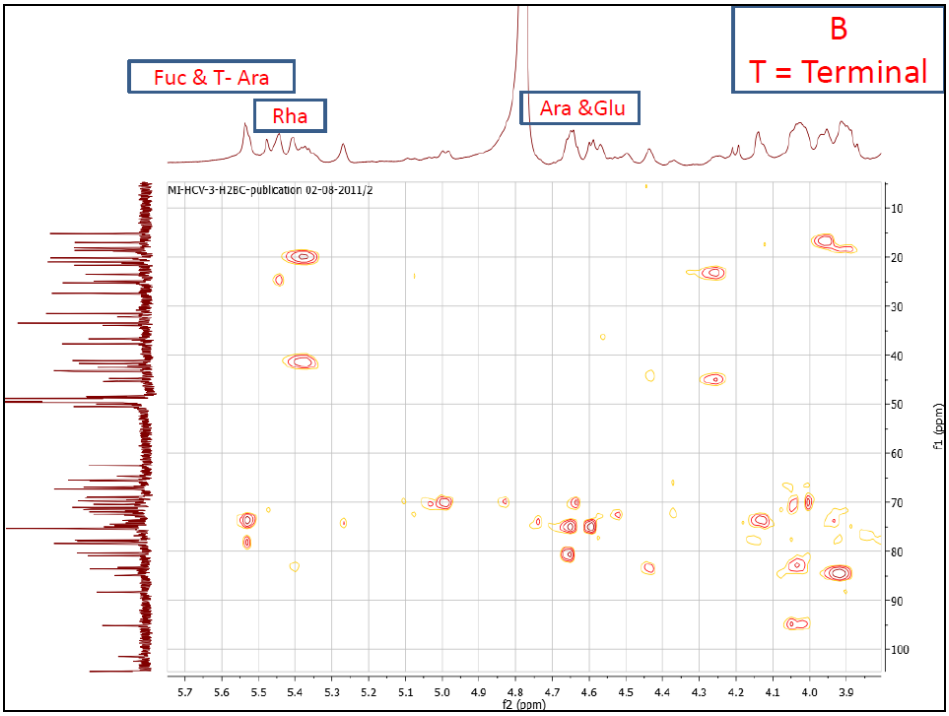

Figure 168. H2BC spectrum of rhododendrosaponin **II** in methanol-d_4 (400 MHz); A) the full spectrum, B) the downfield region

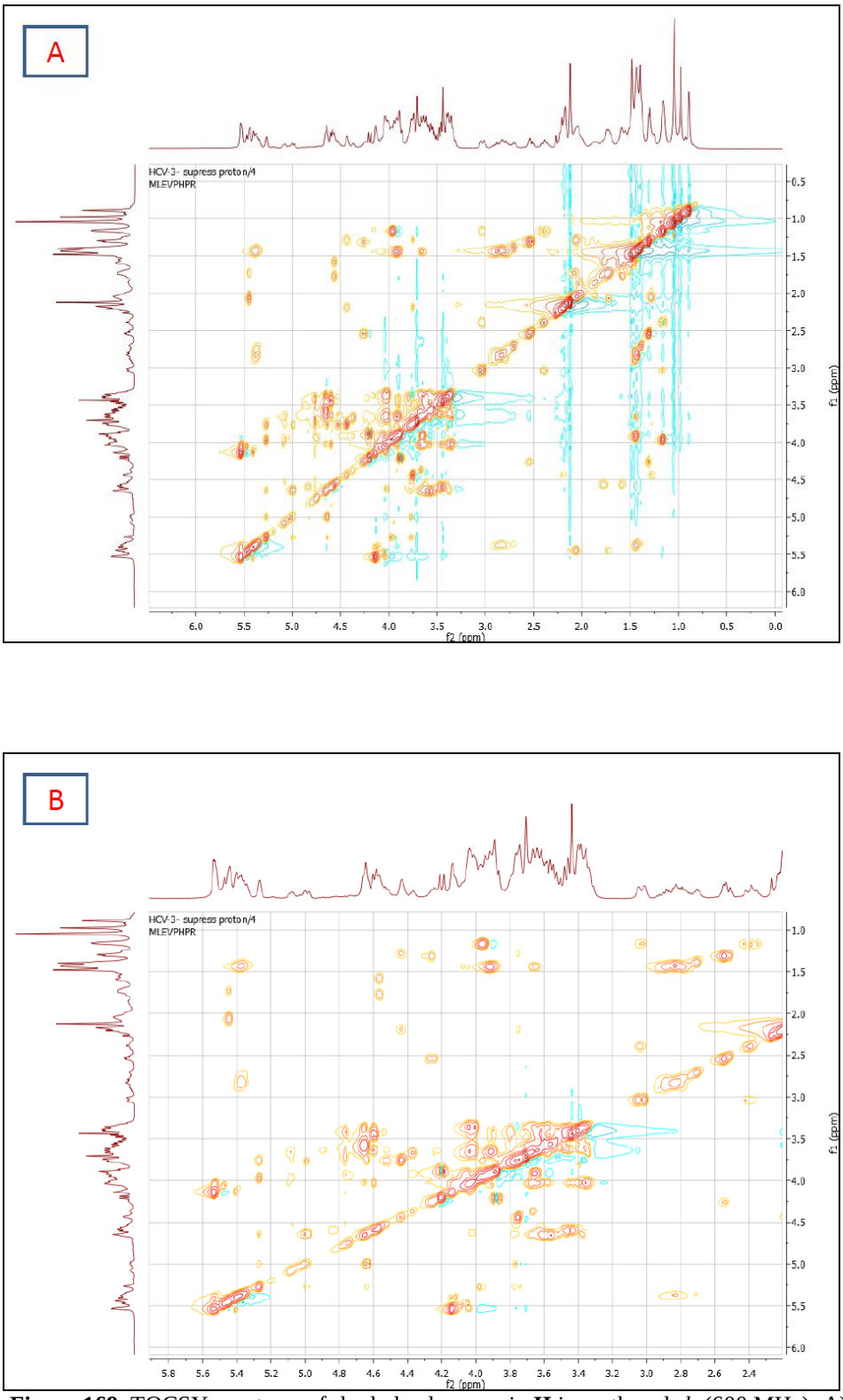

Figure 169. TOCSY spectrum of rhododendrosaponin **II** in methanol-d_4 (600 MHz); A) the full spectrum, B) the downfield region

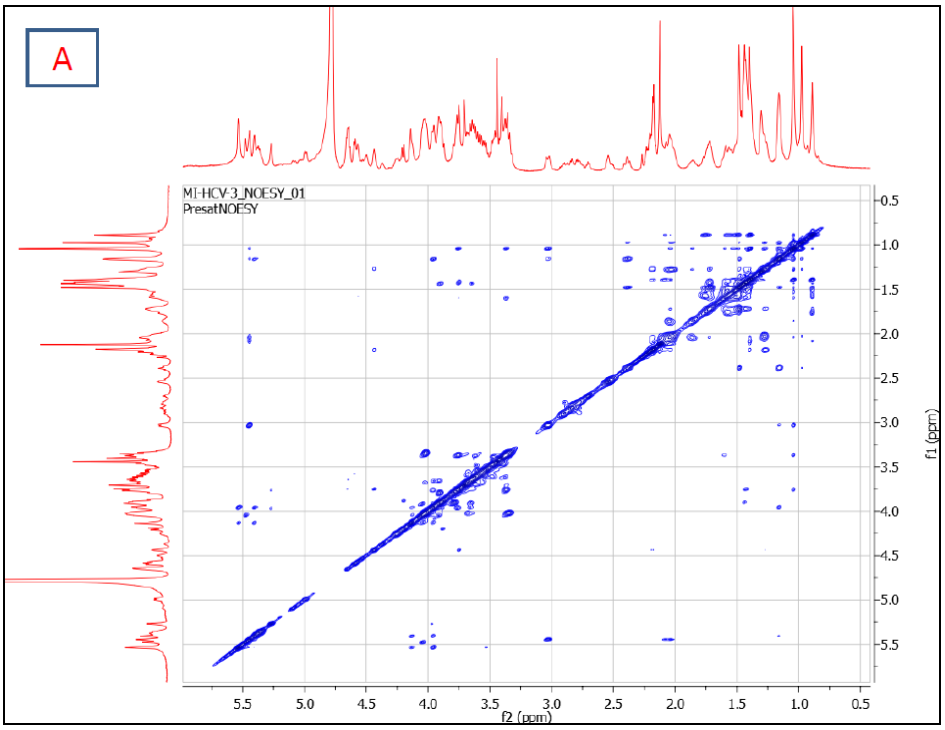

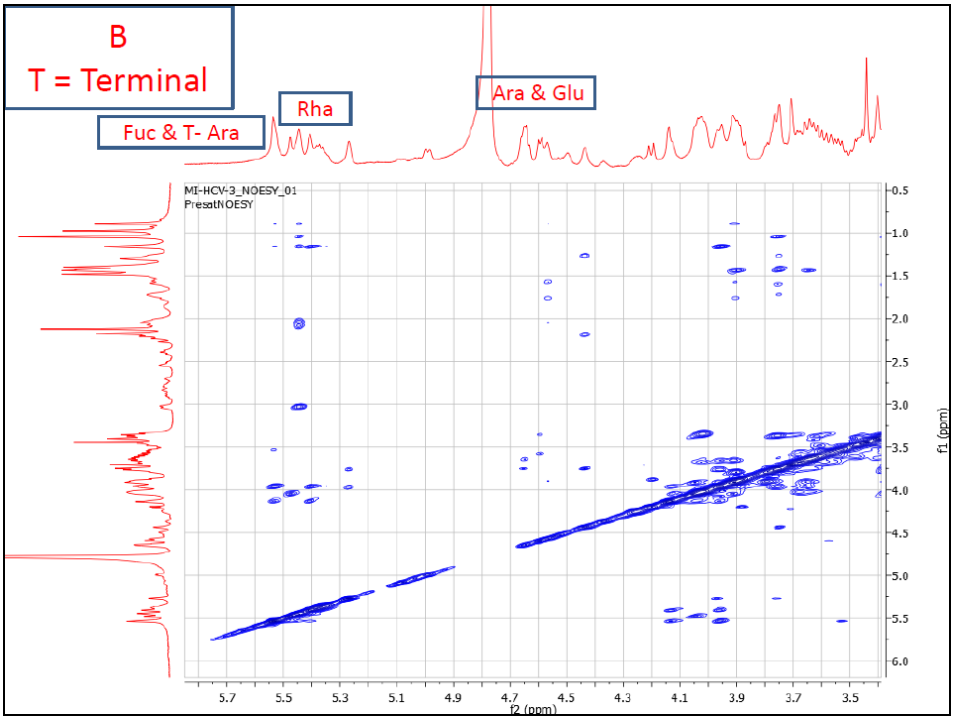

Figure 170. NOESY spectrum of rhododendrosaponin **II** in methanol-d_4 (600 MHz); A) the full spectrum, B) the downfield region

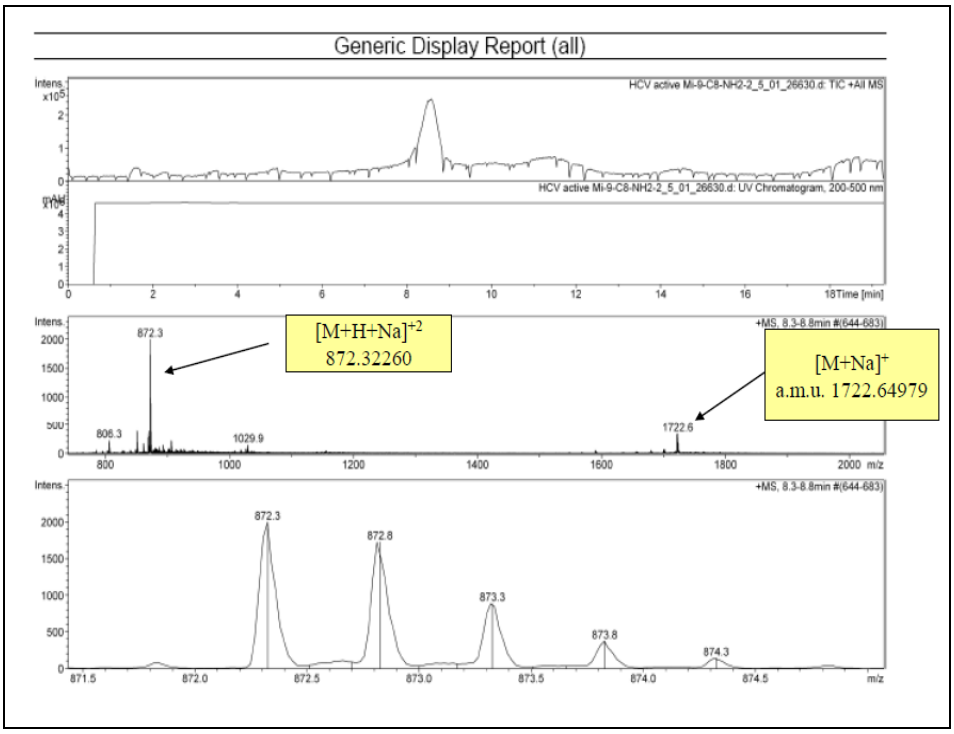

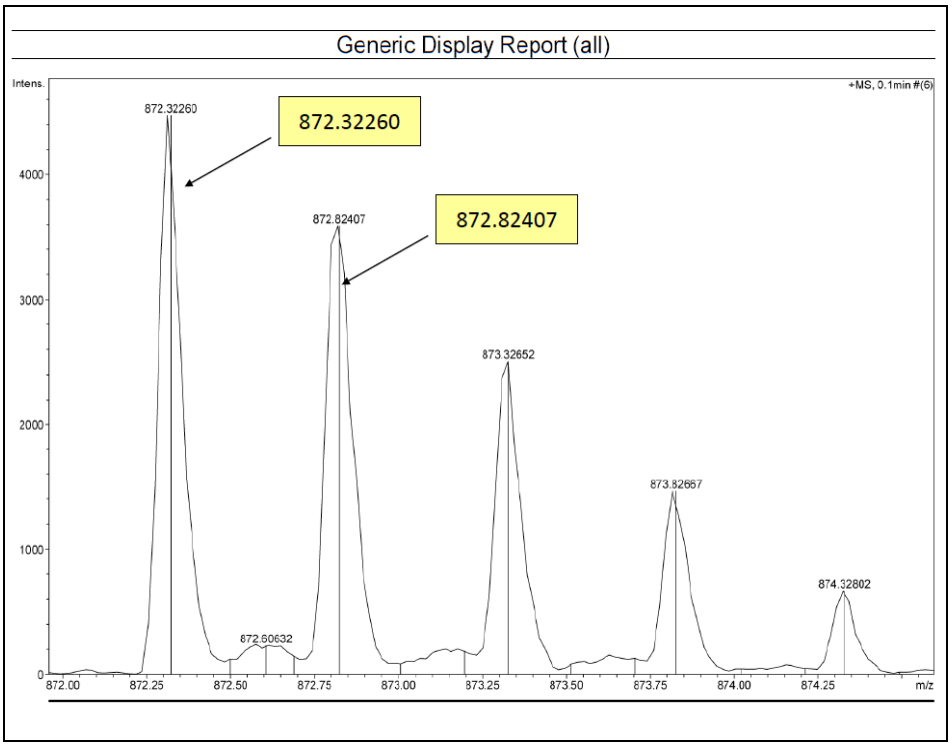

Figure 171. LC/MS chromatogram of rhododendrosaponin **III**

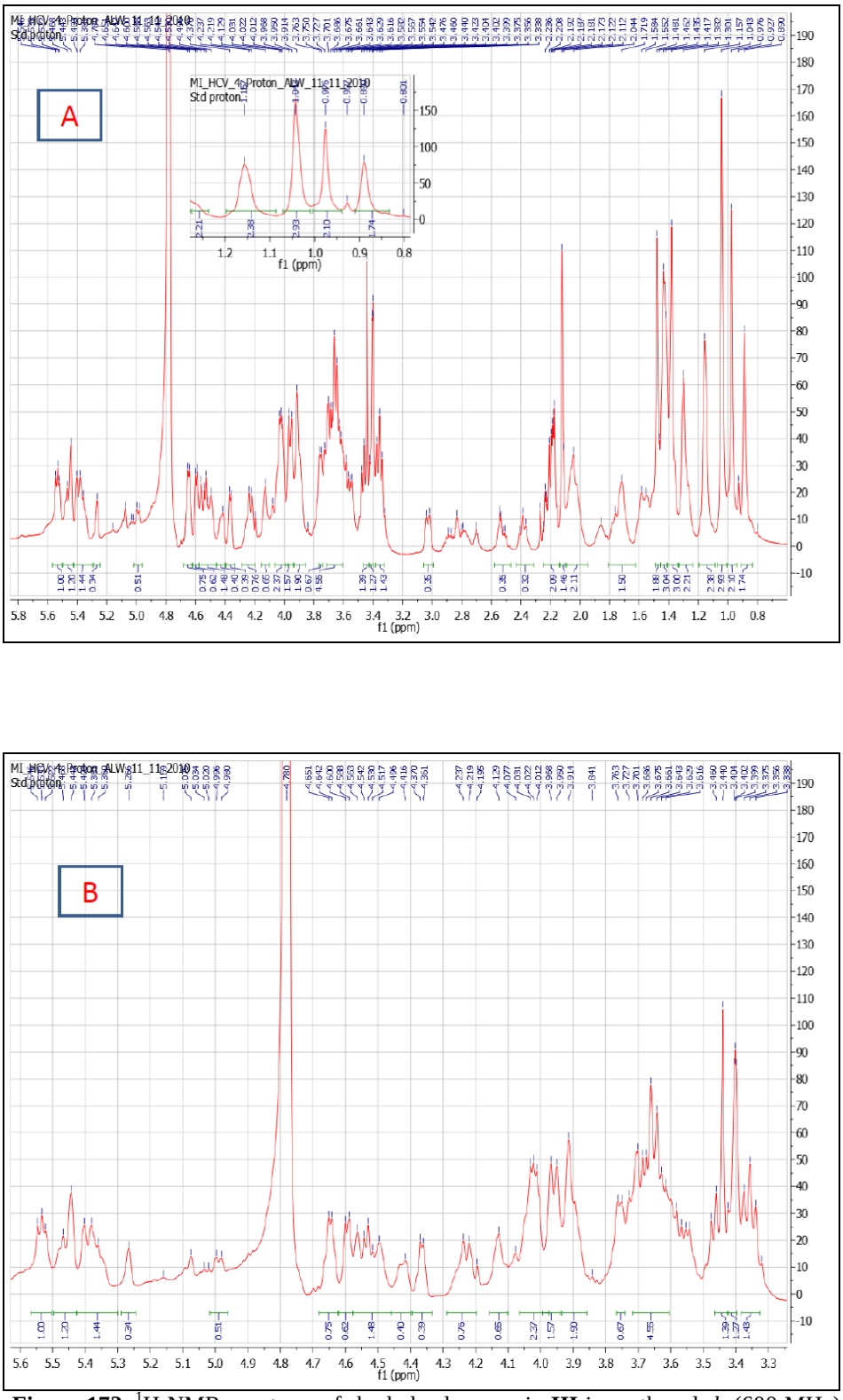

Figure 172. ^{1}H NMR spectrum of rhododendrosaponin **III** in methanol-d_4 (600 MHz); A) the full spectrum, B) the downfield region

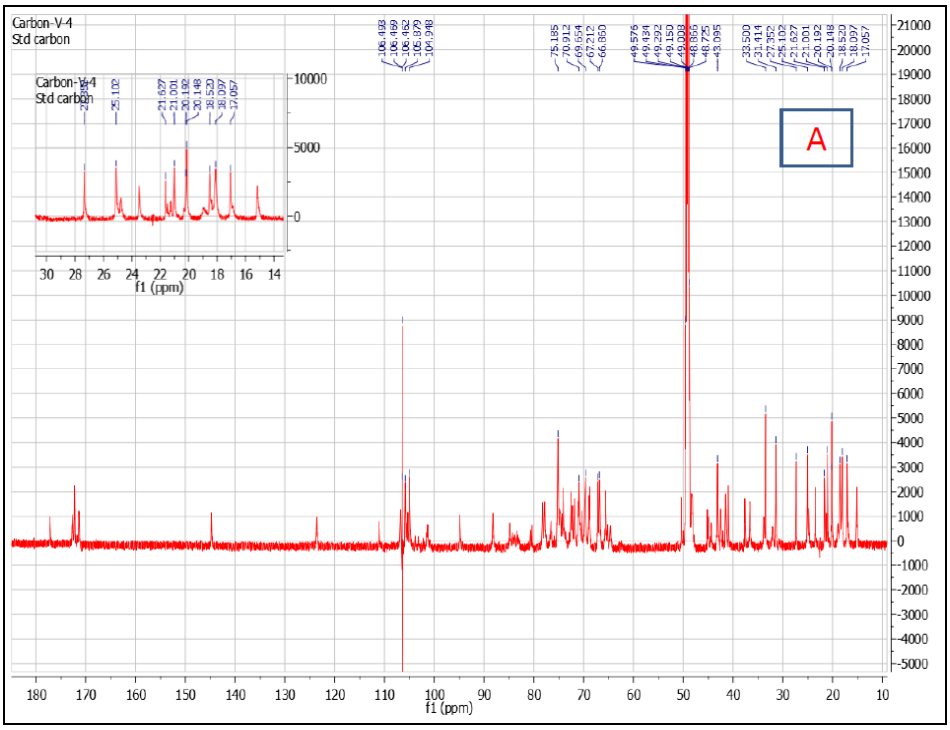

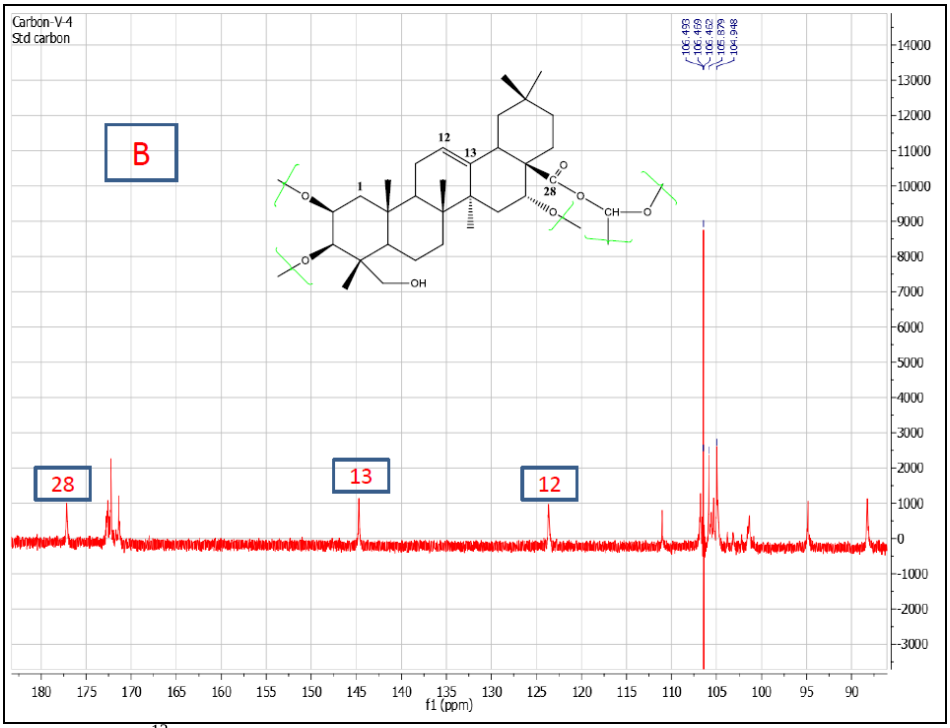

Figure 173. ^{13}C NMR spectrum of rhododendrosaponin **III** in methanol-d_4 (600 MHz); A) the full spectrum, B) the downfield region

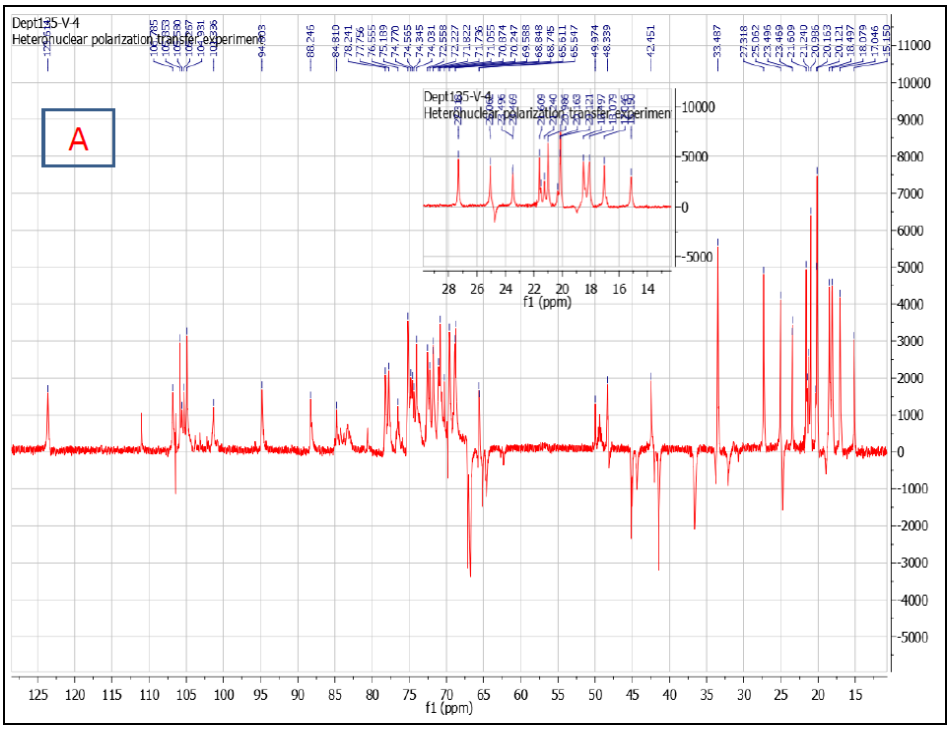

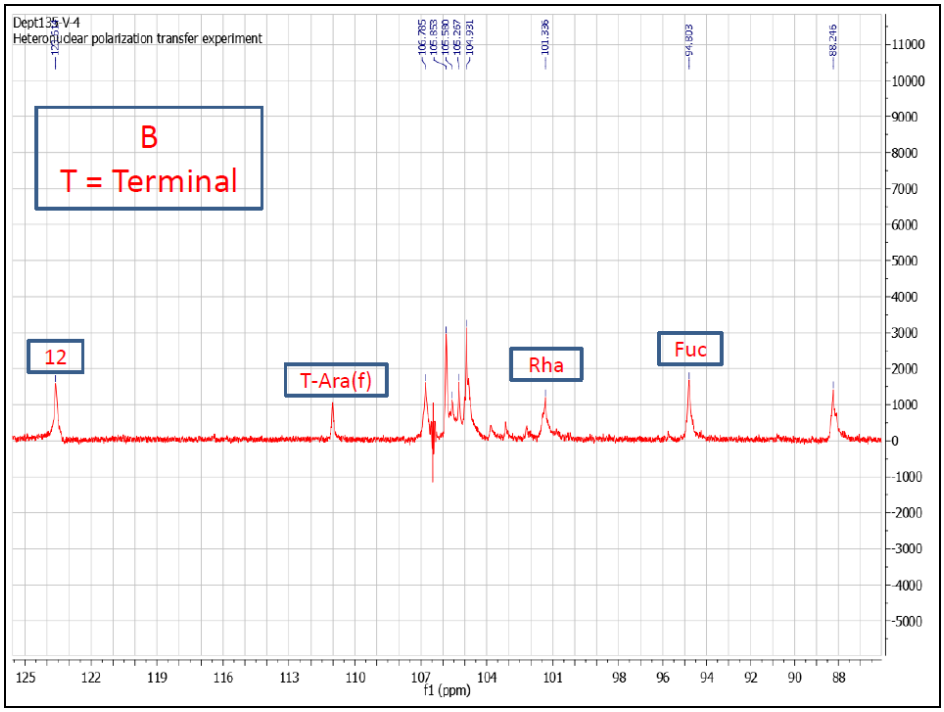

Figure 174. 135º DEPT spectrum of rhododendrosaponin **III** in methanol-d_4 (600 MHz); A) the full spectrum, B) the downfield region

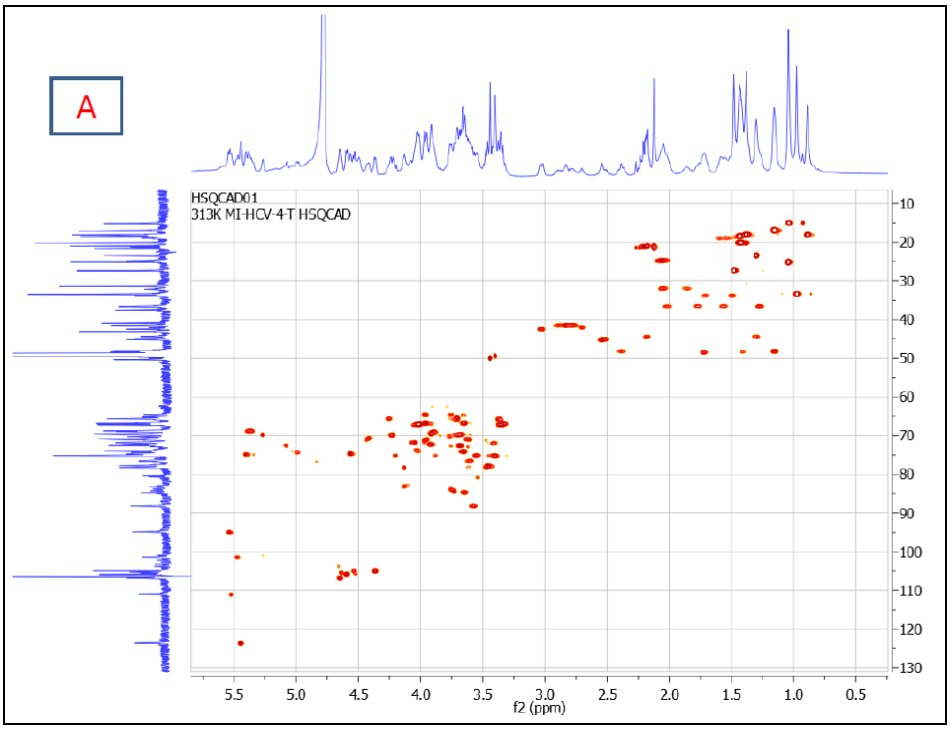

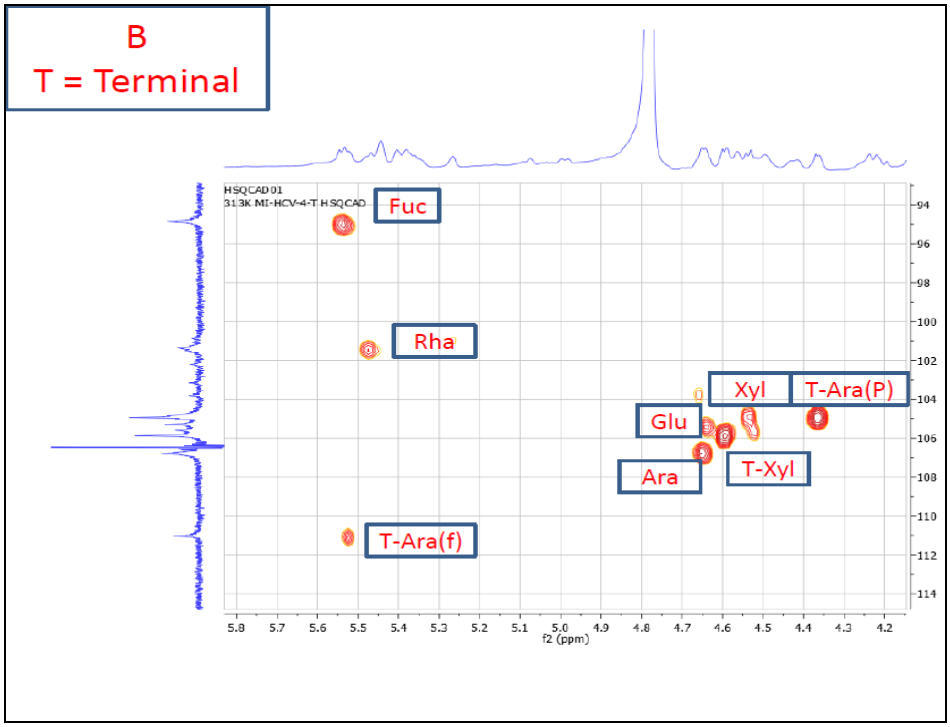

Figure 175. HSQC spectrum of rhododendrosaponin **III** in methanol-d_4 (600 MHz); A) the full spectrum, B) the downfield region

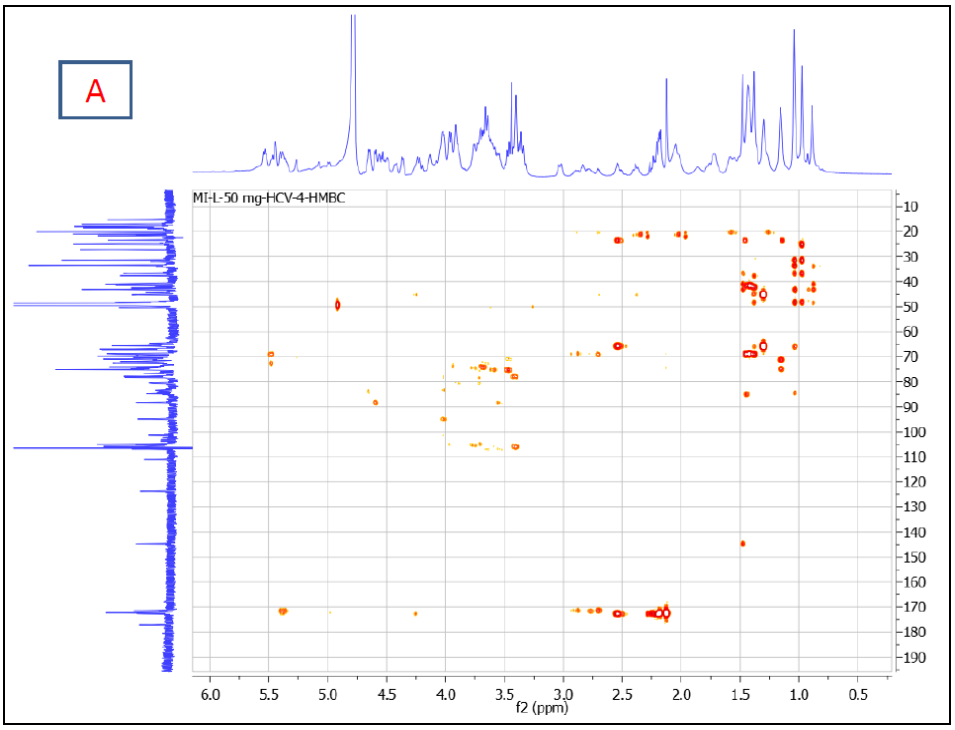

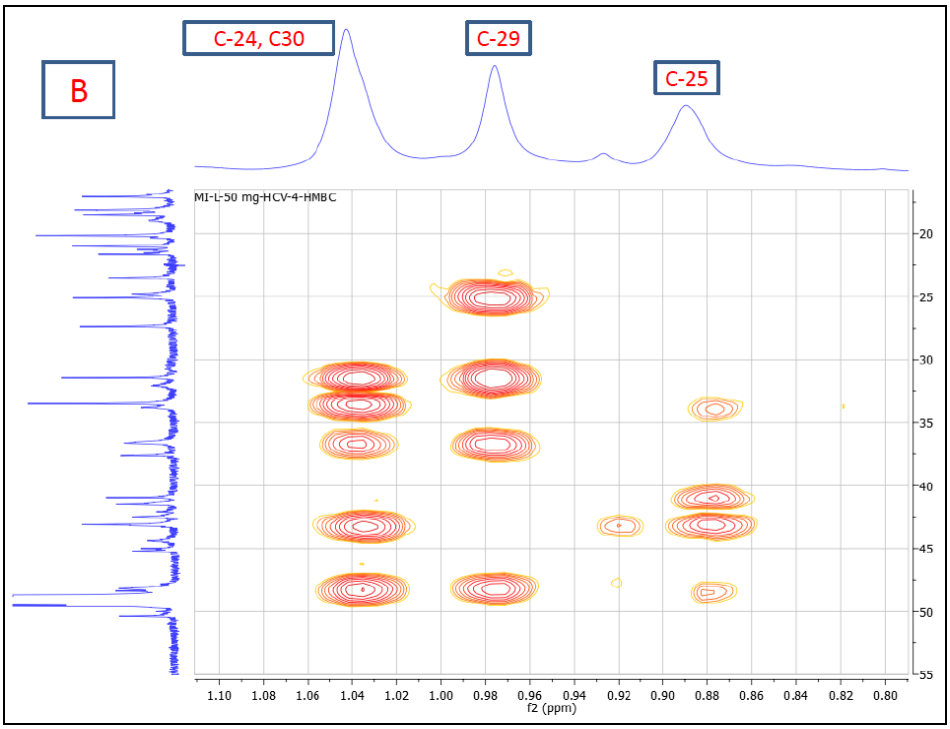

Figure 176. HMBC spectrum of rhododendrosaponin **III** in methanol-d_4 (400 MHz); A) the full spectrum, B) the upfield region

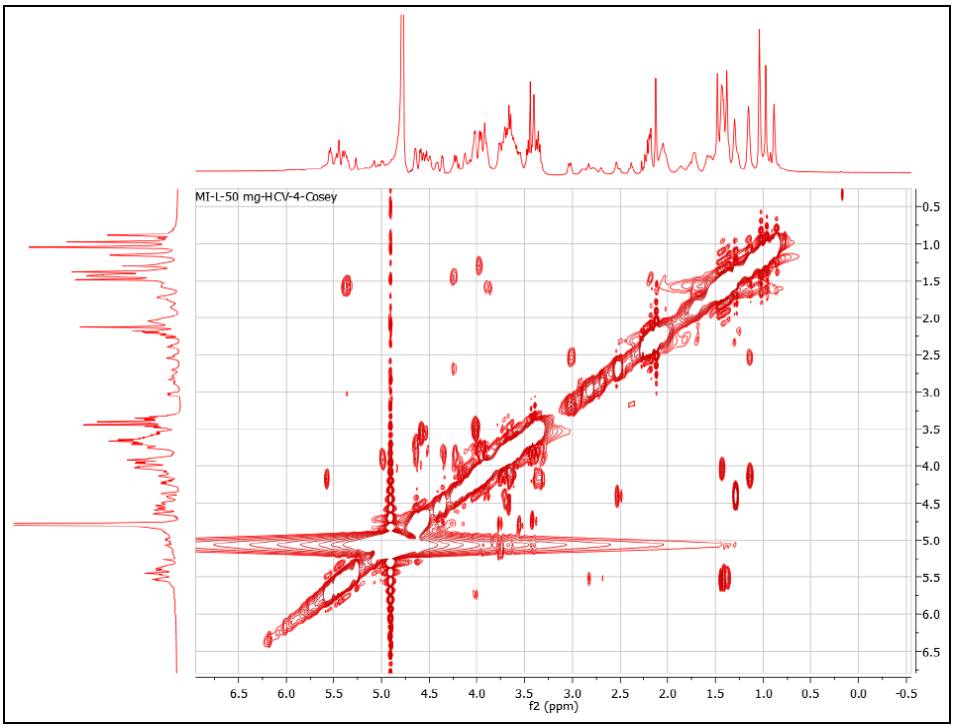

Figure 177. COSY spectrum of rhododendrosaponin **III** in methanol-d_4 (400 MHz)

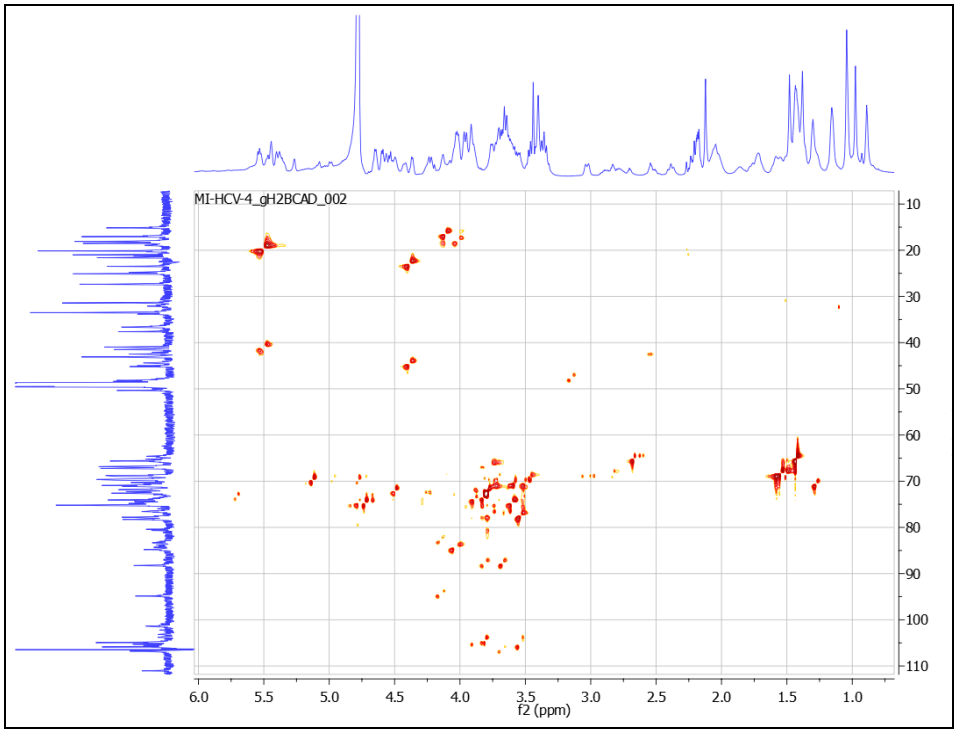

Figure 178. H2BC spectrum of rhododendrosaponin **III** in methanol-d_4 (600 MHz)

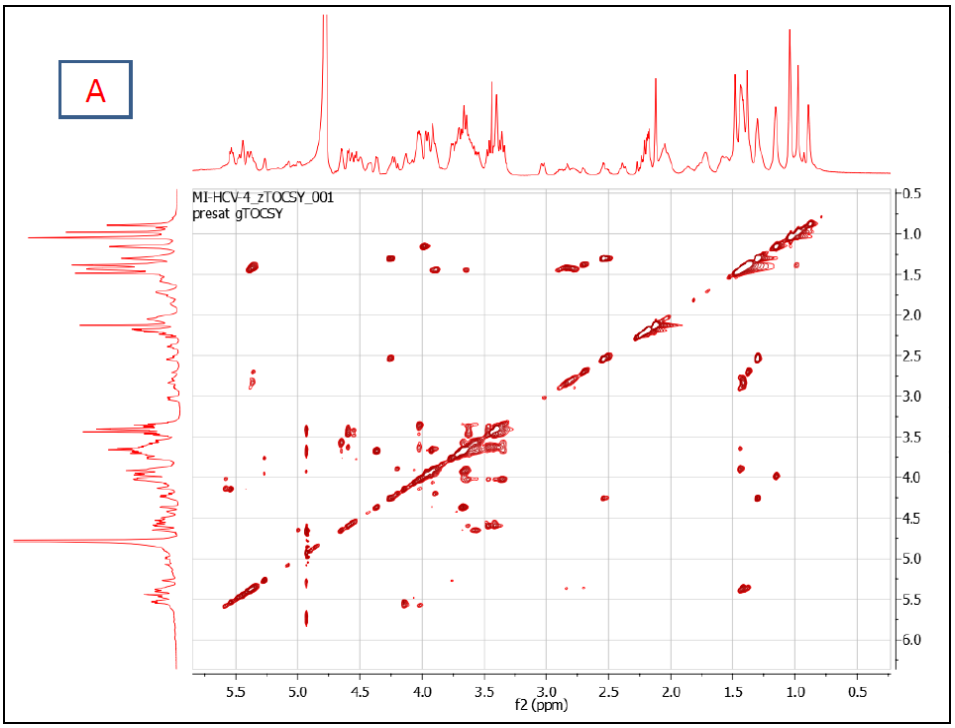

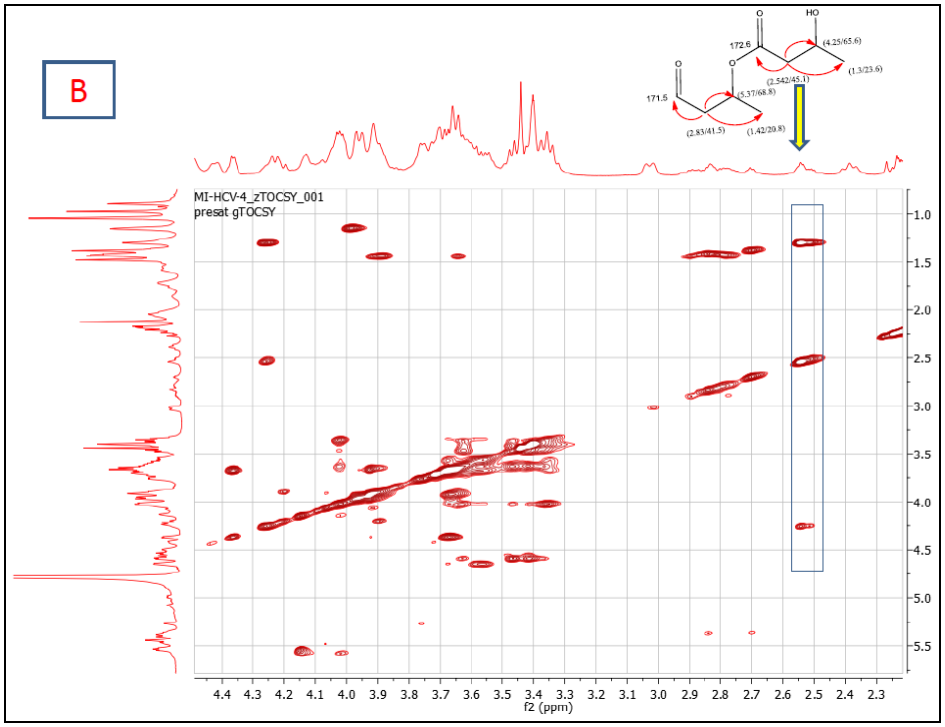

Figure 179. TOCSY spectrum of rhododendrosaponin **III** in methanol-d_4 (600 MHz); A) the full spectrum, B) the downfield region

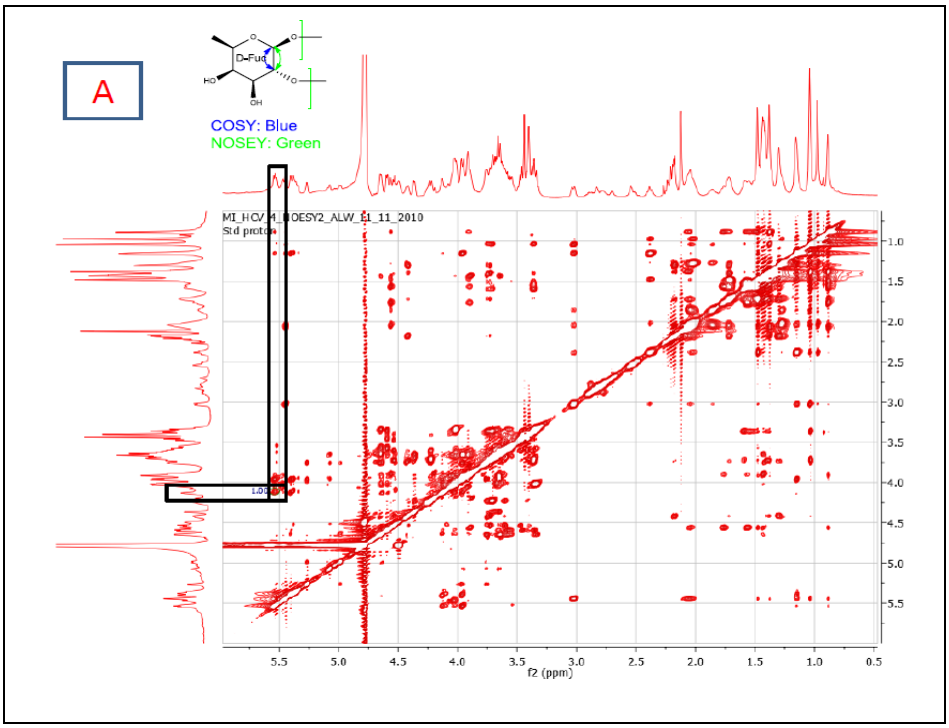

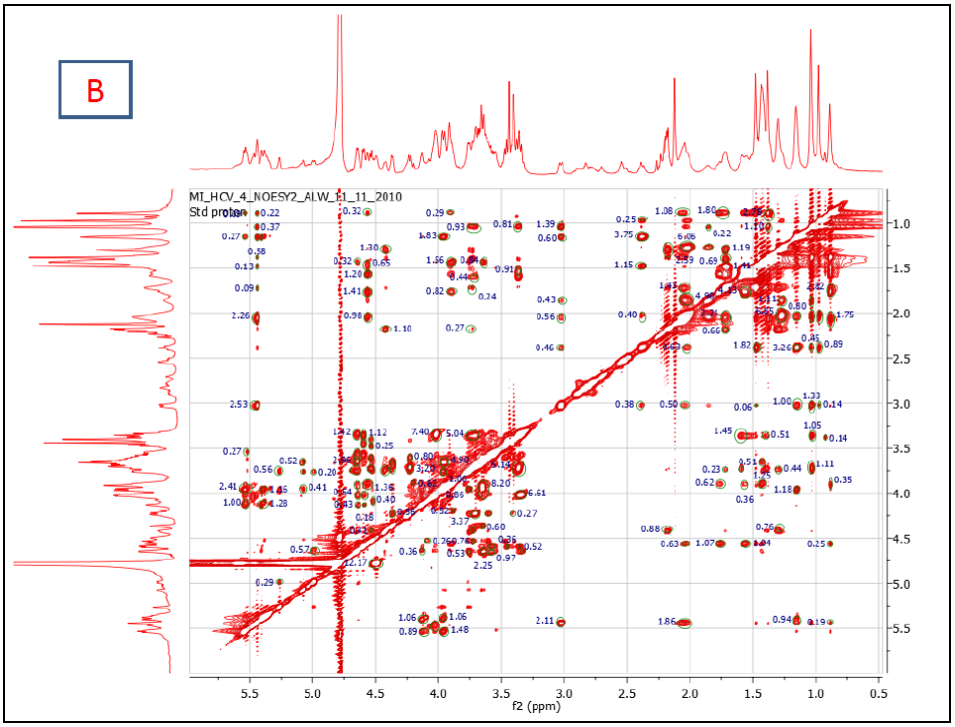

Figure 180. NOESY spectrum of rhododendrosaponin **III** in methanol-d_4 (600 MHz) A) the full spectrum, B) the integrated NOESY

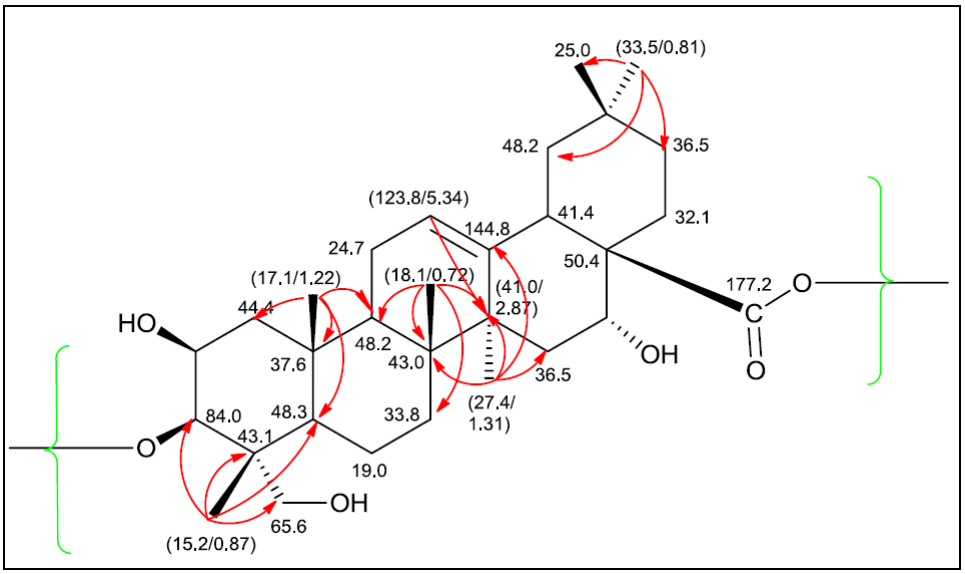

Figure 181. Selected HMBC correlations of the aglycone triterpene

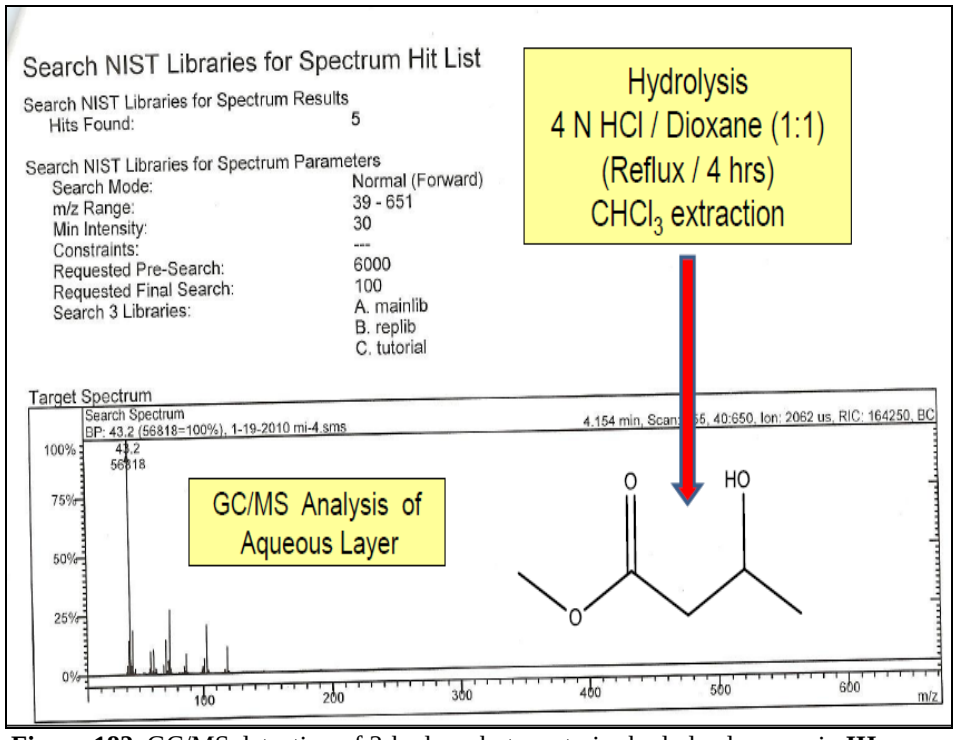

Figure 182. GC/MS detection of 3-hydroxybutanoate in rhododendrosaponin **III**

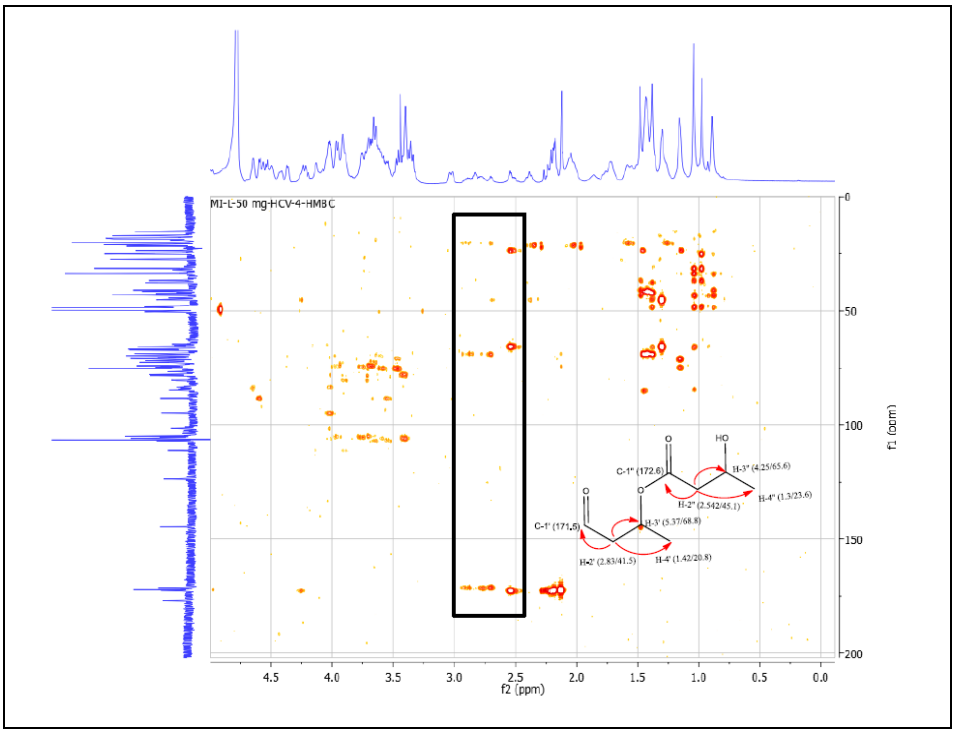

Figure 182. HMBC correlations of 3-hydroxybutanoate dimmer in rhododendrosaponin **III**

Rhododendrosaponins **II** and **III** were shown by (+)-HRESIMS to possess similar masses at *m/z* 1722.6523-1722.6498 for the sodiated species, $[C_{78}H_{124}O_{40}+Na]^+$, calcd 1722.7488 Figures 161 and 171, while rhododendrosaponin **I** shows a mass at *m/z* 1764.7908 for the sodiated species $[C_{80}H_{126}O_{41}+Na]^+$, calcd 1764.7594 Figure 152 and the presence of an extra acetyl group attached at C-23 was confirmed by stacked plot the proton and carbon spectra of rhododendrosaponins **I-III** as well as ROESY spectrum of rhododendrosaponin **I** (Figures 183, 184, and 160).

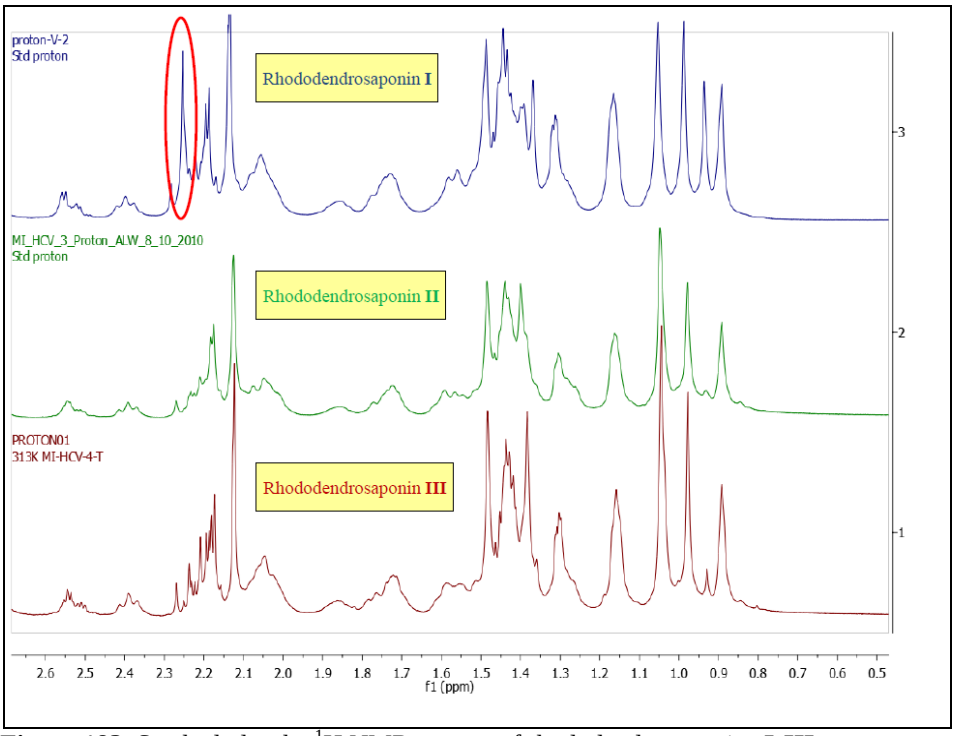

Figure 183. Stacked plot the ^{1}H NMR spectra of rhododendrosaponins **I-III**

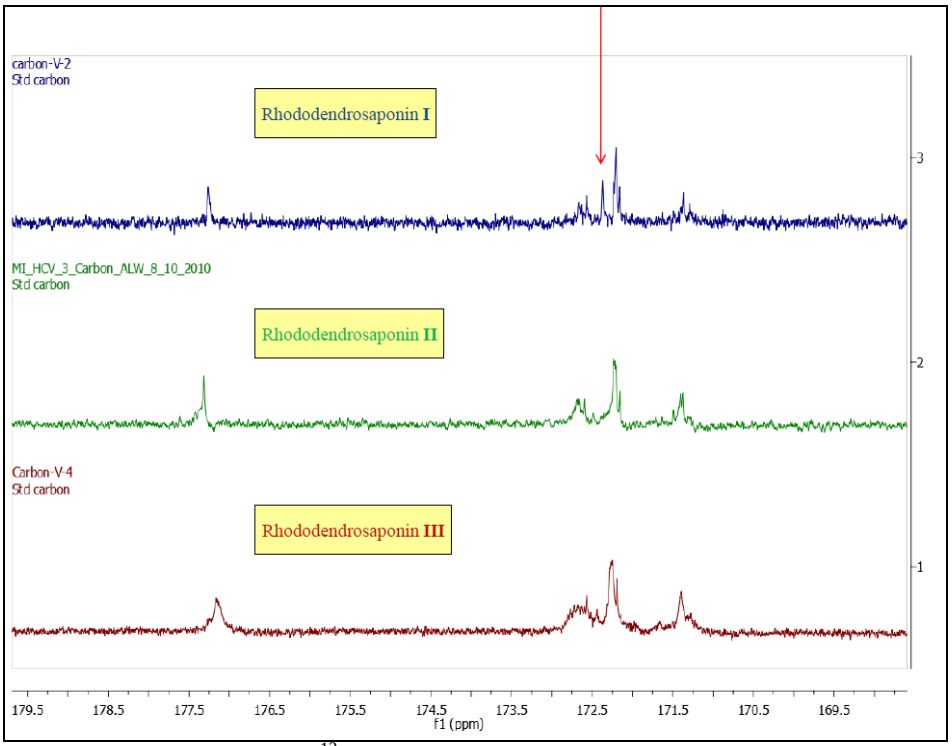

Figure 184. Stacked plot the ^{13}C NMR spectra of rhododendrosaponins **I-III**

Identification and determination of the carbohydrate units were established using ^{13}C NMR and GC/MS/MS data while the determination of the sequence of oligosaccharides was completed through detailed MS studies including fragmentation by Nanospray Ionization-Linear Ion Trap Mass Spectrometry (NSI-MS^n) through collaboration with the Complex Carbohydrate Research Center at The University of Georgia. The total carbohydrate content of the major glycoside rhododendrosaponin **III** was shown by GC analysis to be 73.8% by weight. The processed data revealed the presence of a glucosyl, two arbinosyl, a rhamnosyl, a fucosyl, and two xylosyl units (Table 14). Inositol was added to the sample before derivatization as an internal standard (20 µg/sample) and the monosaccharides are identified by their retention times in comparison to standards and the carbohydrate character of these are authenticated by their mass spectra.

Table 14. Monosaccharide analysis of rhododendrosaponin **III** by GC/MS

Residue	**Weight (ug)[1]**	**mole%**
Arabinose(Ara)	77.2	27.5
Ribose(Rib)	n.d.	n.d.
Rhamnose (Rha)	48.4	15.8
Fucose (Fuc)	43.7	14.2
Xylose (Xyl)	86.7	30.9
Glucuronic acid(GlcUA)	n.d.	n.d.
Galacturonic acid (GalUA)	n.d.	n.d.
Mannose (Man)	n.d.	n.d.
Galactose (Gal)	n.d.	n.d.
Glucose (Glc)	39.2	11.6
N-Acetylgalactosamine (GalNAc)	n.d.	n.d.
N-Acetyl-glucosamine (GlcNAc)	n.d.	n.d.
Heptose(Hep)	n.d.	n.d.
3-Deoxy-2-manno-2-octulsonic acid (KDO)	n.d.	n.d.
Sum		100

[1]Values are expressed as mole percent of total carbohydrate, n.d. = none detected. Values under 2 ug are given as rough estimates only due to poor linearity of the assay in these regions.

The glycosyl linkages were summarized in (Table 15). The determination of the sequence of oligosaccharides was done via full MS and fragmentation by (NSI-MS^n) (Figure 185).

Table 15. Glycosyl linkage analysis for rhododendrosaponin **III**

Glycosyl Residue	**Percentage Present**
Terminally linked arabinofuranosyl residue (t-Araf)	2.6
Terminally linked arabinopyranosyl residue (t-Arap)	21.9
Terminally linked xylopyranosyl residue (t-Xylp)	9.2
4-linked rhamnopyranosyl residue (4-Rhap)	19.7
Terminally linked glucopyranosyl residue (t-Glcp)	2.2
2-linked fucopyranosyl residue (2-Fucp)	1.9
3-linked xylopyranosyl residue (3-Xylp)	12.0
2,3-linked fucopyranosyl residue (2,3-Fucp)	16.3
6-linked glucopyranosyl residue (6-Glcp)	8.8
4-linked glucopyranosyl residue (4-Glcp)	0.7
2,6-linked glucopyranosyl residue (2,6-Glcp)	4.7
Total	100

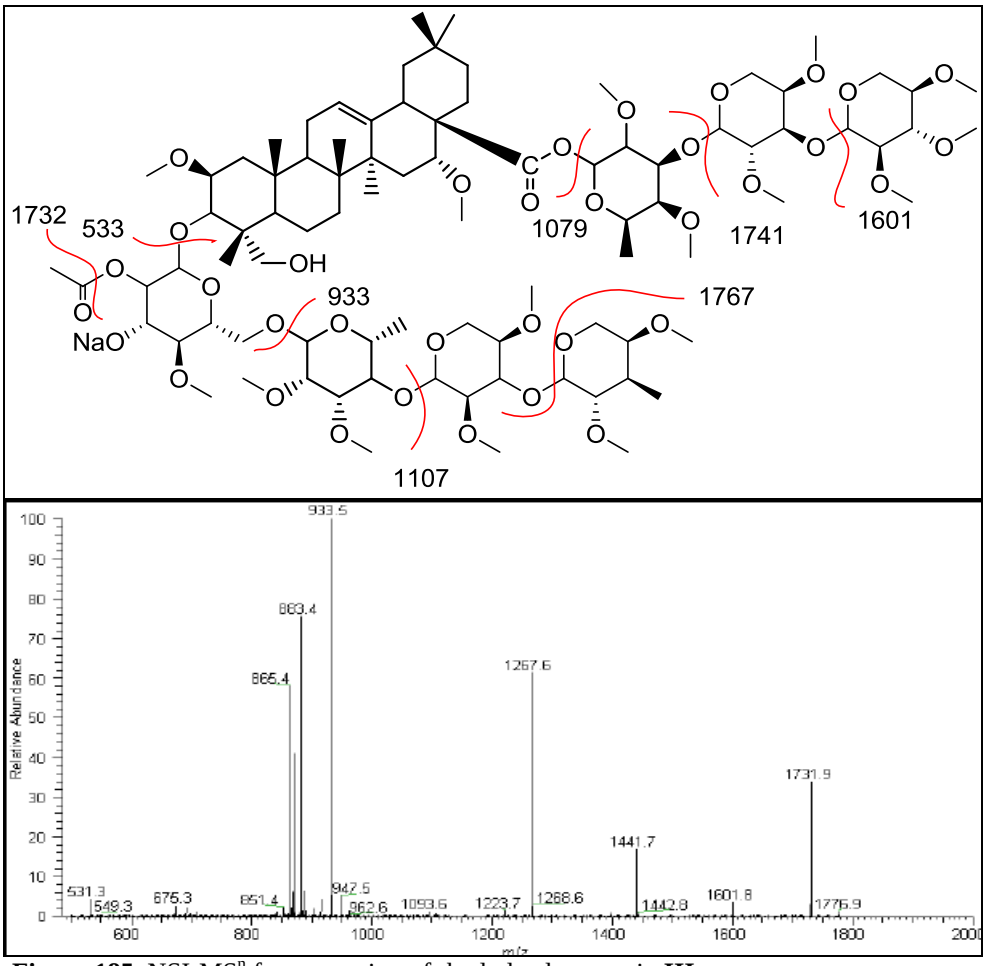

Figure 185. NSI-MS^n fragmentation of rhododendrosaponin **III**

The absolute configuration determination of the carbohydrate units was completed using an HPLC method reported by Tanaka et al.[119] First the compound is hydrolyzed via refluxing in 1 N HCl for 2-3 h followed by extraction with ethyl acetate. The aqueous layer is then neutralized with silver carbonate, centrifuged to remove the insoluble precipitate, dried, refluxed with L-cysteine methyl ester in pyridine for 1 hr at 60-70 °C, followed by the addition of phenylisothiocyanate with extended reflux for an additional 1 hr at 60-70 °C to form the thiazoline derivative that can be detected by UV (Scheme 12). This method was tested using various standards (Figures 186, 187 and Table 16), followed by application to the isolated

metabolites (Figures 188, 190, and 191). The gross structure of the major metabolite rhododendrosaponin **III** was shown in Figure 189.

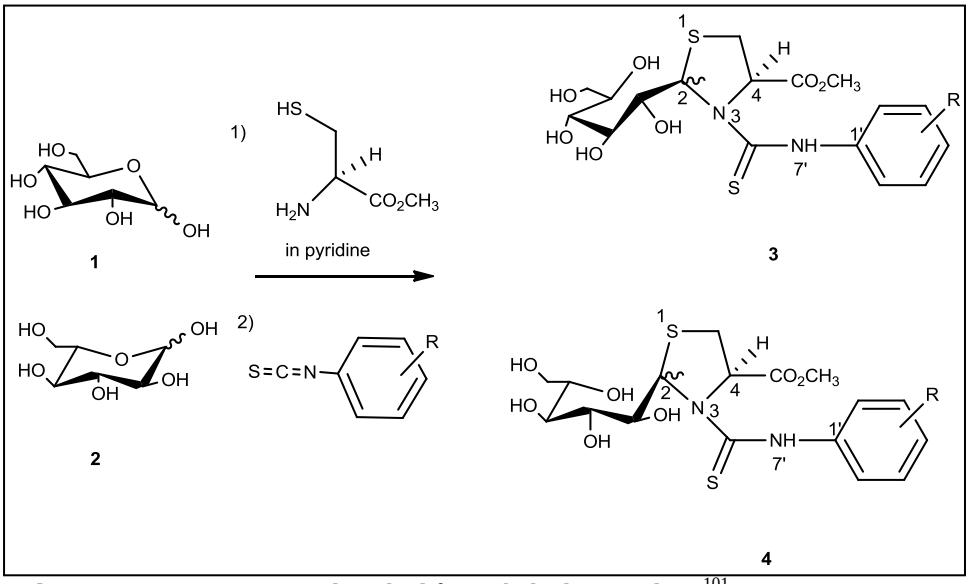

Scheme 12. An investigational method for carbohydrate analysis[101]

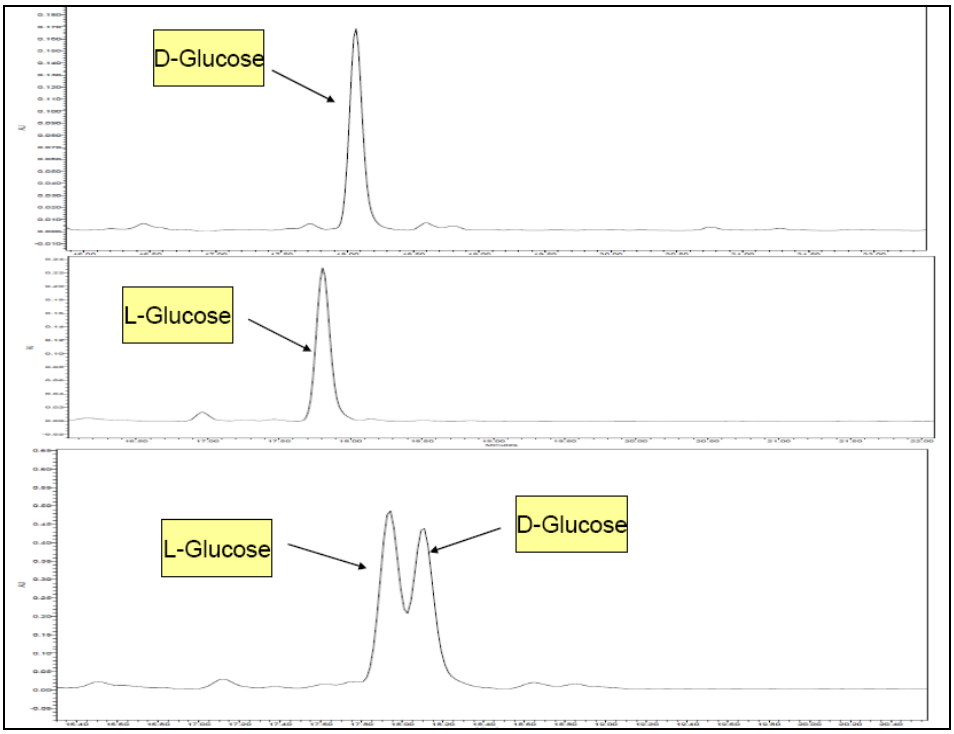

Figure 186. L- and D-glucose standards by carbohydrate analysis method

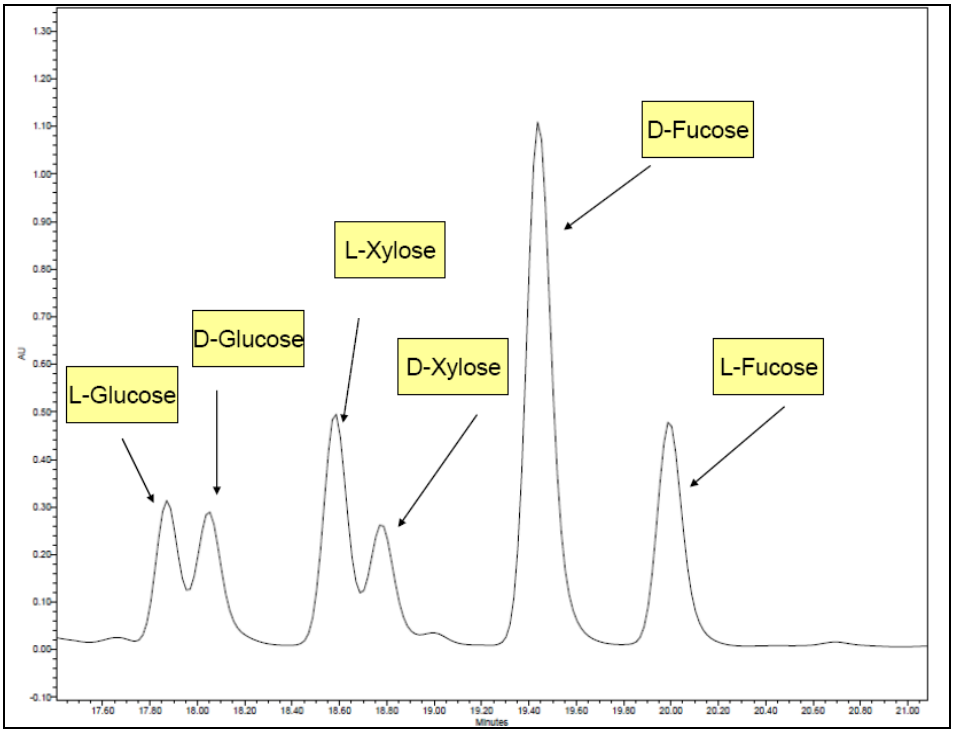

Figure 187. L- and D- glucose, xylose, and fucose standards by the carbohydrate analysis method

Table 16. The retention times of the carbohydrate standards

Carbohydrate	RT
D-Arabinose	18.77
L-Arabinose	18.41
D-Glucose	18.07
L-Glucose	17.81
D-Xylose	18.79
L-Xylose	18.61
D-Fucose	19.42
L-Fucose	20.05
L-Rhamnose	17.10

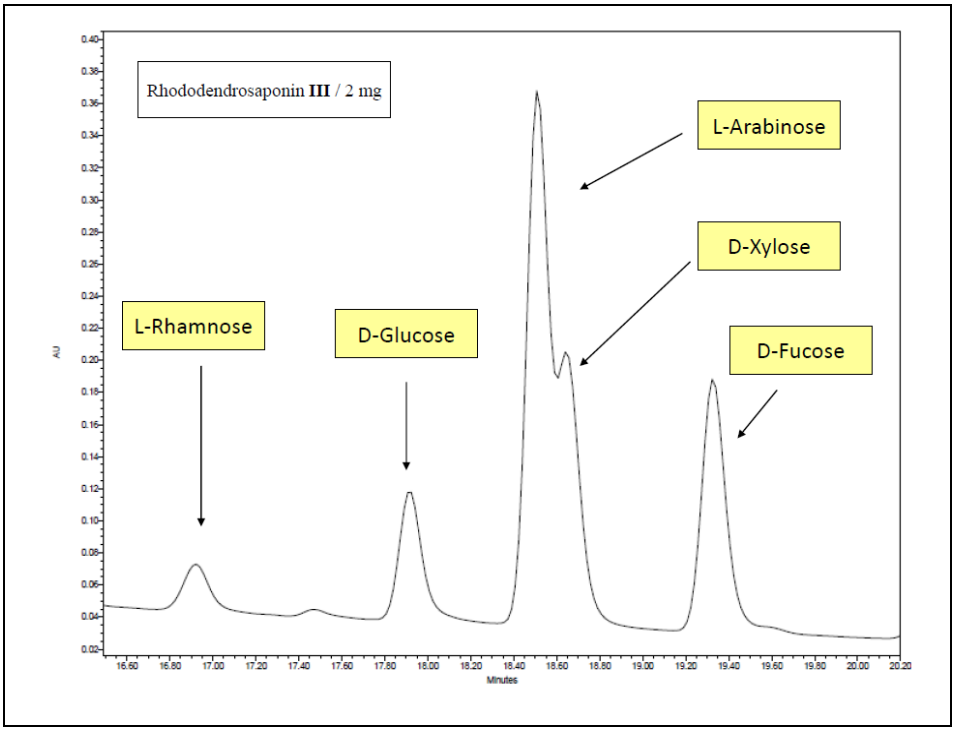

Figure 188. Carbohydrate analysis for rhododendrosaponin **III**

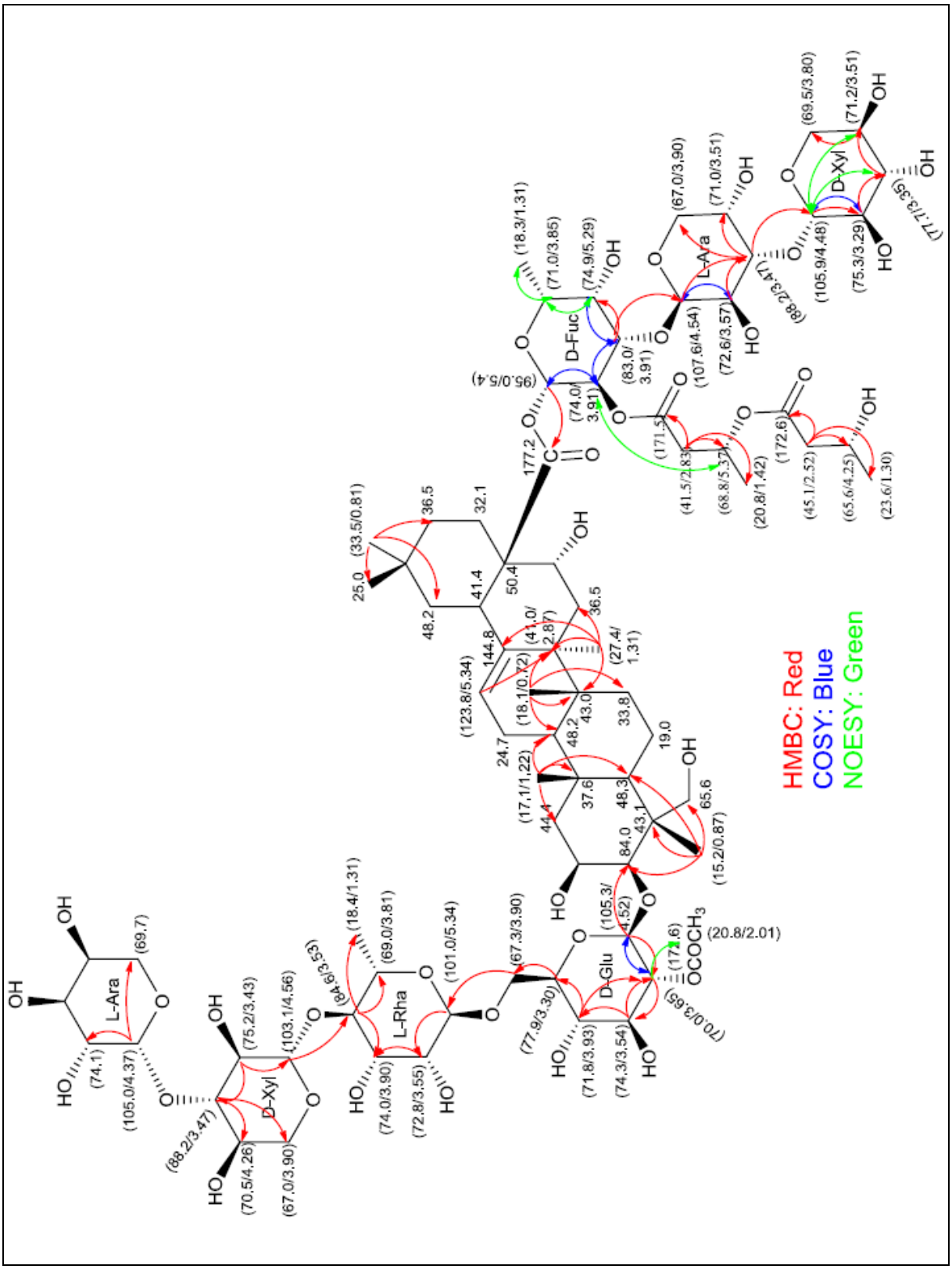

Figure 189. The gross structure of rhododendrosaponin **III**

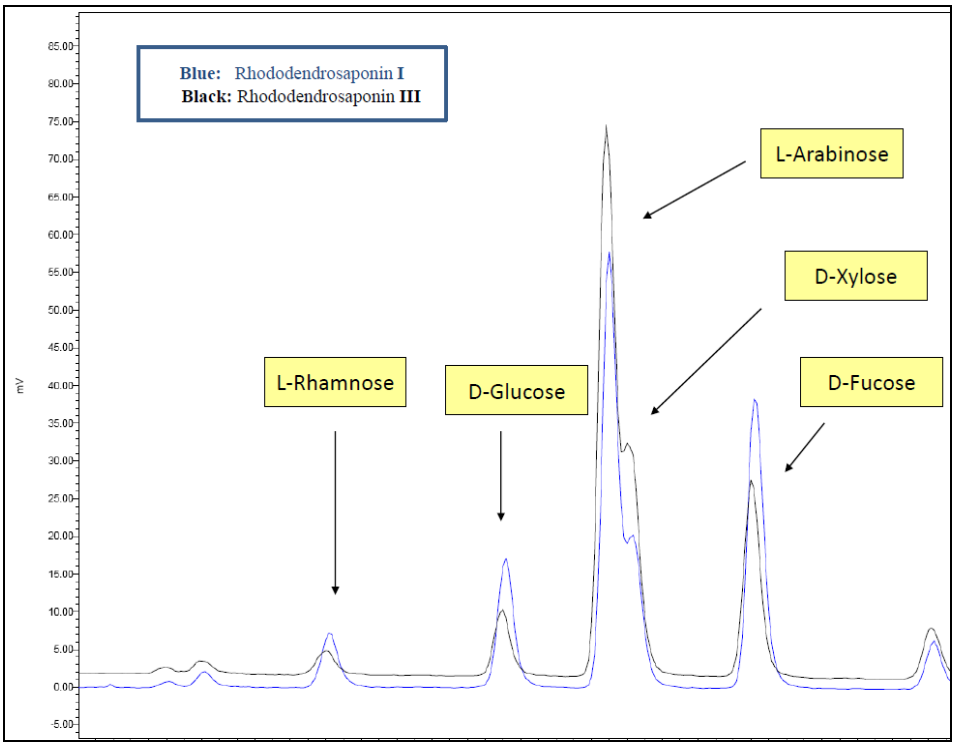

Figure 190. Overlay of the carbohydrate analysis chromatograms of rhododendrosaponins **I** and **III**

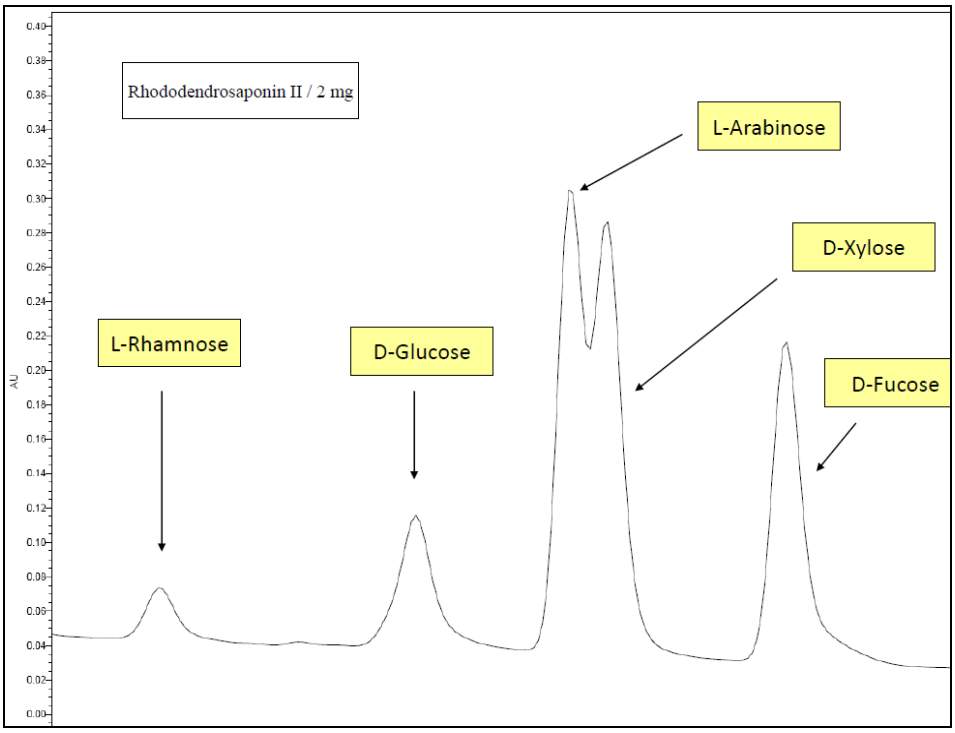

Figure 191. Carbohydrate analysis chromatogram of rhododendrosaponin **II**

Overlaying the most common 2D NMR experiments including ^{1}H-^{13}C) Heteronuclear Multiple Quantum Coherence Spectroscopy (HSQC), ^{1}H-^{13}C (2 and 3 bond) Heteronuclear Single bond Correlation Spectroscopy (HMBC) and ^{1}H -^{1}H Nuclear Overhauser Enhancement spectroscopy (NOESY/ROESY) helped to alleviate the extended time to quickly solve such considerably complex homologous series. Overlaid HSQC data for rhododendrosaponins **I** and **III** revealed a high level of homology (Figure 192) with interchangeable α- and β- configuration at C-24 of rhododendrosaponins **I**. This was confirmed with the HSQC, HMBC, and ROESY spectra of rhododendrosaponins **I** shown in Figures 193, 194, and 195. Interestingly, the superimposed data clearly demonstrated the presence of the uncommon Amadori-type pyranose-furanose isomerism of the terminal L-arbinosyl moiety. It was possible to monitor the presence of acyclic intermediate (-CHO) at 218.1 ppm (Figure196). As further evidence, the glycosyl linkage analysis (Table 15) confirmed the presence of both forms. These data explains the complex NMR spectra for these compounds.

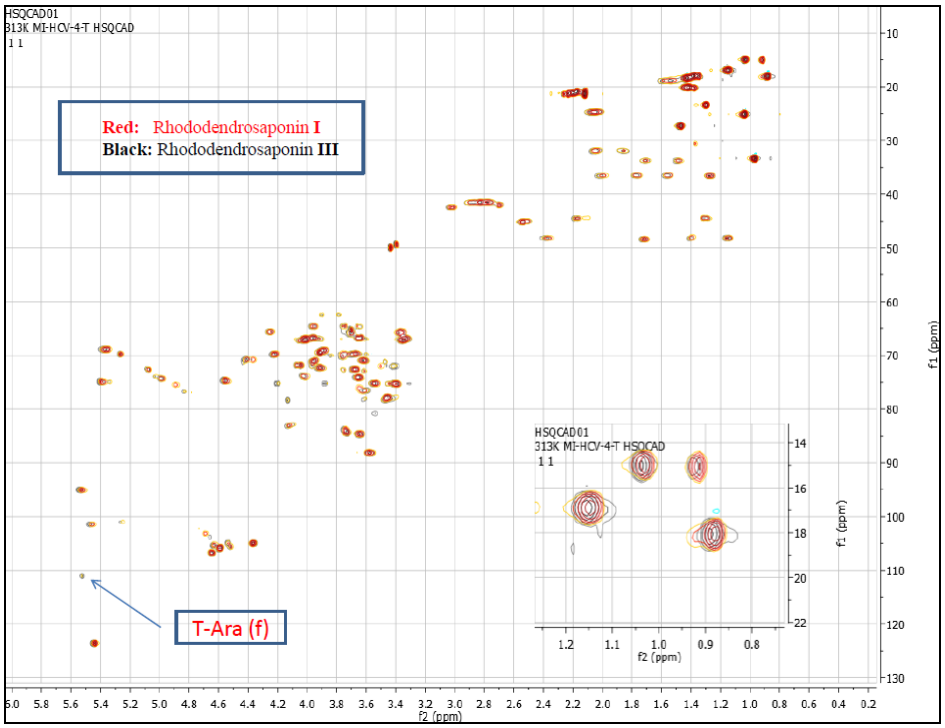

Figure 192. Overlaid HSQC spectra of rhododendrosaponins **I** and **III**

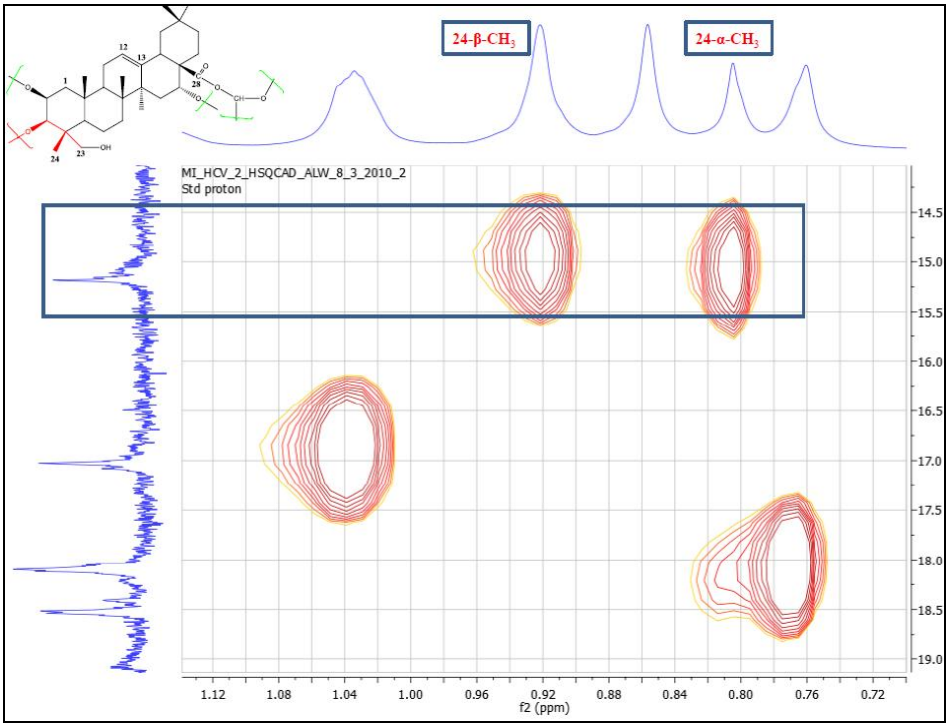

Figure 193. The expanded HSQC spectrum of rhododendrosaponin **I** in methanol-d_4 (600 MHz) shows the presence of α and β isomers at C-24

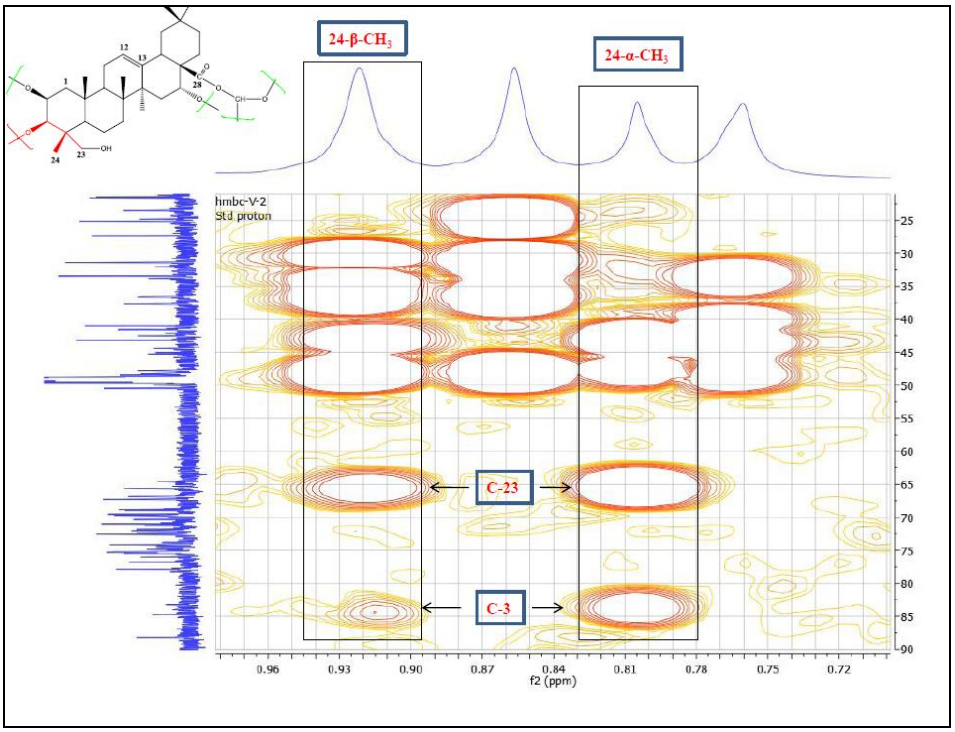

Figure 194. The expanded HMBC spectrum of rhododendrosaponin **I** in methanol-d_4 (600 MHz) shows the presence of α and β isomers at C-24

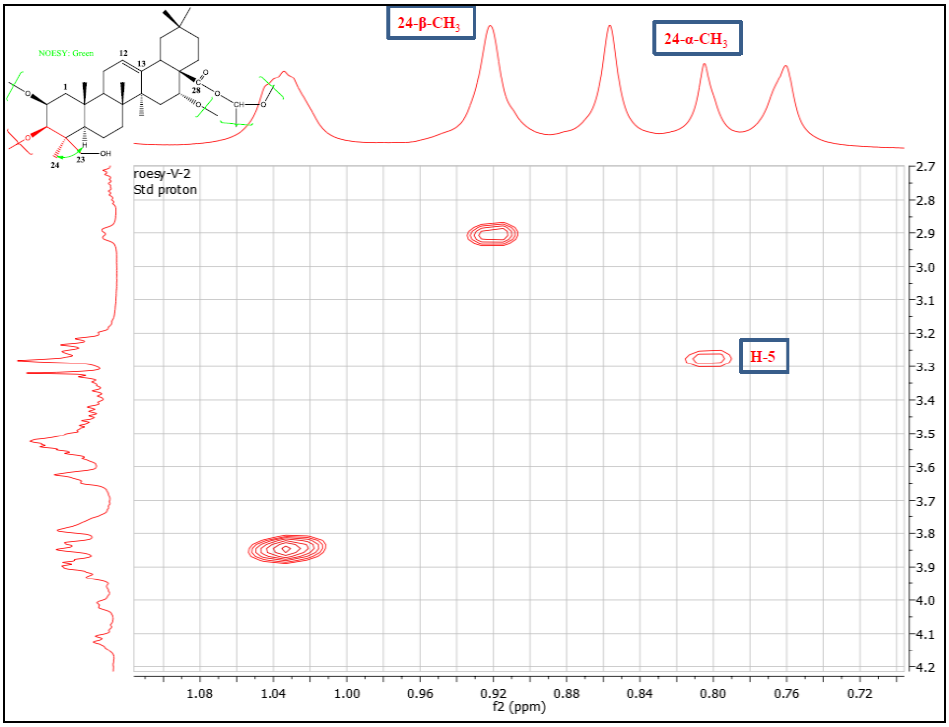

Figure 195. The expanded ROESY spectrum of rhododendrosaponin **I** in methanol-d_4 (600 MHz) shows the presence of α and β isomers at C-24

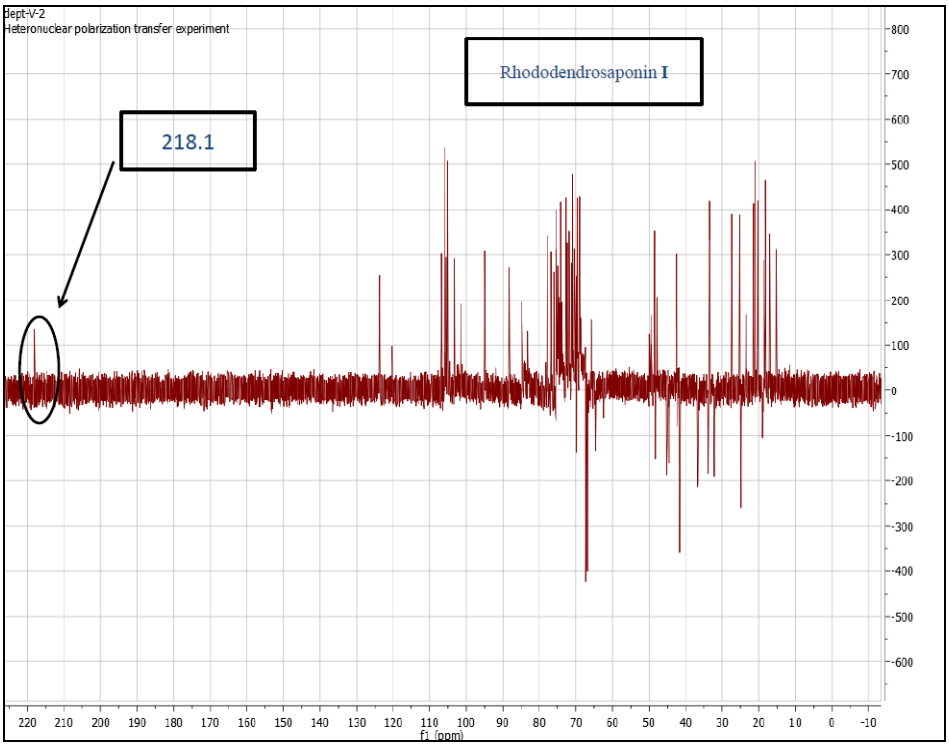

Figure 196. 135º DEPT spectrum of rhododendrosaponin **I** in methanol-d_4 (600 MHz) shows the presence of (-CHO) for the acyclic intermediate

In a similar manner stacked HSQC studies for rhododendrosaponins **II** and **III** revealed high level of similarity (Figure 197) with pyranose-furanose isomerism. This was confirmed by monitoring the presence of the acyclic intermediate (-CHO) at 217.590 ppm (Figure 198), as well as the presence of arbinofuranosyl unit in rhododendrosaponin **II** (Figure 199). Further investigation through co-injection of rhododendrosaponins **II** and **III** on 250 × 21.2 mm NH_2 column with $CHCl_3$-MeOH confirms the isomerization (Figure 200) which may be catalyzed by the NH_2 stationary phase (Figure 201).

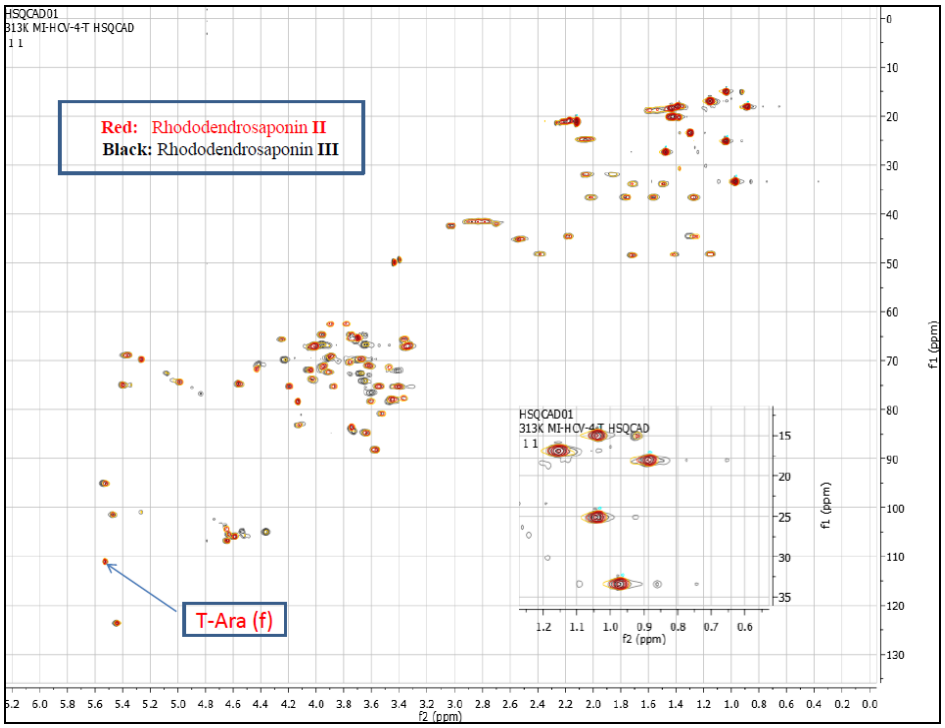

Figure 197. Overlaid HSQC spectra of rhododendrosaponins **II** and **III**

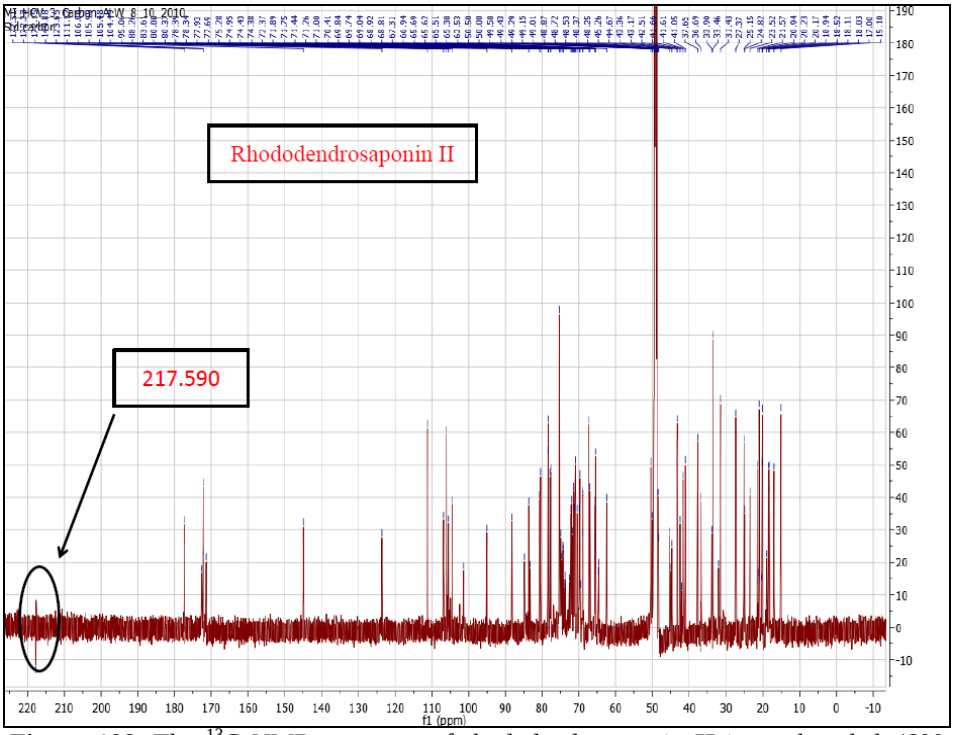

Figure 198. The ^{13}C NMR spectrum of rhododendrosaponin **II** in methanol-d_4 (600 MHz) shows the presence of (-CHO) for the acyclic intermediate

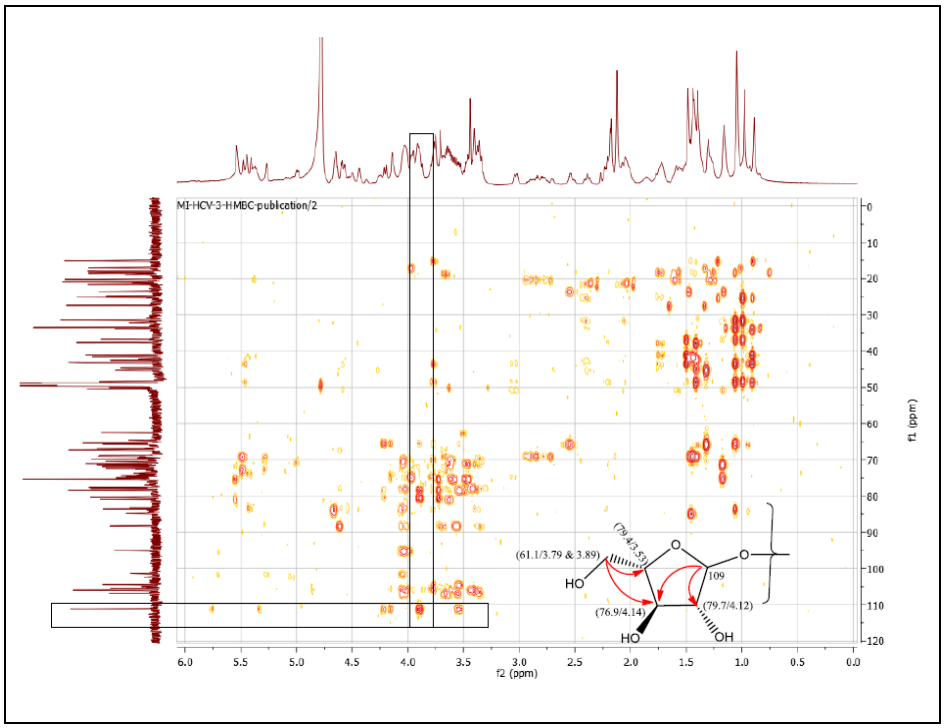

Figure 199. Expanded HMBC spectrum of rhododendrosaponin **II** in methanol-d_4 (600 MHz) shows the presence of arbinofuranosyl moiety

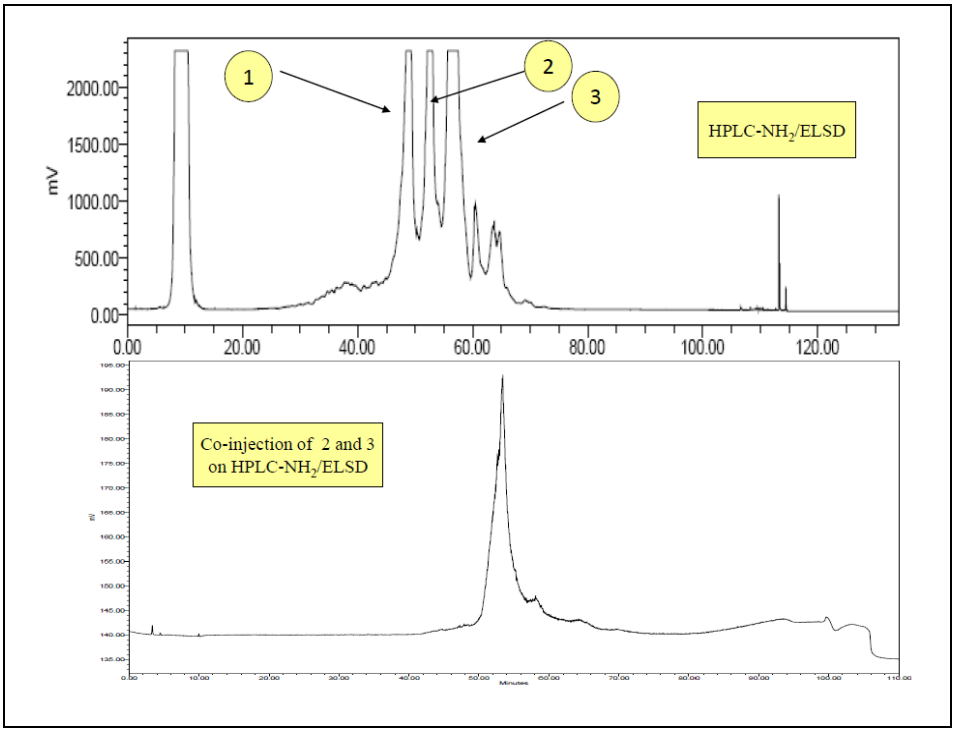

Figure 200. Co-injection of rhododendrosaponins **II** and **III** on 250 × 4.6 mm NH_2 column

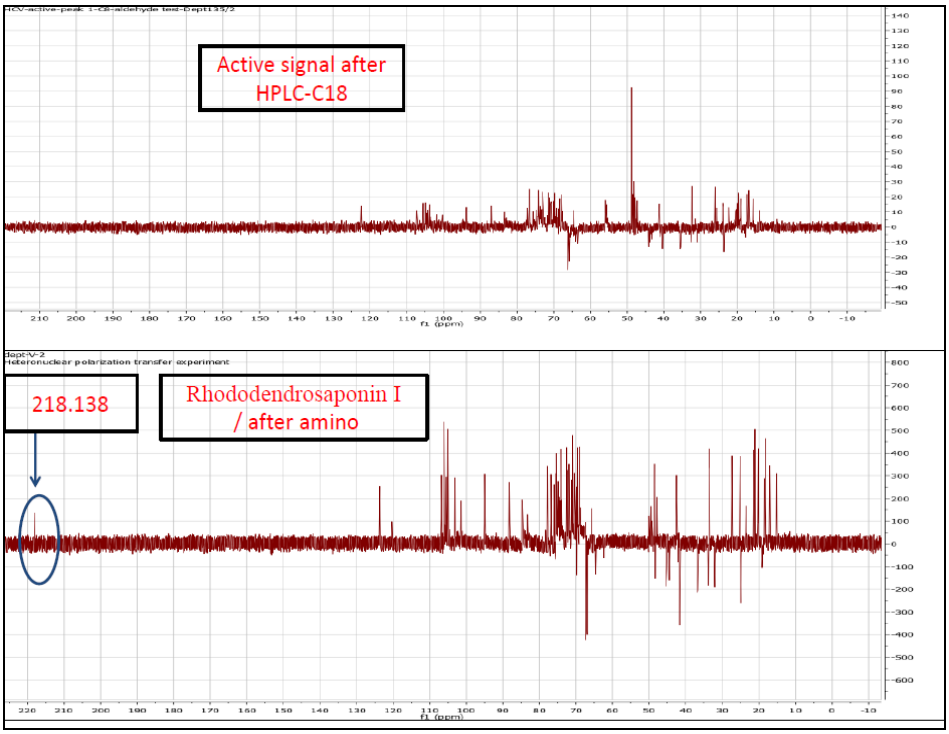

Figure 201. 135º DEPT spectrum of active fraction after 250 x 21.2 mm C_{18} and rhododendrosaponin **I** after 250 x 21.2 mm NH_2 in methanol-d_4 (600 MHz)

^{1}H NMR data for rhododendrosaponins **I** established the β-configuration of the following glycosyl groups: fucosyl (5.42 d, 7.8 Hz), glucosyl (4.57, 7.8 Hz), terminal xylosyl (4.24 d, 6.0 Hz), inner xylosyl (4.52 d, 6.0 Hz), terminal arabinosyl (4.48 d, 7.8 Hz), and inner arabinosyl (4.54 d, 6.6 Hz), while α-configuration of rhamnosyl (5.35, s). The 3β absolute configuration of 3-hydroxybutanoate was determined by acid-catalyzed methanolysis. This was followed by comparison with (R) and (S) standards using a chiral GC column [RESTEK capillary column: St-βDEXsa (30 m x 0.32 mm x 0.25 µm)], Figures 202 and 203.

The proposed structures of the three isolated metabolites are shown in Figure 204. The 3D structure of the major glycoside, rhododendrosaponins **III** was minimized using OPLS_2005 with extended cutoff; Van der Waals of 8.0 K cal/mol, Electrostatic of 20.0 K cal/mol, and H-bond of 4.0 K cal/mol. All stereogenic centers are kept fixed during the calculation. PRCG

method was used with 0.05 as a convergence gradient threshold. Mixed torsional/low-mode sampling was used for conformational analysis with 1000 number of steps. PyMol 1.4 was used to generate the 3D surface with element color scheme as shown in Figure 205. Despite the presence of similarity to previously reported natural products, the rarity of the source, the exceptional activity, and the presence of the uncommon Amadori-type isomerism make this group of metabolites unique.[118,120]

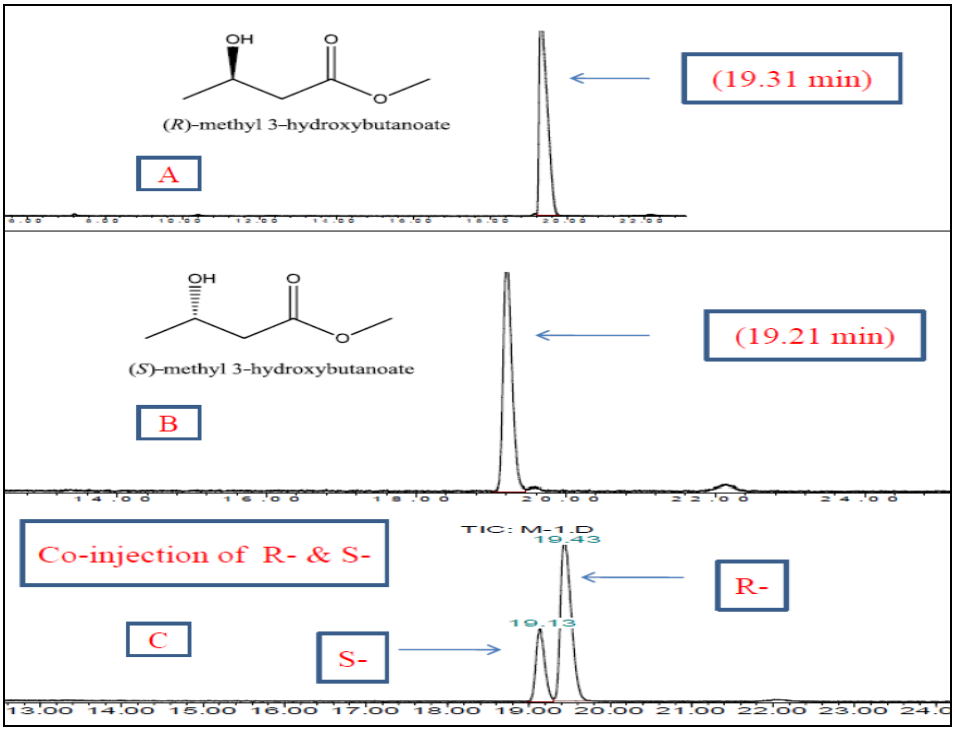

Figure 202. GC chromatograms of: A) (R)-methyl 3-hydroxybutanoate, B) (S)-methyl 3-hydroxybutanoate, C) Co-injection of (R) and (S)-methyl 3-hydroxybutanoate

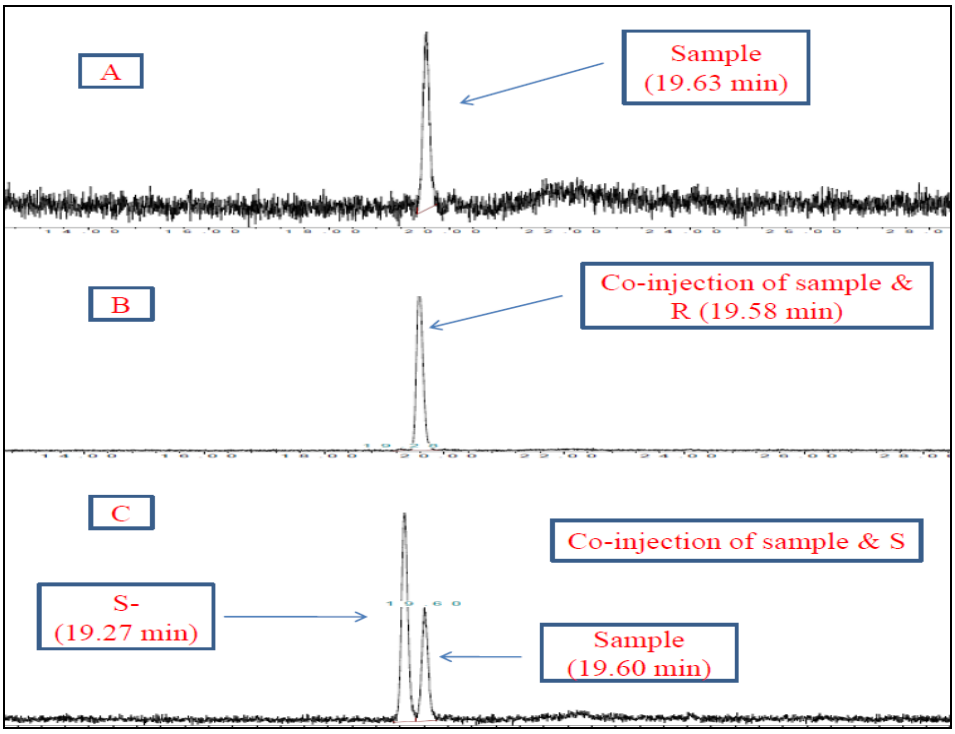

Figure 203. GC chromatograms of: A) rhododendrosaponins **I-III** after methanolysis, B) Co-injection of the sample and (R)-methyl 3-hydroxybutanoate, C) Co-injection of the sample and (S)-methyl 3-hydroxybutanoate

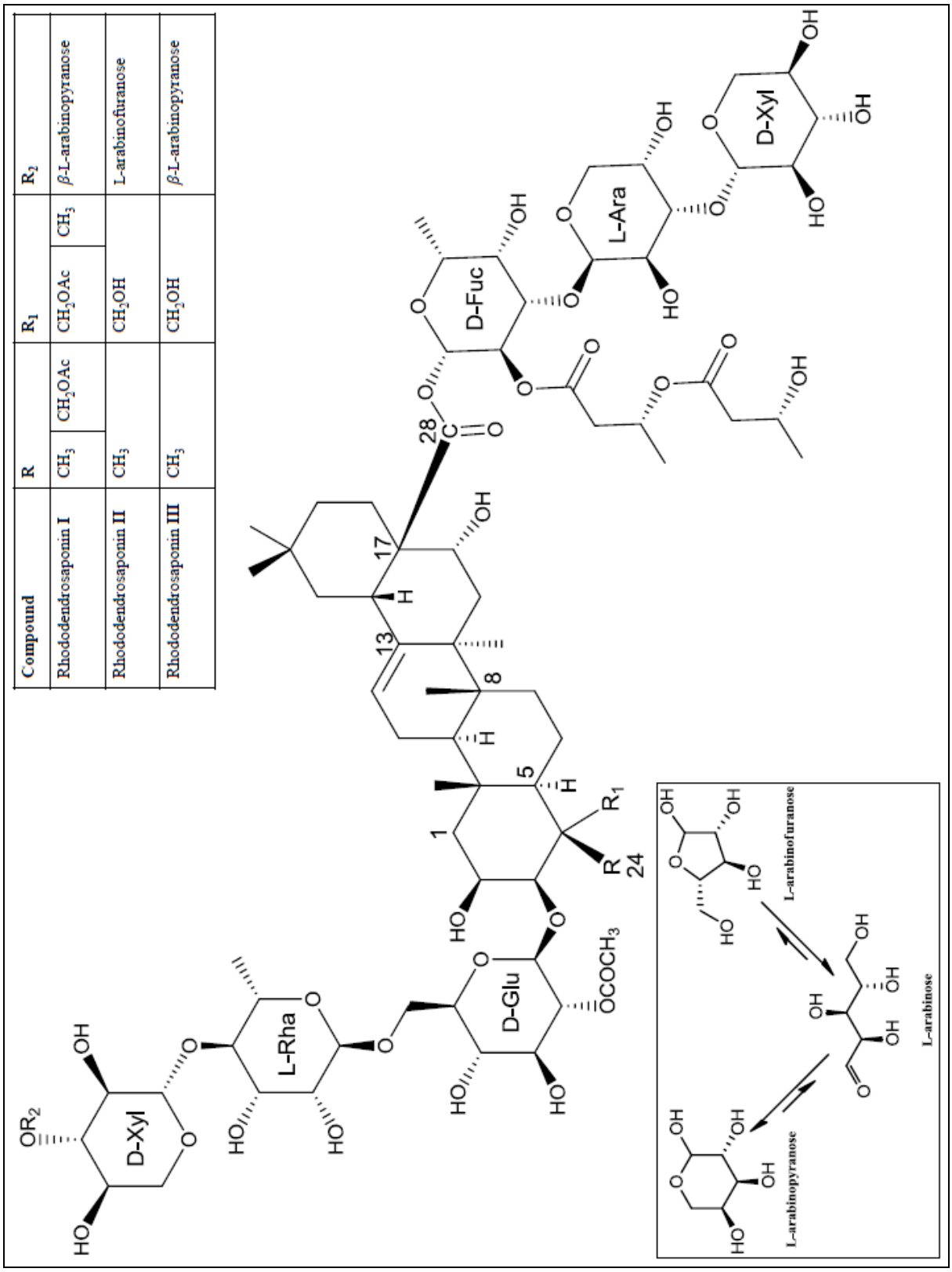

Compound	R		R_1		R_2
	CH_3	CH_2OAc	CH_2OAc	CH_3	
Rhododendrosaponin I					β-L-arabinopyranose
Rhododendrosaponin II	CH_3		CH_2OH		L-arabinofuranose
Rhododendrosaponin III	CH_3		CH_2OH		β-L-arabinopyranose

Figure 204. The proposed structures of rhododendrosaponins **I-III**

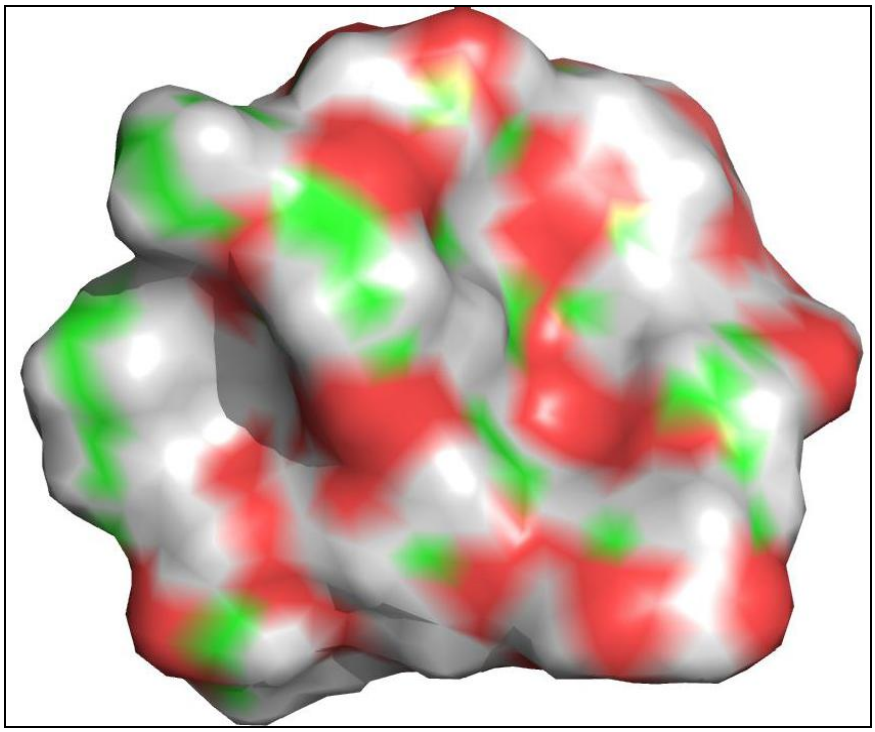

Figure 205. The minimized 3D structure surface generated by PyMol 1.4 for the major glycoside, rhododendrosaponin **III,** red represents oxygen while green and grey represent carbon and hydrogen.

.

Rhododendrosaponins **I-III** were evaluated at six different concentrations for anti-HCV activity and end point determination in Huh-7 replicon Cells (Table 17). Huh-7 B cells containing HCV genotype 1 replicon RNA were seeded in a 96-well plate at 3,000 cells/well and the compounds were added in dose response at 10, 3, 1, 0.3, 0.1, and 0.03 µg/mL in triplicate immediately after seeding. Following five days incubation (37 °C, 5% CO_2), total cellular RNA was isolated using the Manual Perfect Pure RNA 96 Cell Vac kit from 5 prime. Replicon RNA and an internal Control (TaqMan rRNA control reagent, Applied Biosystems) were amplified in a single step multiple Real Time RT-PCR assay.

Table 17. Anti-HCV activity of rhododendrosaponins **I-III** in Huh-7 replicon cells

Sample Code	Concentration µg/mL	ΔCt HCV	ΔCt rRNA	% Inhibition		EC_{50} µg/mL	EC_{90} µg/mL	CC_{50} µg/mL
				HCV	rRNA			
RS-446	0.3	0.49	0.01	28.89	0.69	0.6	2.3	>2.6
	0.8	1.53	-0.57	65.18	-47.93			
	2.6	4.28	-0.63	94.79	-54.19			
Rhododendrosaponin I	0.03	-0.66	-1.10	-57.78	-113.35	0.2	0.6	7.0
	0.1	-0.22	-0.89	-16.69	-85.39			
	0.3	2.60	-0.44	83.37	-35.22			
	1.0	5.35	-0.85	97.51	-79.51			
	3.0	7.08	-0.21	99.25	-15.35			
	10.0	7.04	6.04	99.23	98.46			
Rhododendrosaponin II	0.03	-0.07	-0.23	-5.20	-16.96	0.2	0.9	7.4
	0.1	-0.08	-0.99	-5.68	-98.19			
	0.3	1.84	-1.18	71.89	-126.52			
	1.0	3.67	-0.97	92.10	-95.02			
	3.0	7.44	0.15	99.41	10.05			
	10.0	7.07	1.96	99.24	74.16			
Rhododendrosaponin III	0.03	-0.63	-1.81	-54.19	-249.27	0.2	0.3	5.3
	0.1	-0.42	-0.98	-33.67	-96.38			
	0.3	3.95	0.59	93.49	33.40			
	1.0	5.36	-0.75	97.53	-67.91			
	3.0	6.88	0.44	99.14	26.05			
	10.0	7.50	6.27	99.44	98.69			

The antiviral effectiveness of the compounds was calculated by subtracting the threshold RT-PCR cycle of the test compound from the threshold RT-PCR cycle of the non-drug control (ΔCtHCV). A ΔCt of 3.3 equals a 1-log reduction (equal to 90% less starting material) in replicon RNA levels. The cytotoxicity of the compounds was also calculated by using the ΔCt rRNA values. RS-446 (2′-C-Me-C) Figure 146, was used as the control. To determine EC_{50} and IC_{50} values, ΔCt values were first converted into fractions of starting material and then were used to calculate the percent inhibition.[121] The activity profile clearly revealed significant potency for these metabolites comparable to the recently approved drug Telaprevir (EC_{50} 0.1-0.2 µg/mL)[122] and a therapeutic window warranted to inspire further investigations.

BIBILIOGRAPHY

1. Diekema, D. J.; Boots Miller, B. J.; Vaughn, T. E.; Woolson, R. F.; Yankey, J. W.; Ernst, E. J.; Flach, S. D.; Ward, M. M.; Franciscus, C. L.; Pfaller, M. A.; Doebbeling, B. N. *Clin. Infec. Dis.* **2004**, *38*, 78-85.

2. National Nosocomial Infections Surveillance System Report, Data Summary from January 1992 through June 2003. *Am. J. Infec. Control* **2003**, *31*, 481-498.

3. Reischl, U.; Holzmann, T. *Laboratoriumsmedizin* **2008**, *32*, 253-265.

4. Mahamat, A.; MacKenzie, F. M.; Brooker, K.; Monnet, D. L.; Daures, J. P.; Gould, I. M. *Int. J. Antimicrob. Agents* **2007**, *30*, 169-176.

5. Jappe, U.; Heuck, D.; Strommenger, B.; Wendt, C.; Werner, G.; Altmann, D.; Witte, W. *J. Invest. Dermatol.* **2008**, *128*, 2655-2664.

6. Appelbaum, P. C. *Int. J. Antimicrob. Agents* **2007**, *30*, 398-408.

7. Lodise, T. P.; McKinnon, P. S. *Pharmacotherapy* **2007**, *27*, 1001-1012.

8. Herrick, W. J. *Iroquois Medical Botany*; Syracuse University Press: Syracuse, 1995; p 129.

9. Gilman, F.; Watson, D. G. *Platanus occidentalis*, Sycamore; Adapted from Fact Sheet ST-484, Environmental Horticulture Department, Florida Cooperative Extension Service, Institute of Food and Agricultural Sciences, University of Florida, Gainesville, FL, 1994.

10. Moerman, D. E. *Medicinal Plants of Native America*; University of Michigan: Ann Arbor, 1986.

11. Mitrokotsa, D.; Mitaku, S.; Demetzos, C.; Harvala, C.; Mentis, A.; Perez, S.; Kokkinopoulos, D. *Planta Med.* **1993,** *59*, 517-520.

12. Smith, H. H. Ethnobotany of the Meskwaki Indians; *Bulletin of the Public Museum of the City of Milwaukee* 1928, vol. *4*, pp 175-326.

13. Hamel, P. B.; Chiltoskey, M. U. *Cherokee Plants and their Uses -- A 400 Year History;* Herald Publishing *Co., Sylva*, N.C. 1975, p 58.

14. Stambouli, A.; Paris, R. *Ann. Pharm. Fr.* **1961**, *19*, 732-739.

15. Rieseberg, L. H.; Soltis D. E. *Biochem. Syst. Ecol.* **1987**, *15*, 109-112.

16. Fiorini, C.; David B.; Fouraste I.; Vercauteren, J. *Phytochemistry* **1998**, *47*, 821-824.

17. Kaouadji, M.; Morand, J.; Garcia, J. *J. Nat. Prod.* **1993**, *56*, 1618–1621.

18. Bloor, S. J. *Phytochemistry* **1995**, *38*, 1033-1035.

19. Otsuka, N.; Liu, M. H.; Shiota, S.; Ogawa, W.; Kuroda, T.; Hatano, T.; Tsuchiya, T. *Biol. Pharm. Bull.* **2008**, *31*, 1794-1797.

20. Gao, Z.; Ali, Z.; Khan, I. A. *Phytochemistry* **2008**, *69*, 2856-2861.

21. Hara, S.; Okabe, H.; Nagao, T. *Chem. Pharm. Bull.* **1987**, *35*, 501-506.

22. (a) NCCLS. *Reference Method for Broth Dilution, Antifungal Susceptibility Testing of Yeasts*, Approved Standard M27-A; National Committee on Clinical Laboratory Standards, Hayne, PA, 1997, vol. 17, p 9. (b) NCCLS. *Methods for Dilution Antimicrobial*

Susceptibility Tests for Bacteria that Grow Aerobically M7-A5, National Committee on Clinical Laboratory Standards, Hayne, PA, 2000, Vol. 20, p 2. (c) NCCLS. *Susceptibility Testing of Mycobacteria, Nocardia, and Other Aerobic Actinomycetes; Tentative Standard*, 2nd ed.; M24-T2, National Committee on Clinical Laboratory Standards, Hayne, PA, 2000, Vol. 20, p 26.

23. Bharate, S. B.; Khan, S. I.; Yunus, N. A.; Chauthe, S. K.; Jacob, M. R.; Tekwani, B. L.; Khan, I. A.; Singh, I. P. *Bioorg. Med. Chem.* **2007**, *15*, 87-96.

24. Dandekar, P. K.; Tessier, P. R.; Williams, P.; Nightingale, C. H.; Nicolau, D. P. *J. Antimicrob. Chemother.* **2003**, *52*, 405-411.

25. All in vivo procedures were approved by the University of Mississippi Institutional Animal Care and Use Committee (Protocol # 07-012) and were conducted in accordance with the principles of laboratory animal care as detailed in the Guide for Care and Use of Laboratory Animals (National Research Council, 1996).

26. Ibrahim, M. A.; Mansoor, A.; Gross, A; Ashfag, M.; Jacob, M.; Hamann, M. T. *J. Nat. Prod.* **2009**, *72* (12), 2141–2144.

27. Fortin, D. L.; Banghart, M. R.; Dunn, T. W.; Borges, K.; Wagenaar, D. A.; Quentin, G. Q.; Karakossian, M. H.; Otis, T. S.; Kristan, W. B.; Trauner, D.; Kramer, R. H. *Nat. Methods* **2008**, *5*(4), 331-338.

28. Jiang, Z.; Swem, L. R.; Rushing, B. G.; Devanathan, S.; Tollin, G.; Carl, E.; Bauer, C. E. *Science* **1999**, *285*, 406 - 409

29. Leenders, J. M.; VandeVondele, J.; Bolhuis, P. G.; Meijer, E. J. *J. Phys. Chem. B*, **2007**, *111* (48), 13591–13599.

30. Maxwell, K.; Johnson, G. N. *J. Exp. Bot.* **2000**, *51*, 659-668.

31. Iriyama, K.; Ogura, N.; Takamiya, A. *J. Biochem.* **1974**, *76*, 901-904.

32. Sigala, P. A.; Tsuchida, M. A.; Herschlag, D. *Proc. Natl. Acad. Sci. U.S.A.* **2009**, *106* (23), 9232-9237.

33. (a) Plant Materials http://plant-materials.nrcs.usda.gov/, (b) Plant Fact Sheet/Guide Coordination Page http://plant materials.nrcs.usda.gov/intranet/pfs.html, (c) National Plant Data Center http://npdc.usda.gov, (accessed on December 15th, 2010), (d) Wells, J. M.; Raju, B. C.; Hung, H. Y.; Weisburg, W. G.; Mandelco-Paul, L.; Brenner, D. J. *Int. J. Syst. Bacteriol.* **1987**, *37*, 136-143.

34. a) ENY-683 (IN174), The Department of Entomology and Nematology, Florida Cooperative Extension Service, Institute of Food and Agricultural Sciences, University of Florida, (http://edis.ifas.ufl.edu), (accessed on December 15th, 2010). b) Sinclair, W. A.; Lyon, H. H. *Diseases of Trees and Shrubs*, 2nd Edition; Cornell University Press, *Ithaca*, N.Y. 2005, pp 660.

35. Fava, M.; Kendler, K. S. *Neuron* **2000**, *28*, 335-341.

36. http://www.nimh.nih.gov/health/publications/anxiety-disorders/introduction.shtml, (accessed on August 15th, 2009).

37. Kochanowska, A. J.; Rao, K. V.; Childress, S.; El-Alfy, A.; Matsumoto, R. R.; Kelly, M.; Stewart, G. S.; Sufka, K. J.; Hamann, M.T. *J. Nat. Prod.* **2008**, *71*, 186-189.

38. Diers, J. A.; Ivey, K. D.; El-Alfy, A.; Shaikh, J.; Wang, J.; Kochanowska, A. J.; Stoker, J. F.; Hamann, M. T.; Matsumoto, R. R. *Pharmacol. Biochem. Behav.* **2008**, *89*, 46-53.

39. Cryan, J. F.; Markou, A.; Lucki, I. *Trends Pharmacol. Sci.* **2002**, *23*, 238-245.

40. Cryan, J. F.; Hoyer, D.; Marouk, A. *Biol. Psychiatry* **2003**, *54*, 49-58.

41. Cryan, J. F.; Page, M. E.; Luck, I. *Psychopharmacology* **2005**, *182*, 335-344.

42. Vermeulen, E. S.; Smeden, M.; Schmidt, A. W.; Sprouse, J. S.; Wikström, H. V.; Grol, C. J. *J. Med. Chem.* **2004**, *47*, 5454-566.

43. Porsolt, R. D.; Bertin, A.; Blavet, N.; Daniel, M.; Jalfre, M. *Eur. J. Pharmacol.* **1979**, *57*, 201-210.

44. Crowley, J. J.; Jones, M. D.; O'Leary, J. F.; Lucki, I. *Pharmacol. Biochem. Behav.* **2004**, *78*, 269-274.

45. Petit-Demouliere, B.; Chenu, F.; Bourin, M. *Psychopharmacology* **2005**, *177*, 245-255.

46. Brocco, M.; Dekeyne, A.; Veiga, S.; Girardon, S.; Millan, M. J. *Pharmacol. Biochem. Behav.* **2002**, *71*, 667-680.

47. Shimamura, M.; Tobayashi, K.; Kuratani, K.; Kinoshita, M. *J. Pharmacol. Toxicol. Methods* **2008**, *57*, 80-84.

48. Fontanilla, D.; Johannessen, M.; Hajipour, A. R.; Cozzi, N. V.; Jackson, M. B.; Ruoho, A. E. *Science* **2009**, *323*, 934-937.

49. Hoyer, D.; Hannon, J. P.; Martin, G. R. *Pharmacol., Biochem. Behav.* **2002**, *71*, 533-554.

50. Heisler, L. K.; Chu, H. M.; Brennan, T. J.; Danao, J. A.; Bajwa, P.; Parsons, L. H.; Tecott, L. H. *Proc. Natl. Acad. Sci. U.S.A.* **1998**, *95*, 15049-15054.

51. Parks, C. L.; Robinson, P. S.; Sibille, E.; Shenk, T.; Toth, M. *Proc. Natl. Acad. Sci. U.S.A.* **1998**, *95*, 10734-10739.

52. Cryan, J. F.; Redmond, A. M.; Kelly, J. P.; Leonard, B. E. *Eur. J. Pharmacol.* **1997**, *7*, 109-114.

53. Borsini, F.; Evans, K.; Jason, K.; Rhode, F.; Alexander, B.; Pollentier, S. *CNS Drug Rev.* **2002**, *8*, 117-142.

54. Deakin, J. *Psychopharmacology* **1993**, *7*, 283-289.

55. Pecknold, J. *CNS Drugs* **1994**, *2*, 234-251.

56. Zhunag, X.; Gross, C.; Santarelli, L.; Compan, V.; Trillat, A.; Hen, R. *Neuropsychopharmacology* **1999**, *21*, S52-S60.

57. Mayorga, A. J.; Dalvi, A.; Page, M. E.; Zimov-Levinson, S.; Hen, R.; Lucki, I. *J. Pharmacol. Exp. Ther.* **2001**, *298*, 1101-1107.

58. Duxon, M. S.; Kennett, G. A.; Lightowler, S.; Blackburn, T. P.; Fone, K. C. F. *Neuropharmacology* **1997**, *36*, 601-608.

59. Branchek, T. A.; Blackburn, T. P. *Annu. Rev. Pharmacol. Toxicol.* **2000**, *40*, 319-334.

60. Roth, B. L.; Craigo, S. C.; Choudhary, M. S.; Uluer, A.; Monsma, F. J. J.; Shen, Y.; Meltzer, H. Y.; Sibley, D. R. *J. Pharmacol. Exp. Ther.* **1994**, *268*, 1403-1410.

61. Toure, Y. T.; Oduola, A. *Nat. Rev. Microbiol.* **2004**, 2, 276–277.

62. Ang, K. K. H.; Holmes, M. J.; Higa, T.; Hamann, M. T.; Kara, U. A. K. *Antimicrob. Agents Chemother.* **2000**, *44*, 1645–1649.

63. Chan, K. L.; O'Neill, M. J.; Phillipson, J. D.; Warhurst, D. C. *Planta Med.* **1986**, *52*, 105–107.

64. Wright, C. W.; Bray, D. H.; Oneill, M. J.; Warhurst, D. C.; Phillipson, J. D.; Quetinleclercq, J.; Angenot, L. *Planta Med.* **1991**, *57*, 337–340.

65. Sakai, R.; Higa, T. *J. Am. Chem. Soc.* **1986**, *108*, 6404–6405.

66. El-Sayed, K. A.; Kelly, M.; Kara, U. A. K.; Ang, K. K. H.; Katsuyama, I.; Dunbar, D. C.; Khan, A. A.; Hamann, M. T. *J. Am. Chem. Soc.* **2001**, *123*, 1804–1808.

67. Hu, J. F.; Hamann, M. T.; Hill, R.; Kelly, M. *Alkaloids: Chem. Biol.* **2003**, *60*, 207–285.

68. Rao, K. V.; Santarsiero, B. D.; Mesecar, A. D.; Schinazi, R. F.; Tekwani, B. L.; Hamann, M. T. *J. Nat. Prod.* **2003**, *66*, 823–828.

69. Takasu, K.; Inoue, H.; Kim, H. S.; Suzuki, M.; Shishido, T.; Wataya, Y.; Ihara, M. *J. Med. Chem.* **2002**, *45*, 995–998.

70. Takasu, K.; Shimogama, T.; Saiin, C.; Kim, H. S.; Wataya, Y.; Brun, R.; Ihara, M. *Chem. Pharm. Bull.* **2005**, *53*, 653–661.

71. Takasu, K.; Shimogama, T.; Saiin, C.; Kim, H. S.; Wataya, Y.; Ihara, M. *Bioorg. Med. Chem. Lett.* **2004**, *14*, 1689–1692.

72. Takasu, K.; Terauchi, H.; Inoue, H.; Kim, H. S.; Wataya, Y.; Ihara, M. *J. Comb. Chem.* **2003**, *5*, 211–214.

73. Takasu, K.; Terauchi, H.; Inoue, H.; Takahashi, M.; Sekita, S.; Ihara, M. *Heterocycles* **2004**, *64*, 215–221.

74. Chen, L. B. *Annu. Rev. Cell Biol.* **1988**, *4*, 155–181.

75. Kawakami, M.; Koya, K.; Ukai, T.; Tatsuta, N.; Ikegawa, A.; Ogawa, K.; Shishido, T.; Chen, L. B. *J. Med. Chem.* **1997**, *40*, 3151–3160.

76. Modica-Napolitano, J. S.; Aprille, J. R. *Adv. Drug Delivery Rev.* **2001**, *49*, 63–70.

77. Weissig, V.; Torchilin, V. P. *Adv. Drug Delivery Rev.* **2001**, *49*, 127–149.

78. Srivastava, I. K.; Rottenberg, H.; Vaidya, A. B. *J. Biol. Chem.* **1997**, *272*, 3961–3966.

79. Blom, J. F.; Brutsch, T.; Barbaras, D.; Bethuel, Y.; Locher, H. H.; Hubschwerlen, C.; Gademann, K. *Org. Lett.* **2006**, *8*, 737–740.

80. Hamann, M. T.; Alonso, D.; Martin-Aparicio, E.; Fuertes, A.; Perez-Puerto, M. J.; Castro, A.; Morales, S.; Navarro, M. L.; Monte-Millan, M.; Medina, M.; Pennaka, H.;

Balaiah, A.; Peng, J. N.; Cook, J.; Wahyuono, S.; Martinez, A. *J. Nat. Prod.* **2007**, *70*, 1397–1405.

81. Bax, B.; Carter, P. S.; Lewis, C.; Guy, A. R.; Bridges, A.; Tanner, R.; Pettman, G.; Mannix, C.; Culbert, A. A.; Brown, M. J. B.; Smith, D. G.; Reith, A. D. *Structure* **2001**, *9*, 1143–1152.

82. Jones, G.; Willett, P.; Glen, R. C.; Leach, A. R.; Taylor, R. *J. Mol. Biol.* **1997**, *267*, 727–748.

83. Eldridge, M. D.; Murray C. W.; Auton, T. R.; Paolini, G. V.; Mee, R. P. *J. Comput.-Aided Mol. Des.* **1997**, *11*, 425–445.

84. Lee, B.; Richards, F. M. *J. Mol. Biol.* **1971**, *55*, 379–400.

85. Makler, M. T.; Hinrichs, D. J. *Am. J. Trop. Med. Hyg.* **1993**, *48*, 205–210.

86. Mustafa, J.; Khan, S. I.; Ma, G.; Walker, L. A.; Khan, I. A. *Lipids* **2004**, *39*, 167–172.

87. National Committee for Clinical Laboratory Standards (NCCLS), NCCLS Document M27-A2 **2002**, *22*, 1–51.

88. National Committee for Clinical Laboratory Standards (NCCLS), NCCLS Document M7-A7 **2006**, *26*, 1–64.

89. National Committee for Clinical Laboratory Standards (NCCLS), NCCLS Document M38-A **2002**, *22*, 1–51.

90. National Committee for Clinical Laboratory Standards (NCCLS), NCCLS Document M24-A **2003**, *23*, 1–84.

91. Franzblau, S. G.; Witzig, R. S.; McLaughlin, J. C.; Torres, P.; Madico, G.; Hernandez, A.; Degnan, M. T.; Cook, M. B.; Quenzer, V. K.; Ferguson, R. M.; Gilman, R. H. *J. Clin. Microbiol.* **1998**, *36*, 362–366.

92. Sachs, J. D.; Baillie, J. E. M.; Sutherland, W. J.; Armsworth, P. R.; Ash, N.; Beddington, J.; Tim M. Blackburn, T. M.; Collen, B.; Gardiner, B.; Gaston, K. J.; Godfray, H. C. J.; Green, R. E.; Harvey, P. H.; House, B.; Knapp, S.; Kümpel, N. F.; Macdonald, D. W.; Mace, G. M.; Mallet, J.; Matthews, A.; May, R. M.; Petchey, O.; Purvis, A.; Roe, D.; Safi, K.; Turner, K.; Walpole, M.; Watson, R.; Jones, K. E. *Science* **2009**, *325*, 1502–1503.

93. Gilbert, N. *Nature* **2010**, *467*, 764.

94. Brower, V. *J. Natl. Cancer Inst.* **2008**, *100*, 838–839.

95. Karasov, C. *Environ. Health Perspect.* **2001**, *109*, a582–a587.

96. Reddy, B. A. *Int. J. Pharm. Sci. Rev. Res.* **2010**, *3*, 90–95.

97. Heinrich, M.; Lee, T. H. *J. Ethnopharmacol.* **2004,** *92*, 147–162.

98. Ajikumar, P. K.; Xiao, W. H.; Tyo, K. E. J.; Wang, Y.; Simeon, F.; Leonard, E.; Mucha, O.; Phon, T. H.; Pfeifer, B.; Stephanopoulos, G. *Science* **2010,** *330*, 70–74.

99. Kotiaho, J. S.; Kaitala, V.; Komonen, A.; Päivinen, J. P.; Ehrlich, P. R. *Proc. Natl. Acad. Sci. U.S.A.* **2005**, *102*, 1963–1967.

100. Klironomos, J. N. *Nature* **2002**, *417*, 67–70.

101. Gundale, M. J. *Conserv. Biol.* **2002**, *16*, 1555–1561.

102. Pimentel, D.; Zuniga, R.; Morrison, D. *Ecol. Econom.***2005**, *52*, 273–288.

103. Lee, J. C.; Yang, X.; Schwartz, M.; Strobel, G.; Clardy, J. *Chem. Biol.* **1995**, *2*, 721–727.

104. Choo, Q. L.; Kuo, G.; Weiner, A. J.; Overby, L. R.; Bradley, D. W.; Houghton, M. *Science* **1989**, *4902*, 359–362.

105. Houghton, M. *Liver Int.* **2009**, *29*, 82–88.

106. Fan, H.; Starks, C. M; Hughey, H.; Eldridge, G. R.; Hu, J. F. *Drugs Fut.* **2009**, *34*, 223–236.

107. Chong, T. W.; Smith, R. L.; Hughes, M. G.; Camden, J.; Rudy, C. K.; Evans, H. L.; Sawyer, R. G.; Pruett, T. L. *J. Sur. Res.* **2006,** *130*, 52–57.

108. Fishman, S. L.; Branch, A. D. *Infec., Genet. Evol.* **2009**, *9*, 1158–1167.

109. Alexopoulou, A.; Dourakis, S. P. *Curr. Drug Targets – Inflamm. Allergy* **2005**, *4*, 47–55.

110. Genovese, D.; Dettori, S.; Argentini, C.; Villano, U.; Chionne, P.; Angelico, M.; Rapicetta, M. *J. Clin. Microbiol.* **2005**, *43*, 1902–1909.

111. Murray, C. L.; Rice, C. M. *Nature* **2010**, *465*, 42–46.

112. Gao, M.; Nettles, R. E.; Belema, M.; Snyder, L. B.; Nguyen, V. N.; Fridell, R. A.; Serrano-Wu, M. H.; Langley, D. R.; Sun, J. h.; O'Boyle II, D. R.; Lemm, J. A.; Wang, C.;

Knipe, J. O.; Chien, C.; Colonno, R. J.; Grasela, D. M.; Meanwell, N. A.; Hamann, L. G. *Nature* **2010**, *465*, 96–100.

113. David, D. *Curr. Opin. Investig. Drugs* **2009**, *10*, 860–70.

114. Azzam, H. S.; Goertz, C.; Fritts, M.; Jonas, B. W. Natural. *Liver Int.* **2007**, *27*, 17-25.

115. Kainuma, M.; Ogata, N.; Kogure, T.; Kohta, K.; Hattori, N.; Mitsuma, T.; Terasawa, K. *Phytomedicine* **2002**, *9*, 365–372.

116. Wohlfarth, C.; Efferth, T. *Acta Pharmacologica Sinica* **2009**, *30*, 25–30.

117. Luteyn, J. L. *Memoirs of the New York Botanical Garden* **1999**, *84*, 1–278.

118. Miyase, T.; Inose, Y.; Ueno, A. *Chem. Pharm. Bull.* **1994**, *42*, 617–624.

119. Tanaka, T.; Naskashima, T.; Ueda, T.; Kouno, I. *Chem. Pharm. Bull.* **2007**, *55*, 899–901.

120. Kim, J. W.; Lee, S. W.; Park, S. J.; Shin, J. C.; Yang, J. W.; Lim, J. H. WIPO Patent Application WO/2010/085091.

121. Stuyver, L. J.; Whitaker, T.; McBrayer, T. R.; Hernandez-Santiago, B. I.; Lostia, S.; Tharnish, P. M.; Ramesh, M.; Chu, C. K.; Jordan, R.; Shi, J.; Rachakonda, S.; Watanabe, K. A.; Otto, M. J.; Schinazi, R. F. *Antimicrob. Agents Chemother.* **2003**, *47*, 244–254.

122. Revill, P.; Serradell, N.; Bolos, J.; Rosa, E. *Drugs Fut.* **2007**, *32*, 788-798.

APPENDIX

STUCTURE ELUCIDATION OF HETERONEMIN FROM THE NCI (repository No. 207161),

HYRTIOS RETICULATA

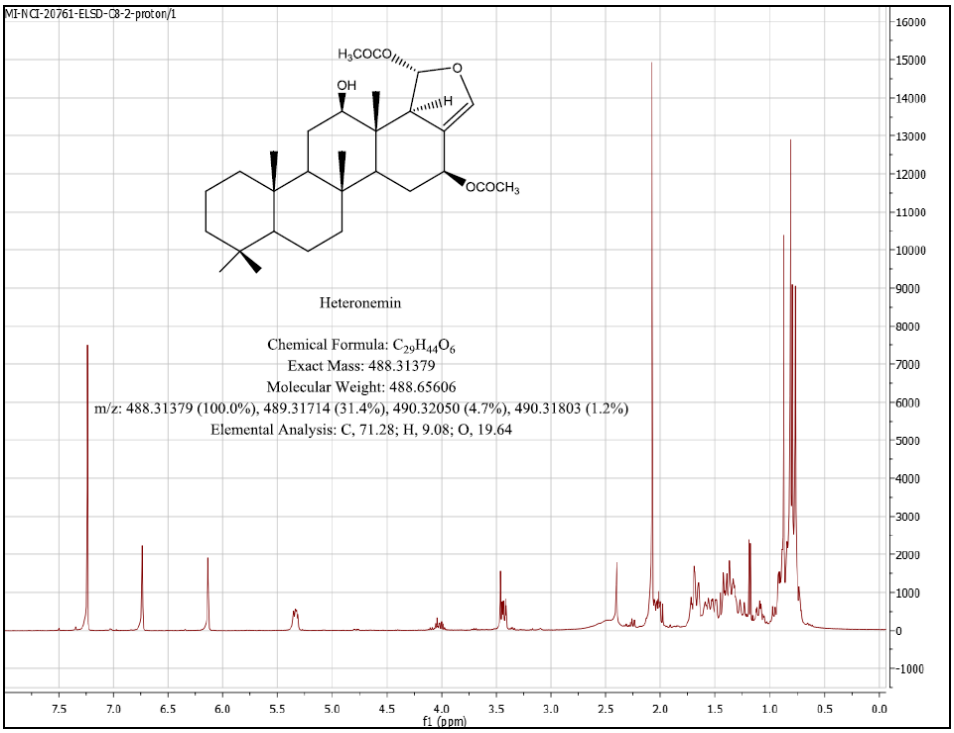

Figure 206. ^{1}H NMR spectrum of heteronemin in $CDCl_3$ (400 MHz)

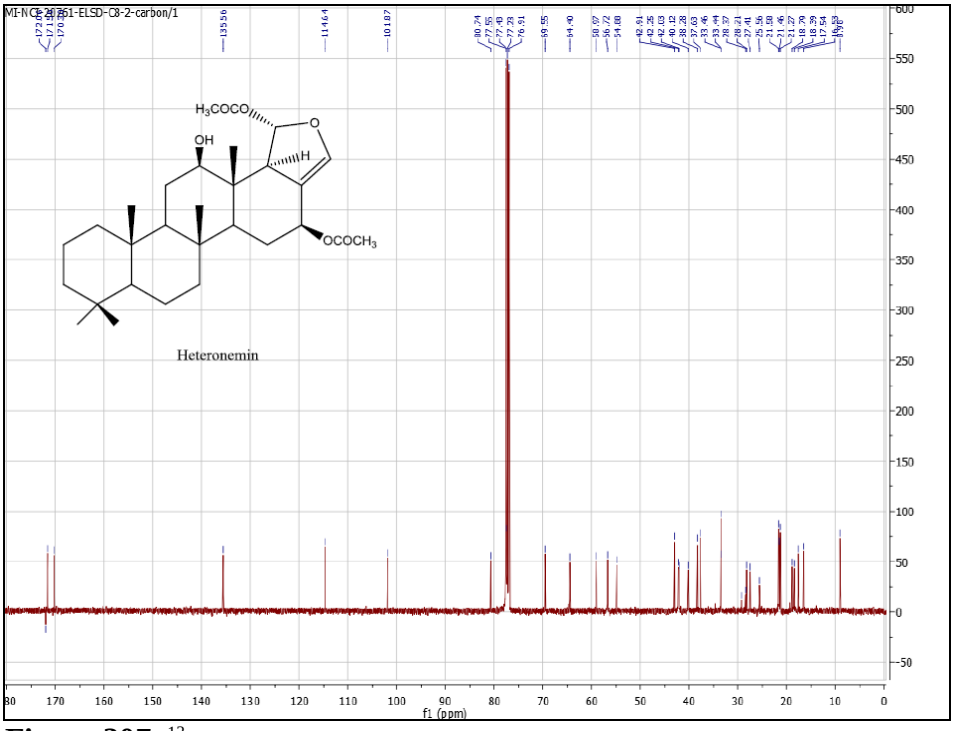

Figure 207. ^{13}C NMR spectrum of heteronemin in $CDCl_3$ (400 MHz)

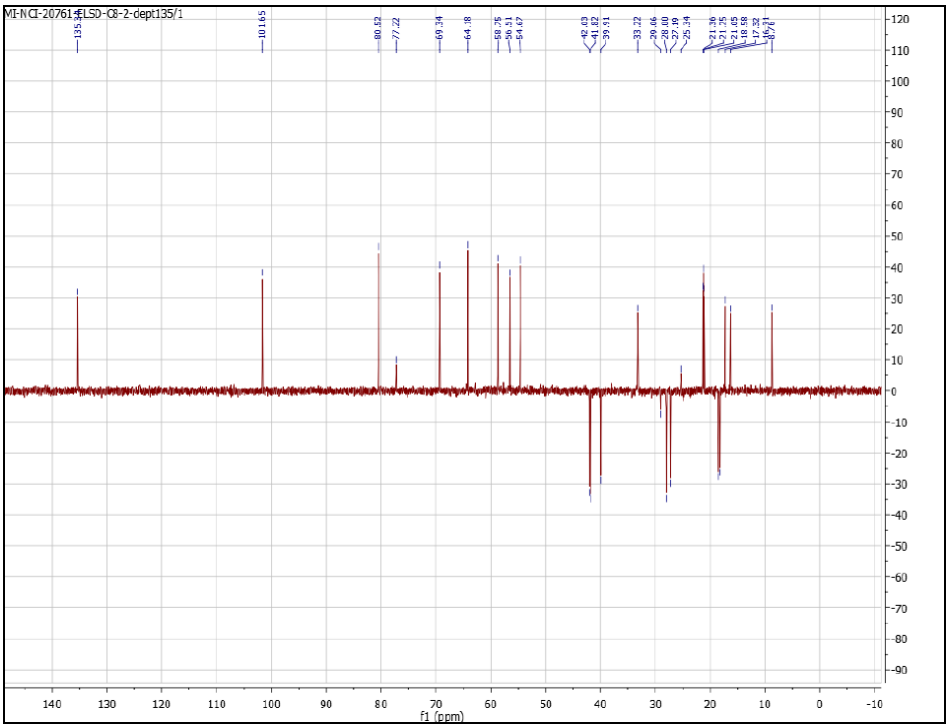

Figure 208. 135° DEPT spectrum of heteronemin in $CDCl_3$ (400 MHz)

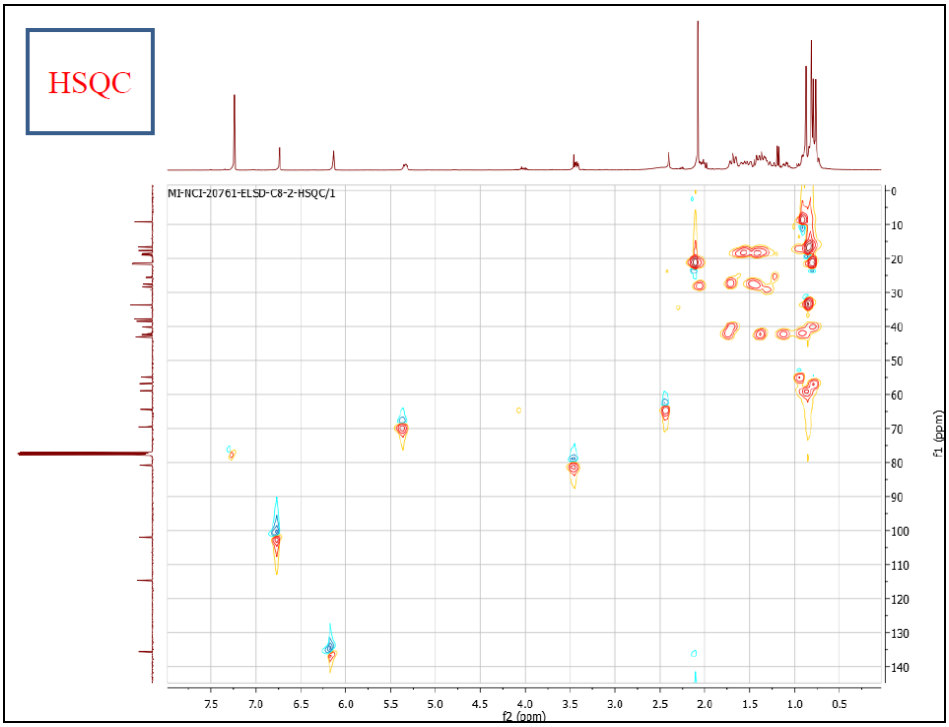

Figure 209. HMBC spectrum of heteronemin in $CDCl_3$ (400 MHz)

VITA

Mohamed Ali Ibrahim was born in Giza, Egypt on October 6th 1976. He graduated from the Faculty of Science, Cairo University with a B. Sc. in Chemistry in May 1997. During his work as a T. A. in the Department of Chemistry, Faculty of Science-Helwan University, Egypt between 1994-2002, he completed his Masters Degree in Organic Synthesis entitled "Synthesis of Antimetabolites using Nitrogen Base as Building Blocks," from the Department of Chemistry, Faculty of Science-Helwan University, Egypt in November 2002 under the supervision of Dr. Galal H. Elgemeie, Dean of the Faculty of Science. Ibrahim joined Dr. Atef G. Hanna's research group as an R. A. in the Department of Chemistry of Natural and Microbial Products**,** Division of Pharmaceutical Industries**,** National Research Center, Dokki, Cairo, Egypt in 2003. In February 2006, Ibrahim was awarded a full Ph.D. scholarship (4 years) from the Ministry of Higher Education and Scientific Research, Egypt, to pursue the doctorate degree in the Department of Pharmacognosy at the University of Mississippi under the supervision of Dr. Mark T. Hamann. During his Ph.D. course studies, Ibrahim was awarded the First place poster presentation award in the graduate student poster competition held at the Annual Poster Sessions of the national Center of Natural Products Research, School of Pharmacy, University of Mississippi, on October 23rd, 2009, and Chi Chapter of Rho Chi Honor Society 2010. During his Ph.D. course, he has filed two patents; the first on April 2009 on "Methods of Controlling Staph Infections Using Glycosides from the American sycamore," while the second has been filed on January 2011 on "Method to Use Compositions Having Antidepressant Anxiolytic and Other Neurological

Activity and Compositions of Matter." In the social field, he has served as ICS Policy Council Member (ICS, INC. PROJECT HEAD START, 2010-2011).